Repulsive Cues & Signalling Cascades of the Axon Growth Cone

Richard Peter Charles Manns
Trinity College, University of Cambridge

Supervisor: Prof. Roger J Keynes, Advisor: Prof. Christine E Holt
Department of Physiology, Development & Neuroscience

A Thesis Submitted
to the University of Cambridge
for the Degree of Doctor of Philosophy

Saturday, 24 November 2012

Declarations

This dissertation submitted for the Degree of Doctor of Philosophy is a result of my own work. It includes nothing which is the outcome of work done in collaboration, except where specifically indicated in the text. No parts of this dissertation have been submitted for any other qualification.

This dissertation is identical in every respect to the soft-bound volume examined for the Degree, except that any alterations required by the Examiners have been made.

This dissertation (39 182 words) does not exceed the 60 000–word limit of the Degree Committee for the School of the Biological Sciences, University of Cambridge.

Signed: _____

Richard Peter Charles Manns, Trinity College

Date: _____

Acknowledgements

I would like to thank my supervisor, Professor Roger Keynes, and my advisor, Professor Christine Holt, for their advice, understanding, insight and encouragement throughout my project.

I also thank Trinity College, Cambridge for funding and Barts and The London School of Medicine, particularly Professors Sir Nicholas Wright and Chris Fowler, for agreeing to pause my clinical studies and for funding my continuing clinical education. I also thank Professor Martin Schwab and Antonio and André Schmandke of the University of Zürich, Switzerland for the samples of Nogo-A NiG-δ20 (Nogo-δ20).

Thanks go to the Library and Harris/Holt labs, with special mention to Dr Geoff Cook, Asha Dwivedy and Jim Blundell for teaching me many techniques, Cátia Ferreira de Sousa for helping with primer design, as well as Clare Ellis and Drs Liz Muir particularly for the cDNA samples, Louis Leung and Aih-Cheun Lee for answering all those niggling little questions and generosity with equipment, Dr Perrine Barraud for donating sections for immunohistochemistry, and Dr Johann Graggaber for stopping me from forgetting my clinical skills.

I would also like to thank Minnie Yung, Pip Warren, João Nuno Alves, Umut Dursun, Dorit Hockman, Dr Sabine Knipp, Ryan Yann Shern Keh and Mark Russell for making the Library Lab so entertaining. I shall also miss Professor Lovely dearly, but not as much as the heavy-duty yet quality coffee shared with Drs Octavian Voiculescu and Mansoor Raza. Finally I thank my family, particularly my parents, for supporting me wholeheartedly whilst considering me insane, and friends for helping me through this project.

Abstract

The aim of the work described in this thesis is to investigate the nature and mechanisms of action of repellent cues for growing axons. In particular I try to resolve the controversy in the literature regarding the need for protein synthesis in the growth cone in response to external guidance cues.

My results resolve the conflicting data in the literature on Semaphorin-3A signalling, where differing labs had shown that inhibiting protein synthesis either blocks or has no effect upon repulsion. They demonstrate the presence of at least two independent pathways, protein synthesis-dependent mTOR activation and -independent GSK3β activation. The higher sensitivity of the synthesis-dependent pathway, and its redundancy at higher concentrations where synthesis-independent mechanisms can evoke a full collapse response alone, resolve the apparent conflict.

My experiments also demonstrated that Nogo-δ20, a domain of Nogo-A, requires local protein synthesis to cause collapse. Unlike Semaphorin-3A, the dependence of collapse upon protein synthesis is concentration-independent and does not involve guanylyl cyclase, but it does share a dependence upon mTOR activity and the synthesis of RhoA, sufficient to cause collapse downstream of Semaphorin-3A. The other axon-repelling domain of Nogo-A, Nogo-66, is partially dependent upon the proteasome instead. It does not share a common pathway with Nogo-δ20, except that both are RhoA-dependent.

I further attempted to identify the nature of a repulsive activity found in grey matter, ruling out a previously suggested candidate identity. Finally, I examined the phenomenon of nitric oxide-induced growth cone collapse. My experiments revealed that *S*-nitrosylated glu-

tathione causes growth cone collapse through the activity of protein disulphide isomerase. This mechanism shows only a partial dependence upon soluble guanylyl cyclase, but I argue that it has total dependence upon an *S*-nitrosylated donor. Coupled with its apparent relation to *S*-palmitoylation, the reciprocal of *S*-nitrosylation, I propose that nitric oxide causes collapse by crossing the cell membrane to inhibit *S*-palmitoylation–determined localisation of proteins.

These results reveal some of the many pathways involved in growth cone collapse, whose further characterisation may provide new targets for the treatment of injuries of the central nervous system.

List of Abbreviations

BSA	Bovine serum albumin
CA	Constituitively active mutant
CHAPS	3-[(3-Cholamidopropyl) dimethylammonio]-1-propanesulphonate
CNS	Central nervous system
DMEM	Dulbecco's modified Eagle's medium
DMSO	Dimethyl sulphoxide
DN	Dominant negative mutant
DRG	Dorsal root ganglion
EDTA	Ethylene diamine tetraacetate
GDP	Guanosine diphosphate
KLH	keyhole limpet hæmocyanin
MαGP	Methyl-α-*D*-galactopyranoside
MVP	Major Vault Protein
NGF	Nerve growth factor
Nogo-δ20	Axon-repulsive fragment of the unique domain of Nogo-A, also *NiG-δ20, amino-Nogo*
Nogo-66	Axon-repulsive 66-amino-acid extramembrane loop of Nogo-A
PAGE	Polyacrylamide gel electrophoresis
PBS	Phosphate-buffered saline
PIC	Protease inhibitor cocktail
PNS	Peripheral nervous system
RNAi	RNA interference
RP	Candidate novel grey matter-derived axon-repulsive glycoprotein
SCI	Spinal cord injury
SDS	Sodium dodecyl sulphate
Sema3A	Semaphorin 3A
TAMRA	Tetramethylrhodamine
TBS	Tris-buffered saline
TBS-T	Tris-buffered saline with Tween-20

Contents

List of Figures

List of Tables

Chapter 1

Introduction

Injuries to the central nervous system (CNS), such as stroke and spinal cord injury (SCI), are a major cause of disease, ill-health and disability around the world. For a long time, they were considered incurable, due in part to the failure of the axons, the long output projections of neurons, to regrow through injured tissue and reconnect with their targets. However, recent advances have rendered SCI in rodents partially treatable through antibodies and enzymes. These have been engineered to target molecules known to hinder regrowth. Other methods range from addition of growth-promoting molecules to disruption of inhibitory intracellular pathways and implantation of growth-permissive 'bridges' through the injured tissue.

My project encompasses several points of investigation: characterising an unidentified axon-repelling protein, elucidating the possible signalling mechanisms of a newly-identified candidate protein and investigating the intracellular signalling pathways of two well-known repulsive molecules in the injured spinal cord: *Semaphorin-3A* and *Nogo-A/Reticulon-4A*.

1.1 The Origin and Structure of Neurons

Neurons are a cell type common to almost all multicellular members of the *Animalia*, excepting almost colonial, sessile structures such as sponges. After gastrulation, where the inner cell mass (or germinal disc of non-mammalian tetrapods) generates the three germ layers (ectoderm, endoderm and mesoderm) from the epiblast, the ectoderm differentiates due to signalling from

the mesoderm notochord (for review, see Kessler and Melton (1994)). The CNS derives from the ectoderm as an invagination which seals over to form the neural tube. Follistatin and inhibition of the TGF-β family by the chelating protein, noggin, allows the invaginated cells to differentiate into presumptive neurons (McMahon et al., 1998) rather than epithelium. In vertebrates only, the border between the presumptive neural tube and the epithelium forms the 'neural crest' first observed by Wilhelm His in 1868, which disaggregates and migrates in cell streams to form various tissues, from melanocytes and the bones of the skull to the peripheral nervous system (PNS). The neural crest has been considered so important that some propose that it be considered a 'fourth germ layer' alongside the ectoderm, endoderm and mesoderm formed during gastrulation (Hall, 2000); strictly, though, its formation is separate. All neurons in vertebrates therefore derive ultimately from the ectoderm *via* neuroepithelium, and then either from the neural tube as most of the CNS, or from the neural crest to form the PNS such as the dorsal root ganglia (DRG).

As all epithelial cells, neurons have a clear apicobasal polarity that is crucial to their function, from stem cell maintenance (Ohata et al., 2011) to migration (Reiner and Sapir, 2009) and the direction of electrical signals in the neuron, from dendrites to axons. Polarity is seen in cells from single-celled organisms such as *Dictyostelium* (for review, see Swaney et al. (2010)) to neurons in humans, which distribute key molecules 'in front' (such as PI3-kinase and PIP_3) and 'behind' (such as PTEN) to dictate polarity and motility. This polarity is again seen in the growth cones of axons, described by Michael Abercrombie as a 'fibroblast on a leash'.

Neuronally-fated cells *in vitro* are initially roughly spherical, in contrast to the highly branched and complex structure of a mature neuron. Newly-formed neurons send out neurites, one of which becomes the axon, the 'output wire' of the neuron, the rest the dendrites, or 'inputs'. *In vivo*, cortical neurons begin as bipolar, but this switches to multipolar and back during migration, before the extension of neurites at its final destination (for review, see Reiner and Sapir (2009)). Both axons and dendrites form growth cones at the tips of their extending branches, although they differ in their mechanisms of growth (Whitford et al., 2002). Axons are notable in that they can extend to over a metre in the human body and they make up the

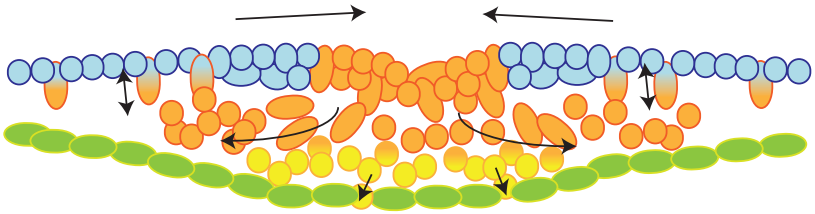

(a) Gastrulation in Mammals and Birds

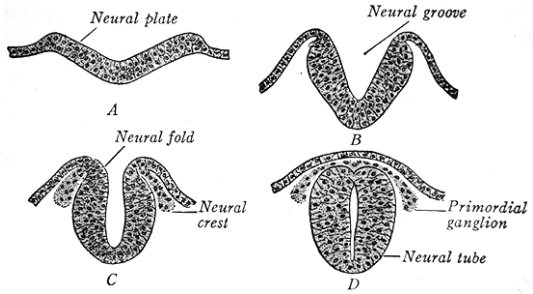

(b) Neural Tube Formation

Figure 1.1: Gastrulation and Neurulation in the Embryo

(a) Hensen's node forms in the epiblast due to signalling from the hypoblast where the head will be, and moves caudally, leaving the 'primitive streak' (centre, orange), through which cells invaginate to either replace the hypoblast (green) to become endoderm (yellow), or fill the intervening space become the mesoderm (orange). Those cells which do not delaminate form the ectoderm (blue). More recent evidence suggests (Voiculescu, 2011) that initially, cells delaminate stochastically and co-operatively, some far from the streak, before the indentation of the primitive streak occurs. (b) Later, the mesoderm induces neuroectoderm from the ectoderm to allow neural tube formation and neural crest migration (neurectoderm in cross-section, early to late). The 'primordial ganglion' will form the DRG. Image from Lewis and Gray (1918).

long-distance, myelinated tracts that fail to regrow after injury in the human CNS. Dendrites, by contrast, branch heavily rather than extend as a single process, leading to many thousands of dendritic 'spines' on the average neuron (Sanes et al., 2006).

Initially *in vitro*, all extending 'neurites' are equivalent and all are tipped with GAP-43, but at some point one neurite grows faster and axon-specific markers, like GAP-43, are only found in the new axon. All other neurites assume a dendrite identity. We know that this is determined by the axon, as removing the newly fated axon (Goslin and Banker, 1989) causes the next-longest neurite to become an axon instead. The axon-derived signal may be Par3 (Shi et al., 2003), an apicobasal polarity-signalling protein in other cells, and axon determination may be triggered by interactions of microtubules and the actin cytoskeleton at the tip of the new axon. This model is supported by evidence that cytochalasin, an actin depolymerising agent, induces all neurites to form axons (Bradke and Dotti, 1999). So does the overexpression of proteins promoting microtubule/actin interactions, such as Tiam1 (Kunda et al., 2001). Conversely, knock-down of Tiam1 induces all of them to form dendrites.

1.2 Glia and Injury in the Central Nervous System

The neuroglia or glia (from the ancient Greek 'glue', γλοία) are cells which provide support for neurons and comprise approximately half of the cells of the human CNS (Azevedo et al., 2009). They provide trophic support, structural support, insulation and immunological functions such as clearance of pathogens and bacteria in this immunologically privileged site. The glia of the CNS consist of the following cell types:

- microglia, which derive from monocytes (and therefore originate from the embryonic mesoderm, not the neuroepithelium), to perform analogous rôles in the CNS,
- ependymal cells, which line the CNS in the ventricles and other cerebrospinal fluid (CSF) spaces, producing and circulating CSF with beating cilia,
- oligodendrocytes, whose processes extend to envelop neighbouring axons to provide myelin insulation, functioning similarly to Schwann cells in this regard, including

- oligodendrocyte precursor cells (OPCs), known to give rise to oligodendrocytes *in vitro* but which may produce other cells *in vivo*, and

- astrocytes, the most abundant type, which regulate the CNS environment such as electrolyte balance and free neurotransmitters. They also control blood flow, signal to one another *via* IP_3 and Ca^{2+} wave propagation through gap junctions (Venance et al., 1997), and may modulate long-term depression and potentiation (Wenzel et al., 1991), although this is disputed (Agulhon et al., 2010).

After CNS injury, the cellular debris is cleared by microglia (Giulian et al., 1989) and the remaining space filled by astrocytes (Latov et al., 1979; Giordana et al., 1994) switching to a 'reactive' phenotype, characterised by hypertrophy and proliferation, to form the 'glial scar'. In mammals, this astrogliosis prevents secondary injury (Myer et al., 2006), but axons fail to regenerate through it (Ramón y Cajal, 1928).

This is not a property of the glial scar alone, but of the adult CNS environment in general. Previous experiments, inserting axon-free PNS tissue into the CNS, revealed little regrowth. What little there was, was thought to derive from the vasculature (le Gros Clark, 1943). David and Aguayo (1981) showed that PNS and fetal CNS tissue was permissive to adult CNS axon growth through 'bridging' experiments across lesions, but that when the regenerating axons recontacted the uninjured, adult CNS tissue on the other side of the bridge, they ceased regenerating. They also proved that the regenerating axons were CNS-derived by retrograde labelling. But even in PNS tissue, CNS axons regenerate more slowly than their PNS counterparts. Thus there are two issues in CNS regeneration: extrinsic factors that repel axons and limit their growth, and intrinsic factors that render CNS axons less capable of regenerating.

We know that age is a factor; young mammalian brains have a 'critical period', during which projections are highly malleable (Hubel and Wiesel, 1962; Wiesel and Hubel, 1963). Injection of immature astrocytes can 'replasticise' the cortex, showing that glia exert control over plasticity (Müller and Best, 1989). So can injections of chondroitinase ABC by lysing chondroitin sulphate proteoglycans (CSPGs) (Pizzorusso et al., 2002), and inhibition of Nogo-A's effects (Syken et al.,

2006; Luo et al., 2011; Delekate et al., 2011). These factors also boost regeneration after injury (Filous et al., 2010; Freund et al., 2006), indicating the link between maturation, reduction of plasticity and regenerative potential. Notably, however, reactive astrocytes revert in some ways to the immature phenotype (Yuan et al., 2007), so they may offer support rather than barriers to regeneration if the balance of growth promotion and inhibition can be modulated.

Ramón y Cajal (1928) showed that while mammalian PNS axons will regenerate after injury, extending over a metre in some cases, injured neurons in the adult CNS will not extend new axons beyond 1–2mm. Even regenerating PNS axons frequently travel aberrantly and rarely reach their exact destination. Cajal noted that beyond the axon's inherent ability to grow, regeneration depended on

"external conditions, the presence or absence of auxiliary factors that are indispensable to the regenerative growth"

and suggested that in the mature CNS

"once development has ended, the founts of growth and regeneration ...dry up irrevocably."

Subsequent research has tried to elucidate the intrinsic and extrinsic limits in CNS regeneration.

1.2.1 The Glial Scar

The CNS response to serious injury is the 'glial scar', a reactive gliosis, which involves mainly astrocytes (Fedoroff and Lindsay, 1986). After a lesion, surrounding astrocytes change their morphology (Mothe and Tator, 2005), proliferate and migrate into the centre (Chirumamilla et al., 2002) and, with their secreted factors and synthesis of new ECM, they profoundly alter injury site over the following days and weeks.

Despite initial claims (le Gros Clark, 1943), sprouting from within the lesion site and from surviving axons occurs (Guth et al., 1985, 1986) but they do not leave the lesion locale. They form dystrophic, bulbous endings (Misgeld et al., 2007) although Kerschensteiner et al. (2005) question their irreversibility, showing high levels of membrane dynamics and turn-over with

repeated episodes of endocytosis and attempts to form membrane veils (Tom et al., 2004), as in growth cones. The glial scar inhibits regeneration in several ways: molecules such as Sema3A (Pasterkamp et al., 2001), SLITs (Hagino et al., 2003), ephrins (Bundesen et al., 2003), CSPGs such as neurocan and versican (Rhodes et al., 2006; Apostolova et al., 2006) inhibit growth, as well as a possible physical barrier of hypertrophied astrocytes with a high density of enlarged processes. Fibroblasts can infiltrate the core in severe lesions (Kimura-Kuroda et al., 2010) which can produce Sema3A (Kaneko et al., 2006), but astrocytes generate most of the ECM post-injury (Ridet et al., 1997).

Astrocytes may pose a mechanical barrier to axon regeneration. One of the hallmarks of severe astrogliosis, when the gliosis does not resolve to the *status quo ante*, is that the 'tiling' of each astrocyte in its own volume is not longer preserved; their processes interdigitate which could pose a mechanical barrier to growth (Bush et al., 1999). Guth et al. (1986) showed that removal of the meshwork did not allow regeneration, but East et al. (2010) showed that insertion of a scaffold which aligned astrocytic processes and axons in one direction allowed regrowth; it is unclear whether this was due to astrocytes' alignment or axons'; it could be both (Sørensen et al., 2007).

Reactive astrogliosis can range from a localised, non-proliferative reaction which resolves to a pre-insult state, to failure of the blood-brain barrier (BBB), permanent infiltration of fibroblasts, astrocyte proliferation and involvement of blood-derived macrophages as well as CNS-derived microglia. It occurs both at the lesion site and at denervated targets far from the lesion (Massey et al., 2006), but the mechanism for the latter is unknown. There is also evidence that astrocytes, defined by their stellate morphology and the presence of glial fibrillary acidic protein (GFAP), consist of several sub-types (Stephens et al., 1993; Imura et al., 2006; Yeh et al., 2009) and that *in vitro* at least, astrocytes generated by different differentiation pathways have different effects when injected into CNS injury sites (Davies et al., 2008).

The glial scar was initially seen as a negative event which inhibits regeneration, but specific elimination of proliferating astrocytes revealed that the scar does have a protective rôle (Myer

et al., 2006; Li et al., 2008). Further, vertebrates with the capacity to regenerate still generate a glial scar; their axons can extend through them (Reier, 1979), showing that the scar is not always a barrier. Aiming to modulate the scar, specific knock-outs of hallmark proteins in scar formation have been performed, such as GFAP and vimentin, (the intermediate filaments required for extensive processes in astrocyte hypertrophy), the aquaporin AQP4 (to alter post-injury œdema), signalling molecules such as interleukin-6 (Il-6) and gene regulators such as STAT3 and NF-κB (for review, see Sofroniew (2009)). Many either exacerbated the extent of injury or improved recovery only in certain situations; only targeting the inflammation regulators SOCS3 and NF-κB had beneficial effects (Okada et al., 2006; Brambilla et al., 2009), suggesting that aspects of inflammation in the CNS do more harm than good; activated macrophages cause axon retraction (Horn et al., 2008), and dendritic cells from the CNS skew responses to a B-cell, humoural response (Hatterer et al., 2006). Recently, PTEN and SOCS3 knock-outs have been combined to induce more extensive, longer and longer-surviving axon regeneration (Sun et al., 2011).

The Glial Scar over Time

Reactive astrocytes re-establish the BBB and limit the extent of injury, but many of these protective reactions block later regeneration. Examples include metalloproteinase-3 (MMP-3), which is one of several proteases released by reactive astrocytes (Hsu et al., 2008). Its initial activity is associated with local recovery and reduced spatial learning deficits but if high MMP-3 activity remains, the effect becomes negative (Falo et al., 2006). The effects of tumor necrosis factor α (TNF-α) are the reverse: high levels of this immune response molecule initially destabilise the BBB, but help to maintain excitatory synaptic strength (Beattie et al., 2002).

Despite these protective effects, there is evidence that CNS glia inhibit regeneration *per se*. Simply depleting a tract of CNS glia allows extensive regeneration until the glia reappear (Moon et al., 2000). The end of the 'critical period' of mammalian plasticity correlates with the maturation of glia such as myelinating oligodendrocytes and astrocytes (Varga et al., 1995*a*; Bavelier et al., 2010) which correlates with a loss of regenerative capacity (Varga et al., 1995*b*). In contrast,

even adult glial scar tissue from frogs, capable of regeneration, is permissive to axons (Reier, 1979). Antibodies against Nogo-A, an axon growth inhibitor found in myelin, and knock-outs of its receptor, NgR1, can partially reverse this change (Varga et al., 1995*b*; McGee et al., 2005), showing the link between the end of plasticity and the end of axon regeneration.

One rather surprising finding is that the 'stiffness' of a substrate reduces axons' capacity to regenerate (Lu et al., 2011); the increased GFAP and vimentin of reactive astrocytes are necessary for the structural integrity of the scar, but those molecules increase the cells' stiffness. In competitive growth assays, glia outcompete axons in a high stiffness environment (Franze, 2011). This bias may explain why even the most chemically-inert CNS probes invoke gliosis within months, and why inhibition of regeneration seems to correlate with GFAP/vimentin expression (necessary for extensive hypertrophy), even though similarly dense scars in frogs do not prevent regeneration (Reier, 1979).

Therapies in CNS Injury

Myelin-derived inhibitors, such as Nogo-A, and CSPGs are the two main targets of the most advanced therapies in development. Nogo-A has been targeted by the monoclonal antibody, IN-1 (Caroni and Schwab, 1988*b*), whereas the family of CSPGs has been degraded by bacterium-derived chondroitinase ABC (ChABC) (Zuo et al., 1998). Corticosteroids to modulate inflammation have long been used, but clinical studies suggest that they do not have an effect (Bracken et al., 1990).

CSPGs are secreted by several cell types at the site of the lesion (Katoh-Semba et al., 1995). They are known to inhibit growing axons both *in vitro* (Niederöst et al., 1999) and *in vivo* (Davies et al., 1999). CSPGs are characterised by one or more polysulphated glycosaminoglycan (GAG) chains that attach to a core protein, and much of the axon repulsive activity is due to them; when degraded by ChABC, axon regeneration and functional recovery is promoted in rats (Bradbury et al., 2002) and cats (Tester and Howland, 2008), whilst Muir et al. (2010) induced growth cone-specific synthesis of functional ChABC, aiming to avoid repeated injections or a continuous pump.

The myelin-derived axon inhibitors have been targeted with antibodies (for review, see Zörner and Schwab (2010)), including humanised monoclonal antibodies in primates (Freund et al., 2006). Short, receptor-blocking peptides (NEP1–40) have also shown promise (GrandPré et al., 2002; Li and Higgs, 2003). However, both these approaches have been contested (Steward and Schuman, 2003); effectiveness may vary according to type of assessment. Genetic studies (Lee et al., 2009, 2010; Zheng et al., 2005; Wang et al., 2010; Nakamura et al., 2011) of Nogo-A- and NgR-deficient mice have revealed conflicting data on the rôle of the Nogo-A/NgR pathway, although gene expression data suggest that expression of CSPGs may up-regulate when Nogo-A is truncated in certain ways (Cafferty and Strittmatter, 2010).

Cell transplants to replace or substitute the lost glial cells, which are retained in PNS damage, are another avenue of research. Olfactory ensheathing cells (OECs) show promise in supporting regeneration across lesions (Ramón-Cueto et al., 1998), as physiologically they support the repeated regeneration of axons from the olfactory bulb throughout life. They are known to improve myelination (Sasaki et al., 2006) and functional recovery (Verdú et al., 2003), and recent evidence of their neural crest origin (Barraud et al., 2010) may allow clinical use. Further, Nakamae et al. (2010) and Filous et al. (2010) suggest that the effects of these therapies may be cumulative.

1.3 Structure of the Axonal Growth Cone

The tip of a growing axon bulges out to form the 'growth cone' first observed by Ramón y Cajal (1899); initially he suspected that the axon forced its way through tissue using the growth cone as a ram. But when living, growing axons were examined under a microscope in tissue samples (Harrison, 1910) and *in vivo* (Speidel, 1942), long, thin processes were observed extending and retracting, with veil-like structures extending between them, all extending and receding an order of magnitude faster than the growth cone as a whole.

Axon growth cones consist of three distinct domains, from the tip of the trailing axon proper to the distal edge:

- The axon shaft proper, consisting of multiple stable, parallel bundles of microtubules with interspersed organelles, making the shaft cylindrical under its own structure, rather than a dynamic area like the growth cone. *In vitro* 2-dimensional substrates cause the growth cone to adopt a flattened form .

- The central, or 'C', domain, filled with organelles such as mitochondria, endosomes and endoplasmic reticulum (ER) (Dailey and Bridgman, 1989), and dominated by stable, aligned microtubules from the axon proper defasciculating as one moves distally. There are arcs of contractile myosin and microtubule cross-linking proteins so that, as the growth cone moves forward, the microtubules are brought together and bound together.

- The peripheral, or 'P', domain, dominated by actin structures, consisting of the thin 'filopodia' and veil-like 'lamellipodia' observed by Harrison (1910) and Speidel (1942). The filopodia are highly dynamic, studded with receptors and filled with aligned actin filaments and microtubules which extend into them from the C-domain. Lamellipodial actin is a meshwork of crossing actin fibres and few microtubules, which instead tend to associate with the filopodia.

At the two boundaries, we also find functionally critical regions:

- The transition, or 'T', zone between the C and P domains, an area where actin structures delivered by retrograde flow break up for disassembly and recycling, through which dynamic microtubules extend and retract radially into more distal areas from the C domain. These microtubule/actin interactions are crucial for effective guidance and growth (for review, see Geraldo and Gordon-Weeks (2009)). A key feature of the 'retraction bulbs' of growth cones during failed regeneration is the inappropriate curling back and disorganisation of microtubules within them (Ertürk et al., 2007).

- The axon 'wrist', at the boundary between the central domain and the axon shaft. This area bundles the more spread microtubules of the C-domain with contractions and microtubule-bundling proteins to convert the rear of the C-domain into new axon shaft. This boundary is also the point at which the growth cone appears to 'pivot' during turning.

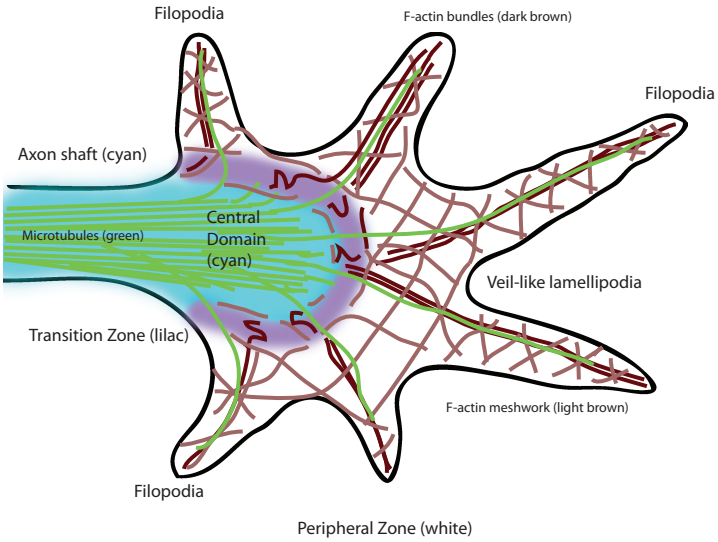

Figure 1.2: The Structural Domains and Features of the Axonal Growth Cone
A stereotyped image of a growth cone: the microtubules (green) of the axon (cyan) spread out into the C-domain. One population remains stable and largely in the C-domain; the other extends dynamic tubules radially, through the T-zone into the P-domain, where they associate with the F-actin bundles of the filopodia. The veil-like lamellipodia do not consist of F-actin bundles, but a meshwork. In the 'treadmill' hypothesis, both forms of F-actin are continuously added to by polymerisation whilst myosin linking the F-actin to the central regions, pulls them back into the T-zone, where they break to form F-actin arcs. The rate of extension or retraction is determined by these two forces, while exposing unprotected actin-ADP ends allows their rapid hydrolysis to release actin monomers back into the pool.

Actin

Actin can spontaneously polymerise in the presence of ATP and Mg^{2+} or Ca^{2+} *in vitro*, and even in steady-state is dynamic, as the 'pointed' end has a lower affinity than the 'barbed' end (defined by the appearance once myosin heads have been attached), thus the pointed ends disassemble as the barbed ends elongate, hydrolysing ATP in the process. The actin monomer comprises of two peanut-shaped domains, hinged with an ATP/Ca^{2+}-binding cleft. The amino-acid sequence of this protein is ancient and highly conserved, perhaps reflecting the extensive range of proteins with which actin must interact. Monomeric (G-) actin polymerises to form the double-helix F-actin, and the directional association of myosin heads to F-actin under the electron microscope

gave rise to the terms 'pointed', which are slow-growing or shrinking, and 'barbed' ends which are fast-growing.

G-actin can attach to F-actin and extend it, but nucleation is slow *in vitro*; once nucleation has occurred (or nucleating short stretches of F-actin are added), filaments grow until the G-actin supply falls to sub-micromolar concentrations (Bray, 2000), whereupon the less-stable pointed end loses actin-ADP monomers which recycle by exchanging ADP for ATP and binding to the barbed end. In the cell, there must be sufficient G-actin for the cell to build structures when required (such as presumptive neurites), even though a large network of F-actin, and therefore binding sites for G-actin, fills the cell 'cortex' and any rapid polymerisation would be quickly limited by local depletion of G-actin. To supply free G-actin ready for polymerisation, concentrations in the lamellipodia of moving cells reach approximately 500 μM and 150 μM, respectively (Koestler et al., 2009). Yet this presents a problem; it is well above the levels (~0.2 μM) needed for spontaneous nucleation *in vitro*. The cell maintains such a level of monomers to allow steady supply by tightly controlling polymerisation, nucleation and break-down of filaments through various proteins and, perhaps, covalent modifications of actin.

To maintain high concentrations of G-actin without spontaneous polymerisation, free actin is sequestered by several small proteins, such as thymosin, which binds most G-actin with a weak K_d of 0.7 μM to allow rapid buffering. The control of actin filament formation was first studied through extreme examples, such as *Thyone* sperm which generate 90 μm-long egg-penetrating actin spikes in seconds, and the intracellular bacterial pathogen, *Listeria*, which travels by generating F-actin behind itself to force itself from one cell to another (Tilney et al., 1973; Tilney and Portnoy, 1989). *Thyone* sperm generate rapid polymerisation through a complex with profilin at its heart. Profilin and related proteins sequester actin, like thymosin, but profilin's behaviour is more complex: there is less profilin than thymosin, it catalyses ADP-ATP exchange to promote barbed-end polymerisation, and it catalyses G-actin transfer from thymosin to the filament. It is also regulated by PIP_2, a signalling lipid from the membrane, allowing control by membrane-based signals.

Cofilin and actin-depolymerising factor (ADF) are members of a separate protein family; they bind the F-actin, and can break filaments with the torsion generated. They are regulated by pH, phosphorylation and phosphoinositols, such as phosphorylation by LIM kinase, downstream of the Rho-family GTPase, Rac (Yang et al., 1998), a GTPase known for promoting lamellipodial extension.

Beyond polymerising, depolymerising and sequestering, many proteins interact with F-actin. Myosin and tropomyosin apply tension and linking proteins such as fimbrin, filamin and spectrin interconnect to form different actin superstructures; organelles such as mitochondria and ribosomes associate with actin (Toh et al., 1980) and many proteins often considered 'cytoplasmic' are likely to bind to the actin cytoskeleton.

Actin Nucleation

There are several proteins downstream of guidance cues which act as nucleating and branching points for actin filaments, such as the Arp2/3 complex, the diaphanous (Dia)-related formins (mDia1–3 in mammals), IRSp53, the ERM family and the ENA/VASP homology proteins (in mammals, they are Mena, VASP and Evl). The Arp2/3 complex binds to the side of existing F-actin (Egile et al., 2005) to create a branch at 60° from the main filament, but although this seems suited for creating the actin mesh of the lamellipodia, Arp2/3 is associated with the actin-rich patches which precede filopodia too, and inhibition reduces the numbers of axonal filopodia (Spillane et al., 2011). Formins, on the other hand, can nucleate actin filaments without existing F-actin (Pruyne et al., 2002).

Tubulin

Microtubules consist of the 110-kDa αβ-tubulin dimer, binding to two GTP molecules, one of which is hydrolysed during polymerisation. These strands form hollow cylinders of 13 protofilaments each, twisting around one another. Microtubules have polarity, as does F-actin: the *plus* end, which extends faster, and the *minus* end. Proteins such as dynein and kinesin, which transport organelles and material necessary for axon growth, travel along the microtubule in a

specifed direction.

Microtubules extend and retract like F-actin, but unlike F-actin, they do so stochastically with slow periods of growth and rapid periods of 'catastrophic' depolymerisation. Further, while F-actin generates the treadmilling effect in the growth cone from net depolymerisation at one end and polymerisation at the other, microtubules in the axon are dynamic at the distal *plus* end only, and do not 'treadmill', even though the axon lacks an anchoring organising centre, like a centrosome, which anchors the minus ends near the nucleus (Stiess et al., 2010). The growth-catastrophe pattern is attributed to the strain of curvature that ATP hydrolysis during polymerisation puts in the microtubule; GDP-tubulin is under stress, and if a cap of GTP-tubulin or another microtubule-capping complex is removed, the GDP-tubulin springs out, disintegrating the structure.

Actin and Tubulin Control of Axon Guidance

F-actin filaments in the filopodia are aligned, with the barbed ends generally pointing distally and the pointed ends towards the C-domain, whereas the lamellipodial F-actin forms a looser, more branched network. The barbed end of F-actin polymerises 10 times more efficiently than the pointed, forcing the filament back as it extends. This simultaneously drives the filopodia and lamellipodia forward, and pushes the pointed ends into the T-zone (for review, see Pak et al. (2008)). Goldberg and Burmeister (1986) imaged live *Aplysia* growth cones to show that axon growth, rather than undergoing constant, persistent movement, consists of three cycling phases: *protrusion*, *engorgement* and *consolidation*.

Actin polymerisation during *protrusion* drives the filopodia and lamellipodia forward, but may also push back the coupled membrane structures near the T-zone, maintaining the border; this is the 'retrograde flow'. Myosin II, the contractile protein linking the F-actin to the C-domain, contributes to this force by pulling the actin filaments further back, and differential modulation of myosin activity across the growth cone is a control point for guidance (Turney and Bridgman, 2005). The combined force of polymerisation from the edge and myosin retraction may cause actin filaments to bend and break in the T-zone to create the actin arcs (Schaefer

et al., 2008), although the precise causes of depolymerisation are unknown. The creation of actin arcs forms a barrier to invading microtubules, as application of cytochalasin D (which binds to and sequesters G-actin to prevent polymerisation) causes microtubules to extend *en masse* into the periphery; this invasion may be the method which cytochalasin D evokes to artificially specify a specific neurite as the presumptive axon (Bradke and Dotti, 1999), as it does not occur in the growth cones of dendrites.

During *engorgement*, this actin arcs disassemble, freeing the microtubules to grow into the P-domain (Schaefer et al., 2008). These are followed by the organelles and vesicles of the C-domain through Brownian motion and active transport along the microtubules into the P-domain. With the removal of the vesicles and organelles, and the suppression of actin polymerisation and the bundling of microtubules, the proximal section of the C-domain can condense to form new axonal shaft during *consolidation*, completing the cycle.

The shape of the growth cone overall also varies according to its surroundings (Bovolenta and Mason, 1987); fluorescent tracers such as DiI revealed that growth cones in areas where guidance decisions must be made, or those pioneering axons with no prior tracts to follow, have traditional spread morphologies with filopodia in all directions. But those following straight paths or guided by fascicles of prior axons are 'bullet-shaped' and the few filopodia extend in the direction of travel. Growth cones with the former morphology travel more slowly but can change direction very easily. The latter are more polarised and extend more quickly, but must turn rather than switch direction (for a review of polarity and turning, see Swaney et al. (2010)). Integration of extrinsic signalling determines the state of the axon (Berman et al., 1993) such as cues specifying 'turning points'.

1.4 Axon Guidance

The main period of axon growth and guidance is during development. These axons originate from different cells in different regions, but must react to cues along their path, and fasciculate and defasciculate with other axons as tracts form, converge, diverge and disperse in order to

each reach unique destinations.This is simplified by the use of 'pioneer' axons, for example in the grasshopper leg, in which the first sensory axon grows proximally *via* 'guidepost cells', then other axons follow its path. If the guidepost cells are destroyed (Bentley and Caudy, 1983), then the pioneer axon no longer finds its way up the leg, and nor do following axons. If the pioneer axon is destroyed after tracing its path, the following axons do not reach their targets irrespective of the guidepost cells and their signals.

But what causes the pioneer axons to grow towards the guidepost cells? And once they have reached them, what then drives them away, to the next guidepost cell? Surface proteins are key (Chang et al., 1992); if phospholipase C is applied to remove surface proteins linked by glycophosphatidylinositol (GPI), early pioneer axons turn away, grow distally instead of proximally and fail to turn ventrally at a cell boundary. The failure at the cell boundary was due to loss of the GPI-linked 'fasciculin IV', later renamed semaphorin 1A (Kolodkin et al., 1992, 1993). But how does the axon sense, then react to the presence of semaphorin 1A on the guidepost cells?

1.4.1 Filopodia and Guidance Cues

Filopodia are key structures for both sensing and effecting guidance decisions in the growth cone; a single filopodium contacting a guidepost cell can induce the entire growth cone to divert course onto the cell (O'Connor et al., 1990). When it contacts an axon shaft, the adhesion and tension from a filopodium can pull its own shaft entirely away from its substrate (Heidemann et al., 1990), proving that the effect is not solely due to signalling to the rest of the growth cone.

However, filopodia do not act entirely autonomously from the rest of the growth cone, allowing the forces of opposing filopodia to average out; filopodial contact with repulsive neurites (Kapfhammer and Raper, 1987) can induce retraction of neighbouring filopodia as well and induce longer-term retraction of the growth cone back down the axon shaft.

These findings imply that filopodia can sense and react to cues autonomously, and can control the growth cone both through application of force directly and signalling to the rest of the structure. But what structures and proteins in the filopodium perform this? And what is the rôle

of the highly dynamic veil-like lamellipodia, which also shrink in response to repulsive signals in the filopodium?

1.4.2 Cellular Mechanisms of Guidance

Actin Nucleation

Although the NGF-induced creation of actin patches (Ketschek and Gallo, 2010) and their conversion by netrin-1 into filopodia (Lebrand et al., 2004) are two methods for cues to exert influence, filopodia once formed can be long-lived, so regulation of extension and retraction becomes the dominant factor during axon guidance (Mallavarapu and Mitchison, 1999). Depolymerisation is governed by a separate set of proteins, such as gelsolin, ADFs and cofilin. Gelsolin may not play a significant rôle in growth cones, unlike other cells, as its knock-out in growth cones seems only to slow filopodial retraction (Lu et al., 1997). ADFs and cofilin colocalise near the T-zone of growth cones, and there is indirect evidence that they sever the proximal ends of actin filaments brought back by treadmilling and myosin contractions. These fragments can be further broken down into monomers, or they may provide new sites for nucleation depending upon the activity of other proteins (for review, see Sarmiere and Bamburg (2004)).

The Clutch Hypothesis

The retrograde flow of actin and the contraction of myosin in the periphery provide the force to both pull the growth cone forward and pull the periphery away, whilst focal adhesions containing integrins bind to the substrate to allow traction. In order to switch between pulling forward and pulling back, there must be a 'clutch' determining whether the actin will be held still and pull the growth cone towards it, or whether myosin contraction will pull unanchored actin into the centre. Hu et al. (2007) used speckle and internal reflection fluorescence microscopy in fibroblasts to examine the proteins forming the connection between actin and integrins.

The speed and direction of focal adhesion kinase (FAK) and paxillin (core proteins of the focal adhesion) and vinculin, talin and α-actinin (actin-binding proteins linking to the focal adhesion) were measured. Those proteins of the first group, despite being considered 'core'

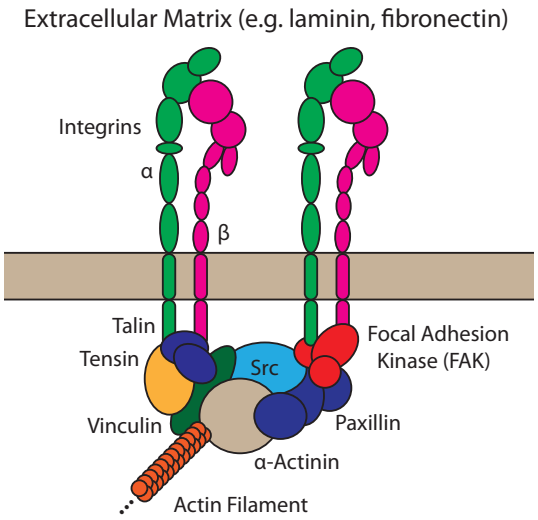

Figure 1.3: The Focal Adhesion

An example focal adhesion. Integrins bind to the ECM and pass through the membrane to contact the cytoskeleton and signalling cascades. The 'core proteins' such as FAK and paxillin, can bind directly to the intracellular domains of integrins, whereas actin-binding proteins (vinculin and α-actinin shown here) link actin filaments directly to the adhesion. Talin can perform both functions. The structures are repeatedly created and dissolved in the growth cone and member proteins are variable, and recent research (Hu et al., 2007) suggests that the structures are fluid *in vivo* and slide readily.

proteins of the complex, move relative to α-integrin. Those of the 'actin-binding' group move more quickly, and vary in their speed and coherence. This suggests that the connections between the proteins of the adhesion are flexible and many slip, rather than one specific point of control between actin and integrins. The presence of multiple sliding points suggests one reason why focal adhesions involve many different proteins in differing combinations; each complex could be an amorphous, transient structure *in vivo*.

However, Aratyn-Schaus and Gardel (2010) have revealed another clutch, this time between the integrins and the extracellular matrix, where newly formed focal adhesions slip under low levels of myosin contraction, through controlled, cycling integrin association and dissociation. On unphysiologically high-tensile surfaces *in vitro*, such as glass cover-slips, the extent of slip falls below detection, explaining why previous studies observed immobile focal adhesions. The location of the 'slip' may depend upon which connections are the weakest, each of which is in turn an opportunity for regulation. Further, these weak initial links to the ECM might allow new extensions to act as highly motile sensory structures for guidance, independent of the 'clutch' mechanism of P-zone extension and retraction. But it remains unknown how such a clutch would be controlled during axon guidance.

1.4.3 Actin and Tubulin Dynamics, and Turning

Actin filaments are predominantly found in the P-domain of the growth cone, whereas microtubules reside in the C-domain and only a few extend into the periphery. However, those that do are highly dynamic and associate with the filopodia, structures key to guidance. Gradients of the actin- or microtubule-destabilising molecules, such as cytochalasin or nocodazole respectively, cause growth cones to turn away from the gradient (Buck and Zheng, 2002; Yuan et al., 2003), showing that local variations in either actin or tubulin polymerisation are enough to induce turning and conversely, a gradient of the microtubule-stabilising molecule, taxol, is attractive to growth cones. Tellingly, however, Buck and Zheng (2002) also found that attractive turning by taxol begins with the extension of lamellipodia (which contain no microtubules), mediated through Rho GTPases, and that using cytochalasin to block actin polymerisation can block this

turning effect. Thus turning responses can be generated through the control of actin or tubulin dynamics, but tubulin generates responses from actin to initiate the turn.

Interestingly, Cheever et al. (2011) have found that actin is not required for motor axon regeneration in the adult mouse, implying that although tubulin requires actin to co-ordinate growth cone guidance, tubulin alone can regenerate motor axon tracts, perhaps by following myelinated tracts. However, these experiments use direct manipulations of the growth cone cytoskeleton, so do not explain how responses to cues are processed. Early experiments with cytochalasin D and taxol (Marsh and Letourneau, 1984; Letourneau et al., 1987) demonstrated that actin was not required for axon elongation *per se*, and may even slow it down through the inhibition of microtubule extension through the T-zone.

The Rho GTPases

The small GTPases are cytosolic, low-molecular-weight signalling proteins, homologous to the α-subunit of G proteins associated with serpentine, or G-protein-coupled, receptors (GPCRs). Like G proteins, fatty acid moieties are attached to them post-translationally to associate them with the inner cell membrane, they constitutively have either GDP or GTP bound to their catalytic sites and they are in general active when bound to GTP, and inactive bound to GDP. Unlike G proteins, they function without β/γ-subunits. They constitutively have some GTPase activity, although often with half-lives in the ranges of seconds to minutes, and are also slow to exchange the resultant GDP for GTP from the cytosol without regulatory co-factors.

Small GTPase activity is modulated by many proteins, grouped as three types:

- guanosine nucleotide exchange factors (GEFs), which facilitate the exchange of GDP for GTP (whose cytosolic concentration is some 10 times higher), and thus activate GTPases,
- GTPase activating proteins (GAPs), which accelerate the hydrolysis of GTP to GDP and thus deactivate GTPases and
- guanosine nucleotide dissociation inhibitors (GDIs), which prevent exchange of GDP for GTP;

GDIs also surround the membrane localisation signals (such as palmitoyl side-chains) to sequester GTPases from their site of activity, the membrane, so maintaining them in an 'off' state.

GEFs and GAPs are not necessarily independent proteins; they can be domains of a larger structure such as integrins or plexins and those domains need not be structurally related to one another.

There are 20 known RhoGTPases in humans (Burridge and Wennerberg, 2004), subdivided into 5 groups according to cladistic analysis of structure and function (Figure 1.4).

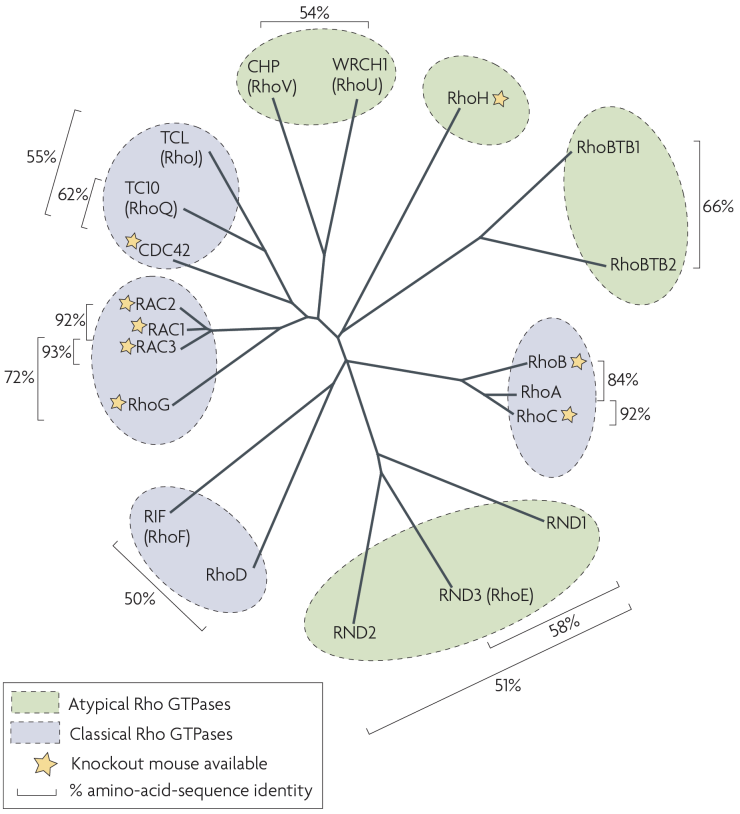

Figure 1.4: The Mammalian Rho GTPase Family

The 20 mammalian Rho GTPases are divided here into 4 classical subfamilies and 4 atypical by cladistic analysis; the best characterised are RhoA, Rac1 and Cdc42. Line lengths indicate genetic distance. Image from Heasman and Ridley (2008).

The effects on actin of RhoA, Rac1 and Cdc42 were first characterised in fibroblasts; constitutitively active mutants caused stress fibres and focal adhesions (RhoA), formation of lamellipodia (Rac1), and filopodia (Cdc42) (Ridley and Hall, 1992; Nobes and Hall, 1995). Beyond the actin cytoskeleton, these proteins influence transcription, membrane trafficking and microtubule dynamics. Together, these have obvious implications for neurons in growth control, motility and adhesion to the extracellular matrix.

Phæochromocytoma and neuroblastoma cells sprout neurites upon application of NGF or serum starvation, respectively, but otherwise remain as globular cells and are models for neurite formation and retraction. As in a rain-drop, the globular shape is energetically stable, and forces must be applied and maintained to warp the cytoskeleton into generating surface protrusions; the forces are largely generated by actin and the neurites are stabilised by growing microtubules (da Silva and Dotti, 2002). Knock-outs (KOs) of various RhoGTPases showed that neurite formation depended on both Rac1 and Cdc42 activity (Sarner et al., 2000; Aoki et al., 2004) and FRET-based probes revealed that their localised activity was key: first to the periphery of the cell, and later further localised around the budding neurites. Aoki et al. (2004) revealed that Rac1 is more active in the distal neurite, with Cdc42 in the proximal half of the bud.

Where Rac1 and Cdc42 are increased in response to NGF, RhoA activity falls (Yamaguchi et al., 2001). RhoA activation or expression of constitutively active (CA) RhoA causes retraction of any neurites present and inhibition of further sprouting (Kranenburg et al., 1997; Amano et al., 1998), whereas dominant-negative (DN) RhoA increases neurite formation over control, and also generates filopodia and lamellipodia at the tips of the neurites (Kranenburg et al., 1997; Sebök et al., 1999). From these experiments, the general conclusion was that Rac1 and Cdc42 activity together cause neurite formation and elongation, and RhoA activity antagonises both of these. However, CA and DN studies of Rac1 and Cdc42 reveal further complexity: CA Rac1 and Cdc42 mutants in *Drosophila* both fail to extend neurites (Allen et al., 2000) whilst both CA and DN Rac1 mutants in chicks display the same neuronal phenotype of slow growth cone extension and differentiation (Kuhn et al., 1998). Such studies, taken together, suggest that regulation of the cycling and localisation of Rac1 and Cdc42 are critical for normal growth and initiation,

rather than activation alone.

Rac1 and Cdc42

What is clear is that Rac1, Cdc42 and RhoA all have some baseline activity, and that to maximise the effect of one necessitates suppression of the activity of others. NGF, for example, signals through the Ras-linked TrkA receptor and both activates Rac1 *via* PI-3 kinase and inactivates RhoA (Nusser et al., 2002). The three can cross-regulate (Yamaguchi et al., 2001), thus causing Rho-kinase activity to fall when Rac1 or Cdc42 are active (Nusser et al., 2002). Other upstream components of Rac1 include the GEFs, Tiam1, STEF and FIR. As an example, Tiam1 is Rac-specific, its expression in the developing nervous system is very high, and it increases outgrowth through α6β1 integrin/laminin interactions (Leeuwen et al., 1997). PI-3 kinases activate Tiam1 and outgrowth increases with RhoA inhibition, whilst CA RhoA abolishes its effects. Tiam1 is not solely dependent upon PI-3 kinases, as Tanaka et al. (2004) showed that Tiam1- and EphA2-expressing cells were activated by ephrin-A1, and this effect was found to be dependent upon all 3 *via* DN mutants.

Rac1 and Cdc42, although targets for a range of pathways, are not effectors in themselves; they bind to and activate effector molecules, such as PAK1. The PAK kinases are a family of serine/threonine kinases (Edwards et al., 1999) that, when inactive, are found in the cytoplasm. Binding to Rac1-GTP localises PAK1 to the cell membrane, which by itself drives neurite formation without kinase activity (Daniels et al., 1998). Rac1 and PAK1 form a membrane-bound complex with p35, a neuron-specific Cdk5 regulator, and Cdk5 itself. This complex requires p35, but active p35 reduces its neurite-forming ability by driving hyperphosphorylation of PAK1 when complexed with Rac1 (Nikolic et al., 1998); the complex encompasses activation and regulated, time-delayed deactivation of PAK1, presumably to control PAK1 activity tightly. PAK5 is another family member which induces neurites, but its activity is kinase-dependent, and not cumulative with DN RhoA mutations (Dan et al., 2002), suggesting that it acts through antagonism of RhoA.

Besides the PAK family, the targets of Rac1/Cdc42 include N-WASP, Cdc42-binding kinase α (MRCKα) and Cdc42Hs-associated kinase-1 (ACK-1).

RhoA and the Rho-Kinases

RhoA is a 24-kDa small GTPase with a geranylgeranylated, methylated *C*-terminus to associate it with the membrane (Katayama et al., 1991). RhoA's most important binding partners in axon guidance are the Rho-kinases (ROKα/ROCK2 and ROKβ/ROCK1) and early experiments with DN and CA RhoA mutants established its rôle in growth cone collapse and axon retraction (for review, see Sebök et al. (1999)).

The *Rho-kinases* consist of a pleckstrin homology domain for membrane and cytoskeletal localisation, a coiled-coil domain with a highly conserved RhoA-binding region (Dvorsky et al., 2004) and an autoinhibitory kinase domain. RhoA, arachidonic acid and sphingosylphosphorylcholine (Fu et al., 1998; Shirao et al., 2002) binding remove the autoinihibition, and caspase-3 cleaves it away (Coleman et al., 2001). Other small GTPases inhibit Rho-kinases by binding either the coiled-coil (RhoE (Riento et al., 2003)) or kinase domains (Gem and Rad (Ward et al., 2002)).

Immunofluorescence and cell fractionation have localised Rho-kinases mainly to the cytoplasm. Typically, they target (R/K)X(S/T) and (R/K)XX(S/T) motifs, and target multiple proteins crucial to the growth cone:

- Myosin light chain (MLC) *via* inactivation of MLC phosphatase (Kimura et al., 1996), leading to contraction of myosin-II in the growth cone, to either retract filopodia or draw the *C*-domain forward, and RhoA can also inhibit MLCP Rho-kinase–independently (Kimura et al., 1996),
- Akt/PKB downstream of plexin B in endothelial cells (Basile et al., 2007),
- LIM kinases, leading to phosphorylation and inactivation of cofilin (Maekawa et al., 1999) also involved in growth cone collapse (Aizawa et al., 2001),

- α-adducin, causing spectrin to bind to and cap the barbed end of F-actin, slowing polymerisation (Fukata et al., 1999),

- the ERM proteins (ezrin, radixin, moesin), modulating their cross-linking function between cell surface proteins and F-actin

and many others, such as the microtubule-modifying proteins Tau (Amano et al., 2003) and CRMP2 (Leung et al., 2002).

RhoA also acts through the mDia family, which possess FH2 domains to nucleate F-actin, resulting in parallel, unbranched F-actin filaments (Ridley, 2006). Citron kinase is another target; although its loss seems more relevant for neurogenesis and cytokinesis of progenitors (Di Cunto et al., 2000; Ackman et al., 2007), recent evidence implies that it might limit axon regeneration downstream of myelin-derived inhibitors (Ahmed et al., 2011).

1.4.4 An Example of Axon Guidance: Crossing the Mid-Line

Axons crossing the mid-line are a well-studied example of axons showing both attraction and repulsion to the same cue, found in both vertebrates and invertebrates. The growth cones of the pioneer axons in the grasshopper leg must be attracted to the guidepost cells. But they must also be repelled by the epithelium near their origin, which makes up the leg's surface, and they must rapidly switch from attraction to repulsion or indifference to the cues of a particular guidepost cell when and only when it is reached. Too early and it will not reach the cell at all. If the attraction is not lost soon after arrival, the growth cone will not continue to the next guidepost cell. Further, at any one time a growth cone will receive several cues and gradients from different directions, such as the leg epithelium surrounding it.

In a related situation common to bilaterally symmetrical *Animalia*, axons crossing the midline of the spinal cord in vertebrates, or the commissural axons of the invertebrate ventral nerve cord, must first be selected from the axons fated not to cross, cross the midpoint, then lose sensitivity to the mid-line guidance cue to prevent recrossing and continue along the contralateral

tract. Axons typically respond to attractive signals whilst approaching the floor-plate and its homologous fly structure, the mid-line glial cells, and repress repulsive signals. Once across, the repression is released to propel the axons across into the contralateral side. In both *Drosophila* and mice, the floor-plate secretes the diffusible cue, netrin (Harris et al., 1996; Shirasaki et al., 1996), which binds to the 'Frazzled' (Fra) or 'deleted in colorectal carcinoma' (DCC) receptor – homologues – on the growth cone. The high-ventral, low-dorsal gradient of netrin in vertebrate spinal cords has been imaged directly (Kennedy et al., 2006), although in absence of netrin, the 'sonic hedgehog' (Shh) gradient from the mid-line also allows some axons to successfully cross the mid-line in both flies and mice (Charron et al., 2003). Further, there is a second receptor for netrin, DSCAM, which can also mediate attractive netrin signals (Andrews et al., 2008), illustrating the layers of complexity found in one instance of guidance.

Once the axon has reached the mid-line in *Drosophila*, the growth cones are repelled abruptly to the contralateral side. This requires the cue Slit from the mid-line and the receptor 'Roundabout' (Robo); in flies without Robo expression, the axons enter, exit and re-enter the commissures in circles, hence the 'Roundabout' name (Kidd et al., 1998). *Drosophila* axons express Robo receptor before reaching the mid-line, but the protein 'Commissureless' (Comm) is expressed to bind Robo receptors and redirect them to late endosomes (Keleman et al., 2002) rather than the cell surface. Comm may block Robo function independently of sorting too (Gilestro, 2008). Comm is only transiently and locally expressed, near the mid-line, controlled by Fra in *Drosophila*. Despite the presence of the netrin gradient, the activation of transcription and translation of *comm* mRNA is netrin-independent (Yang et al., 2009), thus presumably there is an as-yet-unknown third ligand in addition to netrin and Shh in the mid-line.

After crossing the mid-line, Comm is down-regulated to allow Robo to reach the cell surface through unknown mechanisms. In vertebrates, Robo3.1/Rig1 takes the place of Comm to silence repulsion until crossing (Sabatier et al., 2004), whereupon the splice variant Robo3.2 replaces it and aids in repulsion. Work by Kuwako et al. (2010) has further shown that, in the olivary nuclei (but not the spinal cord) of mice, the RNA-binding protein Musashi1 is needed to bind Robo3 mRNA, controlling expression of the repulsive form. The rôle of mRNA-binding

proteins of the axon, such as Fragile X mental retardation (FXR) 1/2 and zipcode-binding protein (ZBP) 1/2, are an growing area of axon research, and will be expanded upon in a later section.

However, even the additional repulsion of Robo3.2 expression is insufficient; knocking down Stem Cell Factor, a specific growth promoter for post-crossing axons, causes the axons to fail to continue away from the floor-plate but stop shortly after crossing (Gore et al., 2008). This may be due to the growth-suppressing properties of many repulsive agents through their receptors, which have been suggested to be tumour suppressor genes (for review, see Mehlen et al. (2011)).

1.4.5 Families of Guidance Cues

All guidance cues can be divided into either repulsive or attractive cues, and each of those into soluble and insoluble cues. Thus insoluble ephrins can support the growth of certain RGC axons on their surfaces (Walter et al., 1987), while axons preferentially avoid tracts with myelin inhibitors (Oertle et al., 2003*a*). Areas of soluble attractive and repulsive cues can appose one another, funnelling axons into tracts. Soluble guidance cues, on the other hand, generate gradients of attraction and repulsion and can influence guidance from afar (Keynes et al., 1997).

There are several large families of cues that guide axons, from semaphorins to CSPGs, and from components of the ECM to fatty acid derivatives from the membrane. In the past decade, it has become clear that morphogens during development such as Engrailed, Wnt and Shh (Brunet et al., 2005; Liu et al., 2008; Charron et al., 2003) guide axons as well. Similarly, the semaphorins have established themselves as morphogens in the layers of the retina (Matsuoka et al., 2011) as well as one of many axon guidance molecules pivotal in guiding vasculature (for review, see Adams and Eichmann (2010)); its receptor, neuropilin 1, is also a receptor for vascular endothelial growth factor (VEGF) (Soker et al., 1998). The divisions between guidance factors and morphogens are thus blurring.

I have focussed upon Sema3A and Nogo-A in my investigations and the rôle of local protein synthesis in both, as both are repulsive, and both are found in injured CNS scar tissue

(Pasterkamp et al., 1999; Sandvig et al., 2004) and local protein synthesis has been indicated as a target to promote growth post-SCI (Liu et al., 2010). But the glial scar also produces other molecules not covered here such as the ephrins, CSPGs and other myelin inhibitors (Goldshmit et al., 2011; Bradbury et al., 2002; Llorens et al., 2010).

1.5 Semaphorins

Semaphorin-3A (Sema3A), also known as collapsin-1/semD/SemaIII, was first identified as a component of *Gallus gallus* brain which induced reversible collapse and paralysis in chick sensory neurons (Luo et al., 1993). Sequence analysis revealed Sema3A's relationship with fasciculin IV of the grasshopper, renamed Sema1A, and SemaIII, the mammalian homologue, leading to the grouping and renaming (Kolodkin et al., 1992, 1993).

Semaphorins are found in most *Metazoa* and although members within the family show high divergence in sequence, with 50% homology at best (Yazdani and Terman, 2006), all share a ~500-amino-acid, cysteine-rich Sema domain, critical for binding to Sema domains in receptors such as plexins (Takahashi and Strittmatter, 2001). The cysteines in extracellular conditions cross-link to form integrin-like β-propellers to interact with plexins and, in Class 3, neuropilins (Antipenko et al., 2003). Humans have 20 different forms, *Drosophila* have 5 and there are 2 identified from DNA viruses. Later research established that a receptor complex of neuropilin-1 and a Class-A plexin were sufficient to allow Sema3A-induced retraction (Kolodkin et al., 1997; Takahashi et al., 1999; Deo et al., 2004).

1.5.1 The Semaphorin Family

Sema3A is one member of a large family spanning 7 classes 1.5, in both invertebrates and vertebrates, and a virus class (Figure 1.5; Ensser and Fleckenstein (1995)). The *Sema* domain is critical for their function (Eickholt et al., 1997); in Sema3A, there is a 70-residue section within the *Sema* domain which is crucial for axon repulsion and collapse (Eickholt et al., 1997). Semaphorins have conserved *N*-linked glycosylation sites and some are alternatively spliced, but the significance of splicing is unknown. Other domains are found in different families, such as the plexin-

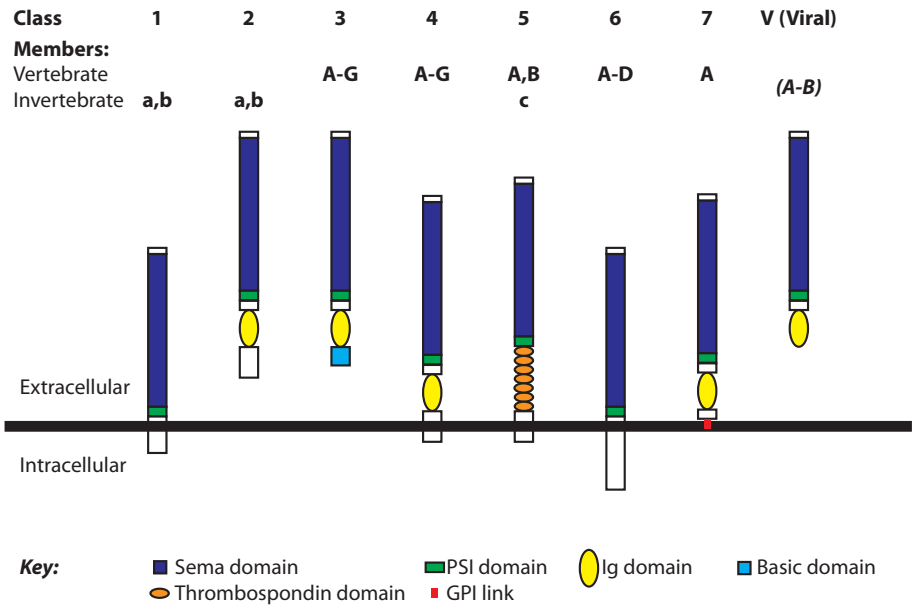

Figure 1.5: The Schematic Structure of the Classes of Semaphorins

The primary structures of the Semaphorin family. Schematic diagrams of the key features of the members of the Semaphorin family, all shown with their N-termini towards the top of the image. Class 1 and 2 are only seen in invertebrates, but Class 1 are structurally and phylogenetically most related to the vertebrate Class 6, and Class 2 are closely related to the vertebrate Class 3, which carry a C-terminus stretch of highly basic residues; these may control soluble Class 3's diffusion through and adhesion to negatively charged ECM. Classes 4-7 are all found in vertebrates, and Class 5 are shared with invertebrates, and all but Class 7 are transmembrane. Class 5 are distinguished by their 7 Type I thrombospondin repeats (TSRs), Class 6 are notable for their alternative splicing in their intracellular domains and Class 7 has one member, Semaphorin 7A, the only GPI-linked member and closely related to the virus-born Class V (Yazdani and Terman, 2006).

semaphorin-integrin (PSI) domain in all but viruses, TSRs in Class 5 and the C2-class Ig domain. Some of their functions are known, such as the basic tail and Ig domain of Sema3A which potentiate axon repulsion (Eickholt et al., 1997), and the TSRs of Sema5A which regulate its effects on axons (Kantor et al., 2004). The basic tail may also affect adhesion to negatively-charged ECM molecules, modulating diffusion.

1.5.2 Semaphorin Expression and Function in the Developing and Adult Nervous System

Semaphorins have a repulsive effect upon axons in development in general, although there are important exceptions (Bagnard et al., 1998):

- Falk et al. (2005) demonstrated Sema3B's rôle in attraction and repulsion in the anterior commissure through null mutations and neurons' responses to the signal *in vitro*. They showed that both signals use neuropilins to transduce the signal, but only attraction recruits FAK Src-dependently.

- *In vivo* experiments by Bagnard et al. (1998) revealed that Sema3C can simultaneously repel the axons and attract the dendrites of the same cells in the cortex, driving axonal projections into white matter whilst creating dendritic networks in the cortex. These results indicated that differing responses to semaphorins are found in differing compartments of the same cell.

Semaphorins are expressed in most tissues and this varies greatly with time; this is best visualised in the developing nervous system. There seems to be no clear relationship between class and pattern. Expression decreases with time in the nervous system overall, and semaphorin patterns seem to dictate boundaries to block ingress of inappropriate axons into specific areas, such as surround repulsion in DRG axon growth (Keynes et al., 1997). Semaphorins are also long-distance guidance cues in the PNS; Fasciculin-IV, now Sema2A, was identified as a null mutation in grasshoppers which drove pioneer axons along their limbs, whilst semaphorin 3A-producing dermomyotomes and notochord 'focus' the trajectories of DRG projecting axons between them (Keynes et al., 1997).

1.5.3 Semaphorin-Induced Repulsion, Dimerisation and Cleavage

After exposure to Sema3A, DRG axons collapse in a time-scale of minutes. Within the growth cone, F-actin depolymerises, microtubule motility falls and the ability to polymerise more F-actin falls. These actions can also control migration, engulfment, polarisation and movement in non-neuronal cells (Walzer et al., 2005).

Newly-synthesised semaphorins, however, often have little repulsive activity. Mouse Class 3 semaphorins require proteolytic cleavage by furins to have an effect (Adams et al., 1997). There are multiple cleavage sites, which lead to isoforms with differing effects. Sema3A repulsive activity depends upon dimerisation (Koppel and Raper, 1998), mediated by the *Sema* domain, cysteine residues and the C-terminus (Eickholt et al., 1997); transmembrane semaphorins also rely on dimerisation for at least some of their effects (Klostermann et al., 1998).

1.5.4 The Neuropilins, Plexins and Co-Receptors

Most semaphorin receptors are in the plexin family of transmembrane receptors, which have a Sema domain in their extracellular sections and thus may be related to the semaphorin family. Class 3 semaphorins cannot bind to plexins alone, excepting Sema3E (Casazza et al., 2010); they bind instead to a neuropilin in a neuropilin-plexin complex. The neuropilin intracellular domain, however, is short and does not seem to be necessary to propagate the Sema3A signal, which implies a co-receptor (Nakamura et al., 2000). Complexity is increased as certain semaphorins will act as competitive inhibitors to others, as although Sema3B and C activate neuropilin-2-containing receptor complexes, they still bind to (but do not activate) neuropilin-1-only complexes, blocking Sema3A's binding.

Further studies of semaphorins' affinities to neuropilins showed that there was little variation *in vitro*, contrary to differences seen in neuronal subsets *in vivo*, which suggests that co-receptors modulate affinity. Neuropilins and plexins are necessary for both the attractive response of cortical apical dendritic growth cones to Sema3A (Polleux et al., 2000) and the repulsive response of the same cells' axons (Polleux et al., 1998). Again, additional sub-units such as VEGFR2 appear

to be crucial, allowing attraction to Class III semaphorins, where deletion of the cytoplasmic domains of the plexins showed that they transduced repulsive, but not attractive, signals (Bellon et al., 2010). Unlike netrins, which have differing binding partners (such as UNC-5 for repulsion and DCC for attraction), neuropilins bind Sema3A to induce both attraction and repulsion.

Beyond VEGFR2, other surface molecules are known to be involved in semaphorin signalling: the 'dead' receptor tyrosine kinase Off-track (Winberg et al., 2001), which seems to contribute to plexin phosphorylation through recruitment of other proteins, and L1CAM (Castellani et al., 2000) and related adhesion molecules such as integrins and CD-72 (Kruger et al., 2005; Pasterkamp and Kolodkin, 2003).

1.5.5 Collapsin Response Mediating Proteins (CRMPs)

The first of the CRMPs was discovered through a genetic screen for expression that caused *Xenopus lævis* eggs to respond electrophysiologically to Sema3A (Goshima et al., 1995), and they are now an established effector of Sema3A signalling (Figure 1.6). This gene (CRMP2) was similar to Unc-33 in *Cænorhabditis elegans*, null mutants of which developed severely deranged axons. There are 5 members of the mammalian family (CRMP1-5), which strongly interact to form heterotetramers.

CRMPs are cytosolic proteins strongly associated with the membrane, and concentrated on the leading edge of neurites (Minturn et al., 1995). CRMPs are expressed early on, as far back as neurogenesis (Minturn et al., 1995) and remain throughout life. In neurogenesis and in the adult neurogenic areas, CRMPs 1, 2 and 5 predominate, whereas later on, expression falls and CRMP2 is the main form, with some CRMP3; as they function as heterotetramers, variations in a single form's expression may entail whole-sale changes to CRMP behaviour in the cell, to the point of function disruption, as CRMP2 over-expression drives ectopic neurite formation in hippocampal neurons (Inagaki et al., 2001). They are also highly conserved, with 95% homology between human and mouse, 50–75% homology across the group and 30% homology with Unc-33 of *C. elegans*.

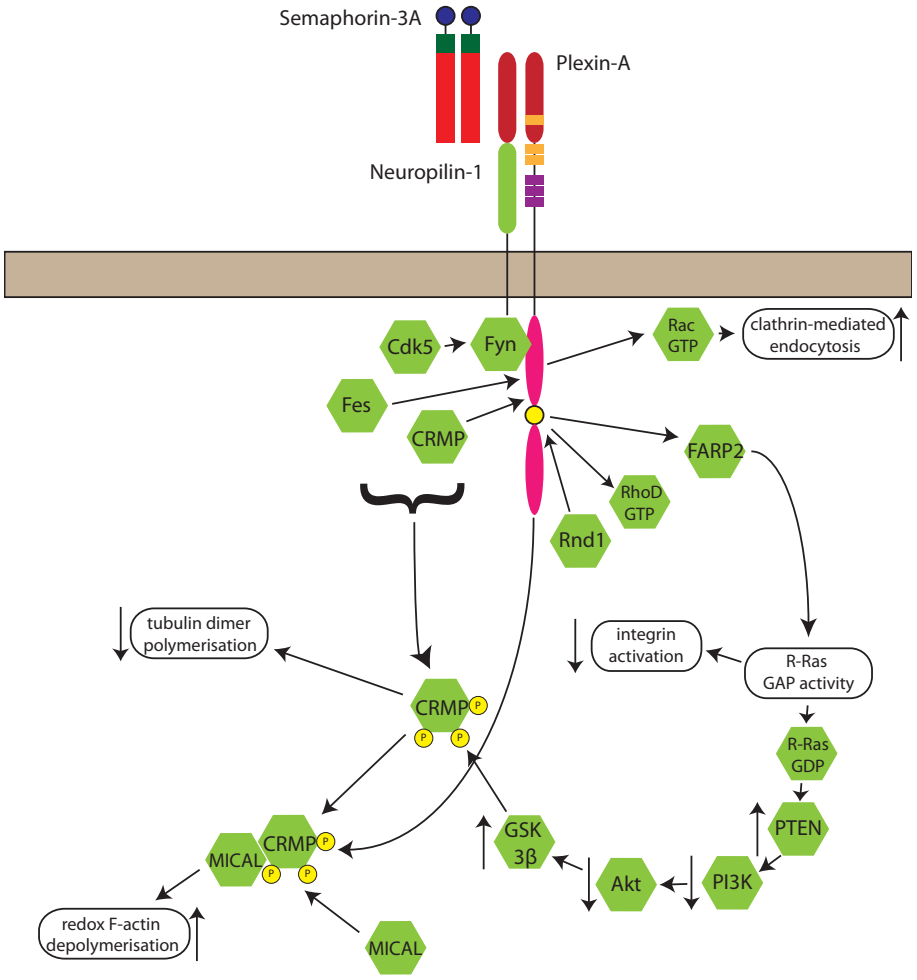

Figure 1.6: Downstream Effectors of the Semaphorin-3A/Neuropilin-1/Plexin-A Complex
Sema3A's binding to neuropilin-1 causes the binding of several proteins to the plexin intracellular domain: Fyn is activated and recruits and activates Cdk5, a serine/threonine kinase, to the complex (Sasaki et al., 2002). Cdk5 phosphorylates CRMPs 1, 2, 4 and 5. This 'priming' phosphorylation allows activated GSK-3β to phosphorylate several other sites on CRMPs 2 and 4 (Cole et al., 2004). Fes can phosphorylate all CRMPs as well as plexin A1; Sema3A enhances its activity and causes CRMPs to bind to plexins (Mitsui et al., 2002). RhoD and Rnd1 antagonise one another in plexin activation, Rnd1 activating plexin A1 (Zanata et al., 2002). In order to activate GSK-3β, plexin A1 releases FARP2 to activate its R-Ras GAP activity (Toyofuku et al., 2005). This can both inactivate integrins, leading to focal adhesion disassembly, and up-regulate PTEN activity, suppressing the PI3K/Akt pathway, leading to increased GSK-3β activity at the leading edge (Eickholt et al., 2002; Chadborn et al., 2006). Increased Rac1 activity also drives clathrin-mediated endocytosis in collapse (Fournier et al., 2000; Tojima et al., 2010). Phosphorylation of CRMPs allows the recruitment of MICALs for F-actin depolymerisation, and CRMP activity to modulate microtubules.

When Cos7 cells co-express neuropilin-1 and plexin A1, they contract in response to Sema3A (Takahashi et al., 1999), and the speed of contraction greatly increases with co-expression of CRMPs (Deo et al., 2004). With plexin A1 alone, the CRMPs form a stable (but inactive) complex, but the addition of neuropilin-1 blocks that binding; only when Sema3A is added, does the plexin/neuropilin/CRMP complex become active. The plexin/neuropilin complex recruits kinases such as Cdk5 *via* fyn activation, leading to phosphorylation of CRMP sites that are conserved between species (Minturn et al., 1995). Deo et al. (2004) discovered a constitutively active mutant of CRMP1, and one that requires only plexin binding, not neuropilin/Sema3A interactions. This suggests that conformational change, in concert with or driven by phosphorylation, controls CRMP2's activity.

1.5.6 'Molecule Associated with Cas Ligand' (MICAL) Proteins

Discovery of the MICAL family by Terman et al. (2002) provided a much-needed link between the semaphorin/plexin/CRMP receptor complex and the control of the cytoskeleton. MICALs consist of a redox domain, a calponin homology domain, a LIM domain, coiled-coil motifs and a proline-rich CasL-binding domain (Suzuki et al. (2002); Figure 1.7).

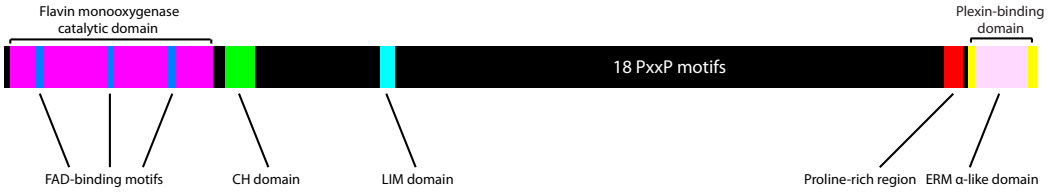

Figure 1.7: The Structure of MICAL
The N-terminus (left) bears the catalytic domain with motifs to bind flavin adenine dinucleotide (FAD), followed by the calponin homology (CH) domain for binding to actin. LIM domains are highly variable zinc-finger domains that bind to a variety of substrates in cytoskeletal organisation, also found in LIM-kinase, a downstream effector of growth cone collapse. The rest of the protein consists of variable regions with high levels of proline and the plexin-binding domain, which contains the ERM α-like motif, known for binding to surface adhesion molecules in the ERM proteins. Image adapted from Hung et al. (2010).

There are three vertebrate MICALs (MICAL-1, -2 and -3) as well as several MICAL-like proteins (e.g. MICAL-L) which lack a highly conserved domain. MICALs are expressed widely

in neurons and in oligodendrocytes, where activation seems to drive retraction of processes, analogous to growth cone collapse, as well as directing oligodendrocyte precursor cell (OPC) migration (Spassky et al., 2002; Cohen et al., 2003).

Once the CasL-binding domain associates with plexins, integrin-associated focal adhesions dissociate and cells retract (Barberis et al., 2004), giving a Rho-independent pathway for MICAL-mediated retraction, although this may be through sequestration of the CasL domains of integrins, or by decreasing the activity of kinases downstream of the integrins. FAK binds to integrin through the CasL ligand as well, so MICAL may block this, reducing phosphorylation of FAK and causing focal adhesions to dissociate. Furthermore, Sema3A binding causes release of the RacGEF FARP2 from plexin-A1, activating Rac, causing Rnd1 to bind to plexin-A1 and activate the plexin R-RasGAP domain, directly antagonising integrin's signalling through R-RasGEF activity (Oinuma et al., 2004; Negishi et al., 2005). Suzuki et al. (2002) also demonstrated that the *C*-terminus domains of MICALs bind to vimentin, although this has only been seen thus far in non-neuronal cells so its relevance is unclear.

The redox catalysis domain (Figure 1.7) is unusual in proteins that interact with the cytoskeleton (Suzuki et al., 2002; Nadella et al., 2005). Redox activity is necessary in *Drosophila* as Hung et al. (2010) demonstrated that MICAL$^{-/-}$ fruit-flies had deformed bristles, structures that rely upon the actin cytoskeleton for structure as the chitin forms, and also showed that the redox domain with the calponin homology domain alone were more active than the full protein, suggesting that the CasL-binding domain exerted control over activity. The redox domain is an active, conserved flavoprotein mono-oxygenase, one which inserts one atom of oxygen into its substrate using FAD^+/FADH (Nadella et al., 2005). Studies by Terman et al. (2002) and Pasterkamp et al. (2006) indicated that the domain is necessary for function *via* flavoprotein mono-oxygenase inhibitors, which abolished growth Sema3-mediated collapse *in vitro*. Mutation of residues in the catalytic site also attenuated responses to Sema1a *in vivo*. These suggest that redox reactions are specifically involved in semaphorin signalling. More generally, reduction of reactive oxygen species levels in axons seems to impede growth and, *in extremis*, leads to loss of the actin cytoskeleton (Munnamalai and Suter, 2009).

Structural studies of the domain suggest that MICALs switch conformation when FAD binds to the domain, but that unlike other mono-oxygenases which perform redox reactions upon small molecules (e.g. steroids and amino acids), MICAL's domain opens up to allow a protein-sized substrate into the catalytic area (Siebold et al., 2005). It is also possible that MICALs may generate reactive oxygen species (ROS) involved in signalling (Milzani et al., 1997) that may drive F-actin depolymerisation through Rac1 GTPase (Moldovan et al., 1999).

In summary, MICALs have been established as transducers of semaphorin-mediated signals in neuronal and non-neuronal cells, and this may occur through any (or all) of 3 ways:

- the FAD-binding domain may directly perform redox reactions upon downstream molecules or cytoskeletal components (e.g. actin) themselves,
- the proline-rich, LIM, calponin homology, ERM and variable domains may act as a protein scaffold to assemble signalling complexes of Rho GTPase modulators and their effectors or
- the FAD-binding domain may simply release ROS into the immediate milieu to modulate nearby proteins and proteins bound to other domains of the MICAL protein.

1.5.7 L1CAM and Semaphorin Signalling

Although Takahashi et al. (1999) demonstrated that a neuropilin and plexin were sufficient to impart Class 3 semaphorin sensitivity, Castellani et al. (2000) revealed a rôle for the transmembrane adhesion molecule, L1CAM, through guidance errors *in vivo* and loss of sensitivity to Sema3A *in vitro* of cortical neurons of L1-deficient mice. The importance of L1 was further emphasised by application of soluble L1, which converted responses to Sema3A from repulsive to attractive. Castellani et al. (2002) later demonstrated that the soluble L1 caused this reversal through binding to neuropilin-1 and NO/cGMP signalling, not homophilic binding.

L1/Sema3A-induced collapse involves clathrin-mediated endocytosis. L1 and neuropilin-1 are endocytosed together in response to Sema3A (Castellani et al., 2004) and further, Cos7

cells expressing L1 and neuropilin-1 endocytose and contract in response to Sema3A, as did the plexin/neuropilin-bearing cells of Takahashi et al. (1999). Tojima et al. (2010) later demonstrated that the clathrin-mediated endocytosis is Ca^{2+}-dependent, linking L1, and perhaps NO/cGMP downstream, to Ca^{2+}/clathrin-dependent endocytosis. Tojima et al. (2010) also demonstrated a direct rôle for clathrin in repulsion through the effects of inhibitors; Tojima et al. (2011) suspected a more general rôle for clathrin in growth cone repulsion.

Finally, (Bechara et al., 2008) have shown that the disassembly of focal adhesions downstream of L1/neuropilin-1, necessary for local retraction of the growth cone, involves FAK recruitment and that loss of either plexin-A or L1CAM reduces sensitivity to Sema3A in cortical neurons.

1.5.8 Protein Synthesis-Dependent Guidance

Sema3A-induced collapse involves protein synthesis (PS) (Campbell and Holt, 2001). Sema3A is not alone in this respect; other cues that induce PS in guidance responses include netrin-1 and brain-derived neurotrophic factor (BDNF) (Campbell and Holt, 2001), as well as Engrailed-2 (Brunet et al., 2005), Slit-2 (Piper et al., 2006) and PACAP (Guirland et al., 2003). On the other hand, chemorepulsion from lysophosphatidic acid (LPA) does not require PS, and indeed requires proteasomal degradation of proteins instead (Campbell and Holt, 2001). These mechanisms are not exclusive; netrin-1 and BDNF are blocked by both inhibitors of PS and degradation, and both attractive and repulsive cues can involve PS.

Use of the inhibitors rapamycin and wortmannin, respectively, upstream demonstrated that attractive netrin-1 and repulsive Sema3A share a dependence on mTOR signalling, but only netrin involves PI3K upstream of mTOR (Campbell and Holt, 2001). Downstream of mTOR, both netrin-1 and Sema3A cause the phosphorylation of eIF4E-BP1, causing the release of eIF4E, a rate-limiting transcription factor in cap-dependent eukaryotic translation. Leung et al. (2006) demonstrated that β-actin is the transcription target of attractive signalling from netrin-1. The *Xenopus* paralogue of zipcode-binding protein (ZBP), Vg1RBP, was shown to bind *Xenopus* β-actin mRNA and move within the growth cone towards attractive sources of netrin-1.

ZBP is known to bind to the 'zipcode' 3′ untranslated region (UTR) of β-actin mRNA and direct its localisation (Ross et al., 1997). Further, the 3′ UTR is sufficient to induce synthesis preferentially nearer to the netrin-1 source, and eIF4E-BP1 phosphorylation has a similar spatial bias. BDNF also drives β-actin synthesis (Yao et al., 2006). NGF, another attractive cue but not one which requires rapid PS for attraction, induces the synthesis of cAMP-responsive element-binding protein (CREB) (Cox et al., 2008) instead, which is retrogradely transported to the soma to modulate cell survival.

Wu et al. (2005) revealed a differing mechanism for Sema3A; in the rat, Sema3A induces synthesis of RhoA, and inhibition of this prevents collapse. siRNA against RhoA mRNA attenuates Sema3A-induced collapse too (Hengst et al., 2006). The collapse activity of Slit-2, however, requires synthesis of cofilin instead (Piper et al., 2006). Li et al. (2009) revealed that fragile X mental retardation protein (FMRP), an RNA-binding protein known for influencing dendrites in synaptic plasticity, was required for PS-dependent collapse due to Sema3A, which binds to a large class of mRNAs bearing U-rich sequences (Chen et al., 2003).

The links between known second messengers of netrin-1 and Sema3A and the mRNA-binding proteins ZBP and FMRP are still unclear. Sasaki et al. (2010) established a specific phosphorylation site on ZBP1 on a tyrosine required for mRNA binding. FMRP may instead require dephosphorylation to drive RhoA synthesis (Narayanan et al., 2007), but direct evidence in the axon is lacking. Curiously, protein phosphatase 2A (PP2A) seems to activate RhoA synthesis (Narayanan et al., 2007) while it inhibits BDNF-induced β-actin synthesis, perhaps implying cross-inhibition.

Sema3A's mechanism in activating mTOR is less clear; BDNF seems to act through a PI3K- and intracellular Ca^{2+}-dependent mechanism (Zhou et al., 2010), but Sema3A inhibits PI3K *via* PTEN (Chadborn et al., 2006). However, one possibility is mTOR activation *via* Erk (p42/p44 MAPK) (Winter et al., 2011); Erk activity is necessary for Sema3A-induced growth cone collapse (Campbell and Holt, 2003).

1.6 Nogo-A

1.6.1 Discovery, Role and the Reticulon Family

After the work of David and Aguayo (1981) demonstrated that failure of regeneration in adults was due to both axon-intrinsic changes, and cues from the CNS itself, CNS myelin was identified as a poor substrate for growth (Schwab and Caroni, 1988; Caroni and Schwab, 1988*b*). The development of antibodies against the non-permissive components of myelin, shown to be active against NI-35/NI-250/Nogo-A (Caroni and Schwab, 1988*a*), lead to the antibody being trialled as a therapeutic agent (Schnell and Schwab, 1990). Nogo-A was demonstrated to reside in oligodendrocytes, not Schwann cells (Caroni and Schwab, 1988*b*), suggesting a rôle in the CNS's failure to support regeneration as the PNS. The antibody's induction of collateral sprouting in uninjured tissue suggested a physiological rôle in controlling plasticity in the CNS (McGee et al., 2005) similar to the CSPGs (Pizzorusso et al., 2002), and Nogo-A remains a target for future therapy (Tsai et al., 2011).

The *Nogo* gene is part of the Reticulon family (Reticulon-4), so-called due to their localisation in the ER (van de Velde et al., 1994). There are 4 members in vertebrates, Reticulons-1 to -4 (Rtn1–4), which share the reticulon homology domain (RHD) in their *C*-terminus (Figure 1.8). The RHD is necessary and sufficient to localise the reticulons to the ER (Iwahashi et al., 2007) although a dilysine at the very *C*-terminus is needed to retain them there. The *N*-termini of the reticulons are unique and give them their cell-specific rôles, and although they number only 4, their various promoters and differential splicing give a large range of isoforms (Oertle et al., 2003*b*).

The *Rtn4/Nogo* gene gives rise to 3 main isoforms (A, B, C), of which Nogo-A is the largest. It is confined to the CNS, and found in neurons and oligodendrocytes (Liu et al., 2002*b*), where ~99% of it is localised to the ER (Oertle et al., 2003*a*). The rest is seen in the myelin of the oligodendrocytes, where it interferes with neural regeneration in the CNS (David and Aguayo, 1981). Nogo-A causes collapse of a wide variety of growth cones *in vitro* and some antibodies produced against it, e.g. IN-1, prevent this effect in *in vitro* models of SCI (Schnell and Schwab,

1990). They are presumed to sterically block Nogo-A's function and, in rats and primates, cause both enhanced regeneration beyond experimental glial scars and improvements in functional recovery (Schnell and Schwab, 1990; Freund et al., 2006).

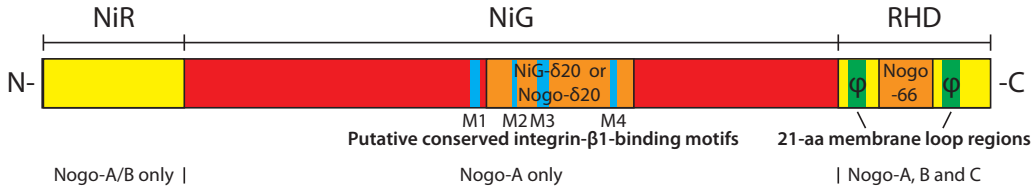

Figure 1.8: Schematic Structure of the Rtn4A/Nogo-A Protein
Nogo-A consists of 3 domains: NiR (yellow), which is present in Nogo-B as well, NiG (red), a Nogo-A-specific domain which contains the axon-repulsive Nogo-δ20 region (orange) and 4 putative integrin-binding motifs (cyan) next to or within it, and the reticulon homology domain (RHD) (yellow), shared with Nogo-A, B and C and homologous to the rest of the reticulon family (RTN1-3). The NiG domain may be distantly related to neurocan, an axon-repulsive CSPG, and is flanked by transposable elements (Shypitsyna et al., 2011). The RHD domain consists of the Nogo-66 repulsive sequence, flanked on either side by 21-residue hydrophobic regions (φ) thought to loop in and out of the membrane. Nogo-δ20 and Nogo-66 are each sufficient to cause collapse, but residues adjacent to Nogo-66 increase its bioactivity (Hu et al., 2005), and the presence of M1 outside the Nogo-δ20 region may imply the same for Nogo-δ20.

1.6.2 The Reticulon Homology Domain

The RHD consists of 2 hydrophobic (φ) regions and a linking stretch. Each of the φ regions is ~35 amino acid residues long, in contrast to the ~20 residue length needed for an α-helix to traverse the membrane, and this implies a more complex structure. Cysteine modification experiments by Voeltz et al. (2006) implied that instead of forming a transmembrane domain, the φ regions both form a hairpin structure, such that the *N*-terminus, *C*-terminus and the loop in the RHD are all on the cytoplasmic side of the membrane. Such a one-sided, wedge-like structure implies a structural rôle for these proteins in the ER, and indeed they only localise to highly-curved ER, such as tubular ER, and not to the sheet-like membrane structures of the ER that make up the nuclear membrane (Voeltz et al., 2006).

When Nogo-A is overexpressed, tubular structures replace the sheet-like structures of the ER and post-mitosis, the nuclear membrane either fails to reform or does so slowly (Anderson and Hetzer, 2008), whilst the tubular ER is stabilised even with the loss of microtubular support (Shibata et al., 2008). Application of anti-Nogo-A antibodies in an *in vitro* ER formation assay largely blocks the tubular ER from forming in favour of large vesicles (Voeltz et al., 2006) whilst in regions of high curvature in flattened ER, e.g. edges of sheets, Nogo-A is present (Kiseleva et al., 2007). In summary, Nogo-A appears to stabilise, favour and possibly induce tubular ER at the expense of sheets like the nuclear membrane, and stabilises high-curvature ER wherever it is found.

Nogo-66

Although the RHD seems to act through the overall structure of the protein, underpinned by the 2 wedge-like hairpins of the RHD φ regions, the 60–70 residue stretch between the hairpins has a different rôle. As a monomeric peptide, Nogo-66 binds the receptors NgR1 (Fournier et al., 2001) and PirB (Atwal et al., 2008) with a nanomolar EC_{50} both in binding receptors (Wang et al., 2002*b*) and causing growth cone collapse (Oertle et al., 2003*a*). Both of these receptors also bind to 3 other members of the myelin inhibitors of axonal regeneration (Atwal et al., 2008): myelin-associated glycoprotein (MAG), oligodendrocyte myelin glycoprotein (OMgp) and myelin *in vitro*, although new myelin inhibitors are being unearthed (Winzeler et al., 2011).

The Di-Lysine Retention Signal

Although all the Nogo isoforms share a dilysine ER retention signal at the very *C*-terminus, this does not automatically imply that Nogo on the cell surface is residual and physiologically non-functional; myelin proteins MAP and PMP-22 carry them, and work on potassium channels (Ma and Jan, 2002) suggests that the retention signal may be masked once complexes are formed, thus releasing only properly associated proteins from the ER. Such complexes may, in turn, be transient. Other cell surface proteins with retention signals include the AMPA receptor (Greger et al., 2002), the NMDA receptor (Xia et al., 2001) and $GABA_B$ receptors (Margeta-Mitrovic et al., 2000).

1.6.3 The Amino-Terminal Domain

NiGΔ20 (Nogo-δ20/amino-Nogo), an inhibitory region in the NiG domain stretching over amino-acid residues 544–725 (Oertle et al., 2003*a*) and present only in Nogo-A, binds not to the canonical myelin receptors like Nogo-66, but to integrins (Hu and Strittmatter, 2008) and as-yet-unidentified receptors. In general, integrin activation promotes neurite outgrowth (Andrews et al., 2009; Plantman et al., 2008; Gardiner et al., 2007), but the Nogo-δ20 region may bind the integrins (Shypitsyna et al., 2011) and block their signalling (Hu and Strittmatter, 2008); this evidence also suggests that the larger sequence surrounding Nogo-δ20 may potentiate Nogo-δ20's effects. Specifically, Nogo-δ20 inhibits signalling *via* the α4β1 and α5β1 integrins, as demonstrated *via* integrin-activating antibodies and the failure of Jurkat cells, reliant on α4β1 integrins to attach to fibronectin, to bind in the presence of Nogo-δ20 (Hu and Strittmatter, 2008). Integrins in general signal through FAK, a key protein in growth cone dynamics and pathfinding (Robles and Gomez, 2006), and mediate pro-growth responses to laminin and collagen.

Recently, *in silico* work by Shypitsyna et al. (2011) has suggested that the exons of the *Rtn4* gene unique to Nogo-A may derive from a neurocan-like sequence in the ancestor of bony fish.They identified 4 highly-conserved, putative integrin-β1-binding motifs, M1-4, three of which are within the NiG-Δ20, and one which is just outside, which may explain the improved binding of the extended Nogo-δ20 of Hu and Strittmatter (2008). Although overall sequence homology is poor (~30%), the similarity of exon structure supports the view that the amino-terminal domain is evolutionarily ancient, although whether the original influenced axon guidance is not clear. The amino-terminal domain also displays several highly similar regions to NCAM, and may share its structure of an Ig-like V-set domain and a mucin-like region, although the findings of Zander et al. (2007) suggest that, in solution, the domain does not oligomerise and has large, disordered regions.

1.6.4 NiR-Δ2

Work by Oertle et al. (2003*a*) also indicated a region a the very *N*-terminus (amino acid residues 1–172) which, much like Nogo-δ20, inhibits fibroblast cell spreading and neurite outgrowth independently of NgR but it has only marginal growth cone collapsing effects.

1.6.5 Nogo Isoforms

Nogo-A, -B and -C are all found on the cell surface (Dodd et al., 2005), all share the RHD domain and are localised to the ER together. Dodd et al. (2005) showed that Nogo-B and -C co-precipitated in immunoprecipitations of Nogo-A, perhaps physically associating *in vivo*, even across species boundaries. This implies conserved behaviour for the proteins. Rat Nogo-A did not, however, form complexes with itself. If this trimer has a rôle *in vivo*, what are the functions of the other Nogo isoforms?

Nogo-C

Nogo-C is the smallest of the 3 isoforms, at ~25kDa, and its function is not clear. It is expressed in the brain (Di Scala et al., 2005) along with another member of the reticulon family, RTN-3. It is expressed in oligodendrocytes along with Nogo-A post-injury (GrandPré et al., 2000) and, like Nogo-A, is not expressed by Schwann cells. Work by Kim et al. (2003) showed that Nogo-C overexpression in Schwann cells post-injury slows PNS regeneration and Nogo-A expression may do the same (Pot et al., 2002), implying that Nogo-C can inhibit regeneration in a similar manner.

1.6.6 Receptors and Effectors of Nogo-A Repulsion

NgR/Lingo-1/p75^{NTR}

NgR1 is a GPI-linked protein which associates with other, transmembrane proteins to signal to the neuron, whereas the downstream pathways of PirB are less firmly established (Figure 1.9). Both Nogo-66 and Nogo-δ20 ultimately activate the RhoA/ROCK pathway to modulate the cytoskeleton (Niederöst et al., 2002; Hu and Strittmatter, 2008; Laforest et al., 2005), although

Nogo-δ20's rôle may be more tenuous (Fournier et al., 2003). As NgR1 was discovered through its binding to the 66-amino-acid loop of Nogo-A (Nogo-66), the neurotrophin receptor $p75^{NTR}$ was found through immunoprecipitation experiments to bind to NgR1 (Wang et al., 2002*a*), and also LINGO-1 (Mi et al., 2004), a leucine-rich repeat (LRR) protein like NgR1. Further, Park et al. (2005) showed that a TNF family receptor, TROY, can substitute for $p75^{NTR}$ and inhibit axon growth and regeneration (Shao et al., 2005), illustrating how axons not expressing $p75^{NTR}$ may respond to myelin-derived inhibitors.

Although RhoA's association with Nogo-A is long-established (Kuhn et al., 1999), the connection between the NgR complex and RhoA is not clear. We know that $p75^{NTR}$ can displace RhoA from its Rho-GDI in a Nogo-A/MAG-dependent manner (Yamashita and Tohyama, 2003). Kalirin-9, a dual RhoGEF, competes with Rho-GDI for its $p75^{NTR}$ binding site and may activate RhoA (Harrington et al., 2008), although further data is lacking. Further, RhoA is again activated in complexes with TROY in place of $p75^{NTR}$, although it is not known how.

PirB/LILBR2

Spurred by results suggesting that NgR deletion was not sufficient to allow recovery (Zheng et al., 2005), Atwal et al. (2008) discovered a novel receptor for Nogo-A, OMgp and MAG independent of NgR by screening a library *via* expression cloning. The only candidates noted were NgR and human leukocyte immunoglobin-like receptor B2 (LILBR2), whose mouse homologue is 'paired immunoglobin-like receptor B' (PirB).

PirB has now been established as a second receptor for myelin inhibitors; it modulates ocular dominance plasticity in the visual cortex (Syken et al., 2006) much like other molecules in inhibitory pathways (Pizzorusso et al., 2002). Relatively little is known about the intracellular signalling pathway. In immune cells Pereira et al. (2004) showed that it antagonises integrins, and Syken et al. (2006) and Uehara et al. (2001) showed that PirB recruits SHP-1 and -2, both phosphatases known to modulate growth cone activity (Wright et al., 1997; Zhao and Lurie, 2004), possibly through modulation of TrkA–C, receptors for neurotrophins (Fujita et al., 2011).

'Plenty of SH3s' (POSH) is a multidomain scaffold known to bind to PirB, consisting of

- 4 'Src homology 3' (SH3) domains, to bind other proteins, found in Src kinases, Ras and other cytoskeletal proteins,
- a Rac GTPase-binding domain and
- an *N*-terminal RING ('really interesting new gene') domain, related to the RING ubiquitin ligase family.

Dickson et al. (2010) have shown that POSH acts downstream of Nogo-66/PirB, specifically through the kinase LZK/MAP3K13 and the protein Shroom3, known to recruit Rho kinases in other systems and induce cell constriction (Nishimura and Takeichi, 2008). RNA interference of POSH in mouse also increases axon outgrowth (Taylor et al., 2008), implying a generally negative effect on axon outgrowth, but the rôles of its other domains or any other interacting partners are unknown.

1.6.7 Exposure of Nogo to the Cell Surface

One of the more contentious issues around Nogo's rôle is that Voeltz et al. (2006) suggest a double-hairpin structure in the RHD. For the RHD to induce the curve, Nogo-66 and possibly the other domains would be left on the cytoplasmic side of the membrane, which conflicts with any signalling function at the cell surface, since such a molecule must display part of its structure on the extracellular/luminal side of the plasma membrane to directly affect its receptors. Domains of Nogo-A have been found on the surface of fibroblasts, DRG neurons and myoblasts *via* biotinylation (Dodd et al., 2005), indicating that Nogo-A must have some method of translocating through the membrane, and immunostaining with antibodies to several epitopes suggests several concurrent topographies in the plasma membrane (Oertle et al., 2003*a*; Yang and Strittmatter, 2007).

Nevertheless, when expressed in COS or CHO cells, Nogo-A is retained in the ER and Golgi (Oertle et al., 2003*a*), and this retention is also seen in immature oligodendrocytes (Caroni and Schwab, 1988*b*). This implies that Nogo-A's 'default' localisation is intracellular, as seen with

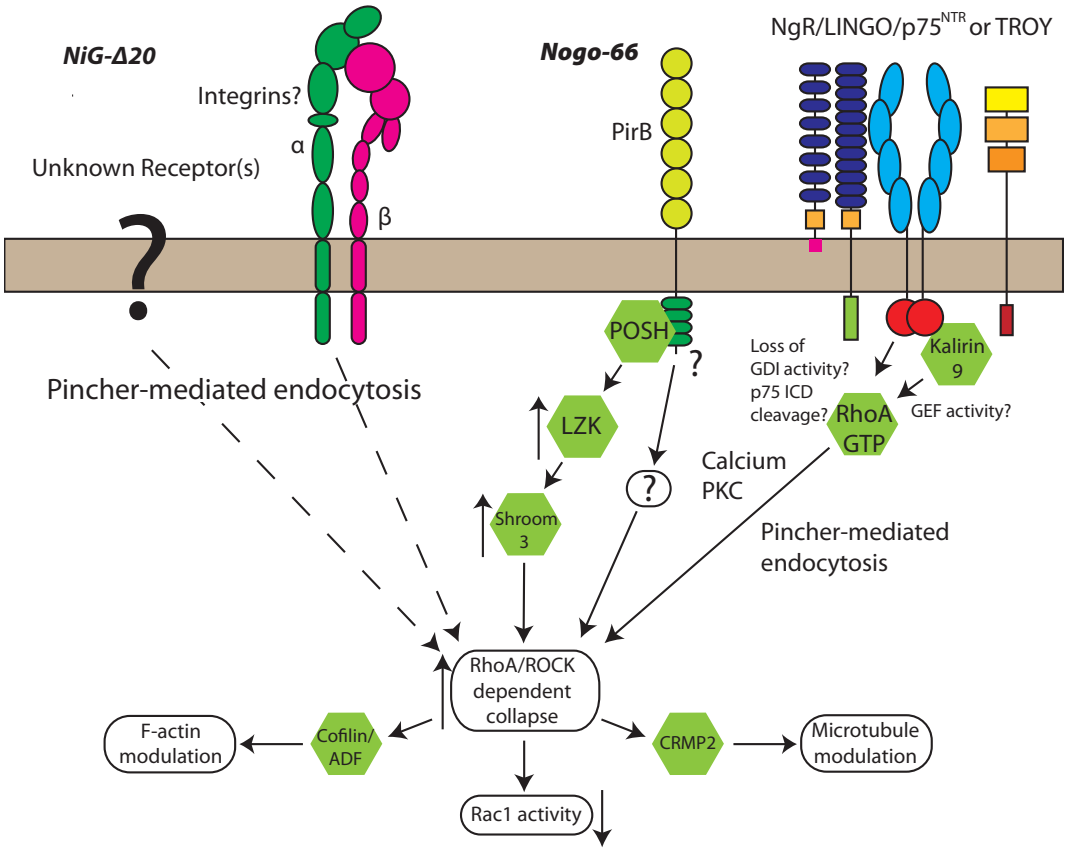

Figure 1.9: The downstream effectors of Nogo-A

NiG-Δ20 may have integrin binding sites (Oertle et al., 2003*a*; Shypitsyna et al., 2011) and is known to cause collapse integrin- and ROCK-dependently, but the mechanisms, whether integrin is a receptor or an effector and any other receptors have not been revealed. Nogo-66's downstream pathways are more clear, but although the complexes NgR, LINGO-1 and either $p75^{NTR}$ or TROY, and the PirB receptor are established, the method of RhoA activation is not proven, may occur through multiple routes and although Pincher-mediated endocytosis, Ca^{2+} and PKC are involved, how they are connected is not yet clear.

other reticulons (Oertle et al., 2003*b*), thus some mechanism presumably drives cell surface expression specifically in certain cell types.

1.7 Posterior Half-Somites and Contact Repulsion

Despite the long-established guidance families such as the semaphorins and morphogens, there remain some repulsive cues expressed in development which remain elusive, such as the surface cue repelling DRG axons from the posterior half-somites, so that they instead pass through the anterior. Somites form from the mesoderm either side of the neural tube, becoming epithelial spheres in pairs, one either side in a cranio-caudal direction driven by a *Notch/Wnt/Fgf* -based clock mechanism (Pourquié, 2004). Ventro-medial somite cells convert back to mesenchyme, forming the sclerotome, fated to create the vertebrae and ribs. The rest of the somite will form skeletal muscle and the axial dermis (dermomyotome) and the tendons (syndetome) (Keynes and Stern, 1988; Brent et al., 2003), whilst streams of neural crest cells migrate through to form the PNS and many other structures.

The appearance of the sclerotome coincides with the shift of crest cell migration to the anterior half-sclerotome of each somite alone, to form the DRGs and sympathetic ganglia (Bronner-Fraser, 1986). Motor axons, projecting shortly after, also exclusively pass through the anterior sclerotome and avoid the posterior halves (Keynes and Stern, 1984) and this occurs in all amniotes (Keynes and Stern, 1988).

We know that the effects are due to the somites, not the migrating cells or axons. Blocks of somites can be inverted, and the motor axons will still grow through the original 'anteriorised' halves. If several anterior halves are joined together, the axons no longer segment (Keynes and Stern, 1984). Similarly, the neural crest cells always migrate through the 'anteriorised' half, and lose their segmentation if 'posteriorised' halves are not present (Kalcheim and Teillet, 1989).

1.7.1 Unknown Signalling Molecules

The molecules preventing motor axons from passing through posterior somites are still not known (Bonanomi and Pfaff, 2010), and nor is the axon-repelling agent released by embryonic lens (Ohta et al., 1999).

The posterior somite repels axons by direct cell-cell contact, unlike the surround chemorepulsion of DRG axons by Sema3A (Keynes et al., 1997), and somite extracts cause motor and sensory axon growth cone collapse (Vermeren et al., 2000; Davies et al., 1990) *in vitro*. Early on, peanut agglutinin (PNA, a lectin which binds to unsialylated Galβ1-3GalNAc) was found to bind selectively to the posterior half (Stern et al., 1986). Davies et al. (1990) used immobilised PNA to identify 2 glycoproteins from the posterior half-somite of 48 and 55 kDa apparent molecular weight, and depleted collapse activity *in vitro* with PNA and antibodies developed against the proteins. Later, Krull et al. (1995) demonstrated this PNA effect in living tissue with migrating crest cells, but the identity of this crucial, evolutionarily ancient and conserved repellant remains unknown.

1.8 Summary

This project spans several aims, from identifying new axon growth inhibitors to elucidating the mechanisms of repulsion and the downstream mechanisms shared by them. This may identify new targets for therapy post-CNS injury, both in the regenerating axons themselves and in the growth-inhibitory milieu which can surround them.

Aim 1 To resolve the apparent conflict of results over whether local protein synthesis has a rôle in repulsive Sema3A guidance activity, following work by Roche et al. (2009) which reported no rôle for local protein synthesis in guidance with any of the guidance cues tested.

Aim 2 To elucidate the intracellular signalling downstream of the axon repulsive domains of Nogo-A, termed Nogo-66 and Nogo-δ20, specifically whether protein synthesis has a rôle, and whether the mechanisms are related beyond RhoA. Their co-operativity, or otherwise,

may suggest whether *in vivo* they share rôles in the CNS, or whether their distinct evolutionary origins have led to distinct developmental rôles.

Aim 3 To investigate candidate grey matter-derived, growth cone-repelling glycoproteins isolated by Keynes et al. (1991), Sandvig (1999) and Jackson (2008), which may play a rôle in controlling plasticity in health and reducing recovery in disease.

Chapter 2

Materials and Methods

2.1 Common Solutions

Phosphate-Buffered Saline	NaCl (137 mM), KCl (2.7 mM), $Na_2HPO_4 \bullet 2\,H_2O$ (10 mM) and KH_2PO_4 (2.0 mM) in 18MΩ water, pH 7.4.
CHAPS Dialysis Solution	*Per 1 l:* as per PBS with 10 g CHAPS, 10 ml 100 mM sodium orthovanadate, 10 ml 500 mM Na-EDTA pH 9.2, protease inhibitors (Roche, 4 693 132) added just prior to use.
4× Separating Gel Buffer	*Per 100 ml:* 75 ml 2 M Tris-HCl pH 8.8, 4 ml 10% SDS, 21 ml 18MΩ H_2O.
4× Stacking Gel Buffer	*Per 100 ml:* 50 ml 1 M Tris-HCl pH 6.8, 4 ml 10% SDS, 46 ml 18MΩ H_2O.
Electrophoresis Buffer	*Per 1 l:* 3 g Tris-base pH 8.3, 14.4 g glycine, 1 g SDS in 18MΩ H_2O.
5× Sample Buffer	*Per 10 ml:* 600 µl 1 M Tris-HCl pH 6.8, 5 ml 50% glycerol, 2 ml 10% SDS, 500 µl β-mercaptoethanol, 1 ml 1% bromophenol blue, 900 µl 18MΩ H_2O.

2.2 Preparation of Protein Samples from CRL-1718 Astrocytoma Cell Line

2.2.1 Medium and Culture Conditions

All CRL-1718 cell cultures were expanded in

- 89% v/v OPTI-MEM + GlutaMAX-1 (Gibco, 51985),

- 10% v/v Fetal Bovine Serum (Invitrogen, 10106169) and
- 1% v/v 100× Penicillin/Streptomycin (Invitrogen, 15140122).

The cells were grown at 37 °C in 5% CO_2, sub-cultured 1:4 at ~95% confluence. To subculture, the cells were washed with 0.5 mM EDTA/PBS pH 7.4, then 0.05% Trypsin-EDTA solution (Invitrogen, 25300054) to free the monolayer of cells from the flask. After re-suspending the cells in new medium, they were spun down at 180×g at 5 °C for 5 min and re-aliquoted into new flasks with fresh medium.

2.2.2 Cell Harvesting, Homogenisation and Ultra-Centrifugation

Cells were harvested by washing the adherent layer in PBS, then scraping the cells into 0.5 mM EDTA/PBS pH 7.4 (Thermo-Scientific, 179693). The cells were spun down as previously, the supernatant was centrifuged once more to collect any remaining cells, and each cell pellet re-suspended into 400µl of Lysis Buffer from the 2-D Fractionation Kit (Amersham, 80-6501-04), containing 1 mM sodium orthovanadate, 5 mM Na-EDTA and 3% v/v protease inhibitor cocktail (Thermo-Scientific, 1860932).

2.2.3 Fractionation of Soluble Protein Component of Astrocytes

The cell suspension was sheared through 0.9×25 mm, then 0.45×12 mm needles and homogenised using the Sample Grinding Kit (Amersham, 80-6483-37) and an electrically-driven pestle. Homogenised material was ultra-centrifuged for 1 h at 100 000×g at 4 °C; supernatant fluid was harvested by aspiration and the microsomal pellet discarded.

Each 500 µl of soluble protein fraction was either used immediately for SDS-PAGE gel electrophoresis, or subjected to ammonium sulphate fractionation on ice as follows:

Fraction I 100 µl of 42% w/w ammonium sulphate pH 5.4 were added drop-wise to 500 µl of the soluble protein fraction; the tube was inverted a few times, allowed to stand on ice for 5 min and centrifuged at 15 000×g at 4 °C for 10 min to pellet the precipitated proteins ('Fraction I'). The supernatant was transferred to a new tube and the pellet was centrifuged once more to remove any residual supernatant, which was added to the new tube.

Fraction II A further 100 µl of ammonium sulphate solution were added drop-wise to the protein/ammonium sulphate solution; the tube was inverted a few times, incubated on ice for 5 min and centrifuged at 15 000×g at 4 °C for 10 min to pellet the newly precipitated proteins ('Fraction II'). The supernatant was transferred to a new tube and the pellet was centrifuged once more to extract residual supernatant.

Fraction III The precipitation was repeated as for Fraction II, but with a further 100 µl added.

Fraction IV As Fraction II precipitation, but with 200 µl.

Fraction V As Fraction II precipitation, but with 300 µl.

Fraction V As Fraction II precipitation, but with 800 µl.

Fraction VI The remaining proteins were precipitated by addition of 6 ml 60% w/v trichloroacetic acid (GE Healthcare, 80-6501-04), inversion and incubation on ice for 10 min, followed by 3 ml cold acetone, vortexing and centrifugation at 8 000×g at 4 °C for 10 min. The supernatant was discarded, a further 200 µl cold acetone added on top of the protein pellet and the sample was centrifuged at 8 000×g at 4 °C for 10 min. I added 100 µl 18 MΩH_2O and vortexed the pellet for 30 s to break it up. The suspension was centrifuged once more at 8 000×g at 4 °C for 10 min, before the supernatant was discarded and the tube inverted on clean paper to air-dry.

The pellets of Fraction VI were air-dried for 1 h and all pellets were stored at -20 °C.

2.2.4 Dialysis

Fractionated pellets were dissolved into 100 µl Solubilisation Buffer (Amersham, 80-6501-04) and transferred to Mini Dialysis Kit tubes (Amersham, 80-6484-13). The 100 µl samples were dialysed twice with stirring at 5 °C for 12 h against 250 ml of solution (2% CHAPS/PBS, 1 mM sodium orthovanadate, 5 mM Na-EDTA and 1 tablet of Complete EDTA-free Protease Inhibitor Cocktail Tablets (Roche, 1 836 170) per 100 ml).

2.3 Experiments Performed with Astrocyte Protein Fractions

2.3.1 Immunoprecipitation

Binding Control To test the ability of a primary antibody (Santa Cruz, SC-18701) against major vault protein (MVP) to bind to recombinant human MVP (Abnova, H00009961-P01), MVP was dot-blotted onto Hybond-C Extra nitrocellulose membrane and air-dried, before being detected by dot blotting, using 1:500 SC-18701 as the primary antibody, and 5% w/v bovine serum albumin (Sigma-Aldrich, B8655) with 1:2000 of bovine anti-goat IgG-HRP (Santa Cruz, SC-2378) as the secondary.

All samples were prepared on wet ice throughout. Fractionated pellets were dissolved into 100 µl freshly-made Solubilisation Buffer consisting of 1 g urea/thiourea per 1.1 ml Diluent (Amersham, 80-6501-04) and dialysed against 2% CHAPS/PBS as described above or against RIPA buffer (0.1% w/v SDS, 1% Nonidet P-40, 0.5% sodium deoxycholate, 0.2 mM EDTA, 1 mM sodium orthovanadate with 1 tablet of Complete Mini EDTA-free Protease Inhibitor Cocktail (Roche, 1 836 170) per 50 ml) and diluted to 200 µl. 40 µl of dialysed fraction were frozen as a control, and 80 µl of dialysed fraction subjected to immunoprecipitation.

MVP Controls 13.3 µl of recombinant MVP (0.12 mg/ml, total protein 1600 ng) were mixed with 10 µl of goat anti-MVP antibody and the total volume brought to 200 µl by the addition of RIPA buffer, and mixed end-over-end for 12 h at 5 °C. I added 100µl Protein A/G Agarose beads (Santa Cruz, SC-2003) which had been washed and spun down 3 times in 1 ml RIPA buffer for 1 min, 1000×g and mixed for 12 h at 5 °C. 6.7 µl recombinant MVP (approx. 800 ng) were used without modification as a control.

The supernatant fluids were aspirated from the immunoprecipitation mixtures after spinning down the agarose beads at 5 °C at 1000×g for 5 min, and stored at -20 °C. The beads were then washed in 1ml RIPA buffer ×3, then in 1 ml PBS. Finally, the beads were re-suspended in 50 µl Laemmli buffer and heated to 100 °C for 5 min. The beads were spun down, and the supernatant was aspirated and stored at -20 °C.

Concentration and Gels The supernatants were concentrated five-fold (Microcon® Concentrator YM-30, Millipore, 42410) and mixed with 20% v/v 5× Sample Buffer. Gel electrophoresis was performed as described below. The blots were detected with 1:4 000 3004.2KLH or SC-18701, as described above in the Binding Control.

2.3.2 Purification with Lectins

Dialysed fractionated protein solution (50 µl) containing the target protein was added to 500 µl of Binding Buffer OG (Qiagen) with 5 µl of 100× Protease Inhibitor (PI) (Qiagen). The jacalin-coated beads were removed from their cartridge into a spin-cup (Thermo Scientific, PN69702) and spun down at 5 000×g for 60 sec at 5 °C to remove the preservative solution. Binding Buffer OG (500 µl) and PI (5 µl) were added to the spin-cup and turned end-over-end for 30 min at 5 °C to equilibrate, the beads were spun down as before, and the flow-through discarded. The sample-bearing Binding Buffer OG was added to the spin-cup in its collection tube, the beads suspended by brief vortexing and the whole mixed end-over-end over-night at 5 °C to allow the glycoproteins to bind to the beads.

The sample-bearing Binding Buffer was spun through the column at 5 °C at 5 000×g for 60 sec, with the flow-through, bearing the non-jacalin-binding proteins, being stored at -20 °C. Binding Buffer (500 µl) with PI (5 µl) was added to the column, spun through and discarded ×2.

The spin-cup was transferred to a new centrifuge tube and Elution Buffer OB (100 µl) was added with PI (1 µl) to the jacalin beads and mixed end-over-end after at 5 °C for a duration varying from 30 min to 48 h. The eluate was spun down for 60 sec at 5 °C at 7 000 rpm ×2; the eluates pooled and stored at -20 °C. The following elution buffers were also used:

Melibiose 0.5 M melibiose (Sigma, M5500) in 0.5% CHAPS/PBS with 1% PI (Qiagen),

Lactose 0.5 M lactose (Sigma, L3450) in 0.5% CHAPS/PBS with 1% PI (Qiagen) and

α-D-GP 0.5 M methyl-α-D-galactopyranoside (Carbosynth, MM05301) in 0.5% CHAPS/PBS with 1% PI (Qiagen).

Later, the following set of elution buffers were also used:

Elu #1 2 M urea, 0.5 M thiourea, 0.5 M methyl-α-D-galactopyranoside in PBS pH 7.4 with proteinase inhibitors,

Elu #2 4 M urea, 1 M thiourea, 0.5 M methyl-α-D-galactopyranoside in PBS pH 7.4 with proteinase inhibitors and

Elu #3 8 M urea, 2 M thiourea, 0.5 M methyl-α-D-galactopyranoside in PBS pH 7.4 with proteinase inhibitors.

To elute any remaining proteins, 200 µl of 5× Sample Buffer (containing 2-mercaptoethanol) was added to the beads, and the slurry was heated to 90 °C for 5 min, before being spun down as before. The protein-bearing supernatant fluid was aspirated and separated directly *via* SDS-PAGE electrophoresis.

2.3.3 Non-Enzymatic Deglycosylation

Proteins were initially deglycosylated *via* β-elimination (Figure 2.1) as per GlycoProfile™ β-Elimination Kit (Sigma-Aldrich, PP0540) protocol; dialysed protein samples were mixed with 20% v/v of β-Elimination Reagent:5 M NaOH (47:3, v/v) for 16 h at 5 °C and neutralised with 1M HCl. Later experiments involved a modified protocol to reduce the length of the reaction to 90 min and neutralisation with 1 M Tris pH 7.0, to minimise protein degradation during pH alteration. Glycans were separated from intact proteins by using 10-kDa concentrators (Sigma-Aldrich, PP0540), spun at 14 000×g for 15 min at 5 °C. The glycan-bearing filtrate was stored at -20 °C, and the protein-bearing solution was recovered from the filter by inversion into another micro-centrifuge tube and centrifuging at 1000×g for 3 min at 5 °C. Recovered proteins were separated by gel electrophoresis as described below.

2.3.4 Enzymatic Deglycosylation

Unfractionated soluble protein fraction was concentrated using Microcon® 30 kDa Concentrators (Millipore, 42410) to less than 700 µl. This was heated to 70 °C for 5 min with 5× Sample

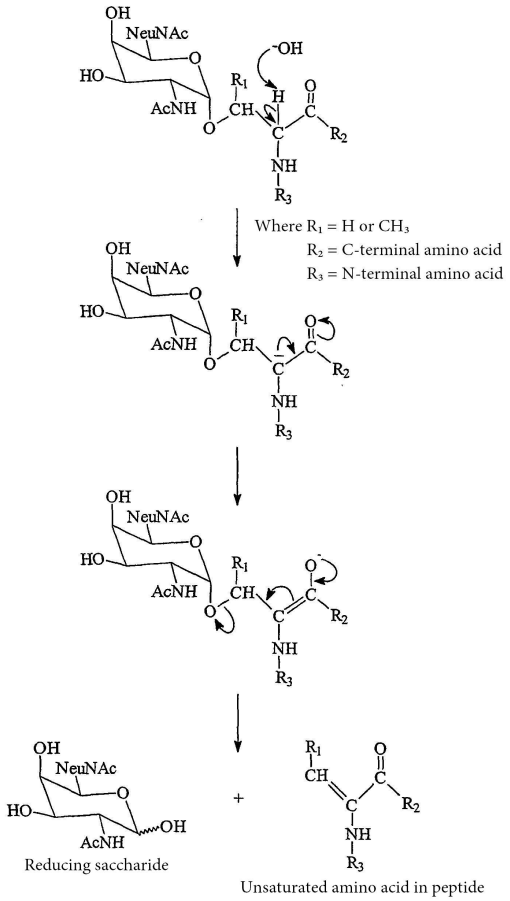

Figure 2.1: Diagram of the Nucleophilic Attack Mechanism of β-Elimination of *O*-Glycans

Buffer to denature, and run on an SDS-PAGE gel with protein ladders (Santa Cruz, SC-2035) and 10 µl of the sample run on either side of the main band, to allow localisation of the main central band of ARP without direct detection. At the end of the separation, the separated proteins were transferred to Hybond-C membrane (see *Western Blot* below); the central section corresponding to the main sample-bearing lane was cut from the membrane and stored at 5 °C, and the sections either side of it, containing the protein ladders and 10 µl lanes of protein concentrate, were enhanced and blocked over-night in 50 ml ChemiBLOCK (Chemicon, 2170) and 50 ml TBS (0.15 M NaCl, 50 mM Tris pH 7.5, 0.5% Tween-20).

The side strips were exposed to 1:4 000 3004.2KLH as primary antibody and 1:7 500 HRP-labelled anti-rabbit antibodies (Santa Cruz, SC-2030) (see *Western Blot* below). The location of the ~115-kDa band was used to guide the excision of a strip of the central section, to select proteins for deglycosylation by apparent molecular weight. The pieces of ARP-bearing nitrocellulose were incubated in the following for 3 h at 37 °C: 200 µl *N*-deglycosylation buffer (Roche, 1 836 552), 40 µl 10% BSA, 5 µl *O*-glycosidase (Roche, 1 347 101), 5 µl neuraminidase (Roche, 1 585 886), 20 µl 20× Complete EDTA-free protease inhibitors (Roche, 4 693 132) and 2 µl 500 mM Na-EDTA pH 7.5.

The pieces of membrane were spun down and the supernatant discarded. The pieces were washed ×7 with 200 µl PBS pH 7.4 with 1× protease inhibitors and 5 mM EDTA, then heated to 90 °C for 5 min in 200 µl PBS containing 1× Sample Buffer and 8 M urea to extract the proteins from the membrane. The protein-bearing sample was then run on a second SDS-PAGE gel, which was either subjected to Western blotting to demonstrate the shift in apparent molecular weight and precise location of the band, or the gel stained directly with silver reagent (see *Silver Stain* below) to determine the location of protein bands for sequencing by mass spectrometry.

2.3.5 Incorporation into Liposomes for Use with DRG Cultures

Phosphatidyl choline in chloroform (20 µl of 100 µg/ml; Sigma, P2772) was mixed with phosphatidyl serine in 1:1 chloroform/methanol (20 µl of 10 mg/ml; Sigma, P5660) and air-dried overnight. The phospholipid residue was then dissolved in 200 µl of 4% w/v CHAPS/PBS pH

7.4. Samples were dialysed against CHAPS/PBS with inhibitors, as described above. 10 µl of the phospholipid solution were added to each sample containing 100 µg of total protein. Controls were prepared with 100 µg BSA in 4% CHAPS/PBS pH 7.4. From each sample, a similar amount was run on an SDS/PAGE gel and Western blotted to detect the presence of the 3004.2KLH antibody-binding band (see below).

Each sample was placed in a dialysis container constructed from the lid of a 1.5 ml microcentrifuge tube, with dialysis membrane held in place by a ring from the top of the same microcentrifuge tube. The dialysis membrane was prepared from 12–14 kDa dialysis tubing by boiling in 18MΩ H_2O for several minutes ×3 to remove plasticising agents, and washed through with cold 18MΩ H_2O ×5 before being cut open and cut into ~15 mm squares. The chambers were loaded with sample, the squares used to seal them, and the samples were dialysed against 1 l PBS pH 7.4 for 12 h ×2. This removes the CHAPS detergent, which would otherwise damage axons, and encourages membrane proteins to incorporate with the phospholipids as they came out of solution to form membrane protein-bearing liposomes.

Cultures of DRGs were prepared as described below, and the liposome-bearing samples were gradually applied directly over the DRGs, slowly, to maximise interactions between the liposomes and the axons. The cultures were incubated for a further 1 h before being fixed and assessed as per the collapse assays (see below).

2.4 Purification of 3004.2KLH Primary Antibody

2.4.1 Purification of Antibodies from Rabbit Serum

Polyclonal antibodies against the astrocyte repulsive protein (ARP) were purified from serum from rabbits exposed to the peptide (YYDEETVAEWTVR) bound to keyhole limpet hæmocyanin (peptide synthesis and rabbit exposure performed by Sigma-Genosys, code 3004). The sequence was determined from rat and chicken grey matter (Sandvig, 1999). 81-kDa cellulose tubing was prepared for dialysis by heating in 18MΩ H_2O at 70 °C for 10min, and the lumina were washed out with same three times. 5 ml of serum were dialysed in treated dialysis tubing

(see *Incorporation into Liposomes* above) against 1000 ml Antibody Dialysis Solution (25 mM Na-CH_3COO, 10 mM NaCl pH 5.4) for 12 h ×2. The Protein A-agarose purification column was washed by passing the following through by gravity in series:

- 2 M urea (10 ml),
- 1 M lithium chloride (10 ml),
- 0.1 M glycine pH 2.5 (10 ml) and
- PBS pH 8.0 until absorbance of eluate at 280 nm was found to be below 0.01.

Dialysed serum was centrifuged at 16 000×g for 10min at 5 °C; the supernatant fluid was aspirated and applied to the Protein A-agarose column. Any pelleted material was discarded. After the dialysed serum had passed through the column, the column was washed with PBS pH 8.0 (15 ml). Absorbance of the eluate was monitored at 280 nm, reading <0.01 at the end of the wash.

Antibodies bound to the column were eluted with 0.1 M glycine pH 3.0, collecting fractions (900 µl), which were immediatedly neutralised with 1 M Tris-HCl pH 8.0 (100 µl).The two fractions (2 ml) with the highest protein levels as assessed at 280 nm were combined and dialysed in treated 81 kDa cellulose tubing against 1000 ml PBS pH 7.4 for 12 h ×2. The column was washed through with 2 M urea, 1 M LiCl and 0.1 M glycine as described above, then preserved in 10 ml PBS pH 7.4 with sodium azide at 5 °C.

2.4.2 Removal of anti-Hæmocyanin Cross-Reacting Antibodies from Anti-Peptide Polyclonal Antibodies

As rabbits were innoculated against the target peptide bound to keyhole limpet hæmocyanin (KLH), as an immunological adjuvant, much of the polyclonal antibodies generated would be directed against hæmocyanin. The antibodies with specificity to hæmocyanin were removed by absorption with suspended agarose/KLH beads (1 ml; Sigma-Aldrich, H5779). These beads were centrifuged at 5 000×g for 30 s at 5 °C and then subjected to six washes in PBS pH 8.0 (1

ml) to remove remaining traces of azide. Dialysed polyclonal antibodies (1 ml) were added to the beads in a 1.5 ml mini-centrifuge tube, and rotated end-over-end for 1 h at 5 °C. The beads were centrifuged at 5 000×g for 30 s at 5 °C and the supernatant fluid carefully aspirated and stored at 5 °C.

The Protein A beads were washed ×3 in PBS pH 8.0 (1 ml) and the adherent, anti-KLH antibodies removed by washing with 0.1 M glycine pH 2.5 (1 ml). The beads were washed again in PBS pH 8.0 (1 ml) until the supernatant from the washes reached pH 8.0, indicating that the glycine had been removed. The rabbit anti-peptide antibody-containing serum was added to the regenerated beads and mixed end-over-end for 1 h at 5 °C to bind any remaining anti-hæmocyanin antibody, before the beads were retrieved by centrifugation (5 000×g for 30 s at 5 °C) and the supernatant fluid removed, aliquoted into 100 µl tubes and stored at -20 °C labelled as '3004.2KLH'. The beads were washed as detailed previously in PBS pH 8.0, 0.1 M glycine pH 2.5 and finally PBS pH 8.0 until the pH stabilised, whereupon 1 mg sodium azide was added to PBS pH 8.0 (10 ml) within the column and the beads were returned to storage.

2.5 SDS-PAGE 1D Gel and Western Blot

2.5.1 Preparation of Gel and Protein Samples and Gel Electrophoresis

Protein samples were combined with 5× Sample Buffer if not already (see *Purification with Lectins*). Aliquots of molecular weight markers ready for electrophoresis consisted of 1 µl Santa Cruz MWt Standards (Santa Cruz, SC-2035), 18MΩ H_2O (2 µl), Lane Marker (1 µl; Pierce, EL67391), and 5× Sample Buffer (1 µl) each.

Gel electrophoresis was performed with a 7.5% w/v separating gel (100×100×1 mm) with 125 mM Tris pH 8.8, 1% w/v SDS and a 5% w/v stacking gel (100×40×1 mm) with 1% w/v SDS, 375 mM Tris pH 6.8 prepared using suitable dilutions of a stock solution of 37.5% w/v acrylamide 0.8% w/v bis-acrylamide (National Diagnostics, EC-890). All solutions were prepared with gentle mixing. Polymerisation of separating gel (10 ml) was triggered with 10% w/v ammonium persulphate (APS) (50 µl) and TEMED (5 µl). The stacking gel (4 ml) was mixed with

APS (50 µl) and TEMED (5 µl) before pouring, and a comb was used to form wells in the gel. The electrophoresis buffer consisted of 0.1% w/v SDS, 192 mM glycine, 25 mM Tris pH 8.3. Gels were run at constant voltage until the bromophenol blue tracking dye reached the end of the gel.

2.5.2 Silver Stain

Gels that were silver-stained for the detection of proteins were treated as follows:

1. Fixation: The gel was trimmed to remove unused columns and fixed in 40% v/v ethanol, 10% v/v glacial acetic acid, 50% v/v 18MΩ H_2O for 60min and washed several times in water overnight.

2. Sensitisation: 0.02% w/v sodium thiosulphate for 1 min and then washed in 18MΩ H_2O for 20 s ×3.

3. Silver Nitrate: 0.1% w/v $AgNO_3$ containing 0.02% v/v freshly-added formaldehyde for 20 min at 4 °C, washed in 18MΩ H_2O for 20 s ×3, transferred to a new tray and washed in 18MΩ H_2O.

4. Developing: 3% w/v Na_2CO_3, 0.05% v/v formaldehyde, until the staining of the bands was sufficient, then washed in 18MΩ H_2O for 20 s.

5. Termination: 5% v/v glacial acetic acid for 5 min.

6. Storage: 1% v/v glacial acetic acid.

2.5.3 Western Blot

Before transfer, the gel was equilibrated in 12.5 mM Tris pH 8.3, 96 mM glycine, 10% v/v methanol for 10 min. The semi-dry electrotransfer was conducted using the following anode-to-cathode configuration: 2× blotting sheets (Sigma, P7921-100EA) soaked in 'Anode I' solution (0.3 M Tris pH 10.4, 20% v/v methanol) and 1 sheet soaked in 'Anode II' solution (0.025 M Tris pH 10.4, 20% v/v methanol), followed by nitrocellulose membrane (Amersham, 'Hybond-C Extra', RPN203E) to which the proteins are transferred, the equilibrated gel and 2× blotting sheets soaked in 'Cathode' solution (25 mM Tris pH 9.4, 40 mM ε-amino-*N*-caproic acid, 20% v/v

methanol). ~100 ml of each solution were used to soak each sheet. Transfer was accomplished at 80 mA constant current for 3 h.

After electrotransfer, the membrane was washed briefly in 18MΩ H_2O, immersed in Enhancer Reagent 1 (Thermo-Scientific, 1859020) for 2 min, washed 5 times in 18MΩ H_2O, followed by Enhancer Reagent 2 for 10 min, then washed 5 times in 18MΩ H_2O and the membrane immersed overnight at 5 °C in ChemiBLOCK (50 ml; Chemicon, 2170) mixed with TBS (50 ml; 0.15 M NaCl, 50 mM Tris pH 7.5, 0.5% Tween-20).

The membrane was exposed to Blotto A (1 g milk protein (Bio-Rad, 170-6404) in 20ml TBS-T (150 mM NaCl, 10 mM Tris pH 8.0, 0.5% Tween-20)) with 5 µl 3004.2KLH primary antibody for 1 h, washed 3 times for 5 min in 150 ml TBS-T pH 8.0 followed by exposure to Blotto A mixed with 5% goat serum (Sigma-Aldrich, G9023-10ML) and 3 µl of HRP-labelled goat anti-rabbit antibody (Santa Cruz, SC2030) for 45 min, followed by three washes for 5 min in TBS-T pH 8.0 (150 ml) followed by one wash for 5 min in TBS (150 ml; 150 mM NaCl, 10 mM Tris pH 8.0). This was followed by exposure to HRP Substrate (20 ml; Millipore, WBKLS0500) for 5 min. The membrane was exposed to CL-XPosure™ Film (Thermo-Scientific, 34091) in the dark room for between 1 and 180 sec before being developed.

2.6 Carbohydrate 1D Gel for Glycan Analysis

Starch-Derived Molecular Weight Markers Molecular weight markers were prepared with wheat starch (Sigma-Aldrich, S5127); the starch was suspended in 0.1 M ammonium acetate buffer pH 5.5 to a concentration of 10 mg/ml and α-amylase (Sigma-Aldrich, A7595) dissolved in 0.1 M ammonium acetate buffer pH 5.5 to a concentration of 0.75 µg/ml. 5.0 µl of amylase solution was added to 50 µl of starch suspension and incubated at 37 °C for 30 min. The reaction was stopped by the addition of cold ethanol (1 ml).

Derivitisation Samples, including the molecular weight markers, were lyophilised in a centrifugal vacuum evaporator (EZ-2, Genevac) below 45 °C, mixed with 0.1 M 2-aminoacridone

(Sigma-Aldrich, 06627) in acetic acid:DMSO (3:17, v/v; 5 µl) and 5 µl 1 M sodium cyanoborohydride (Sigma-Aldrich, 156159). To remove the solvents, the mixture was initially incubated at 37 °C for 16 h and lyophilised in a CVE for 1 h below 45 °C, later at 4 °C, neutralised with 1 M Tris-HCl pH 8.0. The samples were dissolved in DMSO-glycerol-water (2:1:7, v/v) as electrophoresis sample buffer.

Tris–Borate Gel The separating and stacking gels were made with acrylamide concentrations of 20% v/v and 4% v/v, respectively, of dimensions 160×120×1 mm, using 37.5% w/v acrylamide 0.8% w/v bis-acrylamide (National Diagnostics, EC-890) stock solution. The final buffer concentration of the electrophoresis buffer as well as the stacking and separating gels was 0.1 M Tris-borate/boric acid pH 8.3. The gel was run at 250 V for 30 min, and 400 V for 150 min, cooled to 8 °C as per Abelson et al. (1994). The gels were exposed to 365 nm UV light in a transilluminator and photographed using a charge-coupled device (CCD).

2.7 Culture of *Gallus gallus* Dorsal Root Ganglion Axons *in vitro*

2.7.1 Medium for Dorsal Root Ganglia

All dorsal root ganglion (DRG) explants were grown in Ham's F-12 medium (1 ml; PAA, E15-817) supplemented with 2% v/v 50× B-27 additives (Invitrogen, 17504), 80 ng/ml murine NGF-7S (Sigma, N0153) and 100× v/v penicillin-streptomycin (Invitrogen, 15070-063), or DMEM (1 ml; Sigma, D4629) supplemented with 1% 100× v/v insulin/transferrin (Sigma, I2771), 80 ng/ml murine NGF-7S (Sigma, N0153) and 1% v/v 100× penicillin-streptomycin (Invitrogen, 15070-063). Alterations to NGF concentration are indicated in the results.

2.7.2 Preparation of Cover-Slips for DRGs

13 mm-diameter boro-silicate cover-slips (VWR, 631-0149) were cleaned in boiling concentrated nitric acid for 30 min, followed by washing in 18MΩ H_2O and ethanol, stored at room temperature in ethanol until use. Ethanol was removed from individual cover-slips by passing over a lighted spirit burner; the cover-slips were then coated in poly-*L*-lysine (Sigma, P4707) by

'sandwiching' a layer of 30 µl 0.01% poly-*L*-lysine between pairs of cover-slips and incubating them at 37 °C for 60 min. The cover-slips were separated and washed briefly in 18MΩ H_2O to remove excess poly-*L*-lysine and left to dry for 60 min at room temperature. The cover-slips were then coated with laminin by sandwiching the cover-slips with laminin in PBS pH 7.4 (40 µl of 20 µg/ml; Sigma, L2020), and incubated for a further 60 min before washing in 18MΩ H_2O and air-drying at room temperature.

2.7.3 Incubation and Dissection of *Gallus gallus* Embryos

Wild-type fertilised *Gallus gallus* (domestic chicken) eggs were incubated to Hamilton-Hamburger stages 31–34 (Hamburger and Hamilton, 1951), embryonic day 7.5 at 37 °C. The embryos were removed from their associated membranes and washed briefly in medium before decapitation with watchmaker forceps. The embryos were pinned ventral-up on Sylgard®-coated dishes (Dow Corning) in medium under a dissecting microscope with incident light and a dark background. The thoracic and abdominal organs were removed, including the presumptive metanephroi attached retroperitoneally. The remaining embryo was then re-pinned dorsal side up to allow bisection of the embryo along the spinal cord with a cataract knife, which reveals rows of dorsal root ganglia (DRGs) on either side of the embryonic vertebral column.

The DRGs are then removed into fresh medium and cut into ~2 sections with forceps and a cataract knife, so as to completely disrupt the surrounding membranes and increase the number of cultures possible from one embryo. The PLL/laminin-coated plates were distributed into the wells of 4- or 24-well plates and covered in 1 ml medium each; DRG explants were placed onto the cover-slips, bathed in medium, and incubated at 37 °C/5% CO_2, humidified, overnight.

2.8 Culture of *Xenopus lævis* Eye Primordia *in vitro*

2.8.1 Culture of *Xenopus lævis* from Egg to Larva

Xenopus lævis eggs at the one-cell stage were cultured at 18–25 °C, to control rate of development, in 0.1× Modified Barth's Solution (MBS; 1% 10× stock solution consisting of 54.13 g NaCl, 0.75 g KCl, 2.02 g $NaHCO_3$, 2.03 g $MgSO_4.7H_2O$, 0.78 g $Ca(NO_3)_2.4\,H_2O$, 23.83 g HEPES pH 7.5 per litre) with 1% 100× v/v Penicillin/Streptomycin (Invitrogen, 15140122) to stage 32–36, incubation medium replaced daily.

2.8.2 Culture Medium

Eye primordia were grown in a culture medium consisting of 60% Leibovitz's L-15 medium with glutamine (Invitrogen, 31415-029) pH 7.6–7.8, 1% 100× Penicillin/Streptomycin/Fungizone (PSF) (VWR, 733-1809), 39% 18MΩ H_2O.

2.8.3 Preparation of Cover-Slips

Cover-slips were prepared prior to poly-*L*-lysine as above but at room temperature, a concentration of 10 µg/ml and for 3 h or over-night. They were then washed ×2 with 18MΩ H_2O, dried for 1 h and stored until use. Prior to use in tissue culture, they were coated in 250 µl of culture medium with 10 µg/ml laminin (Sigma, L2020) for 1 h, then washed briefly in culture medium.

2.8.4 Dissection of Eye Primordia

The dissection hood was sterilised with UV light for 30 min, then all surfaces were wiped with 70% ethanol and all dissection tools immersed briefly in ethanol, then flamed to sterilise. The embryos were teased out from their egg cases if still within them and washed ×3 in 0.1% MBS with PSF. The embryos were then transferred into 0.1% MBS with PSF with 0.04% w/v MS-222 (Tricaine, ethyl 3-aminobenzoate methanesulphonate, Sigma-Aldrich, A5040) to anæsthetise the embryos and act as a muscle relaxant.

The embryos were pinned lateral side up, and the eye primordia removed with 2 needles. The eye primordia were transferred in groups of 5–6 to the cover-slips and 500 µl culture medium was added, and positioned primordial lens up so that the exiting RGC axons would make contact with the cover-slips. The cultures were left for 2 h at room temperature without moving, so that the eye primordia would adhere to the surface and not roll during transfer, then incubated over-night at 20 °C.

2.9 Experiments Performed upon Axonal Cultures

2.9.1 Preparation of Formaldehyde Fixative

The axon culture fixative was prepared by heating 400 ml PBS pH 7.4 with 40 g paraformaldehyde to 53 °C in a fume hood with 10–20 drops of 10 M NaOH to hydrolyse the paraformaldehyde to formaldehyde, stirring, for 30 min. The heat was removed and 150 g sucrose added, and stirring continued. The pH was adjusted to 7.4 with HCl and the volume made up to 1000 ml with additional PBS pH 7.4.

2.9.2 Co-Incubation with Pharmacological Activators and Inhibitors and Repulsive Cues

After over-night incubation, the cultures were examined briefly under a 40× light phase-contrast microscope to ensure that axons had grown out from the explant, and that the growth cones' morphologies were not collapsed, nor that the axons were thin or blebbed. Those that had collapsed or had blebbed more than minimally prior to experimentation were excluded from further use.

Isolation of Axons from the Cell Body

To demonstrate that protein synthesis-dependent effects of growth cone collapse were localised to the axon, a Pasteur pipette was drawn and cut to give a tip diameter of ~1 mm to remove the main body of the DRG, containing the cell somata, immediately prior to performing the assays. The tip of the pipette was placed over the body, twisted to cut through the axons and the main body then aspirated to ensure that all axons were transected.

Blinding and Application of Agents

Conditions of controls and reagents were applied blind-coded. 1–15 min later, dependent upon the pharmacological agent, the guidance cue and controls were applied by the experimenter, also blind-coded. The cultures were incubated at 37 °C between applications, and after application of cues, the cultures were incubated for a further 30 min at 37 °C/5% CO_2 (unless specified otherwise) prior to fixation.

Fixation and Counting Collapsed Growth Cones

Cultures were fixed by removal of 500 µl of medium, followed by gradual addition of 500 µl warmed fixative. The upper 500 µl was aspirated, being mainly medium, and a final 500 µl of fixative added. The cultures fixed at room temperature for at least 2 h prior to counting the spread and collapsed growth cones. Assessment was performed with a 40× light phase-contrast microscope with the cultures immersed in PBS; each individual growth cone was judged collapsed if it lacked significant lamellipodia and had fewer than two filopodia. Growth cones which had made contact with other axons or were otherwise difficult to categorise (fewer than 1%) were excluded from analysis. All other growth cones were judged 'spread'. Cultures which detached from the cover-slip or whose axons displayed gross morphological abnormalities were excluded from analysis. Rarely, cultures produced less than 50 assessable growth cones, in which case their data were pooled with other cultures'. The data were normalised to a percentage, and the percentages of collapse from each condition were compared with Kruskal-Wallis ANOVA and, if significant, pairs of conditions were compared with non-parametric, two-way Mann-Whitney *U*-test. P-values smaller than 0.05 were considered significant.

Recombinant human Semaphorin-3A-Fc (R&D, 1250-S3-025) and the 66-amino-acid loop domain of Nogo-A (R&D, 3728-NG-050) were purchased from R&D Systems; the Δ-20 domain of Nogo-A (Nogo-δ20) was supplied in dimerised form by André and Antonio Schmandke, of the Schwab lab, ETH Zürich, Switzerland.

2.9.3 Quantitative Immunofluorescence

DRG cultures were prepared as above but with 120 ng/ml NGF in order to slow collapse, and exposed to guidance cues and/or pharmacological agents. Samples were fixed in 4% formaldehyde, 15% sucrose in PBS at 37 °C for 30 min, and washed in PBS. The cover-slips were then incubated in 0.1 M glycine in PBS for 15 min to quench any excess formaldehyde, washed once more in PBS and permeabilised at room temperature in 0.1% v/v Triton X-100/PBS with 2% v/v goat serum (Sigma-Aldrich, G9023-10ML) and 1% w/v BSA for 1 h. Detergents were removed by 3 washes in PBS, and the cover-slips were incubated over-night with 1:100 v/v primary antibody in 1% w/v BSA/PBS.

After 3 washes in PBS, the cover-slips were again incubated at room temperature in 0.1% w/v Triton X-100/PBS with 2% v/v goat serum and 1% w/v BSA for 1 h, followed by 3 washes in PBS and the secondary antibody (1:1000) for 1 h in 1% w/v BSA/PBS, washed in PBS, incubated for 30 min at room temperature in 0.1% v/v Triton X-100/PBS with 2% v/v goat serum (Sigma-Aldrich, G9023-10ML) and 1% w/v BSA for the final time, washed in PBS and mounted in FluoroMount-G (Southern Biotech, 0100-01) on SuperFrost Plus slides (VWR, 631-9483). Slides were stored in a light-tight box at 4 °C until analysed.

The slides were visualised with phase-contrast 500× magnification and under 594 nm light. Images were taken under constant illumination (496 nm for Alexa Fluor® 488 and 590 nm for Alexa Fluor® 594) with OpenLab v5.5.2. Masks were created, blind, from the phase-contrast images of the growth cone, excluding the central domain, and the average fluorescent intensity determined for each growth cone and its background. For each value, the background fluorescence was subtracted from the growth cone's pairwise, and the results were analysed *via* ANOVA.

2.9.4 Astrocyte Immunohistochemistry

To determine whether protein disulphide isomerase was present on the cell surface of cultured CRL 1718 cells, cultured astrocytes were grown on PLL/laminin-coated cover-slips overnight in 1 ml medium (see *Medium and Culture Conditions* for CRL 1718 cells). The cover-slips were

prepared as described above (see *Preparation of Cover-Slips for DRGs*). The cells were fixed in 4% formaldehyde, 15% sucrose in PBS at 37 °C for 15 min to limit permeabilisation by formaldehyde, and washed in PBS. The cover-slips were then incubated in 0.1 M glycine in PBS for 15 min to quench any excess formaldehyde, washed once more in PBS.

To ensure that any signal obtained would be due to cell-surface PDI rather than inadvertent permeabilisation during fixation, the cover-slips were incubated at room temperature in 2% v/v goat serum/PBS (Sigma-Aldrich, G9023-10ML) with 1% w/v BSA for 1 h, with or without 0.1% v/v Triton X-100 to allow complete permeabilisation as a positive control. These solutions were removed by 3 washes in PBS, and all cover-slips were incubated over-night with 1:500 v/v primary rabbit anti-bovine PDI antibody (Sigma, P7496) in 1% w/v BSA/PBS. The cover-slides were then washed, incubated with secondary antibodies, mounted and imaged as for *Quantitative Immunofluorescence* above.

2.9.5 Staining of Axons with Phalloidin

To reveal the actin structure of growth cones, fixed growth cones were stained with Alexa Fluor 488-tagged phalloidin (Invitrogen). The cultures were washed twice with PBS pH 7.4 pre-warmed to 37 °C, and fixed in 4% v/v formaldehyde/PBS with 15% w/v sucrose for 10 min at 37 °C, followed by two washes in PBS pH 7.4 at 37 °C. The labelled phalloidin was diluted to ~6.6 µM in methanol, and 5 µl of this stock was diluted in 200 µl 1 % w/v BSA/PBS pH 7.4 for each cover-slip to reduce non-specific staining. The cover-slips were incubated in this solution for 20 min at room temperature, then washed twice more with PBS pH 7.4. Excess fluid was removed and the cover-slips were mounted on slides with FluoroMount and stored in the dark at 4 °C until imaged.

2.9.6 Analysis of Protein Synthesis with TAMRA and AHA

To demonstrate local protein synthesis directly, the DRGs were transected and aspired from their axons prior to addition of the guidance cue and a methionine analogue, *L*-azidohomoalanine (AHA) in methionine-free medium. Proteins incorporating AHA react

with the alkyne moiety of tetramethylrhodamine (TAMRA) *via* their azido moieties through a 'Click' reaction, specifically an azide-alkyne Huisgen cycloaddition. This provides a fluorescent signal in an SDS-PAGE gel. The method was modified from that described in the Protein Analysis Detection Kit (Invitrogen, C33370). DRG explants were grown overnight as above, with the following modifications:

- approximately 15–25 DRG explants were placed on each cover-slip, arranged geometrically, to allow for ~10 000 axons (~50 DRGs, extending ~200 axons per DRG) per sample and
- the DRGs, after placement on the cover-slips, were warmed to 37 °C and allowed to attach to the cover-slips before transferral to the incubator, to prevent loss of spacing.

The medium was replaced, substituting Ham's F-12 with cystine/methionine/glutamine-free DMEM (Invitrogen, 21013-024) supplemented with 4 mM *L*-glutamine, 0.2 mM *L*-cystine and incubated for 1 h. DRG cell bodies were cut away from the cover-slip surface (see *Isolation of Axons from the Cell Body* above), and both 500 µM AHA in DMSO and 0, 250 or 1000 ng/ml Sema-3A in PBS added to the medium and incubated for 1 h, before the medium was removed and the cover-slips washed ×3 with PBS, before the axons were lysed for 15–30 min on ice in lysis buffer (1% SDS, 5 mM Na-EDTA, 1 tablet of Roche Complete EDTA-free Protease Inhibitors, 1 mM sodium orthovanadate, 50 mM Tris-HCl pH 8.0).

Click Reaction

- 60 µl of Component A (TAMRA-alkyne) was added to a tube of Component B (DMSO) to form the 'TAMRA reagent',
- 500 µl 18 MΩ H_2O to Component E (*tris*-(benzyltriazolylmethyl)amine) to form 'Reagent #1',
- 100 µl 18 MΩ H_2O to Component D (sodium ascorbate) to form 'Reagent #2',
- to 50 µl of lysis buffer, I added 100 µl of 'TAMRA reagent' and 18 MΩ H_2O to a total volume of 160 µl and vortexed for 5 sec,

- added 10 µl of Component C (40 mM $CuSO_4$) and vortexed,
- added 10 µl of 'Reagent #2', vortexed and waited for 2-3 min, and finally
- added 20 µl of 'Reagent #1', vortexed, at which point the solution turned orange.

The tube was covered in foil to protect the reagents from light and rotated end-ever-end for 20 min at 5 °C.

Protein Pellet Extraction To the derivitised protein mix, methanol (600 µl) was added and the mixture vortexed, followed by chloroform (150 µl). The mixture was vortexed again, followed by 18 MΩ H_2O (400 µl) and vortexing. The resultant protein precipitate was centrifuged at 16 100×g for 5 min at 5 °C. The upper layer of chloroform was aspirated and discarded, taking care to keep the fluid interface intact, before 450 µl methanol were added and the mixture vortexed for 5 sec once more. The centrifugation was repeated, and the supernatant bearing excess fluorophore was discarded. The pellet was redissolved in methanol (450 µl) by vortexing, followed by centrifugation at 16 100×g for 5 min at 5 °C and the supernatant fluid discarded. The resulting pellet was air-dried for 15 min with a lint-free tissue covering and stored at -20 °C in a light-tight box.

Electrophoresis The derivitised protein pellet was resolubilised in 20% v/v 5× Sample Buffer (see section 'SDS-PAGE 1D Gel and Western Blot'), 80% v/v PBS pH 7.4 by vortexing and heated to 70 °C for 10 min before being run on an SDS-PAGE 1D gel (see above for method). The gel was fixed in 40% ethanol, 10% glacial acetic acid, 50% 18 MΩ H_2O overnight, washed ×3 in 18 MΩ H_2O and fluorescence imaging performed (see *Quantitative Immunofluorescence* above).

2.10 Gene Retrieval from CRL-1718 cDNA Library

2.10.1 cDNA Amplification *via* Polymerase Chain Reaction

Sema3A cDNA was used as a marker to establish the integrity and completeness of the cDNA library, as its mRNA is synthesised by astrocytes and has only one isoform. To isolate it and

demonstrate its presence, varying amounts of cDNA library template were added to the 'Master Mix'.

Hot-Start PCR Master Mix

5 µl 10× 'Hot Start' buffer,

3 µl 25 mM $MgSO_4$,

5 µl 2mM dNTP mix,

33.5 µl autoclaved ddH_2O subjected to 1 J UV radiation prior to use and

1 µl KOD 'Hot Start' polymerase.

The polymerase was added last and the mixture was homogenised *via* pipetting as vortexing damages the polymerase.

The final reaction mix consisted of the following, per 50 µl reaction:

47.5 µl Master Mix,

1.0 µl cDNA library sample,

0.75 µl 20 µM forward primer and

0.75 µl 20 µM reverse primer to a final volume of 50 µl.

To amplify Sema3A cDNA, the samples were heated to 95 °C for 2 min to denature the inhibiting antibodies from the polymerase, then

95 °C to denature for 20 sec,

60 °C to anneal for 10 sec,

70 °C to allow polymerisation for 75 sec

for 30 cycles, then 70 °C for 10 min and finally 4 °C to end.

2.10.2 cDNA Analysis with Agarose Gel Electrophoresis

Separating 2% agarose gels (*per* 1 l) were prepared with 20 g ultra-pure agarose (Invitrogen, 16500500), 1 l Tris/borate/EDTA (TBE) buffer (10.6 g Tris base pH 8.0, 5.5 g boric acid, 4 ml 0.5 M Na-EDTA), heated to boiling point, cooled to 50 °C and 1:20 000 ethidium bromide 10 mg/ml (Sigma-Aldrich, E1510) added and mixed. This gel mixture was then poured and allowed to set at room temperature.

DNA samples were prepared by adding 10 µl 5× TBE sample buffer (53 g/l Tris base pH 8.0, 27.5 g/l boric acid, 20 ml 0.5 M Na-EDTA, 30% glycerol, 0.25% bromophenol blue) to the sample and adding 18 MΩ H_2O to a total volume of 50 µl. All empty sample wells were filled with 50 µl 1× TBE sample buffer to prevent front distortion and lateral diffusion of DNA during electrophoresis. Gels were run at 50 V constant voltage until the bromophenol blue tracker dye reached the end of the gel, and the gel was imaged with UV transillumination (312 nm) and a CCD.

2.10.3 Amplification of Specific Bands

Bands of interest were cut out from the agarose gel using UV transillumination to visualise them. Samples of gel were stored at –20 °C. To extract a sample for amplification, 2 µl 18 MΩ H_2O were added and the samples centrifuged for 5–10 min at 16 100×g. 1 µl of supernatant then served as the DNA template.

cDNA samples were amplified using the REDTaq ReadyMix PCR Reaction Mix (Sigma, R2523) as follows, per 50 µl reaction:

25 µl Master Mix,

1.0 µl cDNA library sample,

1.0 µl 20 µM forward primer,

1.0 µl 20 µM reverse primer and

22 µl 18 MΩ H_2O to a final volume of 50 µl.

cDNA was amplified using the Hot-Start PCR Master Mix as decribed above (see *Hot-Start PCR Master Mix*).

2.11 PCR Programme for Amplification of CRL17/18 cDNA Library Samples

The cDNA library bears half of the primer recognition site at each of the 5' and 3' ends, cut at recognition sites ready for ligation into plasmids. Initially, the samples were heated to 95 °C for 2 min to denature the inhibiting antibodies from the polymerase, then the first cycle

95 °C for 20 sec,

45 °C for 10 sec and

70 °C for 180 sec

in order to allow the annealing of the initially shortened primer sites (calculated T_m = 46.6 °C initially, then T_m = 63.4 °C thereafter), followed by

95 °C for 20 sec,

60 °C for 10 sec and

70 °C for 180 sec

for 29 cycles, then 70 °C for 3 min and finally 4 °C to end. The polymerisation time was extended to 180 sec to allow for cDNA up to ~3 kbp long.

Amplification of bands using REDTaq occurred with the following cycle. Samples were heated to 95 °C for 2 min, and if amplifying directly from cDNA samples, the initial cycle occurred

95 °C for 25 sec,

45 °C for 45 sec and

72 °C for 240 sec

for 4 cycles, then 95 °C for 2 min,

95 °C for 25 sec,

45 °C for 45 sec and

72 °C for 120 sec

for 36 cycles, then 72 °C for 240 sec and 4 °C to end.

2.11.1 cDNA Gel Extraction for Sequencing

DNA for sequencing was extracted with the High Pure PCR Product Purification Kit (Roche, 11 732 668 001), modified for smaller final volume size. Binding Buffer (300 µl) was added per 100 mg of agarose gel sample and vortexed for 15–20 sec. This mixture was heated to 56 °C to dissolve the agarose and free the DNA, vortexing every 2–3 min. 150 µl isopropanol *per* 100 mg initial agarose were added and the mixture vortexed.

The solutions were transferred to spin-cups with filters and centrifuged for 60 sec, 16 100×g at room temperature; flow-through was discarded. Wash Buffer (500 µl) was added, centrifuged for 60 sec, 16 100×g at room temperature, and the flow-through discarded. Finally, Wash Buffer (200 µl) was added, centrifuged for 60 sec, 16 100×g at room temperature and the supernatant fluid discarded.

The collection tube was replaced, Elution Buffer (20 µl) added and left to stand for 10 min to maximise DNA extraction, and the eluate spun down as before. Elution Buffer (30 µl) was added, left to stand and spun down. The eluate was kept overnight under filter paper to partially evaporate the solvents and concentrate the DNA sample. Concentration and purity of DNA were assessed on a nanodrop spectrometer. Samples were sent to the DNA Sequencing Facility, Department of Biochemistry, University of Cambridge.

2.12 Ligation and Transfection

2.12.1 Ligation and Transfection into CM109 Competent Cells

Purified cDNA was selected for DNA levels and purity *via* nanodrop spectrometry. An aliquot (1.5 µl) of each PCR product sample was mixed with 2.5 µl 18 MΩ H_2O, 0.5 µl T4 ligase (Promega, M1804) and 0.5 µl pGEM-T-Easy plasmid (Promega, A1360), and incubated at 5 °C over-night. These 5 µl samples were then each added to a 20 µl of DH5α transfection-competent *E. coli* cells (kindly provided by Prof. Sarah Bray) and incubated in water ice for 30 min. Samples were then heat-shocked at 42 °C for 45 sec, and returned to water ice for 2 min. An aliquot of SOC medium (50 µl; Sigma, S1797) was added to each sample and incubated at 37 °C for 1 h.

2.12.2 LB Agar Plates and Colony Selection

LB agar (10 g/l bacto-tryptone (BD, 211705), 5 g/l bacto-yeast extract (BD, 210934), 15 g/l agarose, 5 g/l NaCl pH 7.0)) was prepared by mixing all components near-solution, then sterilising *via* autoclave to dissolve the remainder. The liquid agar was then cooled to ~50 °C and 100 mg/l carbenicillin (Melford, C0109) added. The agar was poured into 9 cm Petri dishes in the bacterial hood and allowed to cool with the lids slightly displaced to prevent condensation. They were then sealed in a bag and stored at 4 °C.

Prior to use, the plates were coated with a combination of 0.1 M IPTG (100 µl; Promega, V3955) and 50 mg/ml X-gal (20 µl; Promega, V3941), which was allowed to absorb into the agar for 1 h under the hood at room temperature. The plates were coated with cell-bearing SOB medium and incubated at 37 °C overnight until colonies appeared on the agar surface. Individual white colonies were selected and introduced to 5 ml LB medium with 100 mg/l ampicillin and incubated overnight at 37 °C, rotated at 230 rpm.

2.12.3 Mini-Prep, Midi-Prep and Plasmid Sequencing

Purified plasmids were prepared using the PureYield Plasmid Miniprep System (Promega, A1222). The media (600 µl) of cultures with sufficient growth were transferred to 1.5 ml

microcentrifuge tubes and 100 µl Cell Lysis Buffer added to each. The tubes were mixed by inversion until the solution was clear blue or after 2 min, whichever was the shorter. Neutralisation Solution (350 µl) at 4 °C was added, and the tubes again mixed by inversion, until the samples were uniformly opaque yellow. Precipitates were then spun down for 3 min at 16 100×g, and the plasmid-bearing solution aspirated into PureYield microcolumns in collection tubes. The samples were spun through the filters for 15 sec at 16 100×g, and the flow-through was discarded. Endotoxin Removal Wash Solution (200 µl) was added, and spin through the filters similarly. Column Wash Solution (400 µl) was then added and spun through for 15 sec at 16 100×g.

Nuclease-free 18 MΩ H_2O (30 µl) was added directly to the filters and left to stand for 1 min, before the plasmid-bearing solution was centrifuged for 15 sec at 16 100×g. DNA purity and concentration was measured *via* nanodrop spectrometry and samples were sent to the Biochemistry Sequencing Facility for to obtain their sequences and stored at -20 °C. To expand the culture, 50 µl samples were added to 50 ml LB medium with ampicillin and cultured for 14 h, at 37 °C, 230 rpm. Samples of the bacteria in culture medium (100 µl) were also mixed with 80% v/v glycerol (100 µl) and held at -80 °C for long-term storage.

Plasmids were purified from the 50 ml cultures using the QIAfilter Plasmid Kit (Qiagen, 12245). Cells were pelleted by centrifugation at 6 000×g for 15 min at 4 °C and resuspended in Buffer P1 (4 ml) with RNase A, and LyseBlue as a lysis indicator. Buffer P2 (4 ml) was added and the samples mixed vigorously to a uniform blue, then left to lyse at room temperature for 5 min. Buffer P3 (4 ml) was added to neutralise the lysis solution, and mixed until the lysate turned yellow, formed precipitates and lost its viscosity. These lysates were added to stoppered QIAfilter cartridges to incubate for 10 min at RT. Simultaneously, the QIAGEN-tip 100 DNA-binding columns were equilibrated for 10 min with Buffer QBT (4 ml) allowed to pass through by gravity.

Plungers were inserted into the cartridges, stoppers removed and the filtered lysate placed into the binding columns. The lysate passed through the filter through gravity, followed by Buffer QC

washing solution (20 ml). The DNA was eluted with Buffer QF (5 ml). Isopropanol (3.5 ml) was added and mixed to precipitate the DNA, and the mixture centrifuged at 16 100×g for 30 min at 4 °C to form a DNA pellet. The supernatant fluid was decanted gently and 70% ethanol (2 ml) added to wash. The DNA was centrifuged down at 16 100×g for 10 min, supernatant fluid decanted, the pellet air-dried, redissolved in nuclease-free 18 MΩ H_2O (75 µl) and stored at -20 °C.

2.12.4 Prosaposin Immunohistochemistry

Sections of E6.5 and E10.5 wild-type *Gallus gallus* brain fixed in Histosol (National Diagnostics, HS-100), embedded in wax were kindly donated by Dr Perrine Barraud (Baker lab). The slides were hydrated by sequential 5-min incubations in the following solutions:

2× Histosol,

2× 100% ethanol,

1× 75% ethanol, 25% 18 MΩ H_2O,

1× 50% ethanol, 50% 18 MΩ H_2O,

1× 25% ethanol, 75% 18 MΩ H_2O,

1× 100% 18 MΩ H_2O and

2× PBS.

The slides were blocked in 5% v/v sheep serum/PBS for 1 hour at room temperature, then incubated overnight at 4 °C in 5% v/v sheep serum/PBS with 1:1000 polyclonal rabbit anti-prosaposin antibodies (ProteinTech, 18396-1-AP). Controls were incubated overnight in 5% v/v sheep serum/PBS only.

The slides were washed three times in PBS at room temperature for 15 min, then incubated in 5% v/v sheep serum/PBS with 1:1000 Alexa Fluor 568 anti-rabbit IgG in the dark for 2 h, washed three times in PBS, mounted with Fluoromount G and cover-slips, and viewed under a

fluorescence microscope. Cover-slips and Fluoromount G were removed with multiple washes in PBS, then the neuronal βIII-tubulin was stained by repeating the above, with 1:250 mouse TuJ1 as the primary antibody and 1:1000 Alex Fluor 488 anti-mouse secondary. Nuclei were stained by immersion in 300 nM 4′, 6′ diamino-*2*-phenylindole.2HCl (DAPI)/PBS for 3 min, then washed three times in PBS.

2.13 Pharmacological Agents in Growth Cone Assays and Key to Data

Agent	Target	Concentration	Solvent	Source
Anisomycin	Ribosome	5-40 μM	Ethanol	Sigma A9789
AR-A014418	GSK-3β	500 nM	Ethanol	Sigma A3230
bpV(pic)	PTEN	100 nM	PBS	Enzo ALX-270-205
8-bromo-cAMP	cAMP analogue	25 μM	PBS	Sigma B5386
2-bromopalmitate	Palmitoylation	4 μM	PBS	Sigma 21604
Cycloheximide	Ribosome	25 μM	Ethanol	Sigma C1988
Dynasore	Dynamin	40 μM	DMSO	Sigma D7693
Lithium chloride	GSK-3β	10 mM	PBS	Sigma 62476
MDC	Clathrin	60-100 μM	Methanol	Sigma D4008
Myoglobin	Free NO	20 μM	PBS	Sigma M1882
L_{ω}-nitro-*N*-arginine	NO Synthase	100 nM	PBS	Sigma N5501
S-nitrosoglutathione	NO donor	1-50 μM	PBS	Sigma N4148
ODQ	Guanylyl Cyclase	500 nM	Ethanol	Cayman 61410
PAO	Endocytosis	1 μM	DMSO	Sigma P3075
PD98059	Erk1/2	40 μM	DMSO	Tocris 1213
N_{ω}-propyl-*L*-arginine	NO Synthase-1	450 nM	Ethanol	Tocris 1200
PTIO	Free NO	1 mM	PBS	Tocris 0772
Rapamycin	mTOR Complex 1	100 nM	DMSO	Sigma R0395
SB 216763	GSK-3β	200 nM	Ethanol	Tocris 1616
Wortmannin	PI-3 Kinase	10 nM	PBS	Sigma W1628
Y-27632	Rho-kinase	1.5 μM	DMSO	Cayman 5583
Z-LLnL	Proteasome	100 nM	Ethanol	Sigma A6185
Z-VAD-FMK	All caspases	25 μM	Ethanol	Enzo ALX-260-020

Table 2.1: Pharmacological Agents Used in Growth Cone Collapse and Quantitative Immunfluorescence Assays

Symbol	n.s.	*	**	***	****
Significance	*p>0.05*, not significant	*p<0.05*	*p<0.01*	*p<0.001*	*p<0.0001*

Table 2.2: Key to Significance Levels

Chapter 3

Local Protein Synthesis and Semaphorin-3A

3.1 Introduction

While dendritic protein synthesis is known to be crucial for regulating spine dynamics and synaptic plasticity (Martin and Zukin, 2006; Schuman et al., 2006; Bourne and Harris, 2008), the significance of axonal protein synthesis (PS) was controversial until recently. During the last decade, the importance of axonal PS has been highlighted in growth cone guidance and in axon regeneration (Lin and Holt, 2007; Park et al., 2008; Donnelly et al., 2010). Proteins synthesised locally in the axon account for only 5% of total axonal protein (Eng et al., 1999), and their significance in growth and guidance has been debated. Although mRNAs for cytoskeletal proteins were among those first detected in axons (Kaplan et al., 1992), PS inhibition does not affect the rate of axon growth in the short term (Eng et al., 1999; Campbell and Holt, 2001). Further, although β-actin is a crucial neuronal cytoskeletal protein, isolated axons grow without local PS (Eng et al., 1999). Similarly, work by Leung et al. (2006) suggests that localised synthesis of cytoskeletal proteins directs growth cone polarity and motility, but not outgrowth.

Campbell and Holt (2001) first identified a direct role for local PS in axon guidance, and several groups have reported supporting evidence for this mechanism in the growth cone, for example the presence of active mRNA localisation (Bassell et al., 1998), mRNA-specific transport (Aronov et al., 2001) and phosphorylation-dependent mRNA release (Sasaki et al., 2010). Further, recent genome-wide unbiased studies have revealed thousands of mRNA transcripts in

axon growth cones with cell-type and developmental-stage–specific localisation (Taylor et al., 2009; Andreassi et al., 2010; Gumy et al., 2010; Zivraj et al., 2010).

Notwithstanding the presence of β-actin and RhoA mRNAs in the growth cone, the ability of external cues to influence localisation and synthesis, and the sufficiency of localised synthesis to cause growth cone turning (Wu et al., 2005; Leung et al., 2006; Yao et al., 2006), their relevance has been questioned by Roche et al. (2009), apparently contradicting several studies (Campbell and Holt, 2001; Li et al., 2004; Wu et al., 2005). Roche et al. (2009) investigated the role of PS in mediating responses to several molecular cues using outgrowth, turning and growth cone collapse assays, but despite replicating findings showing that Sema3A activates PS, they concluded that axon guidance mechanisms do not require it.

Sema3A-induced growth cone collapse was therefore examined in chick dorsal root ganglion (DRG) explants (Luo et al., 1993), a model also used by Roche et al. (2009), aiming to identify reasons for their inability to replicate previous findings. It is shown that collapse is indeed refractory to PS inhibition when using high concentrations of Sema3A that induce an extensive degree of collapse in these explants, but it is not refractory at lower Sema3A concentrations. The mTOR-dependent pathway operates at lower Sema3A concentrations alongside activation of GSK-3β signalling, while at higher concentrations GSK-3β signalling becomes predominant, and a combination of reduced NGF and increased Sema3A concentrations replicates the data of Roche et al. (2009).

The role of NO/cGMP signalling downstream of Sema3A was also examined, as reported by Campbell et al. (2001) and Castellani et al. (2002), exploring its relation to these two pathways. Although growth cone collapse assays suggest a relationship with the PS-dependent pathway, it was found that quantitative immunofluorescence data suggest a relationship with GSK-3β–dependent collapse instead.

3.2 Protein Synthesis Dependence of Semaphorin-3A–Induced Growth Cone Collapse

3.2.1 PS inhibitors reduce, but do not eliminate, Sema3A-induced axon growth cone collapse

In the initial experiments, PS inhibitors were added concurrently with Sema3A-Fc to chick embryo DRG axons growing in a medium of DMEM with insulin/transferrin, glutamine and NGF (80 ng/ml). It was found that 250 ng/ml Sema3A induced approximately 40–50% mean growth cone collapse after 30 min (Figure 3.1(a)), equivalent to one 'collapsing unit' (Luo et al., 1993), as opposed to ~10% collapse in with the addition of 1 µl PBS (control) (Figure 3.1). The equivalence of collapse was also demonstrated, assessed *via* comparison of phase contrast microscopy and fluorescence microscopy (Figure 3.1(b)).

Application of 25 µM cycloheximide, a concentration sufficient to inhibit PS (see below), marginally yet significantly increased collapse *vs* control to 17% ($p<0.05$), but when applied concurrently with Sema3A the induced collapse fell from 55% to 28% (Figure 3.2, $p<0.001$). Despite PS blockade, 250 ng/ml Sema3A still increased growth cone collapse relative to cycloheximide alone (28% *vs* 17% respectively, $p<0.05$).

As cycloheximide can also increase cAMP levels (Liu and Ma, 2010), the experiment was repeated using 5 µM anisomycin, a structurally unrelated PS inhibitor (Figure 3.4(a)). The extent of collapse with anisomycin alone (6%) did not differ significantly from control (5%), but when applied concurrently with Sema3A, collapse levels fell from 45% to 18% ($p<0.001$). Again, Sema3A increased the extent of collapse *vs* control, even in the presence of the inhibitor ($p<0.001$). The experiment was repeated using 40 µM anisomycin (Figure 3.4(b)), which alone induced 22% collapse, significantly higher than the 10% collapse in the control samples ($p<0.01$). Despite this increase, the extent of Sema3A-induced collapse in the presence of anisomycin remained lower ($p<0.05$) than in its absence.

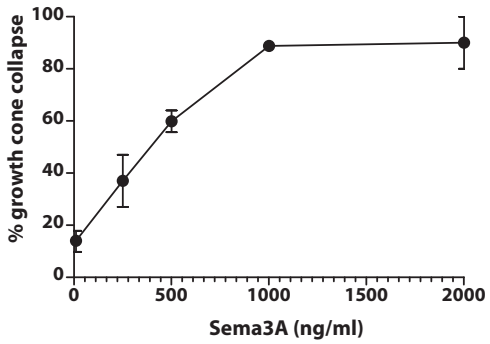

(a) Dose-dependent Collapse

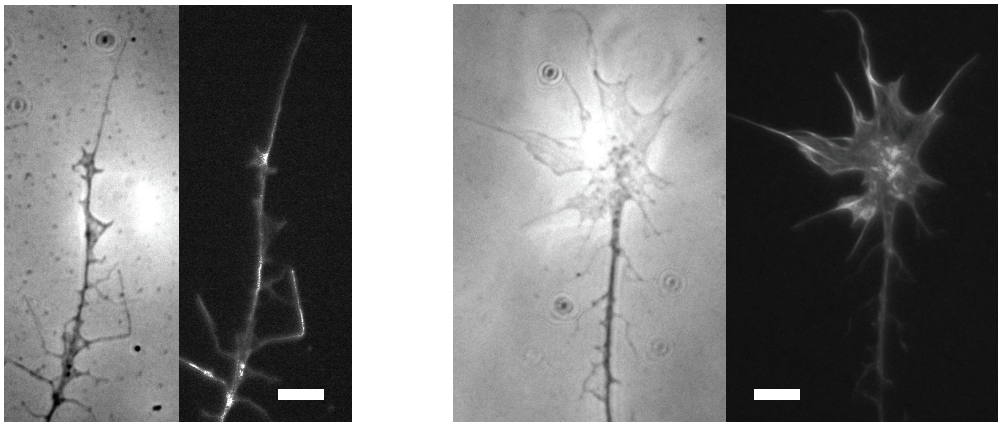

(b) Collapsed and Spread Growth Cones

Figure 3.1: The dose-dependent Sema3A-Induced Collapse of DRG Growth Cones.
DRG cultures grown overnight were exposed to 0–2000 ng/ml Sema3A-Fc for 30 minutes and fixed. Collapse extent ranged from 15% to 90% in a dose-dependent manner (a). Collapsed (b *left*) and spread (b *right*) growth cones under phase-contrast and fluorescence microscopy, respectively, stained with Alexa Fluor 488-tagged phalloidin. Scale bar = 5 μm.

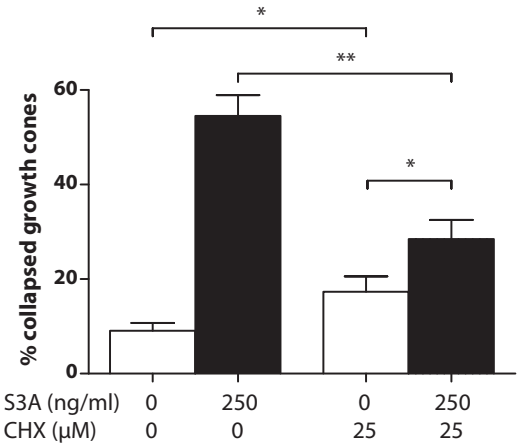

Figure 3.2: The effect of cycloheximide on Sema3A-induced growth cone collapse.
250 ng/ml Semaphorin-3A (S3A) induced half of the axons to collapse. In the presence of 25 μM cycloheximide (CHX), the extent of collapse was reduced but higher than CHX alone. CHX induced a limited level of collapse alone over control.

Last, it was found that 100nM rapamycin (Figure 3.3(a)), an inhibitor of mTOR, produced minimal effects on growth cones alone compared to controls (8% *vs* 5% collapse, respectively; $p<0.05$), but addition of the inhibitor again reduced the extent of Sema3A-induced collapse from 41% to 16% ($p<0.0001$). By contrast, the collapse induced by 1 μM lysophosphatidic acid (Figure 3.3(b)), a repulsive cue unaffected by PS inhibition (Campbell and Holt, 2001), was not reduced by rapamycin (49% *vs* 53%, $p<0.05$).

To confirm the independence of PS-dependent collapse from the neuronal nucleus, the assays were repeated on axons severed from their cell bodies prior to Sema3A application (Figure 3.4(d)). The presence of PS-independent collapse was also confirmed by combining application of cycloheximide and anisomycin (Figure 3.4(c)). To check that any remaining Sema3A-induced collapse did not result from insufficient inhibition of PS, PS was directly measured in growth cones by methionine substitution with azidohomoalanine (AHA) and labeling with tetramethylrhodamine in the presence of the inhibitors, and in the absence of AHA as a negative control. All three inhibitors significantly reduced fluorescence from control ($p<0.001$), and were indistinguishable from the AHA-free negative control (Figure 3.5).

Effect of PS inhibition depends on relative Sema3A and NGF concentrations The initial culture medium included 80 ng/ml NGF, whereas Roche et al. (2009) cultured their explants in 10 ng/ml NGF. Lower concentrations of NGF have been shown to increase the extent of Sema3A-induced growth cone collapse (Dontchev and Letourneau, 2002). Consistent with this, in the presence of 10 ng/ml NGF, although the extent of collapse remained low in controls (5.5%), addition of 250 ng/ml Sema3A caused more collapse than in the presence of 80 ng/ml NGF (87% *vs* 55% respectively; compare Figure 3.6 with Figure 3.4(a)). Collapse was again inhibited by addition of anisomycin at this Sema3A concentration (Figure 3.6), but at 500 ng/ml Sema3A, replicating the conditions of Roche et al. (2009), the effect of PS inhibition declined to a non-significant level (Figure 3.7). Their data were replicated and confirmed, and neither differences in growth media nor time-course of the assays affected PS dependence (see *Appendix*, Figure A.1).

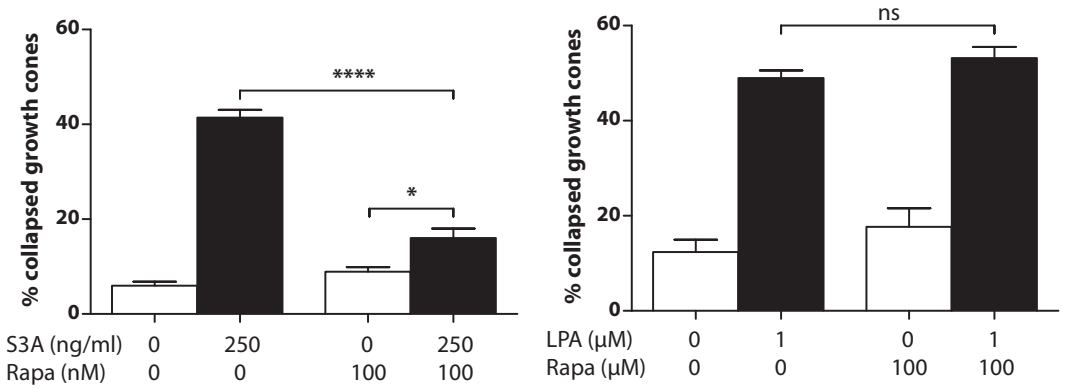

(a) Semaphorin-3A and Rapamycin

(b) Lysophosphatidic Acid and Rapamycin

Figure 3.3: mTOR Inhibition and Growth Cone Collapse

Incubation with 100 nM rapamycin reduces Sema3A-induced collapse (a). Rapamycin alone did not induce collapse above control. In combination with Sema3A, the majority of collapse was inhibited. (b) The collapse induced by 1 μM lysophosphatidic acid (LPA) was not reduced by ribosome inhibition with rapamycin.

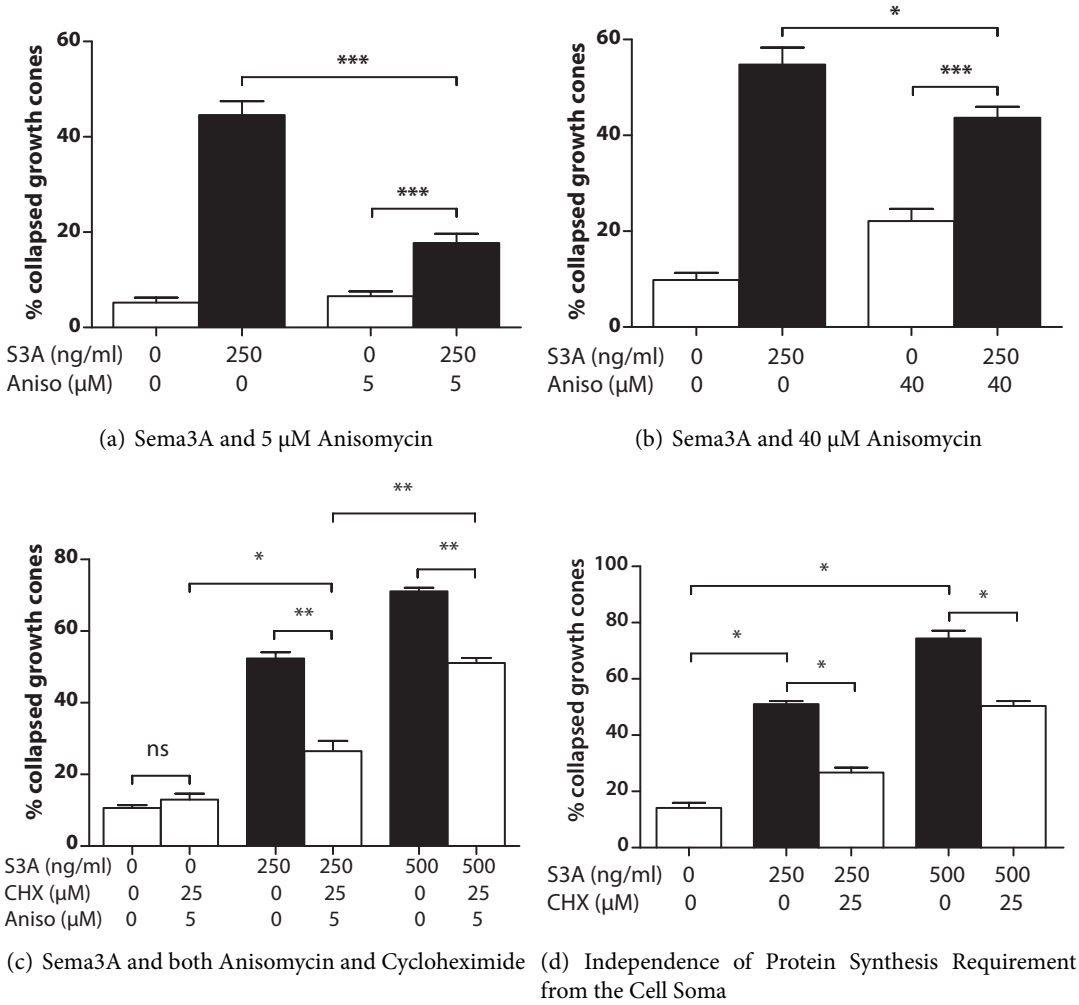

(a) Sema3A and 5 μM Anisomycin

(b) Sema3A and 40 μM Anisomycin

(c) Sema3A and both Anisomycin and Cycloheximide

(d) Independence of Protein Synthesis Requirement from the Cell Soma

Figure 3.4: Anisomycin and Residual Sema3A-induced Collapse

(a) 5 μM anisomycin had similar effects on Sema3A-induced collapse as 25 μM cycloheximide. A residual level of Sema3A-induced collapse remained even in the presence of 5 μM anisomycin. (b) Use of 40 μM anisomycin increased extent of inhibitor-induced collapse relative to 5 μM anisomycin. This increased concentration neither abolished nor reduced the extent of residual Sema3A-induced collapse in the presence of protein synthesis inhibitors, and nor did (c) combining cycloheximide and anisomycin, in the presence of either 250 or 500 ng/ml Sema3A, and this effect was independent of the cell body (d).

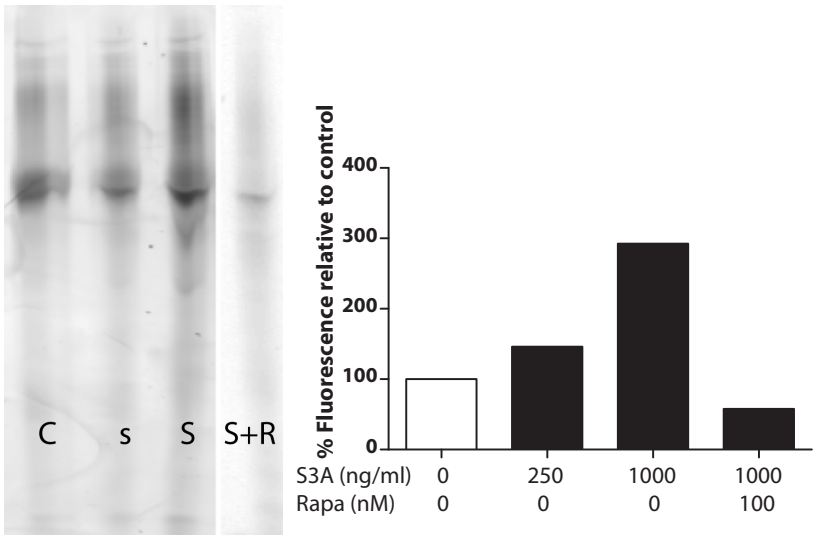

(a) Fluorescence Image of Gel (b) Fluorescence Intensity per Lane

Figure 3.5: AHA-TAMRA Labelling of Protein Synthesis post-Sema3A

(a) The fluorescence of TAMRA-labelled newly synthesised axonal proteins after 1 hour's exposure to control (C), 250 ng/ml Sema3A (s), 1000 ng/ml Sema3A (S) and both 1000 ng/ml Sema3A and 100 nM rapamycin (S+R). There was some axonal protein synthesis in control conditions, which increased little after exposure to 250 ng/ml Sema3A, rising significantly after the application of 1000 ng/ml. The co-application of 100 nM rapamycin reduced protein synthesis to below that of control. (b) Quantification of fluorescence intensity in each lane.

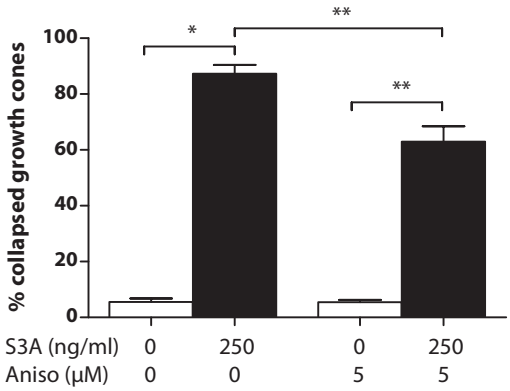

Figure 3.6: The Influence of Low NGF upon Sema3A-induced Collapse

In the absence of Sema3A, collapse remained low in spite of decreased NGF concentrations (10 ng/ml). The presence of Sema3A induced more extensive collapse than in cultures grown in 80 ng/ml NGF. This effect was refractive to protein synthesis inhibition. Anisomycin inhibited some collapse, but the majority of Sema3A-induced collapse was refractive to anisomycin at 10 ng/ml NGF.

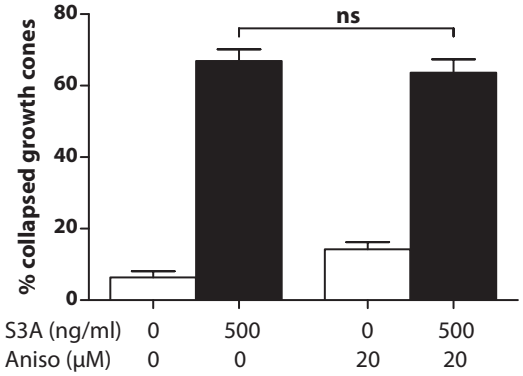

Figure 3.7: The Effects of 10 ng/ml NGF upon Protein Synthesis-Dependence of 500 ng/ml Sema3A-induced Collapse

When two differences in methodology which individually affect collapse were combined, lower NGF and higher Sema3A concentrations, the effect of protein synthesis inhibition upon Sema3A-induced collapse was reduced to insignificance.

The degree of collapse induced by a range of Sema3A concentrations was also assessed, from 67.5 ng/ml to 1000 ng/ml, in the presence of 80 ng/ml NGF and either 20 μM anisomycin or 100 nM rapamycin. This was performed using the same batches of Sema3A and NGF for each experiment (Figure 3.8). Both anisomycin and rapamycin reduced the extent of growth cone collapse induced by Sema3A concentrations ranging from 67.5 ng/ml to 625 ng/ml ($p<0.05$), but with higher Sema3A concentrations neither inhibitor reduced collapse. The effects of rapamycin and anisomycin were broadly similar at all Sema3A concentrations studied. The overall position and shape of the dose–response curve was similar when independent batches of Sema3A and NGF were tested together (from the same suppliers; data not shown).

Local protein synthesis increases with Sema3A concentration As applied Sema3A concentration increased beyond 500 ng/ml, the PS-dependent collapse effect decreases both as a proportion of the total and as an absolute effect (Figure 3.8). There are two non-exclusive explanations for this: either that the PS-dependent and -independent collapse effects 'mask' one another, or that sufficient stimulation of the PS-independent pathway leads directly or indirectly to inhibition of the PS-dependent pathway, as Sema3A and NGF effects on motility interact through the PI3K pathway (Dontchev and Letourneau, 2002), raising the possibility that overstimulation of PTEN by Sema3A (Chadborn et al., 2006) may inhibit mTOR-dependent synthesis (Gingras et al., 2001).

3.2.2 PS-independent collapse is found in *Xenopus* RGC axons

Extensive Semaphorin-3A–induced *Xenopus* RGC axon growth cone collapse is refractory to rapamycin PS-independent collapse was not reported by Campbell and Holt (2001), using *Xenopus* RGC axons. The collapse experiment of Campbell and Holt (2001) with 1000 ng/ml Sema3A was repeated in the presence or absence of 100 nM rapamycin (Figure 3.9). Rapamycin did not reduce the extent of collapse significantly (93% *vs* 84%, $p=0.174$). This shows that the PS-independent collapse effect of Sema3A is not peculiar to *Gallus gallus* DRG axons.

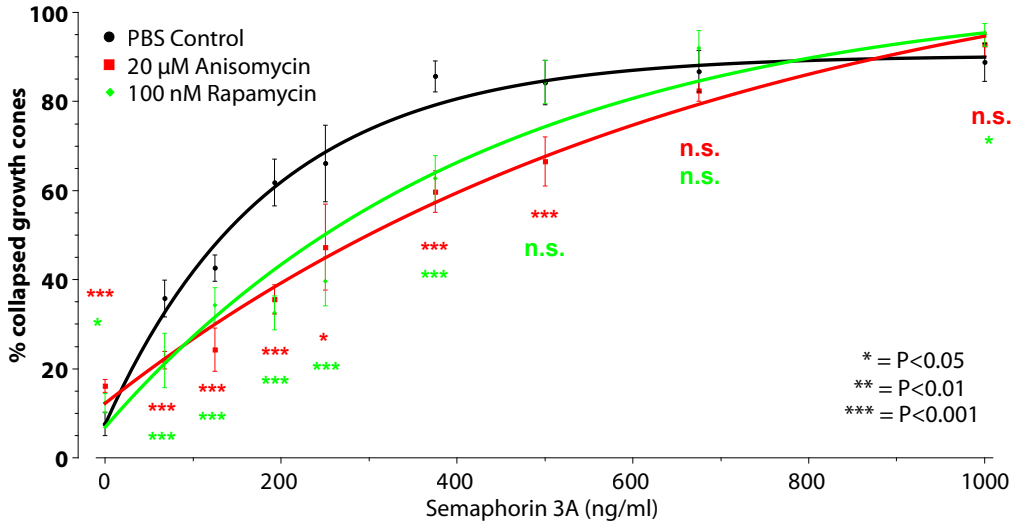

Figure 3.8: Dose response curve of chick DRG growth cones to Semaphorin-3A
The dose-response curve of axon growth cone collapse to 0–1000 ng/ml Sema3A in the presence of PBS control (black), anisomycin (red) or rapamycin (green). Both anisomycin and rapamycin reduce but do not eliminate Sema3A-induced collapse up to 500 ng/ml.

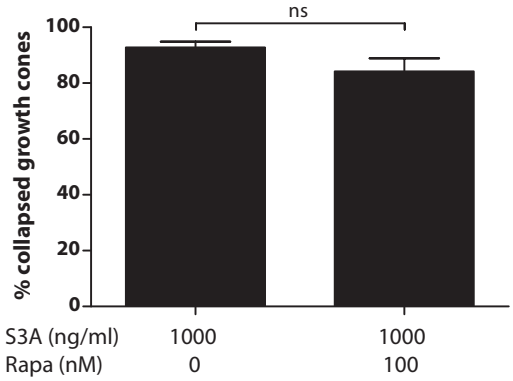

Figure 3.9: *Xenopus lævis* RGC Axons, Rapamycin and Sema3A
Replicating the conditions of (Campbell and Holt, 2001) but increasing the concentration of Sema3A to 1000 ng/ml, 100 nM rapamycin no longer reduced the extent of Sema3A-induced growth cone collapse.

Protein synthesis-independent collapse is caspase-independent Caspases are known effectors of apoptosis, and caspase-3 in particular is activated downsteam of LPA and p38 MAPK in LPA-induced growth cone collapse (Campbell and Holt, 2003). I applied a pan-caspase inhibitor, 25 μM Z-VAD-FMK, as Sema3A-induced apoptosis involves caspases (Gagliardini and Fankhauser, 1999). Application of Z-VAD-FMK concurrently with rapamycin did not reduce the extent of growth cone collapse (Figure 3.10). Failure to inhibit collapse with a caspase inhibitor implies that Sema3A-induced apoptotic mechanisms are not the cause of protein synthesis-independent collapse.

Axonal growth cones recover from collapse induced by 500 ng/ml Semaphorin-3A DRG explants were incubated with 125 or 500 ng/ml Sema3A for 30–390 minutes before fixation (Figure 3.11). Both concentrations induced maximal levels of collapse after 30 minutes (45% and 73%, respectively), and the extent of collapse fell thereafter to the last time-point (14% and 26%, respectively). The longest incubation period (6½ hours) reduced collapse almost to control levels, beyond the reductions achieved by protein synthesis inhibition.

Growth cones can adapt after exposure to 500 ng/ml Sema3A although on a longer time-scale to 125 ng/ml. Whereas growth cones exposed to 500 ng/ml recovered progressively at each time-point ($p \leq 0.01$ for all time-points), those exposed to 125 ng/ml recovered from the majority of collapse by the 2½-hour time-point. This shows that PS-independent collapse is a mostly reversible process and unlikely to be a neurotoxic process. The difference in speed of recovery could be due to different collapse-inducing processes, but it may simply be due to the increase in stimulation. Receptor endocytosis has been proposed as a mechanism of adaptation (Piper et al., 2005), and it is of note that although neuropilin-1 and L1CAM are endocytosed after stimulation with Sema3A, there is no evidence that plexin-A molecules are endocytosed with them (Castellani et al., 2004).

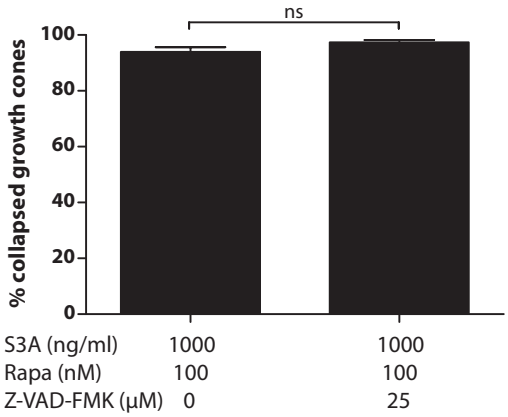

Figure 3.10: The Involvement of Caspases in Synthesis-Independent Collapse
The pan-caspase inhibitor Z-VAD-FMK was applied with 100 nM rapamycin but did not reduce the collapse induced by 1000 ng/ml Sema3A.

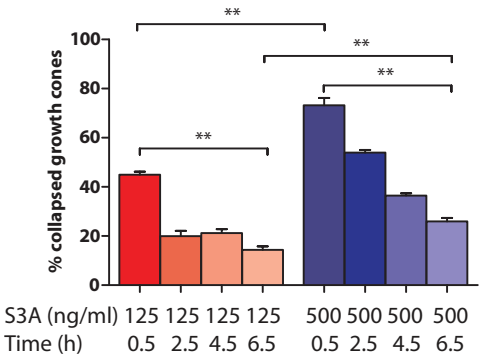

Figure 3.11: Recovery in Differing Concentrations of Semaphorin-3A
Axons exposed to low (125 ng/ml) and high (500 ng/ml) Sema3A concentrations recovered the majority of their spread morphology over a period of hours, demonstrating reversibility of collapse.

3.2.3 Growth cone collapse involves the GSK-3β pathway at both low and high Sema3A concentrations

First, the extent of neuropilin-1 involvement in Sema3A-induced collapse was confirmed by incubating DRG explants in neutralising anti–neuropilin-1 antibodies for 30 min prior to addition of Sema3A (Figure 3.12). While 500 ng/ml Sema3A alone induced 82% collapse, the antibody reduced collapse to control levels. Collapse activity refractory to PS inhibition are inhibited by function-blocking anti–neuropilin-1 antibodies, confirming that the Sema3A-induced collapse requires functional neuropilin-1.

GSK-3β activity is required for Sema3A-induced growth cone collapse (Eickholt et al., 2002), so its relationship with mTOR-dependent growth cone collapse was examined. Inhibition of GSK-3β activity with 10 mM lithium chloride reduced the extent of collapse induced by 500 ng/ml Sema3A (83% *vs* 49%, $p<0.01$), confirming the role for GSK-3β in Sema3A signalling (Figure 3.13(a)). This reduction also summated with that due to rapamycin when both inhibitors were present. Moreover, the reduction caused by inhibiting PTEN upstream of GSK-3β with 100 nM bpV(pic) also summated with that of rapamycin (Figure 3.13(b)).

Additional specific inhibitors of GSK-3β (SB216763 and AR-A014418) were also tested. In the presence of 250 ng/ml or 500 ng/ml Sema3A and 80 ng/ml NGF, the combination of SB216763 and rapamycin reduced collapse more than either alone (Figure 3.16(b)). In the presence of 500 ng/ml Sema3A neither an increased concentration of SB216763 nor the inhibitor AR-A014418, an alternative inhibitor, reduced collapse further (Figure 3.14). In the presence of a lower NGF concentration (10 ng/ml), the proportion of collapse inhibited by SB216763 and AR-A014418 was approximately halved at both low and high Sema3A concentrations (250 ng/ml, 700 ng/ml; Figure 3.17). These experiments indicate a significant role for GSK-3β activity independently of the mTOR pathway.

Control experiments confirmed that the GSK-3β inhibitors did not cause growth cone collapse in the absence of Sema3A (Figure 3.15(a)). It was also confirmed that the GSK-3β inhibitor SB216763 reduced collapse in transected axons to the same extent as intact axons (Figure

3.15(b)).

3.3 Signalling Upstream of Sema3A, Synthesis-Dependent Growth Cone Collapse

3.3.1 The Role of NO/cGMP

Nitroarginine inhibition of collapse Is not additive with rapamycin Castellani et al. (2002) demonstrated that L1CAM, in addition to neuropilins and plexins, is required for Sema3A-induced repulsion through the NO-cGMP pathway. Cyclic nucleotide-gated channels are opened by cGMP to allow calcium influx, inducing protein synthesis-dependent turning (Yao et al., 2006). Nitric oxide synthase (NOS) was inhibited with nitroarginine in the presence and absence of rapamycin to examine its relationship with mTOR-dependent collapse. When added to cultures prior to the addition of 500 ng/ml Sema3A, nitroarginine and rapamycin each reduced growth cone collapse to a similar extent, but produced no further inhibition of collapse when combined ($p<0.05$, Figure 3.16(a)). The two inhibitors may block a NO-cGMP–dependent pathway, which is required for mTOR-dependent, but not mTOR-independent, growth cone collapse.

Similar effects were found when nitroarginine and lithium chloride were replaced by *L*-propyl-*N*-arginine (NPA) and SB 216763, respectively (Figure 3.16(b)). As GSK-3β activity itself inhibits mTOR activity (Inoki et al., 2006), its inhibition would increase PS and would not be expected to reduce PS-dependent collapse. Overall collapse falls, thus GSK-3β activity is involved in synthesis-independent collapse. NOS inhibition blocks collapse independently of GSK-3β activity, consistent with involvement in PS-dependent collapse.

GSK-3β activation inhibits mTOR Lastly, the activation and interaction of the mTOR and GSK-3β pathways were examined more directly by quantitative immunofluorescence analysis of growth cones in the presence of NOS, mTOR and GSK-3β inhibitors (Figure 3.18). Application of 250 ng/ml Sema3A caused an increase in p-4EBP1 fluorescence ($p<0.05$) within 1 hour,

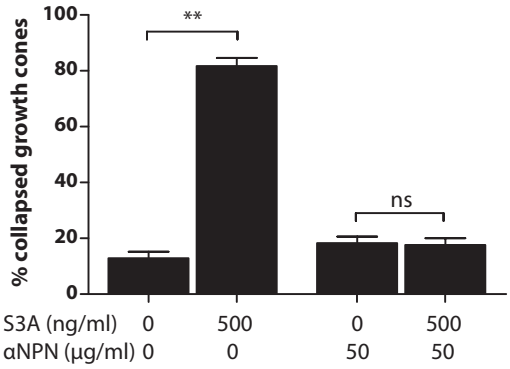

Figure 3.12: The Requirement for Neuropilin-1 Function in Sema3A-induced Collapse
The majority of axons exposed to 500 ng/ml Sema3A collapsed within 30 minutes. Prior incubation with 50 mg/ml α-NPN-1 reduced 500 ng/ml Sema3A-induced collapse to control levels, entirely blocking the collapse effects of 500 ng/ml Sema3A.

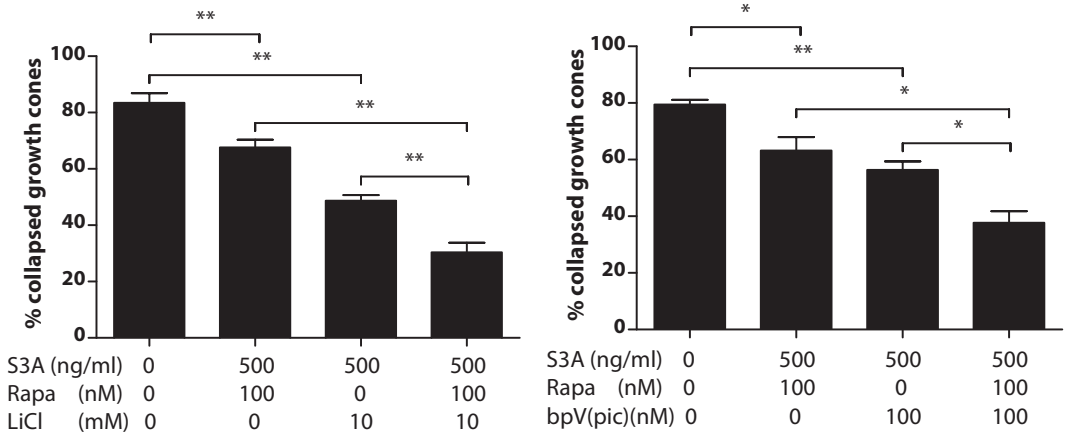

(a) Rapamycin and Lithium Chloride Effects upon Growth Cone Collapse

(b) Rapamycin and bpV(pic) Effects upon Growth Cone Collapse

Figure 3.13: The Combined Effects of Inhibiting the PTEN/GSK Axis and mTOR
100 nM rapamycin marginally inhibited Sema3A-induced growth cone collapse, as did the GSK-3β inhibitor LiCl (a) and the PTEN inhibitor bpV(pic) (b). The effects of inhibiting mTOR and either GSK-3β or PTEN on Sema3A-induced collapse were cumulative. Inhibition of both the mTOR and the PTEN/GSK-3β pathways inhibited growth cone collapse further than either alone.

indicating activation of the mTOR pathway (Figure 3.18(a)). Consistent with this, application of rapamycin with Sema3A reduced p-4E-BP1 fluorescence below control levels ($p<0.0001$). Conversely, however, application of SB216763 with Sema3A significantly increased fluorescence above control levels (Figure 3.18(a)), suggesting that GSK-3β activity is antagonistic to mTOR activation in this system.

Inhibition of NOS activates GSK-3β and inhibits mTOR Application of 250 ng/ml Sema3A reduced growth cone pGSK-3β fluorescence, indicating GSK-3β activation. This response was refractory to rapamycin, thus GSK-3 activation is upstream of, and inhibitory to, mTOR activity (Figure 3.18(b)). However, despite collapse data suggesting that NOS plays a role in the mTOR-dependent pathway (Figures 3.16(a) and 3.16(b)), the fluorescence data imply that NOS activates GSK-3β ($p<0.001$) and thus inhibits mTOR activity ($p<0.05$). Together, Sema3A activates GSK-3β in a NOS-dependent fashion, and GSK-3β activity partially inhibits mTOR activation downstream of Sema3A.

3.3.2 Erk1/2 and Synthesis-Dependent Collapse

Erk1/2 inhibition does not affect Sema3A-induced mTOR activity Campbell and Holt (2003) demonstrated that Sema3A-induced collapse was Erk1/2 (p42/44 MAP kinase)-dependent, and postulated that Erk1/2 induces mTOR activity downstream of Sema3A, an established activity of Erk1/2 (Winter et al., 2011). PI3-kinase is unlikely to transduce mTOR activity downstream of Sema3A, as Sema3A induces PTEN activity, opposing PI3-kinase (Chadborn et al., 2006) and I have demonstrated an apparent opposition of the PTEN- and mTOR-involving pathways (Figure 3.18) downstream of Sema3A. Therefore, Erk1/2 are prime candidates for mTOR activation downstream of Sema3A.

mTOR activity was measured *via* phosphorylation of eIF4E-BP1, as previously, and I attempted to inhibit this phosphorylation with 40 μM PD98059 (Figure 3.19(a)), a highly specific inhibitor of Erk1/2, known to inhibit Sema3A-induced growth cone collapse (Campbell and Holt, 2003). Addition of 250 ng/ml Sema3A increased the fluorescence signal from p4EBP1 by 43% (Figure 3.19(a), $p=0.0005$) within 10 minutes, as expected. However, incubation with

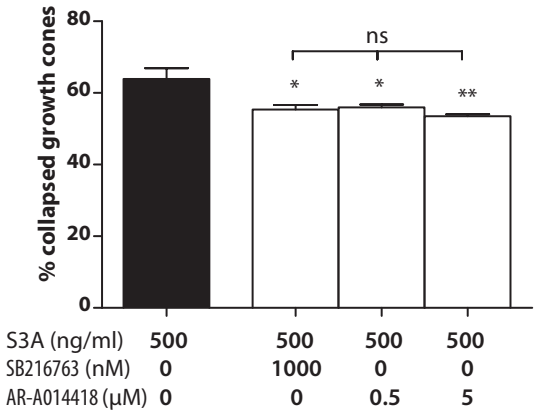

Figure 3.14: Increasing Concentrations of GSK-3β Inhibitors

The effects of high concentrations and alternate GSK-3β inhibitors, both more specific than lithium chloride, on Sema3A-induced growth cone collapse. The four-fold increase in SB 216763 concentration and both concentrations (0.5 and 5 μM) of AR-A014418 reduce the extent of collapse, but the effects of higher concentrations of inhibitor, a more specific inhibitor or both do not differ significantly, and the extent of collapse remains above 50% in all cases. The reduced inhibitory effect may be due to toxicity of such concentrations or an increased role of other pathways in the presence of 80 ng/ml NGF.

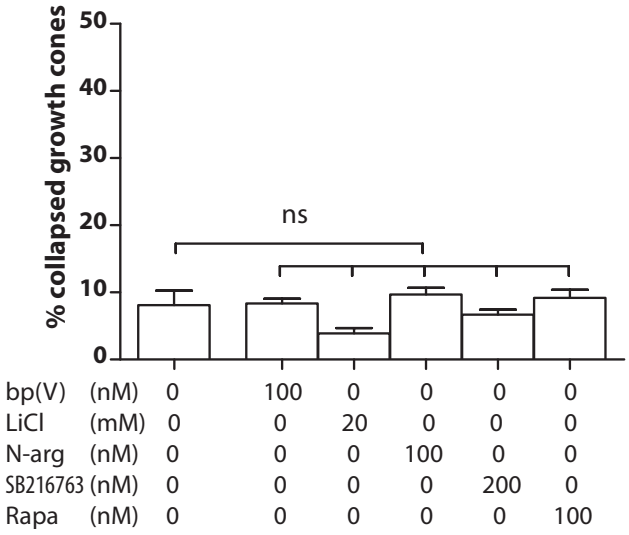

(a) Collapse-Inducing Effects of Inhibitors Alone

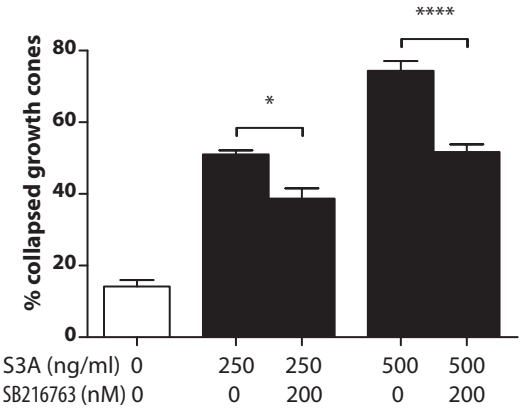

(b) GSK Inhibition in Isolated Axons

Figure 3.15: Control Assays for GSK-3β Activity

(a) Control experiment confirming growth cone collapse is not induced by inhibitors of PTEN (bp(V)pic, 100nM) and GSK-3β (lithium chloride, LiCl, 20mM; SB216763, 200nM; AR-A014418, 0.5μM), nor by the combination of rapamycin and SB216763, nor by DMSO at the solvent concentration used for the latter reagents *(1st column)*. (b) Control experiment confirming that the GSK-3β inhibitor SB216763 reduces Sema3A-induced collapse of growth cones of transected axons.

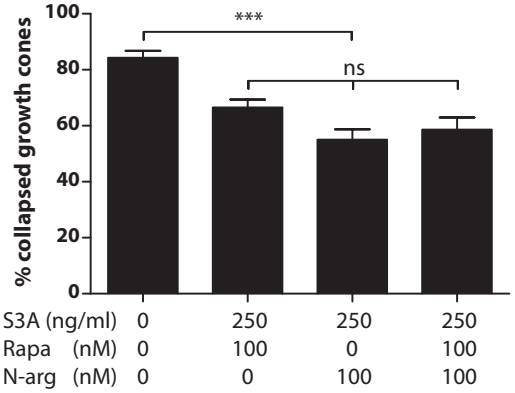

(a) Lithium Chloride and Nitroarginine

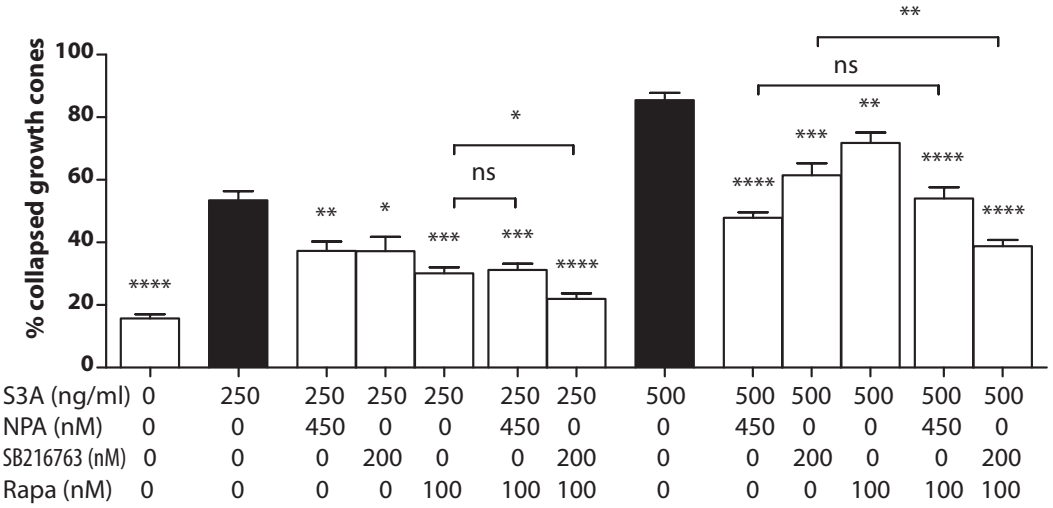

(b) SB 216763 and NPA

Figure 3.16: Inhibiting NOS, mTOR and GSK-3β

(a) Nitroarginine (N-arg), an inhibitor of NOS, marginally reduces the collapse, as does rapamycin, but the effects are not cumulative. (b) Substituting lithium chloride and nitroarginine for SB 216763 and *N*-propylarginine, respectively, demonstrated similar effects to the original inhibitors.

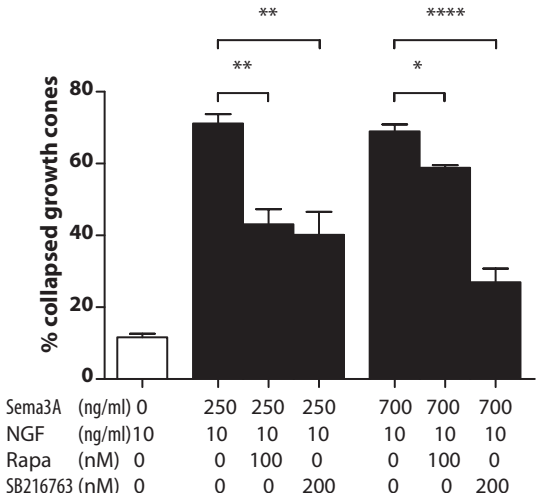

Figure 3.17: The Effect of GSK-3β Inhibition on Sema3A-Induced Collapse in the Presence of 10 ng/ml NGF

Using a lower NGF concentration (10 ng/ml), collapse induced by a low (250 ng/ml) Sema3A concentration is approximately halved by SB216763 (200 nM) or AR-A014418 (0.5 μM), and that induced by a high (700 ng/ml) Sema3A concentration is reduced still further by these inhibitors.

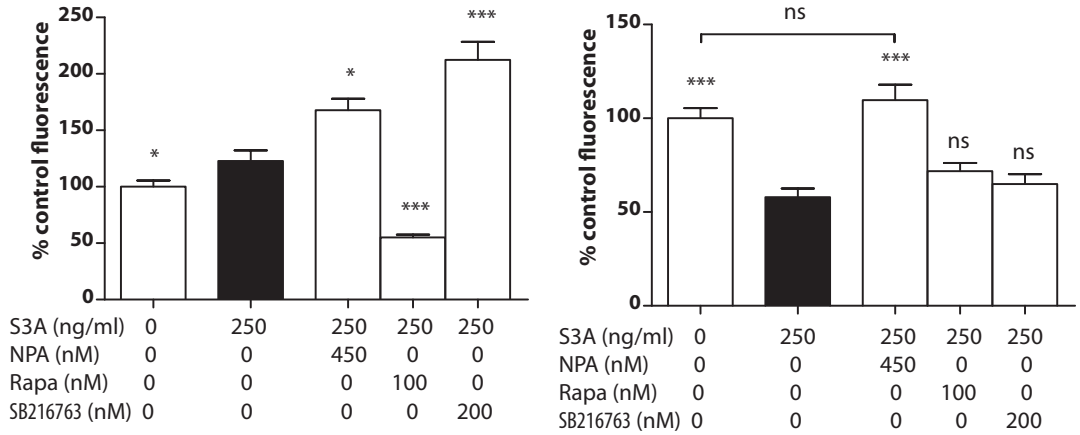

(a) eIF4E-BP1 Phosphorylation

(b) GSK-3β Phosphorylation

Figure 3.18: The Effects of NOS, mTOR and GSK-3β Inhibition on mTOR and GSK-3β Activation

Sema3A activates mTOR indicated by eIF4E-BP1 phosphorylation (a), and GSK-3β through dephosphorylation (b). NOS inhibition increases mTOR phosphorylation an effect similar to GSK-3β inhibition. Rapamycin inhibits eIF4E-BP1 phosphorylation, as expected, but has no effect upon GSK-3β activation.

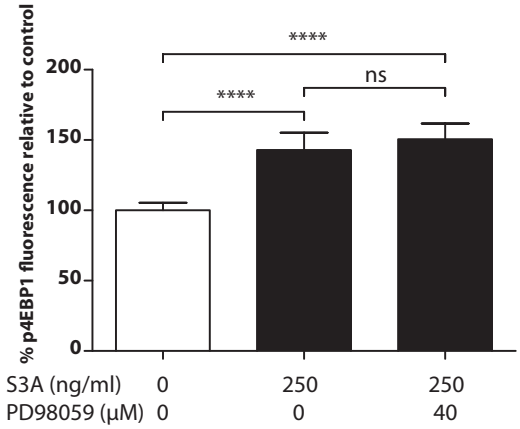

(a) PD98059 Effects upon eIF4E-BP1 Phosphorylation

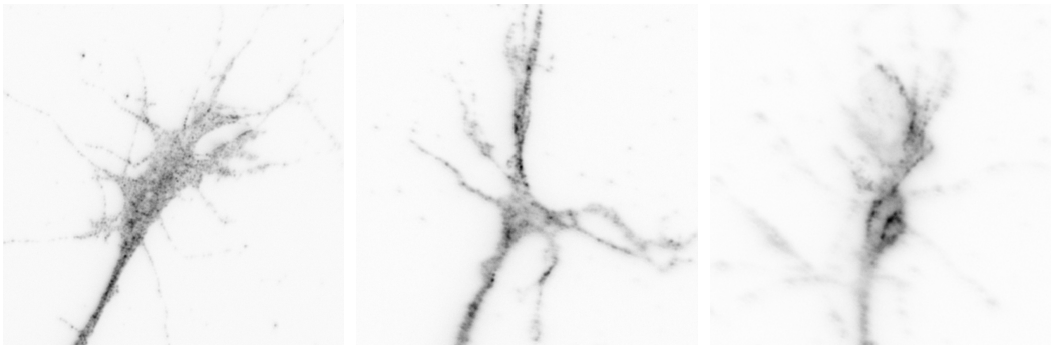

(b) (c) (d)

Figure 3.19: The Erk1/2 Inhibitor, PD98059, Does Not Affect eIF4E-BP1 Phosphorylation
(a) Inhibition of Erk1/2 with 40 μM PD98059 had no observed effect upon Sema3A-induced mTOR activity. (b-d) Example images *(fluorescence intensity normalised and inverted)* of p4EBP1 fluorescence in growth cones exposed to the same three conditions.

both Sema3A and 40 μM PB98059 did not alter eIF4E-BP1 phosphorylation beyond the effects of Sema3A alone (143% versus 151% of control, *p=0.650*). From this, I conclude that mTOR activity is not downstream of Erk1/2 activation in chick DRG growth cones.

3.4 Discussion

Sema3A is one of several guidance cues that have been linked to induction of rapid PS and degradation (Campbell and Holt, 2001; Wu et al., 2005; Brunet et al., 2005; Leung et al., 2006; Li et al., 2009). However, the role of PS within the growth cone has been controversial, particularly regarding its necessity for outgrowth and guidance (Eng et al., 1999; Campbell and Holt, 2001; Piper and Holt, 2004; Wu et al., 2005; van Kesteren et al., 2006; Roche et al., 2009). To resolve apparent differences between laboratories the role of local PS in Sema3A-induced growth cone collapse was reinvestigated.

3.4.1 GSK-3β- and Synthesis-Dependent Collapse

The data show that three structurally unrelated PS inhibitors reduce, but do not eliminate, Sema3A-induced collapse, and both reductions in NGF concentration and increases in Sema3A concentration amplify the PS-independent response. These findings suggest the presence of at least two pathways for Sema3A-induced collapse, which at concentrations greater than 500 ng/ml produce maximal collapse levels, and which function co-operatively across a wide concentration range. The data indicate that the PS-dependent pathway is relatively more active at lower Sema3A concentrations. This model accounts for the findings of Campbell and Holt (2001), where mTOR inhibition blocked turning and collapse responses of *Xenopus* retinal axon growth cones to Sema3A almost to base-line levels, and those of Roche et al. (2009) who used a low concentration (10 ng/ml) of NGF. Moreover, Nédelec et al. (2012) have shown that while certain motor neuron subtypes are more susceptible to PS-dependent Sema3A-induced collapse than others, all tested subtypes undergo PS-independent collapse in the presence of high Sema3A concentrations. A similar concentration-dependence of PS inhibition has also been noted in mammalian (mouse) DRG growth cones (Li et al., 2004). Further, use of 500

ng/ml Sema3A and 10 ng/ml NGF, as in Roche et al. (2009), reduced the collapse-inhibiting effects of PS inhibitors to insignificance.

Neuropilin-1 is a Sema3A co-receptor which binds to plexins A1–4 (Takahashi et al., 1999) and L1CAM (Castellani et al., 2000). As anti–neuropilin-1 antibodies abolished collapse responses in these experiments to control levels, collapse-inducing pathways must require neuropilin-1 and its binding partners. The GSK-3β pathway is involved in plexin-dependent growth cone collapse (Eickholt et al., 2002; Chadborn et al., 2006), and these data indicate that this is PS-independent. Thus GSK-3β inhibition with lithium chloride not only reduced Sema3A-induced collapse, but its combination with rapamycin reduced collapse further than either agent alone.

The residual collapse over control levels, also seen using combinations of cycloheximide/anisomycin (Figure 3.4(c)) and SB216763/rapamycin (Figure 3.16(b)), and at high Sema3A concentrations in the presence of GSK-3β inhibitors (Figure 3.14), may be attributable to the operation of further GSK-3β- and mTOR-independent pathways. It is further noted that different levels of collapse are sometimes obtained using the same reagent concentrations in separate experiments. This is likely to be caused by inevitable biological variation between different DRG cultures and by batch variation in the bioactivity of Sema3A.

Examination of GSK-3β and 4E-BP1 phosphorylation levels, as reporters respectively of the GSK-3β- and mTOR-dependent pathways (Goode et al., 1992; Gingras et al., 1999), showed that while mTOR inhibition did not influence GSK-3β activation, GSK-3β inhibition promoted mTOR activity. This suggests that the GSK-3β pathway may regulate mTOR in the growth cone, but not *vice versa*. A similar GSK-3β/mTOR antagonism has also been identified in the Wnt signalling pathway (Inoki et al., 2006). Since GSK-3β activity dominates at high Sema3A concentrations, growth cone mTOR activity may be correspondingly reduced, and it will be interesting to assess this possibility experimentally.

While it is unknown how these two pathways are deployed relatively during neural development *in vivo*, it can be speculated that different neuronal sub-types may respond through either one or both of these pathways. There is evidence, for example, that Sema3A-responsive neurons differ according to whether neuropilin-1 associates with a plexin-A or L1CAM, and in the downstream consequences (Bechara et al., 2008). The possibility of divergent Sema3A signalling pathways also has the attraction of explaining apparent contradictions in studies showing that RhoA activity is either critical for Sema3A repulsive guidance (Wu et al., 2005) or not (Jin and Strittmatter, 1997).

These data suggest that combinations of mTOR-dependent and mTOR-independent signalling pathways may facilitate axon navigation using adaptive responses (Piper et al., 2006), sharpening responsivity to repulsive gradients of the same guidance cue. Simultaneously, this would enable high concentrations of repulsive molecules to define 'no-go' areas prohibiting entry, for example, to *Xenopus* caudal tectum by retinal axons. Thus, the concentration-dependent activation of distinct signalling pathways can increase the information content of a single cue and may contribute to the general mechanism of cue-mediated axon behaviour *in vivo*.

3.4.2 Upstream of PS-Dependent Collapse

The data above show that collapse involves at least two pathways, mTOR/PS- and GSK-3β–dependent (Figure 3.20). But the signalling cascade between Sema3A and mTOR/PS in growth cone collapse is not fully elucidated. The work of Castellani et al. (2002) demonstrated that Sema3A signalling involves nitric oxide, and Campbell and Holt (2003) demonstrated a dependence on Erk1/2. The involvement of NOS and Erk1/2 in mTOR activation was therefore investigated.

Both NOS and GSK-3β inhibition reduce Sema3A-induced growth cone collapse. The effect of NOS inhibition is not additive with that of rapamycin, whereas that of GSK-3β inhibition is. This leads to the conclusion that NOS is critical upstream of PS-dependent collapse. This would explain the observations by Bechara et al. (2008) that L1-CAM, as well as a plexin, can combine

with neuropilin-1 to form a novel receptor complex for Sema3A. Such a plexin-independent mechanism would explain the origin of a second, independent mechanism of growth cone collapse.

However, immunofluorescence assays of growth cone collapse pathways directly demonstrate that NOS is involved in GSK-3β activation and a reduction in mTOR activity, suggesting that NOS is involved in PS-independent collapse activity. GSK-3β activity reduces mTOR activity, but the reverse was not observed. This finding of NOS activity activating GSK-3β has not been demonstrated before, to the writer's knowledge; eNOS in the endothelium induces the opposite effect, inhibiting GSK-3β through Akt and inducing NFAT transcription factor activity (Drenning et al., 2009).

These findings suggest a more complex interaction between mTOR- and GSK-3β–dependent collapse than previously assumed, as NOS behaves upstream of mTOR/PS in collapse assays, yet upstream of GSK-3β using immunofluorescence. It is possible that NOS plays a role in both, and that the more extensive phosphorylation of 4E-BP1 does not translate into more extensive collapse effects. The pathways may also be separated spatially (for review, see Jung et al. (2011)), an aspect that 'whole growth cone' immunofluorescence does not illuminate.

The immunofluorescence assay was applied similarly to mTOR activity in the presence of an Erk1/2 inhibitor, PD98059. Inhibiting Erk1/2 has no effect upon eI4E-BP1 phosphorylation downstream of Sema3A. However, whether Erk1/2 participates in Sema3A-induced collapse of *Gallus* growth cones rather than than only *Xenopus* growth cones was not confirmed. Erk1/2 is a known effector of RhoA downstream of plexin-B1 (Basile et al., 2007), so Erk may be an effector of RhoA rather than required for its local synthesis. And finally, it may be that mTOR is not a major point of regulation downstream of Sema3A, but that its kinase activity may be controlled by the localisation and/or availability of substrates.

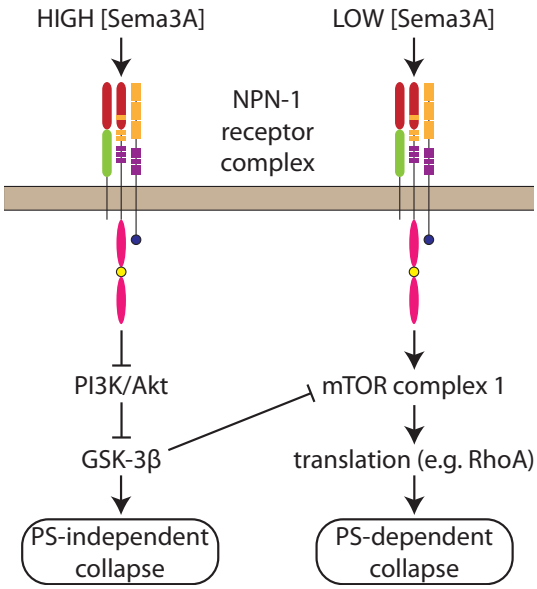

Figure 3.20: The Two Proposed Mechamisms of Collapse Downstream of Sema3A
Schematic of the proposed predominant pathways mediating PS-dependent and -independent growth cone collapse in response to high *(left)* and low *(right)* Sema3A concentrations.

Chapter 4

The Downstream Effectors of Nogo-A

4.1 Introduction

Although the most axon growth cone repulsive region of Nogo-A is the 66-amino-acid loop region, Nogo-66 (Oertle et al., 2003*a*), it is also present in the isoforms, Nogo-B and -C, as part of the reticulon homology domain (RHD). Nogo-B and -C, however, do not inhibit axon growth to a similar extent *in vivo*. This suggests that other regions of the Nogo-A molecule are necessary for Nogo-66's *in vivo* activity. The Nogo-A-specific *N*-terminal domain contains a growth cone repulsive domain, NiG-δ20, (Oertle et al., 2003*a*) also known as Nogo-δ20, whose mechanism of action is more elusive, although it also inhibits fibroblast spreading.

I investigated the inhibitory activities of Nogo-A, focusing on the less well-known Nogo-δ20 and the role of local protein synthesis in Nogo-A signalling. So far, Nogo-δ20 signalling is known to involve integrins (Hu and Strittmatter, 2008), Rho-kinase activity and Pincher-mediated endocytosis of the receptors (Joset et al., 2010). The collapse-inducing pathways downstream of the 66-amino-acid loop, Nogo-66, were also investigated, searching for parallels and convergence in their modes of signalling. This information may shed light on the origins and roles of the two domains, and future pharmacological targets.

4.2 Nogo-A and Local Protein Synthesis

4.2.1 Nogo-δ20 Causes Protein Synthesis-Dependent Growth Cone Collapse

Nogo-δ20–induced collapse is mTOR-dependent Preliminary data and previous data (Oertle et al., 2003*a*) suggested that 150 nM Nogo-δ20 is sufficient to cause 40–50% collapse of chick DRG growth cones. Given the known role of mTOR and protein synthesis (PS) in several guidance cues, whether Nogo-A shared this requirement was also examined. The dependence of the collapse on mTOR activity was assessed using 100 nM rapamycin (Figure 4.1(a)). 150 nM Nogo-δ20 caused 45% collapse after 30 minutes *vs* 15% control ($p<0.0001$). In the presence of 100 nM rapamycin, Nogo-δ20–induced collapse fell to 23% ($p<0.001$), not significantly different from rapamycin alone (21%). Inhibition of mTOR complex 1 reduces the collapse-inducing activity of 150 nM Nogo-δ20 to insignificance.

Nogo-δ20–induced collapse is PS-dependent mTOR complex 1 does not solely direct cap-dependent PS, so the above experiment was repeated with 10 μM anisomycin to directly inhibit the ribosome. The results were similar (Figure 4.1(b)); Nogo-δ20 induced 52% collapse over control (12% *vs* 52%, $p=0.00451$), whereas co-application of anisomycin reduced the difference to insignificance (19% *vs* 19%, $p=0.301$).

Collapse dependence upon mTOR is not dose-dependent It was demonstrated in Chapter 3 that, given sufficient stimulation by Sema3A, PS activity was no longer required to induce full growth cone collapse. Sema3A-induced collapse was maximal and ceased to be PS-dependent at 3–4 'collapsing units' (Figure 3.8). To investigate whether this held true for Nogo-δ20–induced collapse, the initial experiment was repeated with 450 nM (3× greater concentration, Figure 4.1(c)) and 900 nM (6×, Figure 4.1(d)).

Nogo-δ20–induced collapse showed a dose-dependent increase in effect However, whereas Sema3A induced 90%+ collapse, increasing the concentration of Nogo-δ20 by a factor of three and six increased collapse only marginally (45% *vs* 62% *vs* 65%, Figure 4.1). This was not accompanied by signs of axon degeneration, as seen in high concentrations of Sema3A. Further,

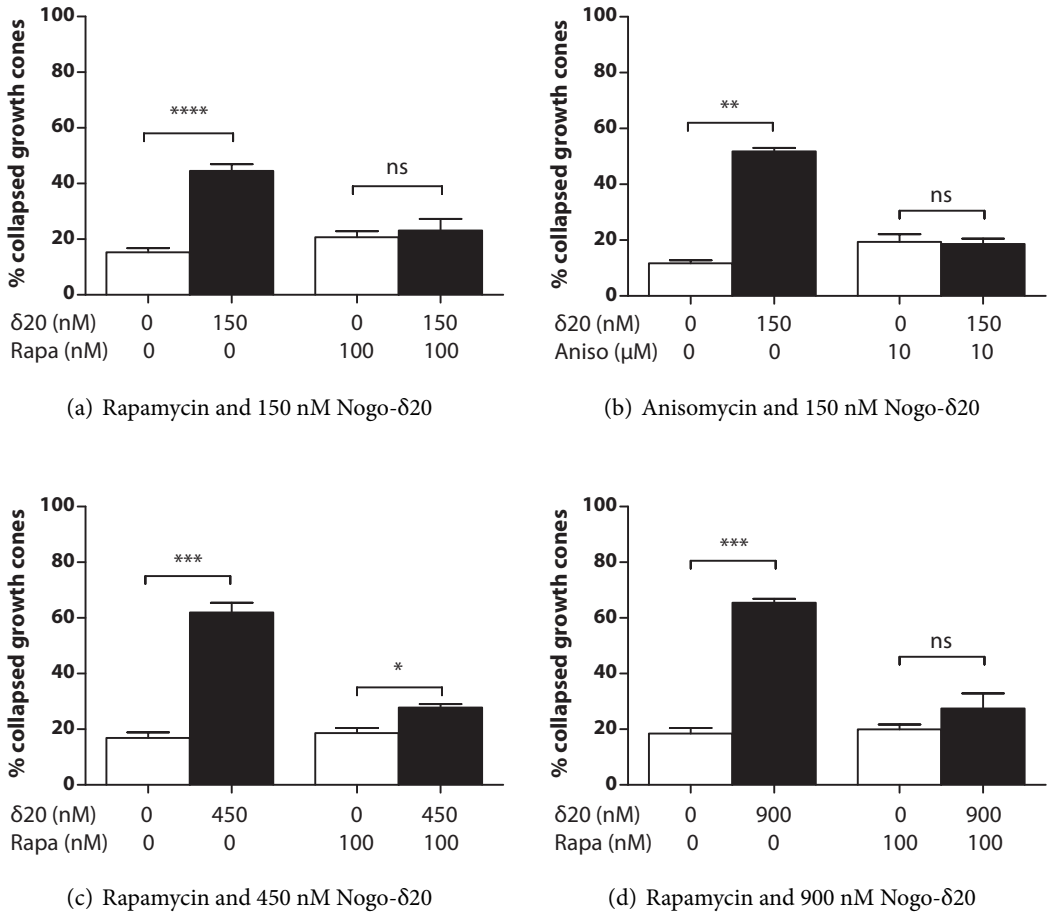

(a) Rapamycin and 150 nM Nogo-δ20

(b) Anisomycin and 150 nM Nogo-δ20

(c) Rapamycin and 450 nM Nogo-δ20

(d) Rapamycin and 900 nM Nogo-δ20

Figure 4.1: The Effects of mTOR and Ribosome Inhibition on Nogo-δ20–Induced Growth Cone Collapse

(a) Nogo-δ20–induced collapse falls to control levels in the presence of rapamycin. This is repeated (b) in the presence of 10 μM anisomycin. 100 nM rapamycin reduces collapse due to 450 nM (c) and 900 nM (d) Nogo-δ20. Only at 450 nM (c) does Nogo-δ20 induce collapse in the presence of rapamycin; this may be a sampling artefact.

the effect of mTOR inhibition on growth cone collapse remained significant at both 450 nM and 900 nM (*p=0.00197* and *p=0.000959*) and the collapse induced by Nogo-δ20 in the presence of inhibitor was marginal at 450 nM (19% *vs* 24%, *p=0.0273*) and not significant at 900 nM (20% *vs* 27%, *p=0.338*). There was little to no Nogo-δ20–induced collapse in the presence of rapamycin at all concentrations tested.

4.2.2 Initial Nogo-δ20–Induced Collapse Is Protein Synthesis-Independent

Nogo-δ20–induced collapse involves a PS-independent phase The experiments just discussed were analysed after 30 minutes, as for Sema3A, and showed no significant evidence of PS-independent collapse. However, growth cones of other species, such as *Xenopus*, attain maximal collapse within 10 minutes and recover extensively within 30 minutes (Campbell et al., 2001) and different collapse mechanisms function over different time-scales (see Figure 3.11). The growth cones were therefore exposed to 150 nM Nogo-δ20 from 2 to 30 minutes with 100 nM rapamycin or control, to examine the time-course of collapse in the presence and absence of the inhibitor.

At time-points 2, 5 and 9 minutes post-exposure, collapse increased to ~30% both in the presence and absence of 100 nM rapamycin; there was no significant difference between the control and rapamycin samples (Figure 4.2). At the 12-minute point and beyond, whilst control collapse increased to 50%, the presence of rapamycin caused collapse to fall to below 20% by the 30-minute time-point (*p<0.01 at 12, 20 and 30 min*). Nogo-δ20–induced collapse therefore involves a less extensive, fast, PS-independent response which reverses within 30 minutes, and a more extensive, PS-dependent response which exerts additional, longer-lived collapse effects after 9 minutes.

4.2.3 Nogo-δ20–Induced Growth Cone Collapse Is Independent of Proteasomal Function

The proteasome is not required for Nogo-δ20–induced growth cone collapse Having established mTOR-dependent PS as critical in Nogo-δ20–induced collapse, the role of the proteasome and ubiquitin-tagged protein degradation was examined. Sema3A-induced axon guidance does

not require proteasomal activity, but lysophosphatidic acid and netrin-1 do (Campbell and Holt, 2001) and further, guidance by netrin-1 requires both PS and proteasomal degradation. Rapamycin was replaced with 25 μM *N*-acetyl-*L*-leucinyl-*L*-leucinyl-*L*-norleucinal (Z-LLnL) to inhibit the catalytic sites of the proteasome (Figure 4.3). Inhibition of the proteasome had no significant effect upon growth cone collapse either with control (16% *vs* 19%, *p=0.100*), or upon the collapse activity of Nogo-δ20 (51% *vs* 47%, *p=0.100*). Therefore the proteasome is not required for Nogo-δ20–induced collapse.

4.2.4 Nogo-66-Induced Growth Cone Collapse Is Independent of Protein Synthesis, but Dependent upon the Proteasome

The ribosome is not required for Nogo-66-induced growth cone collapse Having established a role for PS downstream of Nogo-δ20, PS was inhibited directly with anisomycin and cycloheximide, and *via* mTOR with rapamycin, in the presence of 2 nM Nogo-66, sufficient to cause ~50% collapse under these culture conditions (Figures 4.4(a) and 4.4(b)). Unlike the inhibition of Nogo-δ20 collapse activity, neither cycloheximide and anisomycin combined (53% *vs* 48%, *p=0.6991*), nor rapamycin altered collapse in the presence of 2 nM Nogo-66 (48% *vs* 51%, *p=0.261*) or control. Nogo-66 therefore requires neither PS nor mTOR activity to effect growth cone collapse.

The proteasome is required for full Nogo-66 collapse activity Inhibition of the proteasome with 25 μM Z-LLnL reduced collapse activity by approximately half (Figure 4.4(c), 56% *vs* 27%, *p<0.0001*) without effect upon controls (15% *vs* 13%, *p=0.261*). Z-LLnL is also a potent inhibitor of calpain (IC_{50} = 90 nM) which can influence axon guidance (Robles et al., 2003), so this could be a confounding factor, although recent data argue against calcium involvement in Nogo-66 signalling (Schmandke et al., 2011, *personal communication*).Therefore Nogo-66, in contrast to Nogo-δ20, requires proteasomal activity in place of mTOR/ribosomal activity to induce growth cone collapse.

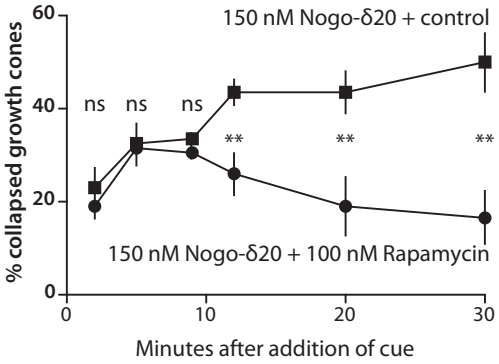

Figure 4.2: Time-Course of Nogo-δ20–Induced Collapse and The Necessity of Protein Synthesis
The extent of collapse over time following addition of 150 nM Nogo-δ20, in the presence (circles) and absence (squares) of 100 nM rapamycin. At 2, 5 and 9 minutes post-exposure, collapse increased to ~30% with and without rapamycin. From 12 minutes post-exposure onward, rapamycin-exposed growth cones recovered, whilst control growth cones continued to increase their extent of collapse.

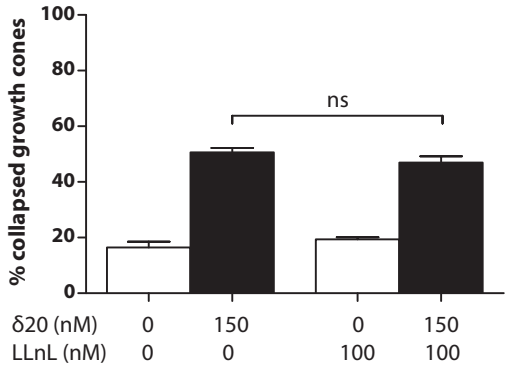

Figure 4.3: Proteasome Inhibition and Nogo-δ20–Induced Growth Cone Collapse
The inhibition of the proteasome with Z-LLnL (LLnL) has no effect upon the collapse activity of 150 nM Nogo-δ20 (δ20) in the chick DRG axon growth cone.

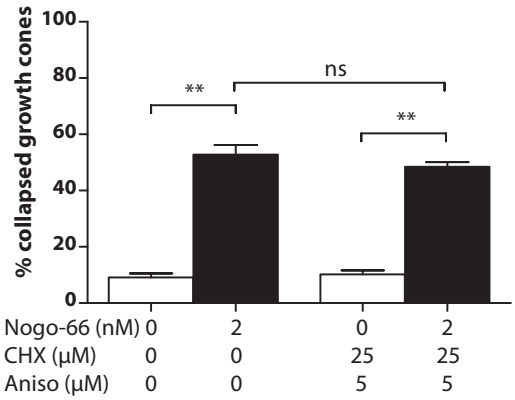

(a) Cycloheximide, Anisomycin and 2 nM Nogo-66

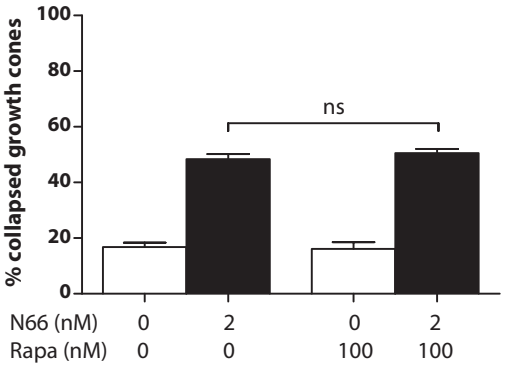

(b) Rapamycin and 2 nM Nogo-66

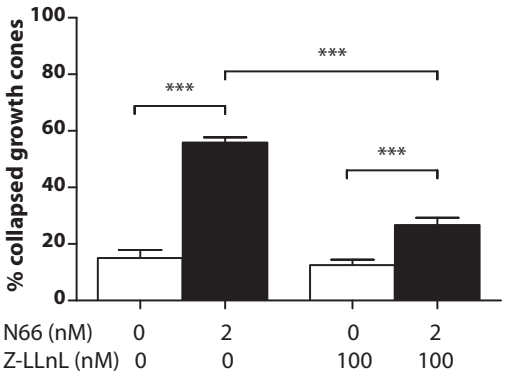

(c) Z-LLnL and 2 nM Nogo-66

Figure 4.4: mTOR and the Proteasome in Nogo-66-Induced Growth Cone Collapse
The collapse activity of 2 nM Nogo-66 (N66) was unaffected by either 5 μM anisomycin/25 μM cycloheximide (a) or by mTOR inhibition by 100 nM rapamycin (b) after 30 minutes. Conversely (c), loss of proteasome function partially but did not totally inhibit collapse activity.

4.2.5 Nogo-δ20 induces mTOR-dependent phosphorylation of eIF4E-BP1, Nogo-66 Does Not

Nogo-δ20 induces phosphorylation of eIF4E-BP1 within 15 minutes To confirm the role of mTOR downstream of Nogo-δ20, the phosphorylation of eukaryotic initiation factor 4E binding protein 1 (eIF4E-BP1) was quantified. This phosphorylation causes the release of eIF4E, a rate-limiting factor in cap-dependent translation, downstream of mTOR complex 1. It is thus a measure of PS activity. Addition of 150 nM Nogo-δ20 (Figure 4.5(a)) increased phosphorylation by 26% over control ($p=0.00185$) within 15 minutes, whereas the combination of 150 nM Nogo-δ20 and 100 nM rapamycin reduced the signal by 58% *vs* control ($p<0.0001$), 66% *vs* Nogo-δ20 alone ($p<0.0001$).

Nogo-66 does not induce phosphorylation of eIF4E-BP1 Nogo-66 collapse activity was not affected by mTOR inhibition (Figure 4.4(b)), but it is possible that Nogo-66 nevertheless induces PS for other purposes as, for example, NGF induces PS of CREB for transport to the soma, which is not required for acute guidance responses (Cox et al., 2008; Roche et al., 2009). Alternatively, Nogo-66 may inhibit axonal PS to limit branching and outgrowth in the mature CNS (Zhao et al., 2011). 15 minutes after exposure to 2 nM Nogo-66, there was no significant change in phosphorylation *vs* control (Figure 4.6, -4%, $p=0.563$). 100 nM rapamycin in addition to Nogo-66 reduced signal levels by 68% *vs* control ($p<0.0001$), demonstrating a basal level of activation in these cultures. These data imply that Nogo-66 does not exert a direct effect upon local PS, although it remains possible that Nogo-66 alters the profile of synthesised proteins without increasing overall PS.

4.2.6 Nogo-δ20 Induces a Rapid Increase in RhoA Levels in the Growth Cone

RhoA levels increase after application of Sema3A. This increase is sufficient to induce collapse, and RNA interference against RhoA mRNA inhibits Sema3A-induced collapse (Wu et al., 2005). As Nogo-δ20–induced collapse involves mTOR complex 1 and PS, as does Sema3A-induced collapse, whether this similarity extended to synthesis of RhoA was examined, or whether another protein, e.g. cofilin (Piper et al., 2006), was synthesised to mediate collapse instead.

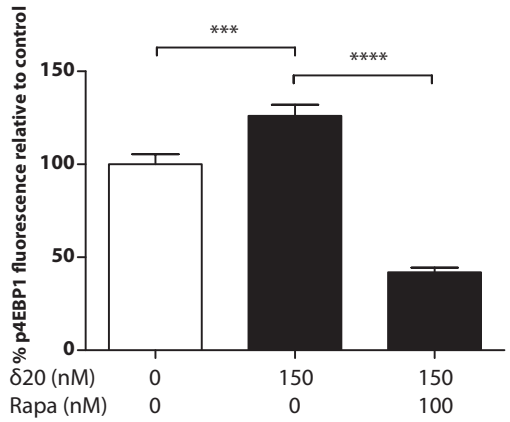

(a) Nogo-δ20 and eIF4E-BP1 Phosphorylation

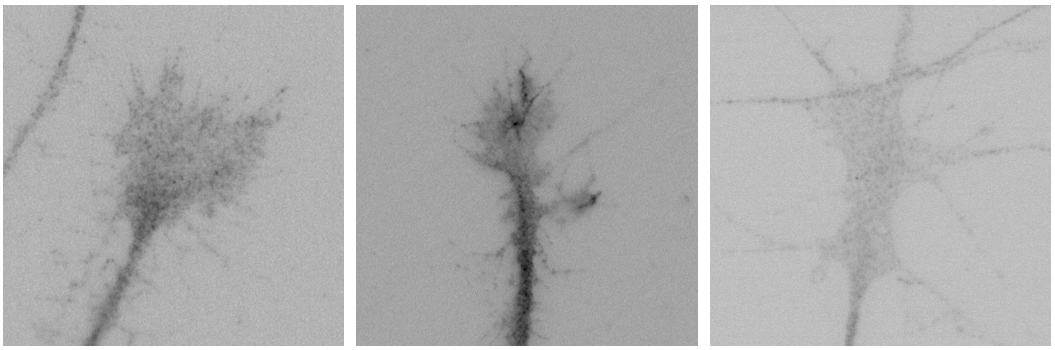

(b) Growth Cone p-eIF4E-BP1 — Control

(c) Growth Cone p-eIF4E-BP1 — Nogo-δ20

(d) Growth Cone p-eIF4E-BP1 — Nogo-δ20 and Rapamycin

Figure 4.5: mTOR Activity after Application of Nogo-δ20

(a) Application of 150 nM Nogo-δ20 increases the phosphorylation of eIF4E-BP1, a key target of mTOR complex 1 to increase local PS, in an mTOR-dependent manner. (b-d) Examples of growth cones *(fluorescence intensity normalised and inverted)* exposed to control, 150 nM Nogo-δ20 and both Nogo-δ20 and 100 nM rapamycin, respectively.

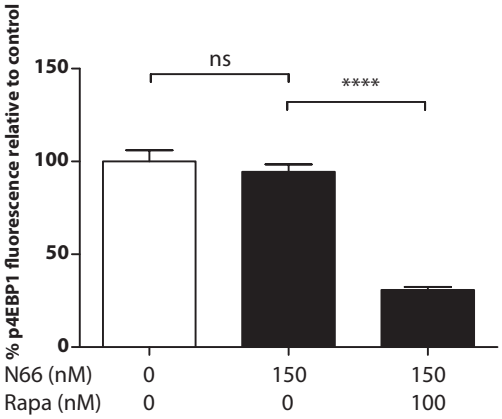

(a) Nogo-66 and eIF4E-BP1 Phosphorylation

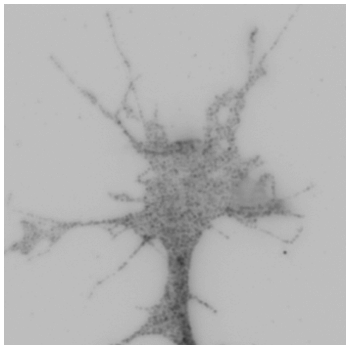

(b) Growth Cone p-eIF4E-BP1 — Control

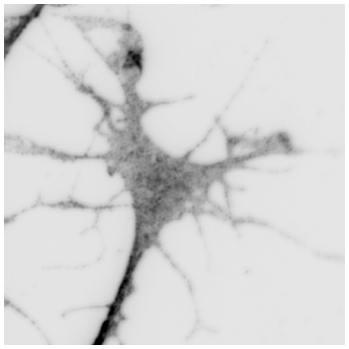

(c) Growth Cone p-eIF4E-BP1 — Nogo-66

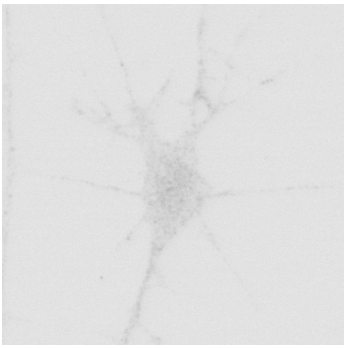

(d) Growth Cone p-eIF4E-BP1 — Nogo-66 and Rapamycin

Figure 4.6: mTOR Activity after Application of Nogo-66

(a) Application of 2 nM Nogo-66 does not alter the phosphorylation levels of eIF4E-BP1. Co-application of 100 nM rapamycin reduces phosphorylation levels to below control, indicating a basal level of mTORC1 activity under these conditions, as seen in Figures 3.18(a) and 4.5(a). (b-d) Representative growth cones *(fluorescence intensity normalised and inverted)* exposed to control, 2 nM Nogo-66 and both Nogo-66 and 100 nM rapamycin, respectively.

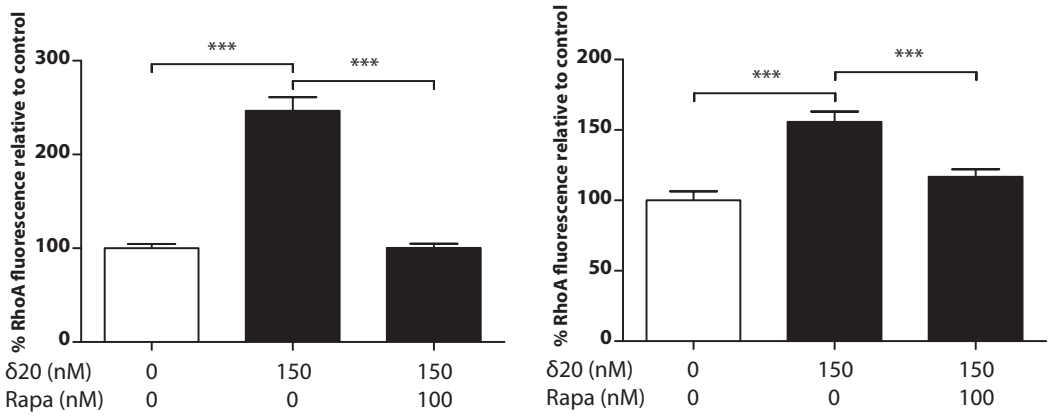

(a) Nogo-δ20 and Growth Cone RhoA Detected with SC-179

(b) Nogo-δ20 and Growth Cone RhoA Detected with 26C4

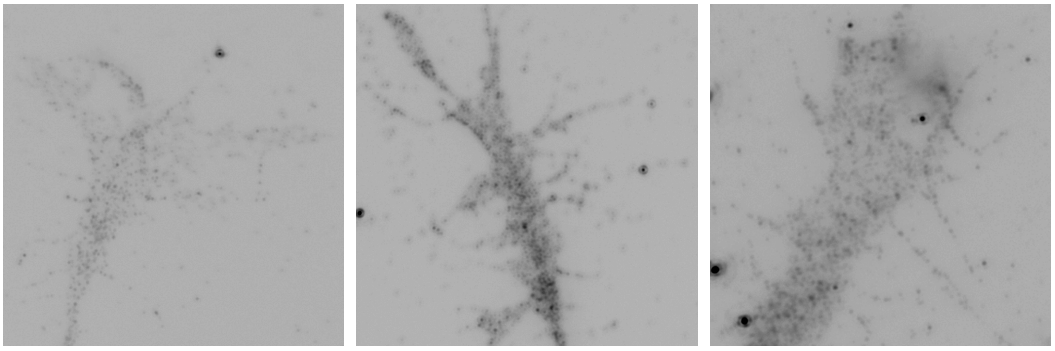

(c) Growth Cone RhoA — Control

(d) Growth Cone RhoA — Nogo-δ20

(e) Growth Cone RhoA — Nogo-δ20 and Rapamycin

Figure 4.7: RhoA Levels after Application of Nogo-δ20

Levels of RhoA in growth cones detected by anti-RhoA monoclonal antibodies sc-179 (119) (a) and 26C4 (b) after 15 minutes' exposure to control, 150 nM Nogo-δ20 and both Nogo-δ20 and rapamycin, respectively. RhoA increases within 15 minutes of exposure to Nogo-δ20, but rapamycin prevents this increase, levels remaining similar to control. (c-e) Example growth cones *(fluorescence intensity normalised and inverted)* exposed to control, 150 nM Nogo-δ20 and both Nogo-δ20 and 100 nM rapamycin, respectively, detected with anti-RhoA antibody 119.

Intra-growth cone RhoA levels increase mTOR-dependently in response to Nogo-δ20 RhoA levels were measured 15 minutes after exposure to 150 nM Nogo-δ20, with two primary antibodies, 119 and 26C4. Both demonstrated an increase in fluorescence (+161% ($p<0.0001$) and +56% ($p<0.0001$), respectively) which reduced almost to control levels with the prior addition of 100 nM rapamycin (+17%, $p=0.0467$, and +7%, $p>0.05$, respectively). Both primary antibodies demonstrate an mTOR-dependent increase in growth cone RhoA levels. Antibody 119 may demonstrate a greater increase as it also binds to RhoB and, to a lesser degree, RhoC, which may also be synthesised. However, further conclusions are difficult to draw as immunofluorescence data can be non-linear.

4.2.7 Nogo-δ20 Increases Total Axonal Protein Synthesis mTOR-Dependently

Direct detection of newly synthesised proteins confirms Nogo-δ20's induction of PS To confirm directly that local PS increased mTOR-dependently after exposure to Nogo-δ20, freshly severed DRG axons were incubated for 1 hour in methionine-free medium with 100 μM azidohomoalanine (AHA, see *Methods*), a methionine analogue capable of undergoing click reactions, before incubation for 1 hour with control, 150 nM Nogo-δ20 or both Nogo-δ20 and 100 nM rapamycin. The proteins were extracted from each culture, the AHA-containing proteins were labelled with tetramethyl rhodamine (TAMRA), separated *via* SDS gel electrophoresis and fluorescence levels imaged with lumination from a 565 nm laser.

Nogo-δ20 induced an increase in labelled proteins within 1 hour (Figure 4.8), an effect inhibited by rapamycin. This confirms directly that Nogo-δ20 induces an acute increase in translation through mTOR complex 1. Notably, the increase of newly-synthesised proteins spanned the length of the lane. This implies that a wide variety of proteins are synthesised in response to Nogo-δ20, not simply RhoA.

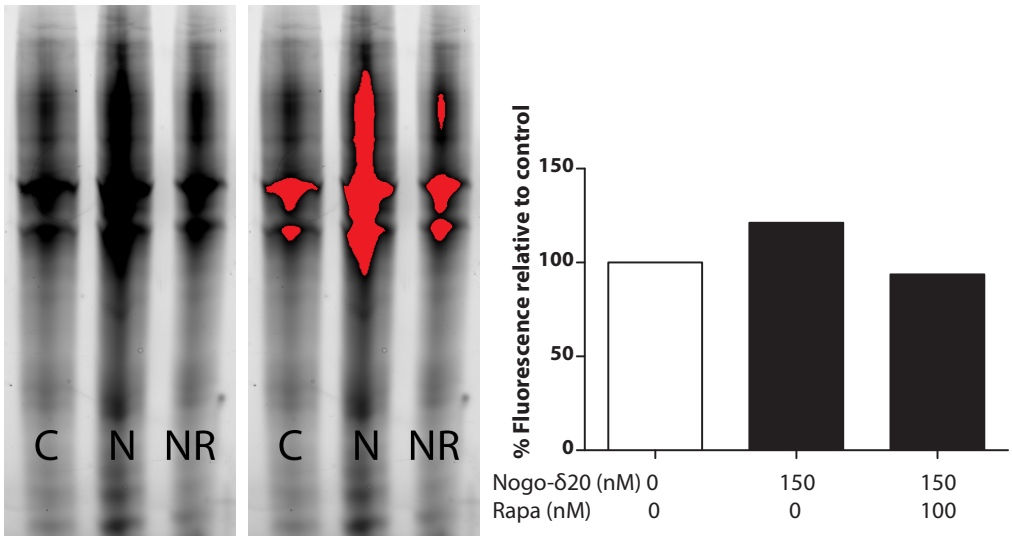

(a) Fluorescence Image of Gel

(b) Fluorescence Image of Gel with Saturated Areas Highlighted

(c) Total Fluorescence per Lane

Figure 4.8: AHA-TAMRA Labelling of Protein Synthesis post-Nogo-δ20

(a) The TAMRA-labelled newly synthesised proteins during 1 hour's exposure to control (C), 150 nM Nogo-δ20 (N) and both Nogo-δ20 and 100 nM rapamycin (NR). The rate of PS increases markedly and across a range of molecular weights after exposure to Nogo-δ20, in an mTOR-dependent manner. (b) The same image with the areas of saturating fluorescence highlighted in red, illustrating the Nogo-δ20–dependent, rapamycin-inhibitable increase. (c) Quantification of the total fluorescence in each lane.

4.3 The Involvement of Erk1/2 in Nogo-δ20–Induced Phosphorylation of eIF4E-BP1

The mechanism upstream of mTOR activation is not established in either Sema3A or Nogo-δ20 signalling. Erk1/2 is involved in Sema3A-induced collapse and therefore Campbell and Holt (2003) proposed that Erk1/2 functions updtream of mTOR in causing collapse. As Sema3A and Nogo-δ20 both require mTOR and synthesis of RhoA to collapse growth cones, Erk1/2 is a clear candidate upstream of mTOR that may be activated.

This analysis was not powerful enough to determine whether Erk1/2 activity downstream of Nogo-δ20 was required for the phosphorylation of eIF4E-BP1 (Figure 4.9). However, we can conclude that Erk1/2 activity is not required for basal levels of PS, as seen downstream of Sema3A (Figure 3.19(a)).

4.3.1 Nogo-δ20–Induced Collapse is Not Dependent Upon NO-cGMP Signalling

500 nM ODQ has no effect upon Nogo-δ20–mediated growth cone collapse NO and cGMP have been linked to repulsive turning *via* L1CAM (Castellani et al., 2002). To explore the parallels of Sema3A and Nogo-δ20 signalling, whether Nogo-δ20–induced collapse shares a dependence on soluble guanylyl cyclase was examined by inhibiting the pathway with 500 nM 1H-[1,2,4]oxadiazolo[4,3-a]quinoxalin-1-one (ODQ).

150 nM Nogo-δ20 induced 41% collapse, *vs* 8% seen in control (*p=0.0451*). Addition of 500 nM ODQ slightly increased collapse *vs* control (14%, *P=0.0142*), and there was no significant effect upon Nogo-δ20–induced collapse (41% *vs* 43%, *p=0.181*). This suggests that soluble guanylyl cyclase is not involved in Nogo-δ20–induced growth cone collapse, and thus cue-dependent synthesis of RhoA, does not require cGMP.

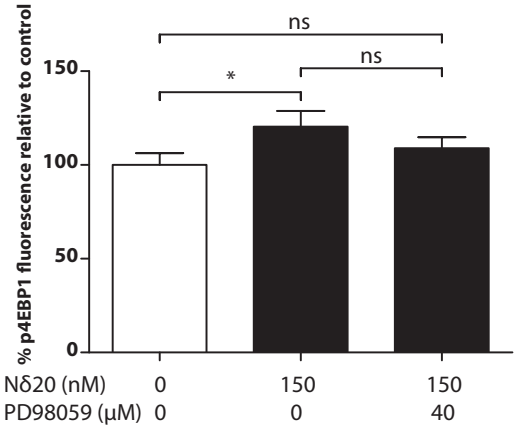

Figure 4.9: The Independence of Nogo-δ20–Induced mTOR Activity from Erk1/2
Although 150 nM Nogo-δ20 induced an increase in eIF4E-BP1 phosphorylation within 10 minutes, as seen previously (Figure 4.5(a)), data were insufficient to determine whether ERK1/2 inhibition would affect mTOR activity downstream of Nogo-δ20.

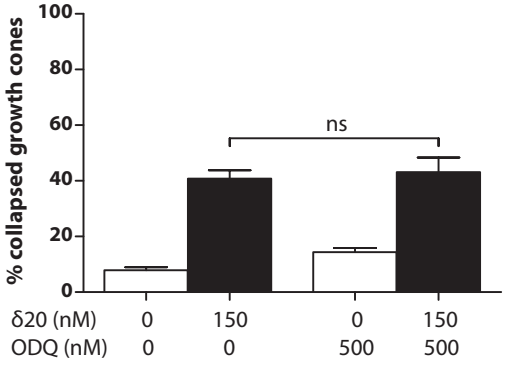

Figure 4.10: Soluble Guanylyl Cyclase and Nogo-δ20–Induced Growth Cone Collapse
Unlike Sema3A-induced growth cone collapse, Nogo-δ20 does not require soluble guanylyl cyclase activity.

4.4 Nogo-A-Induced Growth Cone Collapse and Endocytosis

4.4.1 Inhibition of All Endocytosis Blocks Nogo-δ20–Induced Collapse

Joset et al. (2010) showed that Pincher-mediated endocytosis, but not clathrin-mediated, is required to create Nogo-A–containing signalling endosomes. Expression of dominant-negative Pincher reduces the levels of RhoA activation. However, the requirement of endocytosis to induce collapse was not examined directly and it was conceivable that Nogo-δ20 could also induce collapse Pincher- and RhoA-independently by signalling in another manner. Therefore Nogo-δ20–induced collapse was examined whilst all receptor internalisation was inhibited with 1 μM phenylarsine oxide (PAO), a competitive inhibitor of tyrosine phosphatases (Figure 4.11(a)). Initial results revealed that 30 minutes' exposure to 1 μM PAO caused retraction of neurites (*data not shown*), possibly as PAO is also a metabolic poison (The PubChem Database, 2012) and Pincher-mediated endocytosis is required for NGF signalling (Shao et al., 2002; Valdez et al., 2005), so incubation time was reduced from 30 to 15 minutes for this and the wortmannin experiment.

Phenylarsine oxide inhibits Nogo-δ20–induced growth cone collapse Application of 150 nM Nogo-δ20 increased collapse to 46% *vs* 12% control ($p=0.00197$), and 1 μM PAO alone caused no additional collapse over control (12%, $p=0.292$). However, the combination of Nogo-δ20 and PAO reduced the collapse activity of Nogo-δ20 (46% *vs* 11%, $p=0.0197$) to levels indistinguishable from control (11% *vs* 12%, $p=0.261$). This is consistent with endocytosis being an absolute requirement for Nogo-δ20–mediated growth cone collapse.

4.4.2 Nogo-δ20 Collapse Activity is PI3-Kinase–Dependent

Pincher-mediated endocytosis has been shown to require Rac1 and PI3-Kinase activity during constitutive growth cone activity (Bonanomi et al., 2008), but no association between PI3-Kinase and Nogo-A signalling has thus far been reported. By contrast, Perdigoto et al. (2011) have recently associated PTEN activity, which generally antagonises PI3-Kinase activity, with the axon outgrowth activity of MAG. The study was therefore extended by using 10 nM

wortmannin to examine whether PI3-Kinase was similarly required for Nogo-δ20 activity, or whether Pincher-mediated receptor endocytosis downstream of Nogo-A differed from that downstream of NGF. The duration of incubation was again reduced to 15 minutes to avoid retraction of neurites after 30 minutes (*data not shown*).

Wortmannin inhibits Nogo-δ20–induced collapse Collapse rises from 12% to 45% ($p=0.00197$) upon application of 150 nM Nogo-δ20 (Figure 4.11(b)), whereas wortmannin did not induce collapse (10%, $p=0.356$). 10 nM wortmannin in addition to 150 nM Nogo-δ20 reduced collapse to 14% ($p=0.00197$), similar to controls ($p=0.131$). PI3-Kinase activity is therefore absolutely required for the growth cone collapsing activity of Nogo-δ20.

4.4.3 Inhibition of Clathrin-Mediated Endocytosis Inhibits Nogo-δ20–, Not Nogo-66-Induced, Collapse

Joset et al. (2010) showed that clathrin-mediated endocytosis was not involved in forming signalling endosomes. Clathrin may, however, be involved in other aspects of collapse induced by Nogo-A. Monodansyl cadaverine (MDC) and the dynamin inhibitor, 'Dynasore' were used to explore this, as Sema3A involves RhoA synthesis and requires clathrin activity for collapse (Tojima et al., 2010), and such membrane transfer has recently been proposed as a unifying aspect of growth cone steering (Tojima et al., 2011).

MDC partially inhibits growth Nogo-δ20–induced growth cone collapse, but not that of Nogo-66 100 nM MDC reduces Nogo-δ20–induced collapse from 46% to 29% ($p<0.05$), indicating that although clathrin plays no role in forming the initial signalling endosomes (Joset et al., 2010), it plays a role in collapse. However, p-values were not small, so the conclusion that clathrin-mediated endocytosis plays a role for Nogo-δ20 induced growth cone collapse is tentative.

This experiment was repeated with two inhibitors of clathrin-mediated endocytosis: 100 nM MDC and 40 µM Dynasore, an inhibitor of dynamin GTPase activity. Application of either MDC or Dynasore had no effect upon Nogo-66's collapse-inducing activity after 30 minutes

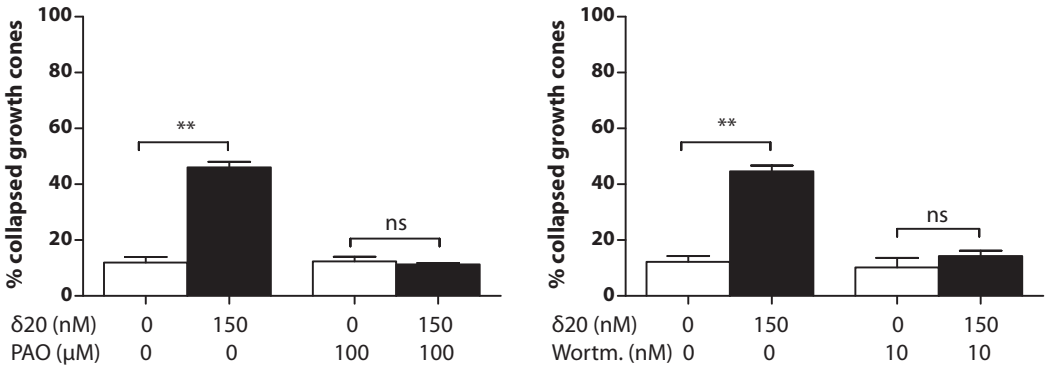

(a) Inhibition of All Endocytosis with Phenylarsine Oxide

(b) PI3-Kinase Inhibition with Wortmannin

Figure 4.11: PI3-Kinase and Endocytosis Downstream of Nogo-δ20

Both inhibition of all endocytosis with PAO (a) and inhibition of PI3-Kinase with wortmannin (b), known to be upstream of Pincher-mediated endocytosis, blocks the collapse activity of Nogo-δ20.

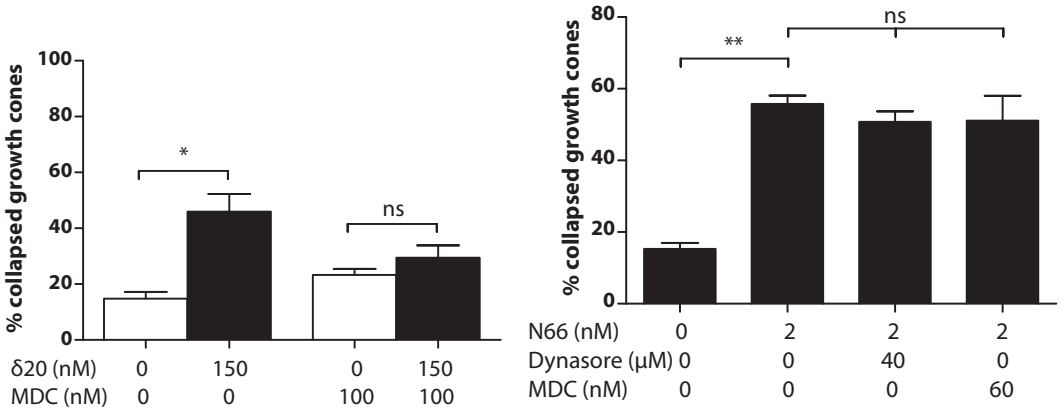

(a) Inhibition of Clathrin-Mediated Endocytosis with Monodansyl Cadaverine

(b) Inhibition of Clathrin-Mediated Endocytosis with Monodansyl Cadaverine and Dynasore

Figure 4.12: Clathrin and Nogo-Induced Growth Cone Collapse

Inhibition of clathrin-mediated endocytosis (a) significantly reduces Nogo-δ20–mediated collapse, but not (b) Nogo-66-mediated collapse.

(56% *vs* 51%, *p=0.233* and 56% *vs* 51%, *p=0.500*, respectively). Therefore neither clathrin nor the dynamin family appear to play a role in growth cone responses to Nogo-66.

4.5 No Synergy Found Between Nogo-A Domains' Growth Cone Collapsing Activity

Combining Nogo-66 and Nogo-δ20 stoichiometrically does not cause synergistic collapse activity The topology and localisation of the Nogo-A protein is controversial (GrandPré et al., 2000; Oertle et al., 2003*a*; Dodd et al., 2005), and it is not clear whether Nogo-66 and -δ20 work independently or co-operatively *in vivo*. The collapse-inducing effects of combining Nogo-66 and -δ20 at equal concentrations was studied, to see whether their collapse effects would be synergistic (Figure 4.13). Such activity would imply that when both are exposed on the plasma membrane *in vivo*, their activities combine.

Addition of 1 nM Nogo-δ20 did not significantly increase growth cone collapse over control (15% *vs* 19%, *p=0.101*), as expected. 1 nM Nogo-66, on the other hand, caused half the growth cones to collapse over control (51% *vs* 19%, *p=0.00308*). However, combining the two at 1 nM concentration each did not increase collapse over expected for 1 nM Nogo-66 alone (53% *vs* 51%, *p=0.218*). Therefore no synergy was detected when both repellent molecules were applied as separate soluble fragments.

However, this interpretation assumes that each Nogo-A molecule presents the Nogo-66 and Nogo-δ20 at a 1:1 ratio on the plasma membrane, which has not been confirmed *in vivo*. It is also possible that the protein fragments require proximity, or a multimeric complex, to act *in vivo*.

4.6 Discussion

Nogo-A has been a target of therapy in spinal cord injury since its identification as a dominant repulsive cue in myelin (Schnell and Schwab, 1990; Schwab, 1990), but the pathways and recep-

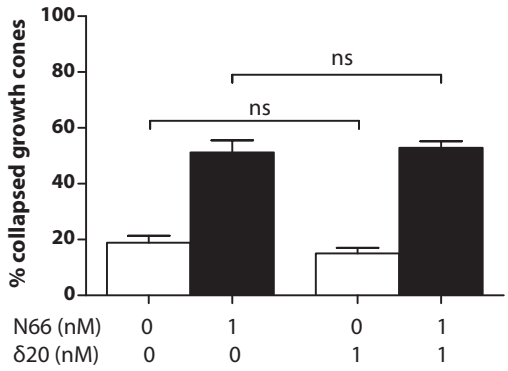

Figure 4.13: The Collapse-Inducing Activity of Combining Equal Amounts of Nogo-66 and Nogo-δ20

The application of 1 nM Nogo-δ20 caused no significant collapse, neither alone nor in addition to 1 nM Nogo-66. 1 nM Nogo-66 induces significant growth cone collapse, irrespective of the presence of 1 nM Nogo-δ20.

tors involved were not identified until much later (Fournier et al., 2001; Niederöst et al., 2002) and both more receptors (Atwal et al., 2008) and more co-receptors have been found since (Mi et al., 2004; Park et al., 2005; Schweigreiter, 2008). Collapse has been associated with RhoA activity (Niederöst et al., 2002; Joset et al., 2010) downstream of both Nogo-66 and Nogo-δ20, and similarly both require the formation of Pincher-mediated endosomes (Joset et al., 2010). Beyond this, little was known about how Nogo-δ20 induces collapse, nor how this might relate to Nogo-66's better-known activity. Further, nothing was known about the role of PS and proteasomal degradation in effecting collapse by either domain of Nogo-A.

4.6.1 The Biphasic Response Downstream of Nogo-δ20

Nogo-δ20–mediated growth cone collapse has been found to be reliant upon mTOR-dependent PS (Figures 4.1(a) and 4.1(b)) at all concentrations tested (Figures 4.1(a), 4.1(c) and 4.1(d)); it induces axonal PS both acutely and mTOR-dependently (Figure 4.8). Time-course experiments in the presence and absence of rapamycin reveal a less potent, faster but short-lived collapse response (Figure 4.2) prior to that of the mTOR-dependent process. This process is maximal after 10 minutes, and recedes within 30 minutes, yet may have a physiological role in guidance, as such short-lived effects are apparently sufficient for guidance in the axons of other species such as *Xenopus* (Ming et al., 2002). These observations may be explained by shrinkage of growth cones due to the Pincher-mediated endocytosis of the receptors (Joset et al., 2010), as Pincher is associated with large-scale pinocytosis, removing large amounts of cell membrane (Shao et al., 2002). Further work is needed to see whether this early-phase retraction is directional and can thus guide the growth cone *in vitro*, and if so whether either phase is redundant *in vivo*. The two phases may instead have differing roles *in vivo*, perhaps one modulating guidance and the other inhibiting growth, respectively, as the two functions' pathways have been separated functionally downstream of Sema3A (Ben-Zvi et al., 2008).

4.6.2 Protein Synthesis and the Proteasome Downstream of Nogo-A

Cue-induced axonal PS has been implicated in several functions, from guidance (Campbell and Holt, 2001) to growth cone resensitisation (Piper et al., 2005). The increase in PS downstream

of Nogo-δ20 (Figure 4.8) yielded no particular bands that could be selected for sequencing to identify the cause of growth cone collapse downstream of Nogo-δ20–induced PS. PS-dependent collapse downstream of Sema3A involves RhoA (Wu et al., 2005), whereas cofilin is thought to mediate Slit2-induced collapse (Piper et al., 2006). It was found that levels of RhoA in the growth cone increased after Nogo-δ20 application in an mTOR-dependent manner (Figure 4.7), similar to Sema3A, which offers a plausible mechanism for collapse as local RhoA synthesis is sufficient to induce collapse (Wu et al., 2005). The phosphorylation of eIF4E-BP1, a target of mTOR complex 1 and a regulator of PS, also increases in a rapamycin-dependent manner (Figure 4.5(a)), implicating a mechanism for mTOR regulation of RhoA synthesis. However, the RhoA-specific primary antibody, 26C4, demonstrated a smaller increase in phosphorylation than 119, which also binds RhoB and RhoC.

Whether RhoA synthesis is sufficient for Nogo-δ20–induced collapse, or whether other molecules are involved, remains to be seen. Further, as the RNA-binding protein implicated downstream of Sema3A, FMR-1 (Li et al., 2009), binds perhaps ~4% of mammalian brain mRNAs (Brown et al., 2001) in addition to RhoA mRNA, including RhoB (Westmark et al., 2011), there may be a range of synthesised molecules involved, and FMR-1's role also remains to be confirmed.

By contrast, inhibition of mTOR has no influence on Nogo-66–induced collapse (Figure 4.4(b)), and similarly the application of Nogo-66 has no effect upon the phosphorylation of eIF4E-BP1 (Figure 4.6(a)). Inhibition of the proteasome with Z-LLnL, on the other hand, reduces collapse induced by Nogo-66 whilst not affecting that due to Nogo-δ20 (Figures 4.4(c) and 4.3). The proteasome has an established role in axon guidance downstream of several cues (Campbell and Holt, 2001, 2003; Strochlic et al., 2008), but a role in Nogo-66 signalling had not hitherto been proposed. One possible mechanism is through the scaffold protein, Plenty of SH3 (POSH), which is downstream of PirB/Nogo-66 (Dickson et al., 2010), and has E3 ubiquitin ligase activity (Kim et al., 2006), but if so, the target ubiquitinated downstream of Nogo-66 is unknown. The partial resistance to inhibition of collapse may relate to NgR-dependent signalling, as POSH interacts with PirB, not NgR (Dickson et al., 2010).

4.6.3 Mechanisms of Endocytosis in Nogo-δ20 Collapse

Joset et al. (2010) demonstrated that Pincher-mediated endocytosis is required to form signalling endosomes to mediate collapse. It was first confirmed that, under our conditions, Nogo-δ20–mediated collapse is entirely blocked by the pan-endocytosis inhibitor, phenylarsine oxide (PAO) (Figure 4.11(a)). Pincher-mediated endocytosis is also required to form NGF/TrkA signalling endosomes (Shao et al., 2002), and it has been found that wortmannin can inhibit Nogo-δ20–induced collapse similarly (Figure 4.11(b)), as seen in NGF/TrkA internalisation (York et al., 2000). Joset et al. (2010) ruled out a role for clathrin in forming the initial endosomes, but whether clathrin-dependent endocytosis could be involved downstream was not explored. Our data (Figures 4.12) suggest that it is not involved downstream of Nogo-66-induced collapse. These data suggest that Nogo-δ20–induced collapse may involve clathrin-mediated endocytosis, but the difference between Nogo-δ20–mediated collapse with and without MDC was only marginally significant ($p=0.05$).

4.6.4 Similarities and Differences to Collapse Downstream of Sema3A

The downstream pathways of Nogo-δ20 and Nogo-66 were explored to see whether the pathways converged with each other or those of Sema3A. Although Nogo-δ20 induced synthesis of RhoA *via* mTOR phosphorylation of 4E-BP1 (Figures 4.1, 4.5, 4.7 and 4.8), mTOR inhibition blocked Nogo-δ20–induced collapse across a 6-fold range of concentrations (Figure 4.1), unlike that seen in Sema3A. Further unlike Sema3A, Nogo-δ20 cannot induce significant collapse after 30 minutes in the absence of mTOR function. The inhibition of soluble guanylyl cyclase had no effect upon the collapse (Figure 4.10), unlike Sema3A (Castellani et al., 2002; Togashi et al., 2008; Nangle and Keast, 2010). These results suggest that NO-cGMP downstream of Sema3A may relate to PS-independent collapse only. Nor does calcium influx seem to play a role, again unlike Sema3A (Schmandke et al, *personal communication*). Thus, while Sema3A and Nogo-δ20 share the mTOR-mediated synthesis of RhoA, the upstream control diverges. An attempt was made to investigate whether Erk1/2 was the upstream modulator of mTOR activity as has been implied downstream of Sema3A (Campbell and Holt, 2003), but initial results were inconclusive (Figure 4.9).

Incidentally, Nogo-δ20 fails to induce more than 70% collapse, even at 900 nM concentration, ~6× that required for 50% collapse (Figure 4.1). This failure to cause more-extensive collapse is shared neither by Sema3A (Figure 3.8), nor Nogo-66 (Kuhn et al., 1999). Taken with evidence that Nogo-δ20 is a stronger inhibitor of neurite outgrowth per gram than Nogo-66 (Oertle et al., 2003*a*), this suggests that growth cone collapse may either be incidental to inhibition of outgrowth, or perhaps Nogo-δ20's function alone cannot prescribe 'no-go' areas for target axons, unlike Sema3A.

4.6.5 Nogo-δ20 and Nogo-66: Similarity or Synergy?

The final experiment was designed to assess whether Nogo-δ20 and Nogo-66 together, as *in vivo* in the Nogo-A molecule, might act synergistically to increase collapse over either fragment alone (Figure 4.13); no synergy was detected when the active fragments were combined. These fragments may function independently *in vivo*, which would imply regulation of each region's exposure to adjacent cells. Alternatively, such regulation may skew the relative abundance of the domains on the cell surface, such that the synergistic effects are seen at differing concentrations. This might be *via* control of the transmembrane regions either side of Nogo-66 (see Figure 1.8), and such regulation may explain the apparently conflicting reports of Nogo-A's topology on the cell surface (for review, see Tessier-Lavigne (2000) and Yang and Strittmatter (2007)).

However, they may still be synergistic: Nogo-A may bring signalling complexes together, or Nogo-66 or Nogo-δ20 may not be long enough fragments to elicit the response. The fragments may not assume the correct fold seen *in vivo*, although the *N*-terminal domain may well be instrinsically unstructured (Shypitsyna et al., 2011). Finally, previous reports suggested that even 100 nM Nogo-66 could not elicit collapse in chick E7 DRG growth cones (Liu et al., 2002*a*); dimerisation may be key to this difference as our Nogo-66 was a disulphide-linked homodimer, mimicking dimerisation *in vivo* (Dodd et al., 2005).

4.7 Conclusion

These results reveal a previously unknown role for both the proteasome and the ribosome in Nogo-A signalling. They also illustrate differences in the signalling mediating collapse between Nogo-66 and Nogo-δ20 and an initial assay revealed no synergy. This unrelatedness of their signalling pathways (Figures 4.14 and 4.15), alongside their 100-fold difference in concentration necessary for collapse, suggests a disparity in their function *in vivo*. One possibility might be control of growth, sprouting and/or guidance during development *vs* maturity. It is feasible that Nogo-δ20 plays a larger role in development, where its growth-modulating properties might come to the fore, whereas Nogo-66 may act to control stability of already-formed connections in the more mature CNS.

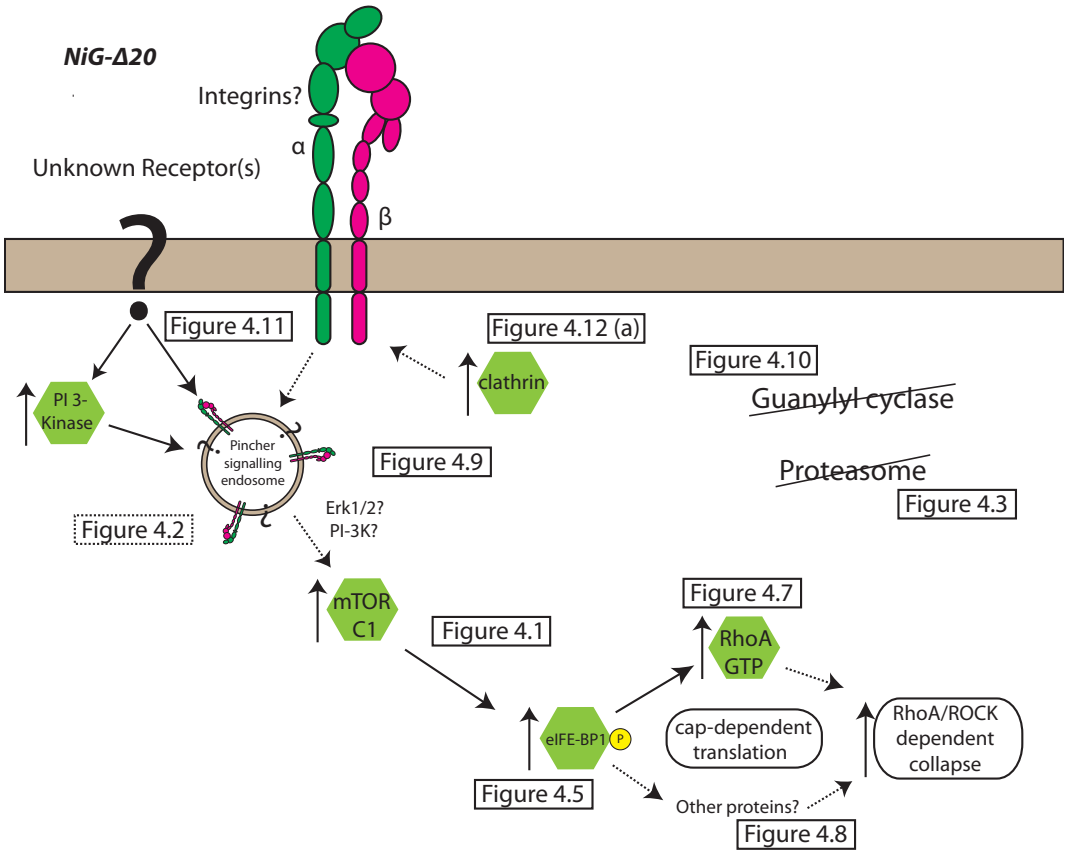

Figure 4.14: Proposed Downstream Signalling of Nogo-δ20 Mediating Growth Cone Collapse
These results indicate that mTOR-dependent synthesis of RhoA is required for Nogo-δ20–induced collapse. A direct connection between synthesised RhoA and collapse was not assessed, although Sema3A also induces RhoA synthesis sufficient to induce collapse. The mechanism differs from Nogo-66 and netrin-1 as the proteasome is not involved.

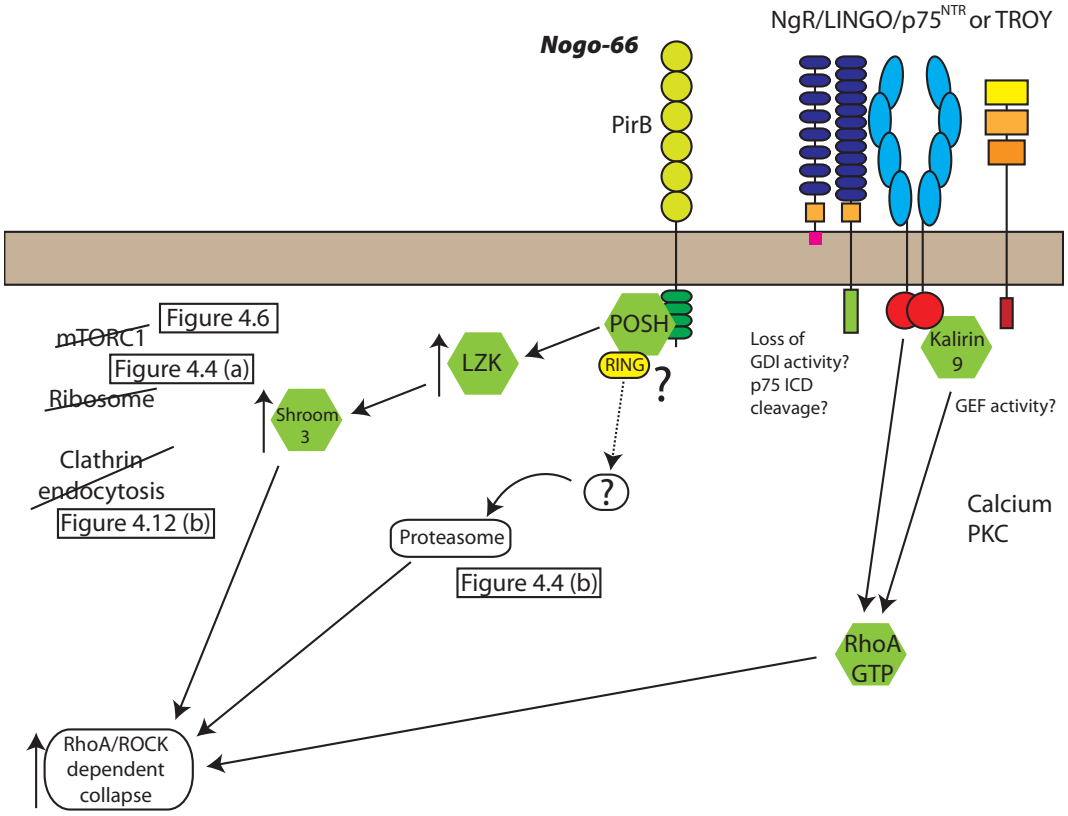

Figure 4.15: Proposed Downstream Signalling of Nogo-66 Mediating Growth Cone Collapse
In contrast to Nogo-δ20, roles for the ribosome and mTOR complex 1 are ruled out as well as clathrin; instead the proteasome is employed in growth cone collapse. The ubiquitinating RING domain of POSH may be involved.

Chapter 5

Candidate Axon Guidance Proteins

5.1 Introduction

Although several families of attractive and repulsive agents have been identified in the last 20 or so years, there remain guidance systems whose cues have not yet been identified. This chapter describes work done to further characterise a protein which is responsible for growth cone-collapsing activity in grey matter (Keynes et al., 1991), and which has been provisionally identified as Major Vault Protein, and later examines the possibility of a protein disulphide isomerase as a guidance molecule, following the work of Hess et al. (1993).

5.2 Major Vault Protein

Following work done in the laboratory by Cook and Johnson (*personal communication*) and Sandvig (1999), detergent extracts of chicken and rat grey matter were fractionated by tissue extraction, hydrophobic interaction chromatography and preparative electrophoresis and growth cone-collapsing activity was followed using the collapse assay described previously. Fractions with a high relative specific activity were examined by 2-D gel electrophoresis and the resultant spot from both chicken and rat preparations was excised. Sufficient protein was extracted to obtain a number of peptide sequences and sequences common to both chicken and rat were used to obtain anti-peptide antibodies (Cook, *personal communication*).

The peptide sequences used for making antibodies did not reveal any links to known guidance proteins, but provided a handle for investigating whether these sequences were found in other species. Using 1718 cells, a line of human astrocytoma cells whose extract also possesses collapse-inducing activity (Cook and Keynes, *personal communication*), Cook and Jackson (2008) separately used these peptides to identify a single spot with an apparent molecular weight of ~120 kDa and a pI of 5.3 through Western blots and 2-D electrophoresis of 1718 proteins. These were sent by each investigator to the Sequencing Facility of the Department of Biochemistry for analysis *via* trypsin digestion and MALDI-TOF sequencing. A single candidate emerged from the two spots submitted, *'Major Vault Protein'* (MVP).

Despite this repeated identification, there remained doubts as to whether the protein identified was likely to be a repellent. MVP is considered to be an exclusively cytosolic protein which forms a large, radially symmetrical 'vault' (thus the name), whose function is largely unknown but binds to RNA (Paspalas et al., 2009). It may have a role in intracellular transport and the telomerase complex (Kickhoefer et al., 1999) and is associated with wide-spectrum drug resistance in cancer (Lu and Shervington, 2008). Further, its published sequence does not match those found in the original sequences from rat and chicken. It thus seems an unlikely candidate for repulsive activity, although the gene *Reticulon-4* from a family of ER-localising proteins shows that alternative splicing can produce proteins (in this case Nogo-A, -B and -C) with widely varying functions from one transcript. Further, the results of Brunet et al. (2005) established the protein Engrailed-2, originally established as a DNA-binding homœobox transcription factor, as an *in vivo* soluble guidance cue, showing that a protein thought to be only cytosolic need not be.

The aim of the work described here was to obtain further evidence to confirm or deny a link between MVP found in 1718 cells and growth cone collapse-inducing activity.

5.2.1 3004.2KLH Binds to a Protein in Astrocytes

Astrocytes are the most abundant cell in the CNS and bear several axon-repulsive molecules. They are therefore a logical place to look for the 3004.2KLH-binding protein. Rabbit serum pre-

pared by Sigma (3004) raised against the peptide bound to keyhole limpet hæmocyanin (KLH) was purified twice *via* KLH-bearing columns to remove KLH-reactive antibodies, to produce the peptide-reactive fraction, termed 3004.2KLH.

CRL 1718 human astrocytoma cell cultures were expanded, harvested, and the soluble proteins subjected to ammonium sulphate fractionation in order to check the fractions for the presence of the protein cross-reacting with the anti-peptide antibody (Figure 5.1). The Western blot revealed strong bands at ~120 kDa in Fractions I and II. This presence correlates with the presence of collapse activity in these fractions. Another strong band was seen in Fraction III at ~50 kDa, with weaker corresponding bands in II and IV, which may be degradation products of the 3004.2KLH-binding protein.

5.2.2 3004 Reactivity Correlates with Growth Cone Collapse in Liposomes

To confirm the presence of growth cone collapsing activity in the protein fractions, liposomes were charged with equal amounts of protein (50 μg) as described in the *Methods*. Chick DRG cultures in 80 ng/ml NGF were then exposed to the liposomes created or controls for 60 min, then fixed and the extent of collapse assessed blind.

Using liposomes formed in PBS pH 7.4 alone as a control, Figure 5.2 shows that liposomes themselves do not induce collapse beyond PBS alone. In contrast, liposomes bearing Fraction I or II proteins induced 35% and 49% collapse, respectively ($p<0.01$ and $p<0.001$), higher than either control alone (9% and 9%). This was not due to non-specific protein, as liposomes bearing proteins from Fractions III–V did not induce significant collapse (5%, 10% and 8%, respectively).

5.2.3 rhMVP Does Not Repel Axons *In Vitro*

To examine whether MVP has axon-repulsive activity, a growth cone collapse assay was performed with recombinant human MVP (rhMVP, $M_r = 124\ kDa$) with chick DRG axons. Similar concentrations of Sema3A ($M_r = 88\ kDa$) were used as a positive control (Figure 5.3).

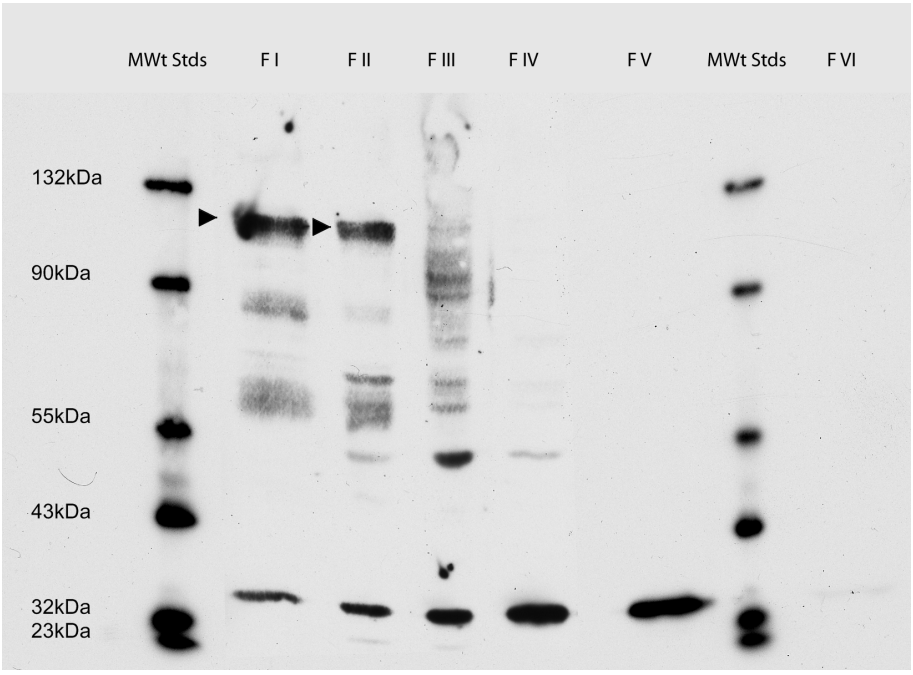

Figure 5.1: Western blot of an SDS/PAGE Gel Showing the Presence of 3004.2KLH-Binding Protein in Astrocytes

30-second exposure of a Western blot of an SDS/Polyacrylamide gel electrophoresis of Fractions I through VI of the soluble fraction of the CRL-1718 cell line. Lanes 'F I' through 'F VI' contained 50 µg protein from Fractions I through VI, as quantified through 280 nm absorption using a BSA standard. 3004.2KLH can be seen to bind to a protein of mass 115 kDa in Fractions I and II (arrowed). There is also a band at 50 kDa, most intense in 'F III', and ~35 kDa bands in fractions 'F I' through 'F V', likely to be degradation products of the target protein. Lanes labelled 'MWt Stds' contained molecular weight standards of 132, 90, 55, 43, 32 and 23 kDa (labelled).

rhMVP combined with liposomes at concentrations up to 1000 ng/ml induced no significant collapse over control (5% *vs* 5%, $p>0.05$), unlike 250 ng/ml Sema3A (5% *vs* 67%, $p<0.05$); even 2.5 ng/ml Sema3A caused significant collapse (5% *vs* 15%, $p<0.05$). MVP therefore shows no evidence of inducing collapse at concentrations equivalent to that of Sema3A, although it is not clear whether the protein integrated into the liposomes.

It is possible that the concentrations used were not enough; Brunet et al. (2005) applied 10 µg/ml Engrailed-2 to induce guidance effects in *Xenopus* RGC axon growth cones. However, 50 µg of total protein was applied to each sample, and the levels of protein detected by Western blot (Figure 5.1) are unlikely to be in the range of micrograms, yet were sufficient to induce collapse (Figure 5.2).

5.2.4 The 3004.2KLH-Binding Protein Does Not Co-Immunoprecipitate with Major Vault Protein (MVP)

It remains possible that MVP and the 3004.2KLH-binding target protein are variants or homologues of one another, thus explaining the identification *via* mass spectrometry. If so, the use of antibodies raised against one may immunoprecipitate both. To examine this possibility, both 3004.2KLH and commercial anti-MVP antibodies were bound to Protein A-coated beads to attempt to precipitate either protein (see *Methods*). The activity of the commercial antibody in Western blotting was confirmed with recombinant human MVP (see Figure 5.4).

3004.2KLH was used to immunoprecipitate the target protein from Fractions I and II on two occasions (Figures 5.5(a) and 5.5(b)). The second time, the stronger detected band had an apparent molecular weight of ~80 kDa, which may reflect degradation of the protein. Immunoprecipitation of MVP and the 3004.2KLH-binding target protein was attempted using the anti-MVP concurrently (Figure 5.5(d)) from both Fraction II and samples of rhMVP. The recombinant MVP revealed a strong band in the control (rMVP), supernatant and eluate lanes of ~120–125 kDa. Tagging of the recombinant protein with glutathione *S*-transferase (GST) explains the discrepancy between MVP's predicted mass and rMVP's apparent mass. In reducing conditions, as

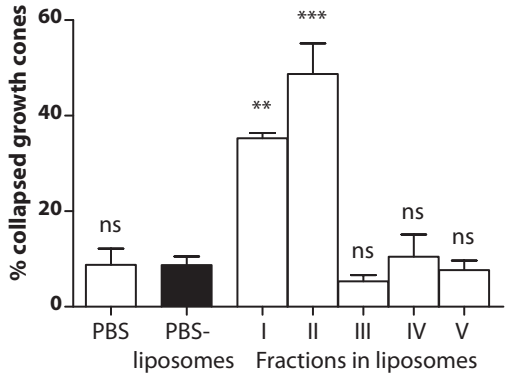

Figure 5.2: Growth Cone Collapse in the Presence Fractions Incorporated into Liposomes
The growth cones were exposed to PBS and liposome controls for 60 min, as well as 50 µg of protein from Fractions I–V incorporated into liposomes. Only Fractions I and II induced collapse beyond control.

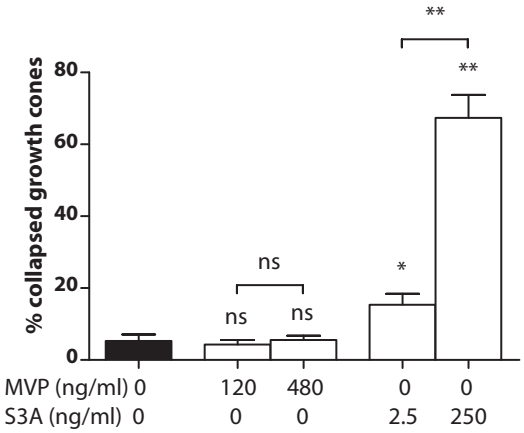

Figure 5.3: The Failure of rhMVP to Induce Growth Cone Collapse
Chick DRG axon growth cones exposed for 60 min to 1% BSA/PBS control, 2 concentrations of recombinant human MVP (120 and 480 ng/ml) and 2 of Semaphorin-3A (2.5 and 250 ng/ml) as positive controls for collapse. The addition of MVP at either concentration fails to increase collapse over control, unlike the positive control Semaphorin-3A (S3A), which causes a significant increase in collapse at a concentrations of both 2.5 and 250 ng/ml.

in SDS-PAGE, GST-tagged proteins are known to degrade, producing a ladder of lower bands, also detected (Thermo-Scientific/Pierce, 2012).

In all three lanes containing Fraction II proteins (F II 'supernatant' containing unbound proteins, the bound 'eluate' proteins eluted from the beads post-immunoprecipitation and the original 'unmodified' protein sample) using SC-18701 to detect MVP, a solitary band was detected with an apparent molecular weight of just under 90 kDa. This protein binds to the antibodies as does rMVP (rMVP supernatant, arrowed, Figure 5.5(d)). This band differs in apparent molecular weight from the 3004.2KLH-binding protein. These data suggest that MVP and the 3004.2KLH-binding protein are unlikely to be identical, and nor does either bear the epitope of the other. However, these data suggest that 3004.2KLH is not a good immunoprecipitation antibody, which would preclude its use as a steric inhibitor in growth cone collapse assays.

5.2.5 The Effects of β-Elimination upon MVP and the 3004.2KLH-binding protein

Earlier experiments in the laboratory had shown that the growth cone collapse activity in 1718 cells could be removed by immobilised jacalin (Cook and Keynes, *personal communication*), suggesting the presence of *O*-glycans on the repellent protein. The β-elimination of *O*-glycans was attempted upon 1718 protein samples containing the 3004.2KLH-binding protein and rMVP, to examine whether (a) MVP is *O*-glycosylated and whether (b) they could be separated biochemically to allow peptide sequencing. Co-localisation of the 3004.2KLH-binding protein and MVP on gels could be overcome by deglycosylation of the 3004.2KLH-binding protein, altering both its apparent molecular weight and charge. Chemical deglycosylation potentially offers differentiation of the 3004.2KLH-binding protein from MVP without the addition of exogenous proteins, simplifying subsequent analysis.

Fetuin, a well-characterised *O*-glycosylated protein, was chosen as a positive control to demonstrate the release of glycans and shift in apparent molecular weight. Initially, the same protocol was applied to fetuin, MVP and the 1718 protein sample (Figures 5.7 and 5.8). Briefly, β-elimination involves incubation with sodium borohydride in alkaline conditions in the absence of a reducing agent to preserve both intact peptides and intact glycans (Figure 5.6(a)).

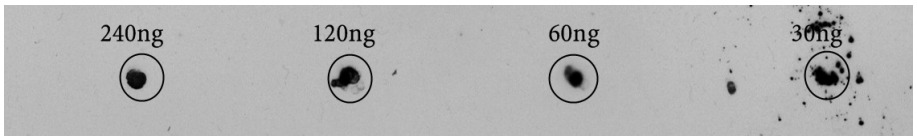

Figure 5.4: Confirming Sensitivity of anti-MVP Antibodies to Recombinant Human MVP
Samples of MVP placed directly onto nitrocellulose membrane, detected with SC-18701 *via* Western blot. The levels of protein are (labelled, left to right) 240, 120, 60 and 30 ng.

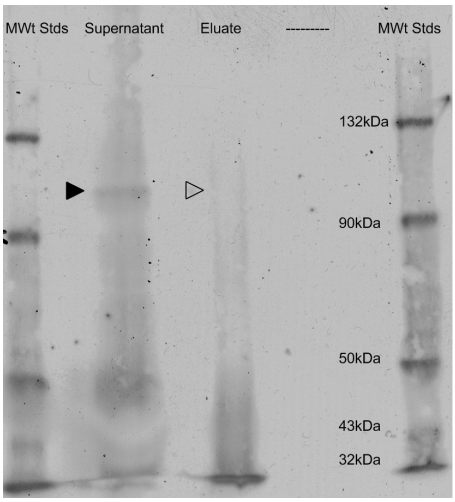

(a) 1st Immunoprecipitation of the 3004.2KLH-binding protein

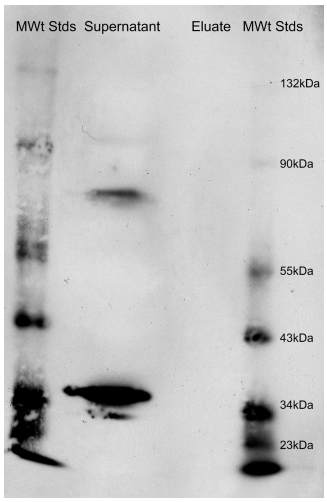

(b) 2nd Immunoprecipitation of the 3004.2KLH-binding protein

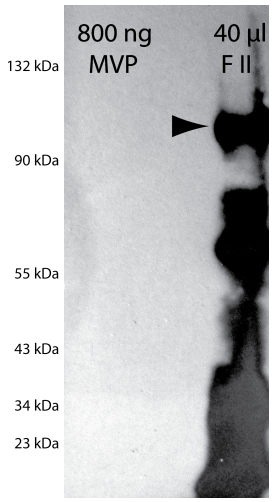

(c) Detecting rhMVP with 3004.2KLH

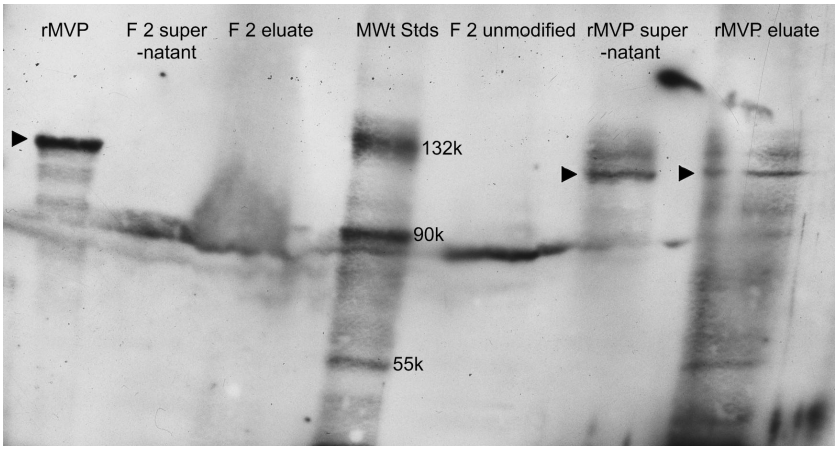

(d) Immunoprecipitation of MVP

Figure 5.5: Immunoprecipitation of MVP and the 3004.2KLH-Binding Protein

(a) The proteins eluted from Protein A beads. One band is present (solid arrow) in the supernatant of ~110 kDa apparent mass. (b) A repeated immunoprecipitation of extended duration to improve protein recovery, revealing a clear band of ~80 kDa, a faint band of more than 90 kDa apparent mass and a strong band of presumed degradation products of ~34 kDa apparent mass. None of these bands are observed in the unbound 'eluate'. (c) A 20-min exposure Western blot, showing the failure of 3004.2KLH to detect 800 ng MVP (left lane) in contrast to the expected location of the 3004.2KLH-binding protein (arrowed) in a 40-µl sample of Fraction II (right lane). Other, lower molecular weight bands are apparent due to 30 min exposure of film to Western blot to increase sensitivity. (d) Immunoprecipitation of MVP using anti-MVP antibody, from recombinant GST-tagged samples (rhMVP) and soluble 1718 proteins. Proteins were detected using the same antibody. Both the rhMVP and 1718 samples were immunoprecipitated, and both were also found in the eluate. The recombinant MVP was GST-tagged, and thus revealed a greater apparent molecular weight than that from the cell-line.

The protein and glycan fractions were separated using spin columns and run on SDS-PAGE or Tris-borate gels, respectively, as described in the *Methods*. To improve the recovery of intact deglycosylated proteins, the reaction temperature could be lowered to 4°C, duration extended to 16 h and neutralisation performed with Tris buffer rather than hydrochloric acid.

Using the standard protocol, the positive control, fetuin, shifts in apparent molecular weight by ~1 kDa and releases glycans (Figures 5.7(b) and 5.7(d)). Recombinant human MVP failed to reveal a shift in the apparent molecular weight of MVP in an SDS-PAGE gel and nor are glycans released (Figures 5.7(a) and 5.7(c)). MVP does not release glycans under these conditions, as opposed to fetuin, a known *O*-glycosylated protein.

Applying the same conditions to a sample of Fraction II proteins aimed to reveal a similar release of glycans and shift in apparent molecular weight of the 3004.2KLH-positive band, as the 3004.2KLH-binding protein binds to the lectin, jacalin, and its weight can be reduced by enzymatic deglycosylation (Cook and Keynes, *personal communication*). Applying the same conditions reduced the 3004.2KLH-binding protein content of the 1718 protein sample below detection (Figure 5.8(a)). Although glycans were released from the sample as a whole, the 3004.2KLH-binding band in SDS-PAGE appeared to be degraded directly to short peptides without the appearance of an intact, deglycosylated form of protein.

When more mild conditions are applied for only 30 min (Figures 5.8(c) and 5.8(b), respectively; see *Methods: Non-Enzymatic Deglycosylation*), the Western blot failed to reveal any intermediate 3004.2KLH-positive band, suggesting the presence of an intact, deglycosylated protein. Figure 5.8(b) instead showed that the original protein was degraded directly to peptide fragments. The 3004.2KLH-binding protein therefore differed markedly from MVP in its stability in the presence of alkali and sodium borohydride, implying significant structural dissimilarity between the two proteins.

Notably, the molecular weight standards produced from partially hydrolysed starch migrated very little in all Tris-borate gels relative to the released glycans (Figures 5.7(c), 5.7(d) and 5.8(c)),

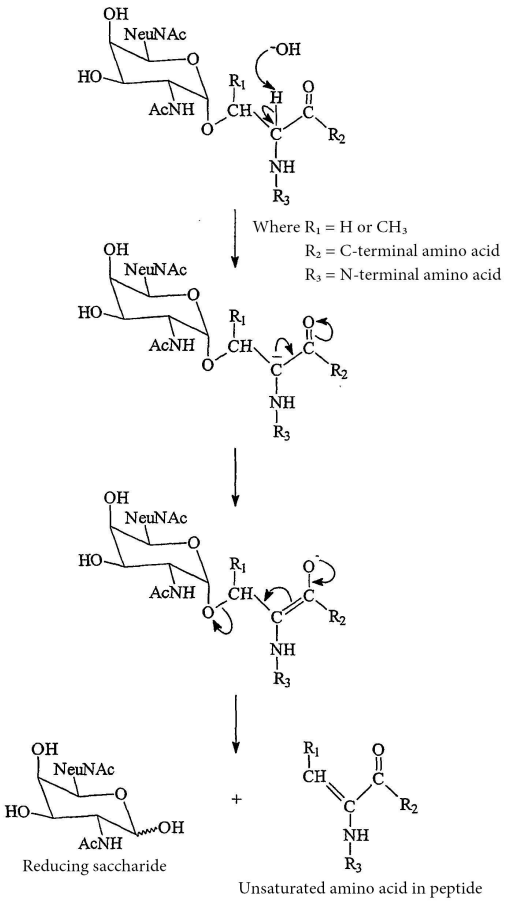

(a) Diagram of β-Elimination of an *O*-Glycan *via* Nucleophilic Attack

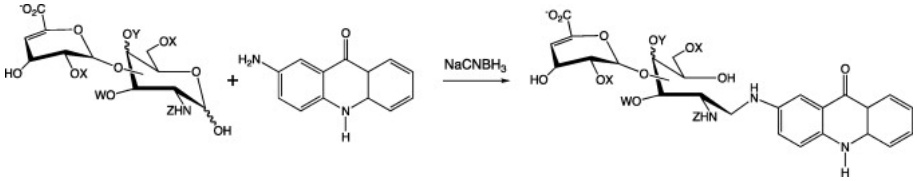

(b) Derivisation with AMAC

Figure 5.6: The β-Elimination of *O*-Glycans and Subsequent Derivitisation

Brief schematics of (a) β-elimination and (b) the binding of the fluorophore AMAC to a complex sugar; W, X, Y and Z indicate varying moieties, typically H or sugars (adapted from Yang et al. (2012)).

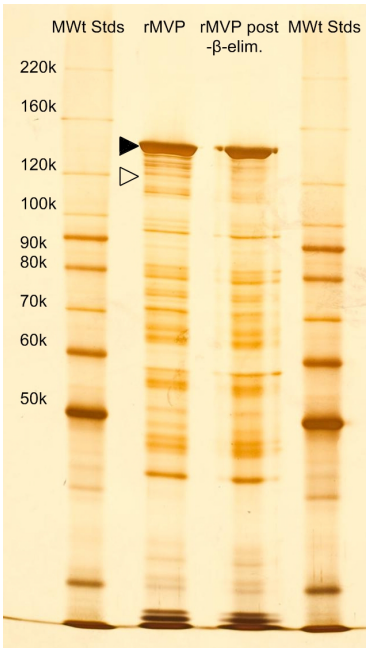

(a) Silver-Stained Gel: β-Elimination and MVP

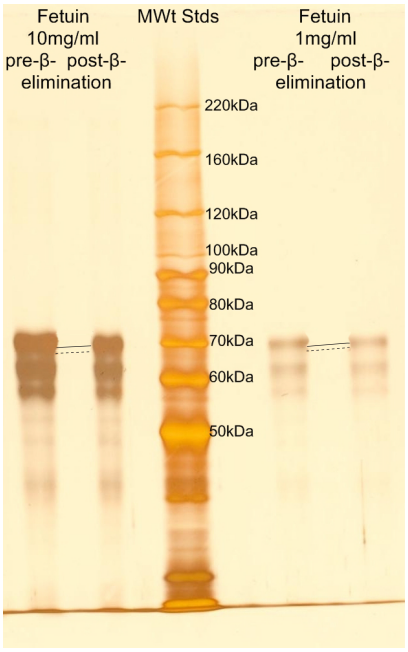

(b) Silver-Stained Gel: β-Elimination and Fetuin

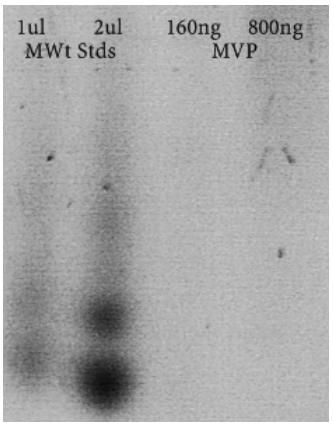

(c) Fluorescence of Released Glycans from MVP

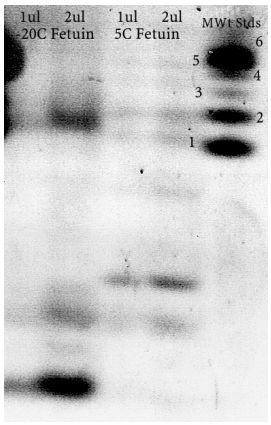

(d) Fluorescence of Released Glycans from Fetuin

Figure 5.7: β-Elimination of Glycans From MVP and Fetuin

(a) Recombinant MVP (rMVP) before and after the original β-elimination protocol at 20°C, flanked by molecular weight standards (MWt Stds). The most intense bands (solid arrow) appear undiminished post-elimination. There is no additional band corresponding to a 20-kDa shift (outlined arrow, as seen when the 3004.2KLH-binding protein is enzymatically deglycosylated). Of note is the lack of purity in the commercial product. (b) β-elimination of *O*-glycans on fetuin causes a small shift in apparent molecular weight (solid lines *vs* dashed). Fetuin reveals more apparent degradation than MVP. There are no detectable glycans released from rMVP (c), but those derived from fetuin form multiple bands (d); temperatures refer to storage conditions.

although there are also faint bands of the same apparent molecular weight as the standards. There may be several causes: AMAC is not known to derivitise peptides, but additional charges from attached peptides, repeated addition of borate or innately charged sugars such as sialic acid might allow faster migration. In contrast, glucose oligosaccharides are uncharged at pH 8.3.

5.2.6 Sequencing of the 3004.2KLH-Binding Protein

MVP differs from the 3004.2KLH-binding protein in apparent molecular weight, repulsive activity and immunoreactivity, so attempts were made to sequence it once more, both through protein purification *via* deglycosylation and lectin binding (see *Appendix*), and through cDNA amplification using samples from CRL 1718 cells. The original sequences from MALDI-TOF analysis, which were used to generate polyclonal antibodies, were also used to generate primers to select possible cDNA sequences from CRL 1718-derived cDNA. This cDNA sample was designed for insertion into plasmids, and thus the sequences bear one half of the *Sfi* endonuclease target sequence on either end for ligation (see *Appendix*).

Primers were created corresponding to the sequences that were used to generate anti-peptide antibodies, and are known to reveal related bands in Western blots. The amino acid sequences used were

- EWTVRLI
- LEDFKAL and
- LDLDYY,

taking into account the residues that mass spectrometry cannot distinguish e.g. leucine *vs* isoleucine (I), and the codon redundancy and bias of the human genome. Primers and their reverse strand equivalents were synthesised by Sigma-Aldrich (see *Appendix*, Table A.2, Primers Sfi 5′, 3′, AP1 to AP3 and their corresponding reverse sequences, AP –1 to –3) so that cDNA stretches either side of the target sequences would be amplified.

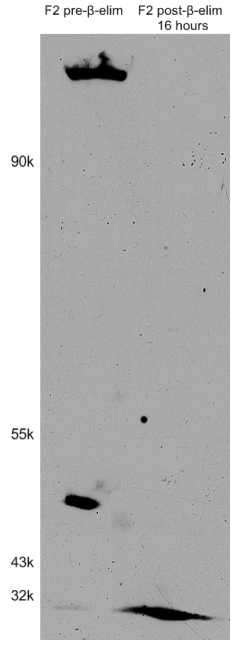

(a) 3004.2KLH-Binding Protein Stability using Standard Protocol

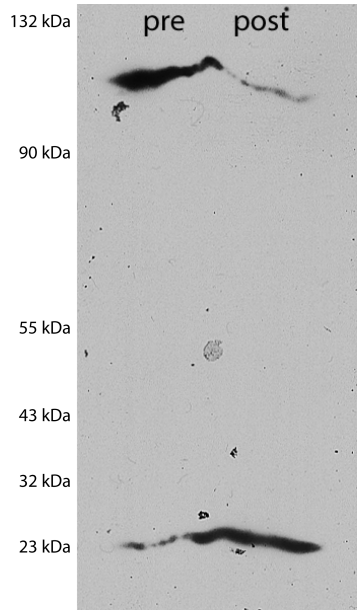

(b) 3004.2KLH-Binding Protein Stability using Modified Protocol

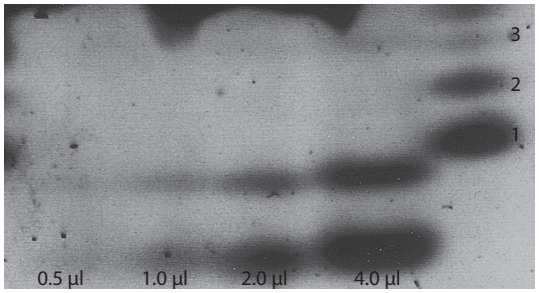

(c) Glycans Released from Fraction II after 30 min

Figure 5.8: β-Elimination of Glycans from 1718 Proteins

Western blots (a, b) of the 3004.2KLH-binding protein and fluorescence (c) of derivitised glycans. Using the β-elimination protocol of Figure 5.7 on Fraction II of 1718 proteins (a) results in the complete loss of the specific 3004.2KLH-positive bands in favour of a degradation band at the gel front (below the 23 kDa point). Reducing the duration of the β-elimination from 16 h to 90 min and temperature to 5°C (b) results in incomplete loss of the higher 3004.2KLH-positive band. The intensity of the band of degradation products correspondingly increases. There is no intermediate-mass band indicating a degylcosylated, but intact, protein at either of these points. Separation and derivitisation of glycans in this negative image of fluorescence under 365 nm light (c) demonstrates that glycan release occurred after 90 min. The right-hand lane contains molecular weight standards of a mono- (1), di- (2) and trisaccharide (3) calibrated against glucose (not shown). The diffusion of free AMAC (irregular dark area, top of image) obscured data from bands of greater apparent molecular weight.

The cDNA samples had been ligated with the SfaI sequence to form small cDNA loops for insertion into plasmids, then cut halfway through the SfaI sequence. To amplify sequences that of candidate mRNAs, only one sequence-specific primer was required with one forward or reverse SfaI primer.

5.2.7 Selecting Candidate cDNA Sequences from PCR Products

The experiment using *SEMA3A* primers was repeated with the following primer combinations:

- AP 1 and Sfi 3′ (1),
- AP –1 and Sfi 5′ (2),
- AP 2 and Sfi 3′ (3),
- AP –2 and Sfi 5′ (4),
- AP 3 and Sfi 3′ (5),
- AP –3 and Sfi 5′ (6),
- AP 1 and Sfi 5′ (7) and
- AP –1 and Sfi 3′ (8).

Bands of cDNA were separated by agarose gel electrophoresis (Figure 5.9(a)) and visualised under UV light. Bands were excised for re-amplification. Concentration of Mg^{2+} was increased to 4 mM to improve the yield of longer fragments and the products were again separated by electrophoresis (see *Appendix*). Bands were repeatedly excised and reamplified to exclude short sequences and non-specific binding (Figure 5.9(b)).

5.2.8 Isolation and Sequencing of Candidate cDNA Sequences from 1718 cDNA Sample

The DNA bands were amplified individually and 5 µl each of the 50 µl reaction volume was separated *via* electrophoresis to confirm that each band was unique (Figure 5.10). Following confirmation, the DNA was purified and sent for sequencing at the Biochemistry Sequencing

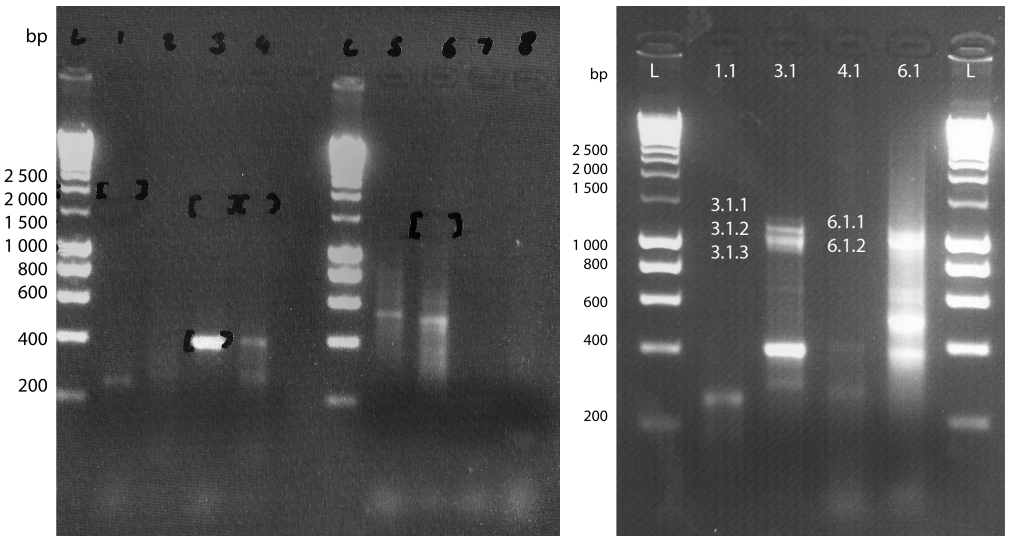

(a) Initial Selection of cDNA with Primers (b) Amplification of Bands of Interest

Figure 5.9: Initial Selection of cDNA Candidates

(a) The PCR products of reactions 1 through 8 (labelled), using Hyperladder I (L) as a reference. The largest visible bands were excised (locations marked by square brackets, as imager was not sufficiently sensitive) and named by their lane and apparent size in that lane, e.g. 4.2 for the 2nd-largest band excised from lane '4'. 5 bands were excised for amplification: 1.1, 3.1, 3.2, 4.1 and 6.1. (b) Amplified, excised bands 1.1, 3.1, 4.1 and 6.1 and Hyperladder I (L). The products of 1.1 and 4.1 did not produce significant bands of interest. 3.1 and 6.1, when amplified, generated several bands of ~1 kb in length. The amplification also produced bands of shorter length, as seen in (a).

Facility, University of Cambridge. The data were of poor quality and the DNA concentration low, so amplification *via* ligation into plasmids and transfection into competent *E. coli* cells was chosen to improve yield. 6 cDNA bands (I–VI) were selected for ligation, on the basis of apparent concentration of DNA (Table A.3).

Samples I (from 3.1.1) and IV (from 6.1.2) were ligated into the pGEM-T-Easy® vector and transfected into JM109-competent *E. coli* cells (Figure 5.11). A positive control, *Amblystoma mexicanum Sox9*, was also ligated and transfected. Plasmids were purified *via* Mini-Prep, the amount of DNA measured (see Table A.3) and sent for sequencing. The results are listed in Table 5.1, using the BLASTn tool against the human genomic + transcript database:

Colony	Closest Sequence	Identity	e-Value
I 1	No significant similarity found	n.a.	n.a.
I 2	Prosaposin	98%	$> 10^{-200}$
IV 1	Actinin-α1	99%	$> 10^{-200}$
IV 2	Mediator Complex Subunit (MED) 20	99%	$> 10^{-200}$
C 1	SRY-box (SOX) 9	94%	10^{-111}
C 2	No significant similarity found	n.a.	n.a.

Table 5.1: Sequencing Data
C 1 and C 2 were analysed using the entire transcript database, and C 1 was of non-human origin and C 2 bore no significant similarity to any human sequences.

5.2.9 Confirmation by Immunohistochemistry of the Presence of Prosaposin in the CNS

MED20 was discounted as a candidate for the identity of the 3004.2KLH-binding protein as the Mediator complex is a ubiquitous regulator of gene expression. Actinin-α1 was also discounted as a ubiquitous cytoskeletal protein. Prosaposin occurs in both membrane-bound and secretory forms and is a neurotrophic factor found on the neuronal surface (O'Brien et al., 1994; Kotani et al., 1996). However, literature searches do not reveal a role for prosaposin specifically on the surface of astrocytes. Immunohistochemistry was performed on *Gallus gallus* embryo sections to examine the relationship between prosaposin and axons in three areas: the optic chiasm, skeletal muscle and the spinal cord/DRGs.

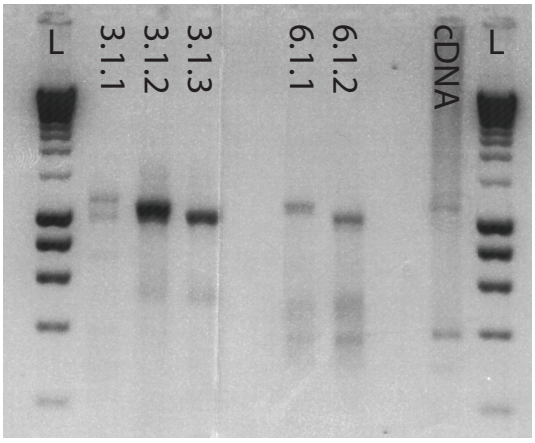

Figure 5.10: Confirmation of Presence of Unique Bands for DNA Sequencing
The DNA samples were re-amplified (labelled) and 5 µl of the 50 µl reaction mixture separated by electrophoresis. Hyperladder I (L) and a sample of the original cDNA with unbiased amplification (cDNA) were used as controls. Having confirmed the presence of high molecular weight bands in all five lanes, the electrophoresis was repeated with the remaining 45 µl and wider lanes to allow tighter bands to be isolated.

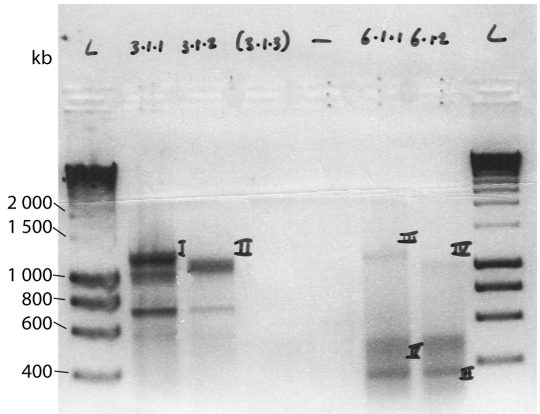

Figure 5.11: cDNA Bands Selected for Ligation into the pGEM-T-Easy® Vector
Gel electrophoresis of amplified samples. Hyperladder I (L) and the re-amplified DNA samples (labelled) were separated, and the bands selected for ligation are labelled (I–VI).

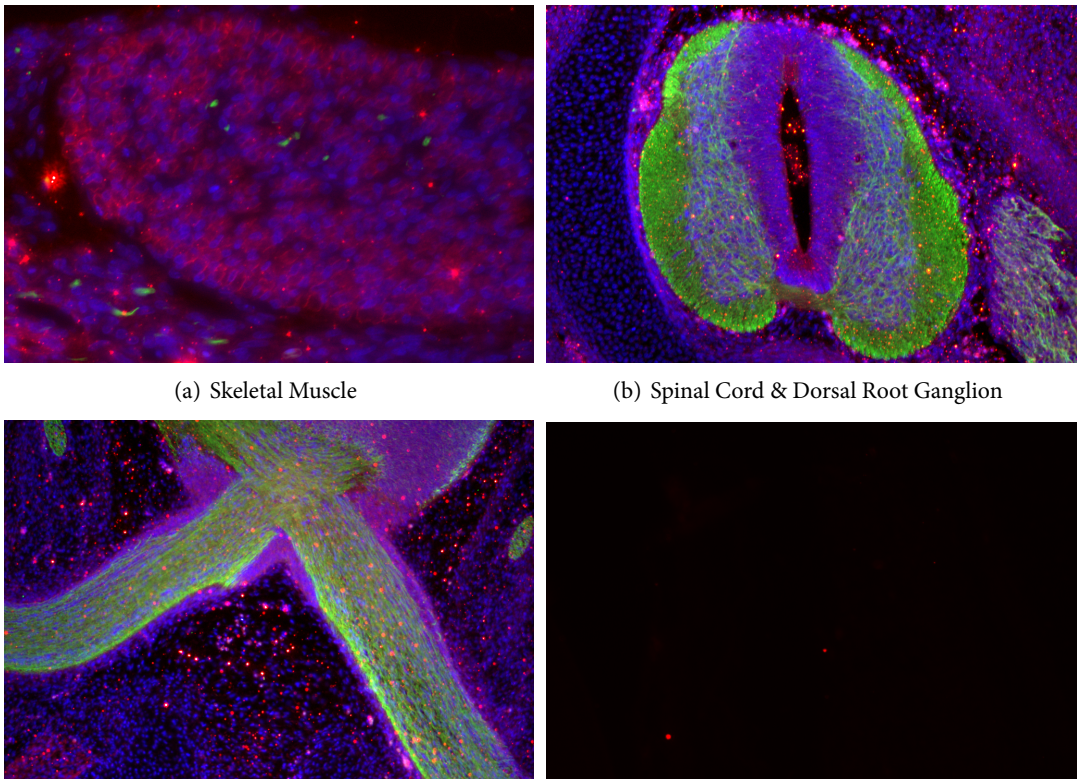

(a) Skeletal Muscle

(b) Spinal Cord & Dorsal Root Ganglion

(c) Optic Chiasm

(d) Control Image of the Optic Chiasm

Figure 5.12: Prosaposin and neuron-specific Tubulin-βIII in a Stage 37 *Gallus gallus* Embryo
Nuclei are stained blue with DAPI, TuJ1 (tubulin) staining is green and α-prosaposin is red. Prosaposin is found extensively on the cell surface of myocytes (a) prior to widespread innervation (green). Prosaposin is found (b) both in the presence of axons and in the relatively axon-poor central region. The region of the optic chiasm (c) displays a similar pattern of prosaposin's localisation both to axons containing β-tubulin and to the surrounding, axon-free support tissues. Image (a) is 600 μm across, images (b-d) are 3 mm across. Control image (d) shows the level of background fluorescence from the Alexa Fluor 594 secondary antibody.

Prosaposin is found in diverse tissues (Figure 5.12) in the Stage 37 embryo. In skeletal muscle (Figure 5.12(a)), prosaposin immunoreactivity (red) forms a ring around many, possibly all, the muscle fibres. This is not greatly associated with axons (green), as their distributions do not overlap and prosaposin encircles the nuclei (blue) stained with DAPI. The levels of prosaposin staining are higher in muscles than in the surrounding tissues.

The spinal cord also shows strong prosaposin staining (Figure 5.12(b)). Curiously, the intensity of staining is reduced in areas of dense TuJ1 staining, i.e. axonal tracts, relative to areas of the cord deep to them. The dorsal root ganglion (bottom right of image) similarly displays high prosaposin levels, but the cartilage of the vertebral arch is (left of image) relatively prosaposin-free. It also lacks nerve fibres. The image of the optic chiasm (Figure 5.12(c)) demonstrates the optic tracts projecting from the eyes to the tectum (top). Discounting noise, prosaposin is found throughout the optic nerve and the section of midbrain, but not elsewhere. Prosaposin distribution is not defined by the axonal tract, but by the optic nerve, as its boundary correlates with a marked fall in nucleus density. As there are no neuron cell bodies in the optic nerve, this suggests that prosaposin is located in the glial cells.

The distribution of prosaposin correlates only partially with that of neurons, and correlates more fully with areas of current and future axon growth, such as muscles and the presumptive grey matter of the spinal cord, as might be expected of astrocytes. Its concentration is markedly lower in tissues that do not and will not contain nerve tracts, such as the presumptive bone of the vertebral arches. These data are consistent with a protein expressed in glia, rather than neurons alone, and are consistent with prosaposin's presence in the 1718 cDNA sample.

5.3 Protein Disulphide Isomerase: Candidate Contact Repulsion Protein?

In addition to the attempt to confirm the identity of the collapse-inducing protein in 1718 cells, attention was given to a possible mechanism of action. As seen in Chapter 3, nitric oxide (NO) is an established second messenger in guidance signalling and is present in inflammation after spinal cord injury (for review, see Conti et al. (2007)). External gradients cause growth cone

turning (Tojima et al., 2009). However, another aspect of NO signalling is now known to occur at the surface of platelets; novel cell-surface protein disulphide isomerases which are expressed upon activation and may modulate adhesion and transnitrosylation distinct from free NO (Root et al., 2004; Xiao and Gordge, 2011). In particular, Hess et al. (1993) proposed that nitric oxide might guide growth cones through modulating fatty acid acylation, and PDI has been detected through live staining of the surface of CRL 1718 cells, causing ring reactions (de Sousa, *unpublished results*). I therefore chose to examine bovine PDI (hereafter simply PDI) as a model molecule, as a source of NO and nitrosylation found on the cell surface and its influence on axon guidance.

PDIs in general were first identified as a protein of the ER, catalysing rearrangement of cysteine–cysteine disulphide bonds to allow proteins to fold correctly. However, later work (Akagi et al., 1988) demonstrated that PDIs were also found on the cell surface and that these proteins were catalytically active (Mandel et al., 1993). Further, PDI can also catalyse the transfer of other *S*-linked moieties, such as nitric oxide (NO), on the cell surface (Zai et al., 1999; Ramachandran et al., 2001) to other proteins, or causing the release of NO.

NO is readily cell-permeable and is well-established as a second messenger of growth cone repulsion (Rentería and Constantine-Paton, 1996; Tojima et al., 2009) and may act as a diffusible guidance cue itself (Berman and Morris, 2011). Alternately, PDI can use an *S*-nitrosylated substrate to *S*-nitrosylate proteins both directly, and indirectly through free NO (Zai et al., 1999; Jaffrey et al., 2001). Further, *S*-nitrosylation can control the localisation of at least one protein involved in signalling in axon guidance, PSD-95 (Ho et al., 2011). Therefore the possibility of PDI as an axon guidance protein was examined.

5.3.1 PDI in the Presence of *S*-Nitrosoglutathione (GSNO) Causes Growth Cone Collapse

A model compound alone, bovine PDI, failed to induce collapse in assays (Cook and Keynes, *personal communication*). However, if *S*-nitrosylation of PDI were required for its axon guidance effects, the absence of activity by commercially available PDI might be due to a lack of NO donors, present *in vivo*.

1 μM *S*-nitrosylated glutathione (GSNO) was chosen as a representative NO donor as *S*-nitrosothiols are found at concentrations from hundreds of nanomoles to tens of micromoles per litre *in vivo* (Jourd'heuil et al., 2000), and GSNO is an established donor of the NO moiety to cell-surface PDI (Root et al., 2004; Shah et al., 2007). DRG growth cones were exposed to either GSNO alone or 250 ng/ml PDI, or in combination (Figure 5.13). As observed before, the addition of PDI alone did not increase growth cone collapse beyond control, and nor did GSNO alone (10% *vs* 9% *vs* 9%, respectively), but the combination induced 37% collapse after 30 min *($p<0.01$)*. Thus neither PDI nor GSNO alone induce collapse, but combining them causes significant collapse within 30 min.

PDI concentration is the limiting factor under these conditions A key factor of many guidance cues is that their effect is dose-dependent. Therefore the growth cone collapse assay was repeated, varying the concentration of PDI from 125 to 1000 ng/ml (Figure 5.14(a)). Increases from 125 to 250 to 500 ng/ml PDI significantly increased the extent of collapse over the previous (28% *vs* 40% *vs* 59%, $p<0.01$), but a further doubling of PDI concentration to 1000 ng/ml failed to do so (59% *vs* 67%, $p>0.05$). Thus the collapse effects of PDI/GSNO are dependent upon the dose of PDI.

The effect of increasing GSNO concentration was also examined. I increased the GSNO concentration from 1 to 5 and 50 μM, and 50 μM in the absence of PDI (Figure 5.14(b)). Varying GSNO concentration did not increase collapse in the presence of 250 ng/ml PDI (44% *vs* 45% *vs* 37%, $p>0.05$), and 50 μM GSNO in the absence of PDI failed to induce similar levels of collapse (12%). PDI/GSNO-induced growth cone collapse is not affected by GSNO concentration above 1 μM. This behaviour suggests that the availability of *S*-nitrosylated substrates is not a limiting factor under these conditions.

Collapse increases with continuing exposure to PDI/GSNO Although significant collapse is seen within 30 min (Figure 5.13), the samples from which the sequences were derived induced maximal collapse after 60 min (Keynes and Cook, *unpublished observations*). I therefore assessed the extent of collapse 0, 15, 30 and 60 min after addition of PDI/GSNO (Figure 5.15).

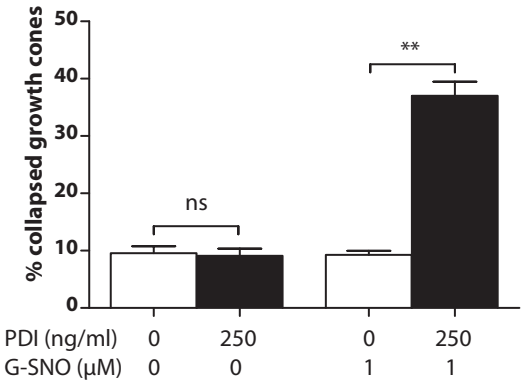

Figure 5.13: Growth Cone Collapse in the Presence of PDI and GSNO
The presence of soluble PDI or GSNO alone does not increase collapse over controls. In the presence of both, collapse occurs within 30 min.

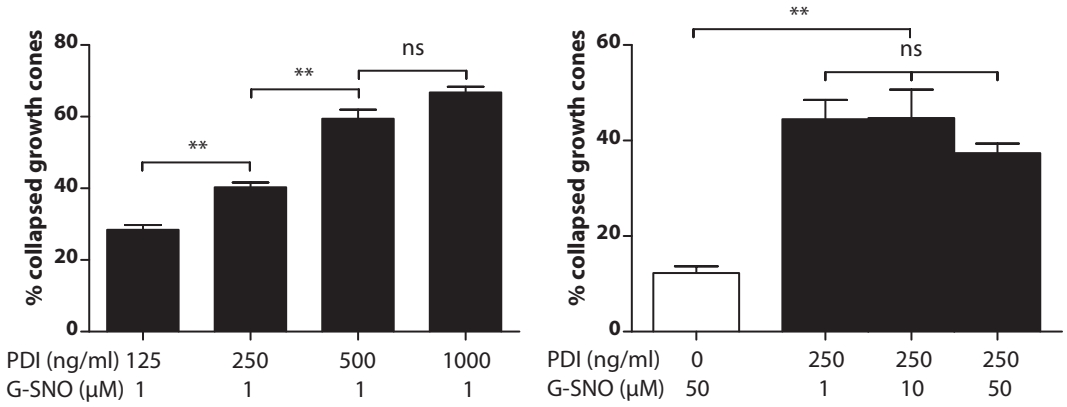

(a) The Dependence of PDI-induced Growth Cone Collapse upon PDI Concentration

(b) Increased GSNO Concentration and PDI/GSNO-induced Collapse

Figure 5.14: The Effects of Concentration on PDI/GSNO-induced Collapse
The collapse effects of combined PDI/GSNO are dependent upon PDI concentration (a), but increasing GSNO concentration (b) does not have similar effects.

Collapse activity increased steadily from 0 to 15 to 30 to 60 min (16% *vs* 36% *vs* 50% *vs* 63%). The PDI/GSNO combination, therefore, induces maximal collapse after at least 60 min.

O-glycans are not involved in inducing PDI/GSNO growth cone collapse Cell-surface PDI *in vivo* appears to bear *O*-glycans, as shown by peanut agglutinin's ability to localise to axon-repelling tissues in the embryo and its ability to deplete extracts of the tissues of collapse activity (Keynes and Cook, *unpublished data*). The PDI/GSNO assay was therefore repeated in the presence of fetuin and asialylated fetuin in order to saturate any such sites (Figure 5.16) to examine whether the *O*- or *N*-glycan moieties had any direct involvement in PDI/GSNO collapse activity, such as binding to receptor molecules on the growth cone plasma membrane.

Neither fetuin nor asialofetuin inhibited bovine PDI/GSNO inhibition, suggesting that the growth cone-collapsing activity of *in vivo* PDI does not require proximity to *O*-glycan–binding sites on axon surface to cause collapse. If there were a site that bound Gal-β(1-3)-GalNAc specifically, the sialic acid residues on fetuin might have sterically inhibited any blocking effect, whereas asialofetuin would have bound to the pocket and blocked collapse. Therefore, asialylated *O*-glycans may not be a critical moiety in PDI/GSNO-induced growth cone collapse.

5.4 The Role of Nitric Oxide in PDI/GSNO-Induced Growth Cone Collapse

PDI collapse activity is partially cGMP-dependent cGMP is a signalling molecule by which NO causes growth cone collapse (Tojima et al., 2009). If PDI/GSNO collapses growth cones through the synthesis of cGMP, then inhibiting NO-activated soluble guanylate cyclase (sGC) with ODQ would inhibit PDI/GSNO-induced collapse (Figure 5.17). The addition of 0.5 μM ODQ to the PDI/GSNO collapse assay reduced the extent of collapse from 49% to 34% ($p<0.05$), but some collapse remained above ODQ alone (34% *vs* 17%, $p<0.05$). sGC activity plays a role in PDI/GSNO-induced collapse, but there may be sGC-independent collapse activity.

PDI collapse activity is partially free-NO–dependent and may function by blocking palmitoylation As the role of cGMP implied a mechanism for NO in growth cone collapse, atten-

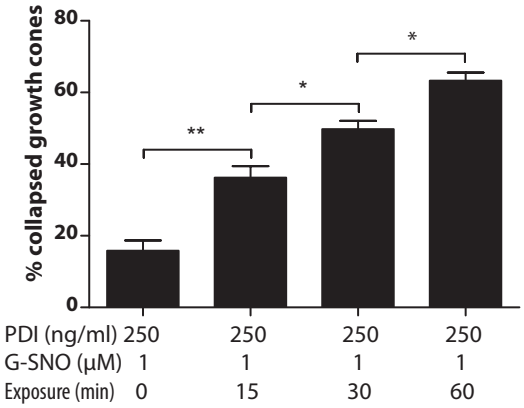

Figure 5.15: PDI-induced Growth Cone Collapse over Time
PDI/GSNO-induced collapse continues to increase after 60 min' incubation.

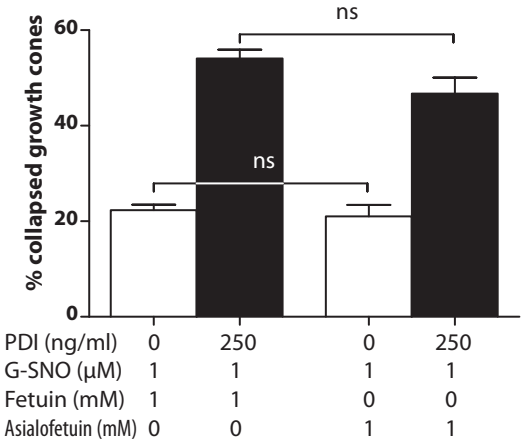

Figure 5.16: *O*-Glycosylated Fetuin Does Not Interfere With Growth Cone Collapse
30 min of pre-incubation with proteins bearing either sialylated (fetuin) or asialylated *O*-glycans (asialofetuin) do not affect the collapse-inducing properties of PDI/GSNO.

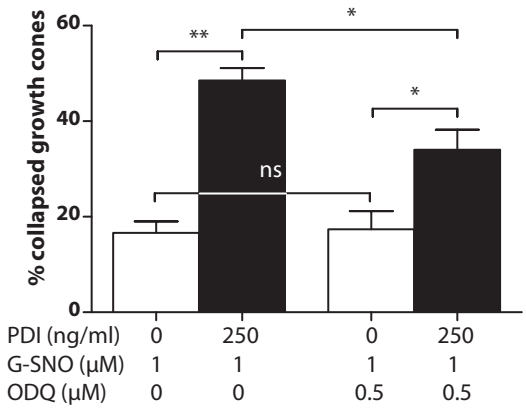

Figure 5.17: The Role of cGMP in PDI-induced Collapse

Inhibition of the hæm group of soluble guanylate cyclase (sGC), preventing NO-induced synthesis of cGMP, reduces the extent of PDI/GSNO-induced collapse.

tion was turned to alternative mechanisms, as NO can also act cGMP-independently through *S*-nitrosylation (Ahern et al., 2002) and cell-surface PDI catalyses *S*-nitrosylation (Root et al., 2004; Shah et al., 2007) directly. The role of NO unbound to protein was assessed by using cell-impermeable myoglobin to bind such NO before cell penetration (Figure 5.18(a)). The effects of *S*-nitrosylation are not fully known, but include competitive inhibition of *S*-palmitoylation, a highly dynamic post-translational modification with a half-life of minutes which causes protein localisation to the cell surface. An increase in *S*-nitrosylation removes proteins from the cell surface to the cytoplasm such as DCC and PSD-95, involved in axon guidance and outgrowth respectively (Hérincs et al., 2005; Ho et al., 2011).

The addition of myoglobin reduces collapse from 45% to 22% ($p<0.01$), further than that achieved by sGC inhibition, but the presence of PDI/GSNO still induced significant collapse over myoglobin alone (22% *vs* 12%, $p<0.05$). To confirm these results, the assay was repeated using PTIO, a small-molecule NO scavenger (Figure 5.18(b)) and with SIN-1 as a positive control for NO-induced growth cone collapse, an unstable compound which spontaneously releases NO in aqueous solution.

The use of PTIO produced variable results, and as such, although the addition of PTIO apparently reduces the mean collapse induced from 39% to 30%, this was not significant ($p>0.05$). In contrast, SIN-1 induces more extensive collapse (52%) and the addition of PTIO apparently reduced this to 27% ($p<0.01$). PTIO therefore inhibits SIN-1-induced collapse more than PDI/GSNO-induced collapse, implying that PDI/GSNO's effect involves more than liberation of free NO into the pericellular space.

The effect of blocking palmitoylation with *2*-bromopalmitate was compared to PDI/GSNO-induced collapse (Figure 5.18(c)), using PTIO to block the effects of free NO. 40 μM *2*-bromopalmitate induced similar collapse to 250 ng/ml PDI and 1 μM GSNO (48% *vs* 49%, $p>0.05$), but the combination of the two only marginally increased collapse to 56% (Kruskal-Wallis ANOVA, $p<0.01$), an effect abolished when PTIO was added to the combination (43%, Kruskal-Wallis ANOVA, $p>0.05$). Therefore combining PDI/GSNO with a palmitoylation-

blocking molecule increases collapse only marginally, and that PTIO, a scavenger of NO, abolishes this increase. This finding is consistent with PDI/GSNO causing growth cone collapse through inhibition of *S*-palmitoylation, but inhibition of PDI/GSNO collapse by blocking depalmitoylation with Palmostatin B would be a more direct and conclusive assay.

5.5 Discussion

5.5.1 3004.2KLH-Binding Protein

The investigation of the molecular nature of the 3004.2KLH-binding protein, which had been provisionally characterised as MVP, began with short sequences from mass spectrometry of a rat brain-derived sample, a polyclonal antibody (3004.2KLH) against one of the sequences and a candidate identity for the protein, major vault protein (MVP), from sequencing of the 3004.2KLH-positive band observed in human cells. MVP is established as a cytosolic protein in cancer biology (Scheffer et al., 1995) with increased expression in chemotherapy-resistant tumours such as the Grade IV astrocytoma from which the human cell line was derived (Lu and Shervington, 2008) and shares no clear homologies with the rat- or chick-derived sequences. However, Brunet et al. (2005) demonstrated that Engrailed-2, a protein previously identified as a DNA-binding Hox gene, also acts as a diffusible guidance cue, demonstrating that proteins thought to be purely intracellular in function and location can also act extracellularly. The recombinant human MVP was compared with the protein identified in 1718 cells through immunoprecipitation, growth cone repulsion and deglycosylation to determine whether MVP was a likely identity.

Recombinant MVP does not induce detectable growth cone collapse at molar concentrations comparable to Sema3A (Figure 5.3). MVP cannot bind to 3004.2KLH, and anti-MVP cannot bind to 3004.2KLH's target (Figure 5.5). MVP is subject only to partial protein degradation and no deglycosylation under conditions of alkaline β-elimination, whereas the majority of the 3004.2KLH-binding protein is lost within 30 min, even after reducing temperature (Figure 5.8(b)).

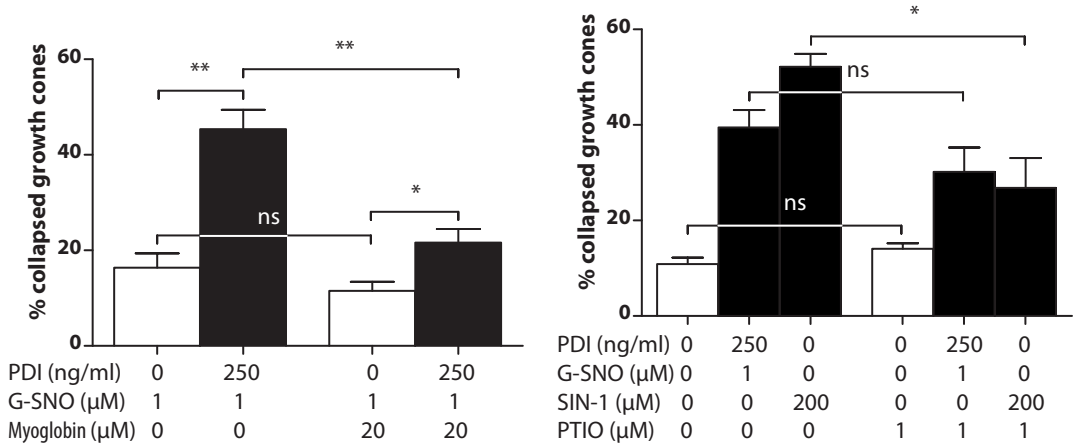

(a) The Effects of Myoglobin on PDI/GSNO Collapse (b) The Effects of PTIO on PDI/GSNO and SIN-1 Collapse

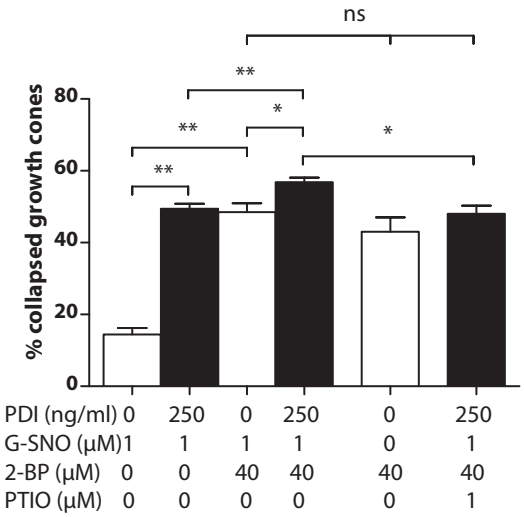

(c) Palmitoylation and PDI-induced Collapse

Figure 5.18: The Role of NO and Palmitoylation in PDI/GSNO Collapse

The collapse of PDI/GSNO are attenuated by the presence of myoglobin (a), which can sequester NO. The use of PTIO has similar effects upon SIN-1 (b), which spontaneously releases NO in aqueous solution, but the assay had insufficient power to determine whether the effect on PDI/GSNO collapse was significant. Both PTIO/GSNO and *2*-bromopalmitate induce collapse (c), which is only mildly synergistic, and this additive effect can be abolished with the addition of PTIO, which implies that they may share a mode of action.

Structural data suggest that MVP forms multimeric vaults within the cytoplasm and analysis of the 'transmembrane tendency' (Zhao and London, 2006) of MVP revealed only short (8 residues or less) stretches of weakly positive scores (<0.720) where solubility is essentially zero beyond +0.8. Established transmembrane proteins, by contrast, have longer stretches of higher scores, reaching +1.75. MVP is therefore likely to be a co-localising protein in 2-D gel electrophoresis.

5.5.2 cDNA and Prosaposin

As protein methods failed to reveal more about the identity of the 3004.2KLH-binding protein, I turned to the sequences known from the rat homologue of the protein, against which the antibody had been generated. I created primers against the sequences and used cDNA samples from the 1718 cell line to fish for similar sequences. Such sequences were selected for their size and band intensity to allow DNA sequencing. Of the sequences identified (Table 5.1), prosaposin was identified as a possible candidate through its localisation to cell membranes of the nervous system and its predicted unglycosylated mass.

Prosaposin without glycosylation has a predicted mass of ~58 kDa, similar to that found after removal of *O*-glycans from the the 3004.2KLH-binding protein (see *Appendix*). However, its primary sequence shows little homology with the original targets of the primers (Tables A.5 and A.2). Further, previous studies have established it as a neurotrophin (O'Brien et al., 1994), which promotes recovery after nerve injury (Kotani et al., 1996).

Prosaposin in the brain has been characterised as primarily or exclusively derived from neurons (Kondoh et al., 1993; Hosoda et al., 2007). My data seem to contradict this, being found both in axon targets such as skeletal muscle fibres, and throughout the optic nerve, rather than simply in association with the nerve fibres. In the developing spinal cord, the β-tubulin–rich (i.e. axon-rich) areas are not correspondingly prosaposin-rich. In addition, the cDNA sample derives from a cultured astrocytoma cell line, indicating that astrocytes synthesise prosaposin. It may well be that non-neuronal expression falls post-development, and the expression of prosaposin mRNA in the astrocytoma reflects dedifferentiation of the tumour cells. However, its

presence in the optic nerve may suggest wider application of its neurotrophic properties than for peripheral nerve lesions alone.

5.5.3 Protein Disulphide Isomerase

Novel cell-surface protein disulphide isomerases, expressed upon platelet activation, modulate adhesion and transnitrosylation distinct from NO synthase-produced NO (Root et al., 2004; Xiao and Gordge, 2011). Bovine PDI was used as a model molecule with GSNO as an *S*-nitrosylated donor of NO to examine a possible role in axon guidance.

PDI's most well-established function is in the ER, where it catalyses the rearrangement of disulphide bonds while proteins fold, speeding their folding. Its mechanism involves a cysteine thiol group, with a lowered pK_a, being protonated and attacking disulphide bonds (Gruber et al., 2006), substituting one half of the disulphide bridge with itself. An oxidoreductin reduces PDI back to its original state with FADH.

This nucleophilic attack can analogously capture NO from nitrosylated thiols (Zai et al., 1999), which can either be transferred to other thiols or reduced to free NO (Figure 5.19). Adding a nitrosylated thiol, GSNO, to PDI as a donor of the NO moiety allows PDI to collapse growth cones, a property not found in either GSNO or PDI alone (Figure 5.13). This suggests that *S*-nitrosylation of the PDI active site is necessary to cause collapse. After *S*-nitrosylation, PDI can release NO either by transferring it to another protein's thiol side-chain, or an oxidoreductase can release free NO. It is also possible that nitrosylated PDI itself binds to an unknown target to induce collapse.

Concentrations of PDI and GSNO, and Duration of Incubation

The extent of PDI/GSNO-induced collapse is dependent upon PDI concentration but not GSNO concentration at the concentrations tested (Figure 5.14). This may reflect saturation kinetics within the signalling, although more data points would be needed for firmer conclusions.

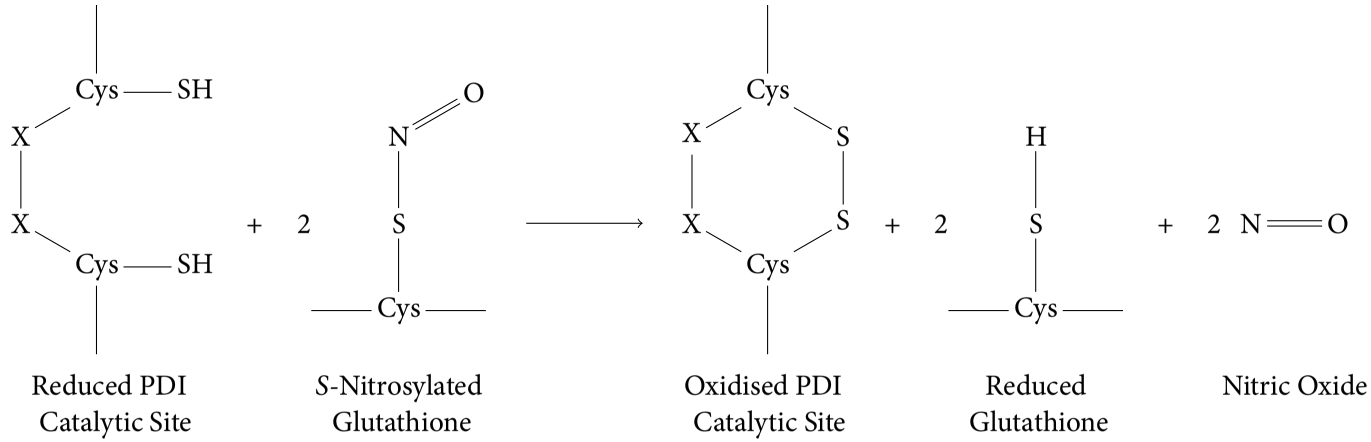

Figure 5.19: Schematic of PDI-Catalysed Release of NO from *S*-Nitrosylated Glutathione

The catalytic site of PDI consists of the CXXC motif, where each thiol group has its pK_a lowered by neighbouring side-chains such that they can form thiolate ($-S^-$) ions, which can then perform nucleophilic attack on the sulphur of *S*-nitrosylated glutathione. This allows the charge to transfer across, releasing nitric oxide. The remaining glutathiones bound to each PDI sulphur are released when they bind protons, allowing the 2 sulphurs of PDI to form a disulphide bridge. The cycle is completed when this bridge is reduced back to 2 thiol groups. Intracellular *S*-nitrosylation is thought to occur *via* a temporary combination with O_2 to form N_2O_3, a powerful nitrosylating agent, as it passes through the membrane (Ramachandran et al., 2001).

169

PDI/GSNO requires at least an hour to achieve the maximum extent of collapse (Figure 5.15). NO is a small molecule, similar in size and mass to diatomic oxygen and diffuses quickly through both plasma membranes and cytosol (Moncada and Higgs, 1993). Little is known about how NO causes growth cone collapse, although Tojima et al. (2009) suggest modulation of Ca^{2+} levels and calcium-induced calcium release (CICR) through cGMP, and Figure 3.18 implies activation of GSK-3β. Guidance mechanisms that involve nitric oxide, such as Sema3A, can induce maximal collapse in shorter time-scales (Dontchev and Letourneau, 2002). This suggests that other mechanisms cause the time lag, such as localisation effects or *S*-nitrosylation. This does not rule out a role for the NO/cGMP axis downstream of PDI/GSNO; several mechanisms may operate in tandem downstream of any given guidance molecule, as seen in Chapters 3 and 4. Different pathways may act on differing time-scales, as seen in Nogo-δ20 (Figure 4.2). The time delay may also be due to slow reduction of PDI after NO release, which *in vivo* might be performed by oxidoreductases in the cell membrane or in the extracellular milieu; soluble PDI in oxygenated medium would have ready access to neither.

There is a limit to the extent of collapse induced by increasing PDI, as doubling the concentration of PDI fails to increase collapse beyond a certain concentration (Figure 5.14(a)). However, 50%+ collapse may be sufficient for guidance. This limit may be due to insufficient GSNO, but there was 1 μM GSNO (58× that of the maximum molar concentration of PDI) present and even in pathological states, NO concentration does not rise much beyond 2.5 nM (Hall and Attwell, 2008), rendering this unlikely. Alternatively, the mechanisms through which PDI/GSNO exert their collapse effect may not fully collapse all growth cones (90%+) under my conditions at maximal effect, as seen with Nogo-δ20 (Figure 4.1), and unlike Sema3A (Figure 3.8) or Nogo-66 (*data not shown*). Failure to cause 90%+ collapse makes it unlikely that PDI/GSNO is inducing collapse through toxicity, which would also induce growth cone collapse. Neither were thinning or beading of the axons observed in any culture (*data not shown*), again suggesting that the collapse effect is non-toxic.

5.5.4 Summary

In this chapter, I have demonstrated that MVP is not our molecule of interest through immunoprecipitation and biochemical techniques. I also identified another molecule, prosaposin, through cDNA techniques, whose presence on glia had not been previously reported. Although reported to be neurotrophic within neurons (O'Brien et al., 1994), its role in glia might prove of interest in spinal cord injury (Kotani et al., 1996). Turning to PDI, another candidate guidance molecule, I have demonstrated that PDI in the presence of an *S*-nitrosylated peptide can mediate growth cone collapse in a dose-dependent manner., and that it is likely to involve both cGMP and other mechanisms. To demonstrate definitively that transnitrosylation or free NO are truly involved will require inhibition and assays to detect NO, but I have shown that cGMP synthesis is unlikely to be the sole mediator of PDI/GSNO's effects on growth cones.

Chapter 6

Conclusions and Future Work

The major aim of this thesis was to establish the extent to which protein synthesis in the growth cone is essential for its response to external guidance cues. This has been investigated with regard to two known cues, Sema3A and Nogo-A, both of which were investigated in relation to their repellent properties. In addition, the thesis covers candidate astrocyte cues and the degree to which they involve novel mechanisms regulating axon growth.

6.1 Semaphorin-3A

Semaphorin-3A induces collapse through separate mechanisms Here it is demonstrated that Sema3A operates through at least two pathways. The effects of inhibiting protein synthesis are dependent upon the concentrations of Sema3A and NGF; the dependence of the collapse upon protein synthesis falls as Sema3A concentration increases and NGF concentration falls. Conversely, the dependence of the collapse upon GSK-3β increases.

This dual mechanism resolves the conflicting data in the literature, with some studies indicating total dependence upon protein synthesis and others claiming that no synthesis is required. Separable pathways are not without precedent; Ben-Zvi et al. (2008) showed that the collapse-inducing and growth-inhibiting effects of Sema3A are independent. Further, Perron and Dodd (2011) demonstrated independent guidance and non-guidance mechanisms that require differing BMP concentrations for activation. This model requires recruitment of differing receptor

complex sub-units, a role that L1CAM may adopt when binding to neuropilin-1.

This new understanding of independent and possibly antagonistic pathways downstream of the same guidance cue, yet both causing collapse, aids understanding of axon guidance. Interventions to aid CNS regeneration, such as PTEN knock-outs (Park et al., 2008; Liu et al., 2010) might therefore simultaneously activate one pathway and inhibit the other. Multiple independent mechanisms may also allow regulation of sensitivity between neuron types, varying their responses to Sema3A-rich environments (Nédelec et al., 2012). Interestingly, NOS up-regulates GSK-3β downstream of Sema3A. Observations of this mechanism have not previously been published to the author's knowledge, but may be linked to Sema3A's suppression of axon initiation *via* cGMP (Shelly et al., 2011).

Signalling upstream of mTOR has yet to be elucidated Although the involvement of mTOR was established early on (Campbell and Holt, 2001), the signalling linking Sema3A with mTOR activity leading to RhoA synthesis is unknown, and inhibition of Erk1/2, posited as an effector by Campbell and Holt (2003), does not influence protein synthesis. Direct assessment of RhoA levels in the presence of Erk1/2 would test this hypothesis. As Welshhans and Bassell (2011) have investigated mRNA-binding ZBP-1 and local β-actin synthesis, future work would target FMR1, the RNA-binding protein which releases *RhoA* mRNA.

The signalling downstream of L1CAM is unclear; it may modulate the GSK-3β–dependent pathway *via* NOS (Castellani et al., 2002), mTOR activity, or disassembly of focal adhesions (Bechara et al., 2008), or any combination of the three. The study of Nédelec et al. (2012), assessing two motor neuron populations, only one of which undergoes PS-dependent repulsion, could offer a starting point to examine L1CAM's role in this difference.

It is also possible that mTOR is not directly regulated by Sema3A. Direct analysis of mTORC1 phosphorylation after exposure to Sema3A may answer this. A large range of guidance cues induce acute protein synthesis, including BDNF, Slit2b and netrin-1. However, beyond the requirement for mTOR complex 1 and phosphorylation of eIF4E-BP1, no definitive control mech-

anisms have been established which could link receptor-ligand interactions to protein synthesis. Similarly, little is known as to how the *RhoA* mRNA is regulated; as protein phosphatase 2 (PP2A) activity appears to cause *RhoA* mRNA release and inhibit ZBP1's release of *β-actin* mRNA (Narayanan et al., 2008; Sasaki et al., 2010), it may be a future target for investigation.

6.2 Nogo-A

Nogo-δ20–induced collapse requires protein synthesis Nogo-δ20 induces an mTOR-dependent increase in RhoA protein within the growth cone, similar to the PS-dependent pathway of Semaphorin-3A–induced collapse. But unlike that of Semaphorin-3A, the dependence is absolute and invariant over the concentration range tested, and nor is cGMP required for collapse. Endocytosis and PI3-K activity are absolutely required, similar to Pincher-mediated endocytosis downstream of NGF/TrkA (Bonanomi et al., 2008), but clathrin-mediated endocytosis is also involved.

By contrast, Nogo-66 displayed no such dependence on PS nor clathrin, and induced no detectable mTOR activity. Nogo-66–induced collapse instead revealed a partial dependence upon the proteasome. This requirement of the proteasome *vs* Nogo-δ20's dependence on protein synthesis may be necessary in differing circumstances of each domain's role or may reflect their postulated evolutionary origins (Shypitsyna et al., 2011). However, none of the proteins acutely degraded in the guidance response to Nogo-66, or indeed in response to other guidance cues such as netrin-1, has been identified to the author's knowledge.

Nogo-A is a major inhibitor of axon regeneration in the injured CNS and an active target of clinical research, and understanding axon-repelling mechanisms may lead to new therapies to counter its effects. The connection between Nogo-66 and the proteasome is novel. Further, these data illustrate the role of protein concentration as a dynamic regulator of the growth cone.

Whether synthesis of RhoA causes collapse should be confirmed These data do not indicate whether the increase in RhoA is from local protein synthesis, or that it is necessary and sufficient

to induce collapse. It is conceivable that RhoA is instead transferred from the central domain (excluded from analysis) to the periphery. There may be other proteins synthesised with other short- or long-term effects; an unbiased analysis of the total newly-synthesised proteins would reveal more comprehensive information. Nogo-66 does not require protein synthesis acutely, but it may instead influence protein synthesis in the soma, as does NGF.

Future assays would also explore the relationship between Nogo-δ20 and Nogo-66, which differ in evolutionary origin, the degree of collapse-inducing effects and signalling pathways. Nogo-A's physiological topology within the cell membrane, how it is regulated and whether this changes after injury may be key to understanding Nogo-A's role in development and disease, and why Nogo-B and -C do not play such a role, despite sharing the Nogo-66 loop domain. Nogo-δ20, on the other hand, is thought to be related to the CSPG neurocan, and its receptor may be similar as well (Schmandke and Schmandke, *personal communication*).

6.3 Astrocyte Repulsive Protein and Protein Disulphide Isomerase

Astrocyte Repulsive Protein is not Major Vault Protein Immunological, collapse assay and sequence data indicate that MVP is not the target protein in CRL 1718 astrocytoma cells. A more likely scenario is that MVP's relative preponderance in high-grade tumour cells co-purified with and overwhelmed any ARP signal during mass spectrometry. However, further experiments failed to present a convincing alternative candidate. The use of rat and chicken brain, from which the original sequences were derived, may uncover more definitive sequence.

Prosaposin is found in muscle and glia Selective cDNA amplification brought forward a possible identity, prosaposin, previously characterised as a neuron-specific neurotrophic factor. Immunohistochemistry suggests instead that it is present in muscle fibres and glia in the chick embryo, suggesting a role in development. However, little is known and manipulation of expression could be used to elucidate embryological roles.

Protein Disulphide Isomerase can repel growth cones Hess et al. (1993) first demonstrated the ability of nitric oxide-releasing molecules to collapse growth cones. Cell-surface PDI is known to be able to release nitric oxide from GSNO, an *S*-nitrosylated peptide, into adjacent platelets, regulating aggregation (Root et al., 2004; Shah et al., 2007; Irwin et al., 2009). Here the data demonstrate that PDI can induce growth cone collapse *in vitro* only in the presence of GSNO, reducing it to gain its NO group (Ramachandran et al., 2001). However, PDI's *in vivo* role in axon guidance is unconfirmed; RNAi targeted specifically against cell-surface PDI during development and inhibition with a specific inhibitor are two directions which may resolve this.

The mechanism of NO release is yet to be confirmed The evidence in this thesis is centred upon growth cone collapse; direct evidence of NO release is needed. Pharmacological inhibitors, such as bacitracin, would show the involvement of the catalytic site and its use *in vivo* would confirm a physiological role. Also, α-tocopherol would test for the involvement of $ONOO^-$ as a mechanism for traversal of the membrane and oxidative activity in the cell. Finally, the use of *2*-bromopalmitate could only confirm that inhibition of *S*-palmitoylation induces acute collapse and may be part of nitric oxide's effects upon the growth cone. Whether inhibition of acyl thioproteinesterase-1 with palmostatin B *in vitro* can inhibit collapse, specifically PDI/GSNO-induced, would resolve this.

The extent of Protein Disulphide Isomerase's role is unknown PDI is expressed on the cell surface in a variety of tissues, and *S*-nitrosylated proteins are thought to be ubiquitous. Whether the presence of PDI at the cell surface is the determining factor in repelling growth cones, or whether only certain PDIs or other molecules determine repulsive activity is unknown; for example, reductases could be required to maintain levels of unoxidised PDI at the cell surface.

6.4 Concluding Remarks

The conflicting data over the relevance of protein synthesis downstream of Semaphorin-3A are resolved: the necessity of synthesis to cause collapse is dependent on concentration. This is due

to parallel collapse-inducing pathways. The role of the protein synthesis and the proteasome in growth cone collapse has also been extended to Nogo-A. However, these findings leave open the extent of cross-talk and the biological relevance of such dual (or more) mechanisms. The mechanism for initiating protein synthesis is also sparsely established. The role of cell-surface PDI in growth cone guidance *in vivo* is possible but not yet proven and, if so, the actions of nitric oxide in guidance may gain a new angle.

6.4.1 Findings' Roles in the Field and Future Directions

Looking further afield, these results add to the growing evidence that single cues have multiple effectors and multiple receptors, and their effects are dependent upon both extrinsic (e.g. NGF) and intrinsic (e.g. local protein synthesis) factors. Not only this, but there remain large gaps in our knowledge, such as the repulsive factors found during somite segmentation, and new discoveries about long-established effects, such as cAMP's regenerative effects being mediated through EPAC rather than PKA, which instead may even oppose regeneration. This complexity and the multiplicity of targets compound to support the view that SCI treatment will require multiple additive lines of attack, whereas many promising individual therapies have produced disappointing results in clinical trials, from corticosteroids to anti–Nogo-A antibodies. Whether multiple therapies might interact negatively, however, remains an open question, and drastic interventions producing impressive results in primary research, such as PTEN knock-outs, may not be feasible clinically.

The role of protein synthesis, however, continues to expand. RhoA synthesis is now known to be required for much of CSPGs' growth-restricting effects. Together with Nogo-δ20's homology to CSPGs, this implies a whole group of inhibitory factors that require local protein synthesis for their full effect. But recent analyses of mRNAs contained and proteins synthesised has not been matched by analysis of proteins degraded by the proteasome, a phenomenon discovered downstream of guidance cues at the same time. Similarly, as the range of growth cone mRNAs reaches into the thousands, our knowledge of regulatory proteins (e.g. ZBP-1 and FXR-1) and microRNAs in the growth cones has been expanding only recently.

Whilst the above focuses upon SCI, there is an arguably greater burden created by the CNS's failure to regenerate elsewhere: loss of vision. Diseases such as glaucoma, diabetic retinopathy and uveitis cause irreversible sight loss to a large and growing fraction of the world's population. Moreover, the eye is uniquely accessible, with the RGCs separated from the injectable vitreous only by a single membrane, with a similar immunological isolation. Such an anatomical arrangement allows ready access to the retina by lasers, antibodies and RNAi, to name a few, and therapies to support survival and regeneration of axons might find easier application and more success in maintaining vision, a major and growing health burden in an ageing world population.

Finally, whilst failure of regeneration is the focus of this thesis, unwanted growth into injured areas such as the inner Achilles tendon or intervertebral cartilage is also an issue. Here, innervation post-injury causes great pain and subsequent disability, and little is known about the original factors that limit their ingress during development. Research into novel factors, such as cell-surface PDI, may suggest solutions in the PNS as well as the CNS.

Current research is focused understandably on spinal injuries due to its devastating impact on mostly young people, but expanding the field to incorporate other medical interventions, such as replasticising the cortex and maintaining visual function, would expand benefit to greater numbers of patients, as anti-VEGF therapies have done moving from oncology to ophthalmology. Nor is this a one-way process; developments in parallel fields could offer fresh perspective. But despite the challenges ahead, it is useful to remember how far the field has come; SCIs have moved from a lethal injury of war for Horatio Nelson and George Patton, to a survivable injury with potential for recovery. Complexity makes it unlikely that a complete cure *ex nihilo* will be found, but the incremental improvements will doubtless continue. Hopefully, in the future, the field will again be able to look back and see how much further we have come.

Bibliography

Abelson JN, Simon MI, Lennarz WJ, Hart GW. *Guide to Techniques in Glycobiology (Methods in Enzymology)* (Academic Press, New York, 1994).

Ackman JB, Ramos RL, Sarkisian MR, Loturco JJ. Citron kinase is required for postnatal neurogenesis in the hippocampus. *Dev Neurosci* 2007;29(1-2):113–23.

Adams RH, Eichmann A. Axon guidance molecules in vascular patterning. *Cold Spring Harb Perspect Biol* 2010;2(5):a001875.

Adams RH, Lohrum M, Klostermann A, Betz H, Püschel AW. The chemorepulsive activity of secreted semaphorins is regulated by furin-dependent proteolytic processing. *EMBO J* 1997;16(20):6077–86.

Agulhon C, Fiacco TA, McCarthy KD. Hippocampal short- and long-term plasticity are not modulated by astrocyte Ca2+ signaling. *Science* 2010;327(5970):1250–4.

Ahern GP, Klyachko VA, Jackson MB. cGMP and S-nitrosylation: two routes for modulation of neuronal excitability by NO. *Trends Neurosci* 2002;25(10):510–7.

Ahmed Z, Douglas MR, Read ML, Berry M, Logan A. Citron kinase regulates axon growth through a pathway that converges on cofilin downstream of RhoA. *Neurobiol Dis* 2011;41(2):421–9.

Aizawa H, Wakatsuki S, Ishii A, Moriyama K, Sasaki Y, Ohashi K, Sekine-Aizawa Y, Sehara-Fujisawa A, Mizuno K, Goshima Y, Yahara I. Phosphorylation of cofilin by LIM-kinase is necessary for semaphorin 3A-induced growth cone collapse. *Nat Neurosci* 2001;4(4):367–73.

Akagi S, Yamamoto A, Yoshimori T, Masaki R, Ogawa R, Tashiro Y. Localization of protein disulfide isomerase on plasma membranes of rat exocrine pancreatic cells. *J Histochem Cytochem* 1988;36(8):1069–74.

Allen MJ, Shan X, Murphey RK. A role for Drosophila Drac1 in neurite outgrowth and synaptogenesis in the giant fiber system. *Mol Cell Neurosci* 2000;16(6):754–65.

Amano M, Chihara K, Nakamura N, Fukata Y, Yano T, Shibata M, Ikebe M, Kaibuchi K. Myosin II activation promotes neurite retraction during the action of Rho and Rho-kinase. *Genes to cells : devoted to molecular & cellular mechanisms* 1998;3(3):177–88.

Amano M, Kaneko T, Maeda A, Nakayama M, Ito M, Yamauchi T, Goto H, Fukata Y, Oshiro N, Shinohara A, Iwamatsu A, Kaibuchi K. Identification of Tau and MAP2 as novel substrates of Rho-kinase and myosin phosphatase. *J Neurochem* 2003;87(3):780–90.

Anderson DJ, Hetzer MW. Reshaping of the endoplasmic reticulum limits the rate for nuclear envelope formation. *J Cell Biol* 2008;182(5):911–24.

Andreassi C, Zimmermann C, Mitter R, Fusco S, De Vita S, Devita S, Saiardi A, Riccio A. An NGF-responsive element targets myo-inositol monophosphatase-1 mRNA to sympathetic neuron axons. *Nat Neurosci* 2010;13(3):291–301.

Andrews GL, Tanglao S, Farmer WT, Morin S, Brotman S, Berberoglu MA, Price H, Fernandez GC, Mastick GS, Charron F, Kidd T. Dscam guides embryonic axons by Netrin-dependent and -independent functions. *Development* 2008;135(23):3839–48.

Andrews MR, Czvitkovich S, Dassie E, Vogelaar CF, Faissner A, Blits B, Gage FH, Ffrench-Constant C, Fawcett JW. Alpha9 integrin promotes neurite outgrowth on tenascin-C and enhances sensory axon regeneration. *J Neurosci* 2009;29(17):5546–57.

Antipenko A, Himanen JP, van Leyen K, Nardi-Dei V, Lesniak J, Barton WA, Rajashankar KR, Lu M, Hoemme C, Püschel AW, Nikolov DB. Structure of the semaphorin-3A receptor binding module. *Neuron* 2003;39(4):589–98.

Aoki K, Nakamura T, Matsuda M. Spatio-temporal regulation of Rac1 and Cdc42 activity during nerve growth factor-induced neurite outgrowth in PC12 cells. *J Biol Chem* 2004;279(1):713–9.

Apostolova I, Irintchev A, Schachner M. Tenascin-R restricts posttraumatic remodeling of motoneuron innervation and functional recovery after spinal cord injury in adult mice. *J Neurosci* 2006; 26(30):7849–59.

Aratyn-Schaus Y, Gardel ML. Transient frictional slip between integrin and the ECM in focal adhesions under myosin II tension. *Curr Biol* 2010;20(13):1145–53.

Aronov S, Aranda G, Behar L, Ginzburg I. Axonal tau mRNA localization coincides with tau protein in living neuronal cells and depends on axonal targeting signal. *J Neurosci* 2001;21(17):6577–6587.

Atwal JK, Pinkston-Gosse J, Syken J, Stawicki S, Wu Y, Shatz C, Tessier-Lavigne M. PirB is a functional receptor for myelin inhibitors of axonal regeneration. *Science* 2008;322(5903):967–70.

Azevedo FAC, Carvalho LRB, Grinberg LT, Farfel JM, Ferretti REL, Leite REP, Jacob Filho W, Lent R, Herculano-Houzel S. Equal numbers of neuronal and nonneuronal cells make the human brain an isometrically scaled-up primate brain. *J Comp Neurol* 2009;513(5):532–41.

Bagnard D, Lohrum M, Uziel D, Püschel AW, Bolz J. Semaphorins act as attractive and repulsive guidance signals during the development of cortical projections. *Development* 1998;125(24):5043–53.

Barberis D, Artigiani S, Casazza A, Corso S, Giordano S, Love CA, Jones EY, Comoglio PM, Tamagnone L. Plexin signaling hampers integrin-based adhesion, leading to Rho-kinase independent cell rounding, and inhibiting lamellipodia extension and cell motility. *FASEB J* 2004;18(3):592–4.

Barraud P, Seferiadis AA, Tyson LD, Zwart MF, Szabo-Rogers HL, Ruhrberg C, Liu KJ, Baker CVH. Neural crest origin of olfactory ensheathing glia. *Proc Natl Acad Sci U S A* 2010;107(49):21040–5.

Basile JR, Gavard J, Gutkind JS. Plexin-B1 utilizes RhoA and Rho kinase to promote the integrin-dependent activation of Akt and ERK and endothelial cell motility. *J Biol Chem* 2007;282(48):34888–95.

Bassell GJ, Zhang H, Byrd AL, Femino AM, Singer RH, Taneja KL, Lifshitz LM, Herman IM, Kosik KS. Sorting of beta-actin mRNA and protein to neurites and growth cones in culture. *J Neurosci* 1998; 18(1):251–65.

Bavelier D, Levi DM, Li RW, Dan Y, Hensch TK. Removing Brakes on Adult Brain Plasticity: From Molecular to Behavioral Interventions. *J Neurosci* 2010;30(45):14964–14971.

Beattie EC, Stellwagen D, Morishita W, Bresnahan JC, Ha BK, Von Zastrow M, Beattie MS, Malenka RC. Control of synaptic strength by glial TNFalpha. *Science* 2002;295(5563):2282–5.

Bechara A, Nawabi H, Moret F, Yaron A, Weaver E, Bozon M, Abouzid K, Guan JL, Tessier-Lavigne M, Lemmon V, Castellani V. FAK-MAPK-dependent adhesion disassembly downstream of L1 contributes to semaphorin3A-induced collapse. *EMBO J* 2008;27(11):1549–62.

Bellon A, Luchino J, Haigh K, Rougon G, Haigh J, Chauvet S, Mann F. VEGFR2 (KDR/Flk1) signaling mediates axon growth in response to semaphorin 3E in the developing brain. *Neuron* 2010;66(2):205–19.

Ben-Zvi A, Ben-Gigi L, Yagil Z, Lerman O, Behar O. Semaphorin3A regulates axon growth independently of growth cone repulsion via modulation of TrkA signaling. *Cell Signal* 2008;20(3):467–79.

Bentley D, Caudy M. Pioneer axons lose directed growth after selective killing of guidepost cells. *Nature* 1983;304(5921):62–5.

Berman S, Morris A. Nitric oxide as a putative retinal axon pathfinding and target recognition cue in Xenopus laevis. *Impulse (Columbia, S.C.)* 2011;2010:1–12.

Berman SA, Moss D, Bursztajn S. Axonal branching and growth cone structure depend on target cells. *Dev Biol* 1993;159(1):153–62.

Bonanomi D, Fornasiero EF, Valdez G, Halegoua S, Benfenati F, Menegon A, Valtorta F. Identification of a developmentally regulated pathway of membrane retrieval in neuronal growth cones. *J Cell Sci* 2008; 121(Pt 22):3757–69.

Bonanomi D, Pfaff SL. Motor axon pathfinding. *Cold Spring Harb Perspect Biol* 2010;2(3):a001735.

Bourne JN, Harris KM. Balancing structure and function at hippocampal dendritic spines. *Annu Rev Neurosci* 2008;31:47–67.

Bovolenta P, Mason C. Growth cone morphology varies with position in the developing mouse visual pathway from retina to first targets. *J Neurosci* 1987;7(5):1447–60.

Bracken MB, Shepard MJ, Collins WF, Holford TR, Young W, Baskin DS, Eisenberg HM, Flamm E, Leo-Summers L, Maroon J. A randomized, controlled trial of methylprednisolone or naloxone in the treatment of acute spinal-cord injury. Results of the Second National Acute Spinal Cord Injury Study. *The New England journal of medicine* 1990;322(20):1405–11.

Bradbury EJ, Moon LDF, Popat RJ, King VR, Bennett GS, Patel PN, Fawcett JW, McMahon SB. Chondroitinase ABC promotes functional recovery after spinal cord injury. *Nature* 2002;416(6881):636–40.

Bradke F, Dotti CG. The role of local actin instability in axon formation. *Science* 1999;283(5409):1931–4.

Brambilla R, Hurtado A, Persaud T, Esham K, Pearse DD, Oudega M, Bethea JR. Transgenic inhibition of astroglial NF-kappa B leads to increased axonal sparing and sprouting following spinal cord injury. *J Neurochem* 2009;110(2):765–78.

Bray D. *Cell Movements: From Molecules to Motility* (Garland Science, 2000).

Brent AE, Schweitzer R, Tabin CJ. A somitic compartment of tendon progenitors. *Cell* 2003;113(2):235–48.

Bronner-Fraser M. Analysis of the early stages of trunk neural crest migration in avian embryos using monoclonal antibody HNK-1. *Dev Biol* 1986;115(1):44–55.

Brown V, Jin P, Ceman S, Darnell JC, O'Donnell WT, Tenenbaum SA, Jin X, Feng Y, Wilkinson KD, Keene JD, Darnell RB, Warren ST. Microarray identification of FMRP-associated brain mRNAs and altered mRNA translational profiles in fragile X syndrome. *Cell* 2001;107(4):477–87.

Brunet I, Weinl C, Piper M, Trembleau A, Volovitch M, Harris W, Prochiantz A, Holt C. The transcription factor Engrailed-2 guides retinal axons. *Nature* 2005;438(7064):94–8.

Buck KB, Zheng JQ. Growth cone turning induced by direct local modification of microtubule dynamics. *J Neurosci* 2002;22(21):9358–67.

Bundesen LQ, Scheel TA, Bregman BS, Kromer LF. Ephrin-B2 and EphB2 regulation of astrocyte-meningeal fibroblast interactions in response to spinal cord lesions in adult rats. *J Neurosci* 2003; 23(21):7789–800.

Burridge K, Wennerberg K. Rho and Rac take center stage. *Cell* 2004;116(2):167–79.

Bush TG, Puvanachandra N, Horner CH, Polito a, Ostenfeld T, Svendsen CN, Mucke L, Johnson MH, Sofroniew MV. Leukocyte infiltration, neuronal degeneration, and neurite outgrowth after ablation of scar-forming, reactive astrocytes in adult transgenic mice. *Neuron* 1999;23(2):297–308.

Cafferty WBJ, Strittmatter SM. Limitation of adult CNS axonal growth by Nogo/NgR1 pathway. In *Axon Guidance, Synaptic Plasticity & Regeneration Meeting, CSHL* (Cold Spring Harbor Laboratory Press, Cold Spring Harbor, NY, USA, 2010) 153.

Campbell DS, Holt CE. Chemotropic responses of retinal growth cones mediated by rapid local protein synthesis and degradation. *Neuron* 2001;32(6):1013–26.

Campbell DS, Holt CE. Apoptotic pathway and MAPKs differentially regulate chemotropic responses of retinal growth cones. *Neuron* 2003;37(6):939–52.

Campbell DS, Regan AG, Lopez JS, Tannahill D, Harris WA, Holt CE. Semaphorin 3A elicits stage-dependent collapse, turning, and branching in Xenopus retinal growth cones. *J Neurosci* 2001; 21(21):8538–47.

Caroni P, Schwab ME. Antibody against myelin-associated inhibitor of neurite growth neutralizes non-permissive substrate properties of CNS white matter. *Neuron* 1988*a*;1(1):85–96.

Caroni P, Schwab ME. Two membrane protein fractions from rat central myelin with inhibitory properties for neurite growth and fibroblast spreading. *J Cell Biol* 1988*b*;106(4):1281–8.

Casazza A, Finisguerra V, Capparuccia L, Camperi A, Swiercz JM, Rizzolio S, Rolny C, Christensen C, Bertotti A, Sarotto I, Risio M, Trusolino L, Weitz J, Schneider M, Mazzone M, Comoglio PM, Tamagnone L. Sema3E-Plexin D1 signaling drives human cancer cell invasiveness and metastatic spreading in mice. *J Clin Invest* 2010;120(8):2684–98.

Castellani V, Chédotal A, Schachner M, Faivre-Sarrailh C, Rougon G. Analysis of the L1-deficient mouse phenotype reveals cross-talk between Sema3A and L1 signaling pathways in axonal guidance. *Neuron* 2000;27(2):237–49.

Castellani V, De Angelis E, Kenwrick S, Rougon G. Cis and trans interactions of L1 with neuropilin-1 control axonal responses to semaphorin 3A. *EMBO J* 2002;21(23):6348–57.

Castellani V, Falk J, Rougon G. Semaphorin3A-induced receptor endocytosis during axon guidance responses is mediated by L1 CAM. *Mol Cell Neurosci* 2004;26(1):89–100.

Chadborn NH, Ahmed AI, Holt MR, Prinjha R, Dunn GA, Jones GE, Eickholt BJ. PTEN couples Sema3A signalling to growth cone collapse. *J Cell Sci* 2006;119(Pt 5):951–7.

Chang WS, Serikawa K, Allen K, Bentley D. Disruption of pioneer growth cone guidance in vivo by removal of glycosyl-phosphatidylinositol-anchored cell surface proteins. *Development* 1992;114(2):507–19.

Charron F, Stein E, Jeong J, McMahon AP, Tessier-Lavigne M. The morphogen sonic hedgehog is an axonal chemoattractant that collaborates with netrin-1 in midline axon guidance. *Cell* 2003;113(1):11–23.

Cheever TR, Olson EA, Ervasti JM. Axonal regeneration and neuronal function are preserved in motor neurons lacking ß-actin in vivo. *PLoS ONE* 2011;6(3):e17768.

Chen L, Yun SW, Seto J, Liu W, Toth M. The fragile X mental retardation protein binds and regulates a novel class of mRNAs containing U rich target sequences. *Neuroscience* 2003;120(4):1005–17.

Chirumamilla S, Sun D, Bullock MR, Colello RJ. Traumatic brain injury induced cell proliferation in the adult mammalian central nervous system. *J Neurotrauma* 2002;19(6):693–703.

Cohen RI, Rottkamp DM, Maric D, Barker JL, Hudson LD. A role for semaphorins and neuropilins in oligodendrocyte guidance. *J Neurochem* 2003;85(5):1262–78.

Cole AR, Knebel A, Morrice NA, Robertson LA, Irving AJ, Connolly CN, Sutherland C. GSK-3 phosphorylation of the Alzheimer epitope within collapsin response mediator proteins regulates axon elongation in primary neurons. *J Biol Chem* 2004;279(48):50176–80.

Coleman ML, Sahai EA, Yeo M, Bosch M, Dewar A, Olson MF. Membrane blebbing during apoptosis results from caspase-mediated activation of ROCK I. *Nat Cell Biol* 2001;3(4):339–45.

Conti A, Miscusi M, Cardali S, Germanò A, Suzuki H, Cuzzocrea S, Tomasello F. Nitric oxide in the injured spinal cord: synthases cross-talk, oxidative stress and inflammation. *Brain Res Rev* 2007; 54(1):205–18.

Cox LJ, Hengst U, Gurskaya NG, Lukyanov KA, Jaffrey SR. Intra-axonal translation and retrograde trafficking of CREB promotes neuronal survival. *Nat Cell Biol* 2008;10(2):149–59.

Dailey ME, Bridgman PC. Dynamics of the endoplasmic reticulum and other membranous organelles in growth cones of cultured neurons. *J Neurosci* 1989;9(6):1897–909.

Dan C, Nath N, Liberto M, Minden A. PAK5, a new brain-specific kinase, promotes neurite outgrowth in N1E-115 cells. *Mol Cell Biol* 2002;22(2):567–77.

Daniels RH, Hall PS, Bokoch GM. Membrane targeting of p21-activated kinase 1 (PAK1) induces neurite outgrowth from PC12 cells. *EMBO J* 1998;17(3):754–64.

David S, Aguayo AJ. Axonal elongation into peripheral nervous system "bridges" after central nervous system injury in adult rats. *Science* 1981;214(4523):931–3.

Davies JA, Cook GM, Stern CD, Keynes RJ. Isolation from chick somites of a glycoprotein fraction that causes collapse of dorsal root ganglion growth cones. *Neuron* 1990;4(1):11–20.

Davies JE, Pröschel C, Zhang N, Noble M, Mayer-Pröschel M, Davies SJ. Transplanted astrocytes derived from BMP- or CNTF-treated glial-restricted precursors have opposite effects on recovery and allodynia after spinal cord injury. *J Biol* 2008;7(7):24.

Davies SJ, Goucher DR, Doller C, Silver J. Robust regeneration of adult sensory axons in degenerating white matter of the adult rat spinal cord. *J Neurosci* 1999;19(14):5810–22.

Delekate A, Zagrebelsky M, Kramer S, Schwab ME, Korte M. NogoA restricts synaptic plasticity in the adult hippocampus on a fast time scale. *Proc Natl Acad Sci U S A* 2011;108(6):2569–74.

Deo RC, Schmidt EF, Elhabazi A, Togashi H, Burley SK, Strittmatter SM. Structural bases for CRMP function in plexin-dependent semaphorin3A signaling. *EMBO J* 2004;23(1):9–22.

Di Cunto F, Imarisio S, Hirsch E, Broccoli V, Bulfone A, Migheli A, Atzori C, Turco E, Triolo R, Dotto GP, Silengo L, Altruda F. Defective neurogenesis in citron kinase knockout mice by altered cytokinesis and massive apoptosis. *Neuron* 2000;28(1):115–27.

Di Scala F, Dupuis L, Gaiddon C, De Tapia M, Jokic N, Gonzalez de Aguilar JL, Raul JS, Ludes B, Loeffler JP. Tissue specificity and regulation of the N-terminal diversity of reticulon 3. *Biochem J* 2005;385(Pt 1):125–34.

Dickson HM, Zurawski J, Zhang H, Turner DL, Vojtek AB. POSH is an Intracellular Signal Transducer for the Axon Outgrowth Inhibitor Nogo66. *J Neurosci* 2010;30(40):13319–13325.

Dodd DA, Niederoest B, Bloechlinger S, Dupuis L, Loeffler JP, Schwab ME. Nogo-A, -B, and -C are found on the cell surface and interact together in many different cell types. *J Biol Chem* 2005;280(13):12494–502.

Donnelly CJ, Fainzilber M, Twiss JL. Subcellular communication through RNA transport and localized protein synthesis. *Traffic* 2010;11(12):1498–505.

Dontchev VD, Letourneau PC. Nerve growth factor and semaphorin 3A signaling pathways interact in regulating sensory neuronal growth cone motility. *J Neurosci* 2002;22(15):6659–6669.

Drenning JA, Lira VA, Soltow QA, Canon CN, Valera LM, Brown DL, Criswell DS. Endothelial nitric oxide synthase is involved in calcium-induced Akt signaling in mouse skeletal muscle. *Nitric Oxide* 2009;21(3-4):192–200.

Dvorsky R, Blumenstein L, Vetter IR, Ahmadian MR. Structural insights into the interaction of ROCKI with the switch regions of RhoA. *J Biol Chem* 2004;279(8):7098–104.

East E, de Oliveira DB, Golding JP, Phillips JB. Alignment of Astrocytes Increases Neuronal Growth in Three-Dimensional Collagen Gels and Is Maintained Following Plastic Compression to Form a Spinal Cord Repair Conduit. *Tissue Eng Part A* 2010;16(10):3173–3184.

Edwards DC, Sanders LC, Bokoch GM, Gill GN. Activation of LIM-kinase by Pak1 couples Rac/Cdc42 GTPase signalling to actin cytoskeletal dynamics. *Nat Cell Biol* 1999;1(5):253–9.

Egile C, Rouiller I, Xu XP, Volkmann N, Li R, Hanein D. Mechanism of filament nucleation and branch stability revealed by the structure of the Arp2/3 complex at actin branch junctions. *PLoS Biol* 2005; 3(11):e383.

Eickholt BJ, Morrow R, Walsh FS, Doherty P. Structural features of collapsin required for biological activity and distribution of binding sites in the developing chick. *Mol Cell Neurosci* 1997;9(5-6):358–71.

Eickholt BJ, Walsh FS, Doherty P. An inactive pool of GSK-3 at the leading edge of growth cones is implicated in Semaphorin 3A signaling. *J Cell Biol* 2002;157(2):211–7.

Eng H, Lund K, Campenot RB. Synthesis of beta-tubulin, actin, and other proteins in axons of sympathetic neurons in compartmented cultures. *J Neurosci* 1999;19(1):1–9.

Ensser A, Fleckenstein B. Alcelaphine herpesvirus type 1 has a semaphorin-like gene. *The Journal of general virology* 1995;76 (Pt 4):1063–7.

Ertürk A, Hellal F, Enes J, Bradke F. Disorganized microtubules underlie the formation of retraction bulbs and the failure of axonal regeneration. *J Neurosci* 2007;27(34):9169–80.

Falk J, Julien F, Bechara A, Fiore R, Nawabi H, Zhou H, Hoyo-Becerra C, Bozon M, Rougon G, Grumet M, Püschel AW, Sanes JR, Castellani V. Dual functional activity of semaphorin 3B is required for positioning the anterior commissure. *Neuron* 2005;48(1):63–75.

Falo MC, Fillmore HL, Reeves TM, Phillips LL. Matrix metalloproteinase-3 expression profile differentiates adaptive and maladaptive synaptic plasticity induced by traumatic brain injury. *J Neurosci* 2006; 84(4):768–81.

Fedoroff S, Lindsay RM. *Reactive gliosis* (Academic Press, Orlando, 1986).

Filous AR, Miller JH, Coulson-Thomas YM, Horn KP, Alilain WJ, Silver J. Immature astrocytes promote CNS axonal regeneration when combined with chondroitinase ABC. *Dev Neurobiol* 2010;70(12):826–41.

Fournier AE, GrandPre T, Strittmatter SM. Identification of a receptor mediating Nogo-66 inhibition of axonal regeneration. *Nature* 2001;409(6818):341–6.

Fournier AE, Nakamura F, Kawamoto S, Goshima Y, Kalb RG, Strittmatter SM. Semaphorin3A enhances endocytosis at sites of receptor-F-actin colocalization during growth cone collapse. *J Cell Biol* 2000; 149(2):411–22.

Fournier AE, Takizawa BT, Strittmatter SM. Rho kinase inhibition enhances axonal regeneration in the injured CNS. *J Neurosci* 2003;23(4):1416–23.

Franze K. Atomic force microscopy and its contribution to understanding the development of the nervous system. *Current opinion in genetics & development* 2011;21(5):530–7.

Freund P, Schmidlin E, Wannier T, Bloch J, Mir A, Schwab ME, Rouiller EM. Nogo-A-specific antibody treatment enhances sprouting and functional recovery after cervical lesion in adult primates. *Nat Med* 2006;12(7):790–2.

Fu X, Gong MC, Jia T, Somlyo AV, Somlyo AP. The effects of the Rho-kinase inhibitor Y-27632 on arachidonic acid-, GTPgammaS-, and phorbol ester-induced Ca2+-sensitization of smooth muscle. *FEBS Lett* 1998;440(1-2):183–7.

Fujita Y, Endo S, Takai T, Yamashita T. Myelin suppresses axon regeneration by PIR-B/SHP-mediated inhibition of Trk activity. *EMBO J* 2011;30(7):1389–401.

Fukata Y, Oshiro N, Kaibuchi K. Activation of moesin and adducin by Rho-kinase downstream of Rho. *Biophys Chem* 1999;82(2-3):139–47.

Gagliardini V, Fankhauser C. Semaphorin III can induce death in sensory neurons. *Mol Cell Neurosci* 1999;14(4-5):301–16.

Gardiner NJ, Moffatt S, Fernyhough P, Humphries MJ, Streuli CH, Tomlinson DR. Preconditioning injury-induced neurite outgrowth of adult rat sensory neurons on fibronectin is mediated by mobilisation of axonal alpha5 integrin. *Mol Cell Neurosci* 2007;35(2):249–60.

Geraldo S, Gordon-Weeks PR. Cytoskeletal dynamics in growth-cone steering. *J Cell Sci* 2009;122(Pt 20):3595–604.

Gilestro GF. Redundant mechanisms for regulation of midline crossing in Drosophila. *PLoS ONE* 2008; 3(11):e3798.

Gingras AC, Gygi SP, Raught B, Polakiewicz RD, Abraham RT, Hoekstra MF, Aebersold R, Sonenberg N. Regulation of 4E-BP1 phosphorylation: a novel two-step mechanism. *Genes Dev* 1999;13(11):1422–37.

Gingras AC, Raught B, Sonenberg N. Regulation of translation initiation by FRAP/mTOR. *Genes Dev* 2001;15(7):807–26.

Giordana MT, Attanasio A, Cavalla P, Migheli A, Vigliani MC, Schiffer D. Reactive cell proliferation and microglia following injury to the rat brain. *Neuropathol Appl Neurobiol* 1994;20(2):163–74.

Giulian D, Chen J, Ingeman JE, George JK, Noponen M. The role of mononuclear phagocytes in wound healing after traumatic injury to adult mammalian brain. *J Neurosci* 1989;9(12):4416–29.

Goldberg DJ, Burmeister DW. Stages in axon formation: observations of growth of Aplysia axons in culture using video-enhanced contrast-differential interference contrast microscopy. *J Cell Biol* 1986; 103(5):1921–31.

Goldshmit Y, Spanevello MD, Tajouri S, Li L, Rogers F, Pearse M, Galea M, Bartlett PF, Boyd AW, Turnley AM. EphA4 Blockers Promote Axonal Regeneration and Functional Recovery Following Spinal Cord Injury in Mice. *PLoS ONE* 2011;6(9):e24636.

Goode N, Hughes K, Woodgett JR, Parker PJ. Differential regulation of glycogen synthase kinase-3 beta by protein kinase C isotypes. *J Biol Chem* 1992;267(24):16878–82.

Gore BB, Wong KG, Tessier-Lavigne M. Stem cell factor functions as an outgrowth-promoting factor to enable axon exit from the midline intermediate target. *Neuron* 2008;57(4):501–10.

Goshima Y, Nakamura F, Strittmatter P, Strittmatter SM. Collapsin-induced growth cone collapse mediated by an intracellular protein related to UNC-33. *Nature* 1995;376(6540):509–14.

Goslin K, Banker G. Experimental observations on the development of polarity by hippocampal neurons in culture. *J Cell Biol* 1989;108(4):1507–16.

GrandPré T, Li S, Strittmatter SM. Nogo-66 receptor antagonist peptide promotes axonal regeneration. *Nature* 2002;417(6888):547–51.

GrandPré T, Nakamura F, Vartanian T, Strittmatter SM. Identification of the Nogo inhibitor of axon regeneration as a Reticulon protein. *Nature* 2000;403(6768):439–44.

Greger IH, Khatri L, Ziff EB. RNA editing at arg607 controls AMPA receptor exit from the endoplasmic reticulum. *Neuron* 2002;34(5):759–72.

Gruber CW, Cemazar M, Heras Bn, Martin JL, Craik DJ. Protein disulfide isomerase: the structure of oxidative folding. *Trends Biochem Sci* 2006;31(8):455–64.

Guirland C, Buck KB, Gibney JA, DiCicco-Bloom E, Zheng JQ. Direct cAMP signaling through G-protein-coupled receptors mediates growth cone attraction induced by pituitary adenylate cyclase-activating polypeptide. *J Neurosci* 2003;23(6):2274–83.

Gumy LF, Yeo GSH, Loraine Tung YC, Zivraj KH, Willis D, Coppola G, Lam BYH, Twiss JL, Holt CE, Fawcett JW. Transcriptome analysis of embryonic and adult sensory axons reveals changes in mRNA repertoire localization. *RNA* 2010;17(1):85–98.

Guth L, Barrett CP, Donati EJ. Histological factors influencing the growth of axons into lesions of the mammalian spinal cord. *Exp. Brain Res, Suppl.* 1986;13:271–282.

Guth L, Barrett CP, Donati EJ, Anderson FD, Smith MV, Lifson M. Essentiality of a specific cellular terrain for growth of axons into a spinal cord lesion. *Exp Neurol* 1985;88(1):1–12.

Hagino S, Iseki K, Mori T, Zhang Y, Hikake T, Yokoya S, Takeuchi M, Hasimoto H, Kikuchi S, Wanaka A. Slit and glypican-1 mRNAs are coexpressed in the reactive astrocytes of the injured adult brain. *Glia* 2003;42(2):130–8.

Hall BK. The neural crest as a fourth germ layer and vertebrates as quadroblastic not triploblastic. *Evolution & development* 2000;2(1):3–5.

Hall CN, Attwell D. Assessing the physiological concentration and targets of nitric oxide in brain tissue. *The Journal of physiology* 2008;586(Pt 15):3597–615.

Hamburger V, Hamilton HL. A series of normal stages in the development of the chick embryo. *J Morphol* 1951;88(1):49–92.

Harrington AW, Li QM, Tep C, Park JB, He Z, Yoon SO. The role of Kalirin9 in p75/nogo receptor-mediated RhoA activation in cerebellar granule neurons. *J Biol Chem* 2008;283(36):24690–7.

Harris R, Sabatelli LM, Seeger MA. Guidance cues at the Drosophila CNS midline: identification and characterization of two Drosophila Netrin/UNC-6 homologs. *Neuron* 1996;17(2):217–28.

Harrison RG. The outgrowth of the nerve fiber as a mode of protoplasmic movement. *J Exp Zool* 1910; 9(4):787–846.

Hatterer E, Davoust N, Didier-Bazes M, Vuaillat C, Malcus C, Belin MF, Nataf S. How to drain without lymphatics? Dendritic cells migrate from the cerebrospinal fluid to the B-cell follicles of cervical lymph nodes. *Blood* 2006;107(2):806–12.

Heasman SJ, Ridley AJ. Mammalian Rho GTPases: new insights into their functions from in vivo studies. *Nat Rev Mol Cell Biol* 2008;9(9):690–701.

Heidemann SR, Lamoureux P, Buxbaum RE. Growth cone behavior and production of traction force. *J Cell Biol* 1990;111(5 Pt 1):1949–57.

Hengst U, Cox LJ, Macosko EZ, Jaffrey SR. Functional and selective RNA interference in developing axons and growth cones. *J Neurosci* 2006;26(21):5727–32.

Hérincs Z, Corset V, Cahuzac N, Furne C, Castellani V, Hueber AO, Mehlen P. DCC association with lipid rafts is required for netrin-1-mediated axon guidance. *J Cell Sci* 2005;118(Pt 8):1687–92.

Herrmann C, Zimmermann H, Volknandt W. Analysis of a cDNA encoding the major vault protein from the electric ray Discopyge ommata. *Gene* 1997;188(1):85–90.

Hess DT, Patterson SI, Smith DS, Skene JH. Neuronal growth cone collapse and inhibition of protein fatty acylation by nitric oxide. *Nature* 1993;366(6455):562–5.

Ho GPH, Selvakumar B, Mukai J, Hester LD, Wang Y, Gogos JA, Snyder SH. S-Nitrosylation and S-Palmitoylation Reciprocally Regulate Synaptic Targeting of PSD-95. *Neuron* 2011;71(1):131–41.

Horn KP, Busch SA, Hawthorne AL, van Rooijen N, Silver J. Another barrier to regeneration in the CNS: activated macrophages induce extensive retraction of dystrophic axons through direct physical interactions. *J Neurosci* 2008;28(38):9330–41.

Hosoda Y, Miyawaki K, Saito S, Chen J, Bing X, Terashita T, Kobayashi N, Araki N, Shimokawa T, Hamada F, Sano A, Tanabe H, Matsuda S. Distribution of prosaposin in the rat nervous system. *Cell Tissue Res* 2007;330(2):197–207.

Hsu JYC, Bourguignon LYW, Adams CM, Peyrollier K, Zhang H, Fandel T, Cun CL, Werb Z, Noble-Haeusslein LJ. Matrix metalloproteinase-9 facilitates glial scar formation in the injured spinal cord. *J Neurosci* 2008;28(50):13467–77.

Hu F, Liu BP, Budel S, Liao J, Chin J, Fournier A, Strittmatter SM. Nogo-A interacts with the Nogo-66 receptor through multiple sites to create an isoform-selective subnanomolar agonist. *J Neurosci* 2005; 25(22):5298–304.

Hu F, Strittmatter SM. The N-terminal domain of Nogo-A inhibits cell adhesion and axonal outgrowth by an integrin-specific mechanism. *J Neurosci* 2008;28(5):1262–9.

Hu K, Ji L, Applegate KT, Danuser G, Waterman-Storer CM. Differential transmission of actin motion within focal adhesions. *Science* 2007;315(5808):111–5.

Hubel DH, Wiesel TN. Receptive fields, binocular interaction and functional architecture in the cat's visual cortex. *The Journal of physiology* 1962;160:106–54.

Hung RJ, Yazdani U, Yoon J, Wu H, Yang T, Gupta N, Huang Z, van Berkel WJH, Terman JR. Mical links semaphorins to F-actin disassembly. *Nature* 2010;463(7282):823–7.

Imura T, Nakano I, Kornblum HI, Sofroniew MV. Phenotypic and functional heterogeneity of GFAP-expressing cells in vitro: differential expression of LeX/CD15 by GFAP-expressing multipotent neural stem cells and non-neurogenic astrocytes. *Glia* 2006;53(3):277–93.

Inagaki N, Chihara K, Arimura N, Ménager C, Kawano Y, Matsuo N, Nishimura T, Amano M, Kaibuchi K. CRMP-2 induces axons in cultured hippocampal neurons. *Nat Neurosci* 2001;4(8):781–2.

Inoki K, Ouyang H, Zhu T, Lindvall C, Wang Y, Zhang X, Yang Q, Bennett C, Harada Y, Stankunas K, Wang CY, He X, MacDougald OA, You M, Williams BO, Guan KL. TSC2 integrates Wnt and energy signals via a coordinated phosphorylation by AMPK and GSK3 to regulate cell growth. *Cell* 2006; 126(5):955–68.

Irwin C, Roberts W, Naseem KM. Nitric oxide inhibits platelet adhesion to collagen through cGMP-dependent and independent mechanisms: the potential role for S-nitrosylation. *Platelets* 2009; 20(7):478–86.

Iwahashi J, Hamada N, Watanabe H. Two hydrophobic segments of the RTN1 family determine the ER localization and retention. *Biochem Biophys Res Commun* 2007;355(2):508–12.

Jackson G. *BA Hons Thesis*. Ph.D. thesis, University of Cambridge, 2008.

Jaffrey SR, Erdjument-Bromage H, Ferris CD, Tempst P, Snyder SH. Protein S-nitrosylation: a physiological signal for neuronal nitric oxide. *Nat Cell Biol* 2001;3(2):193–7.

Jin Z, Strittmatter SM. Rac1 mediates collapsin-1-induced growth cone collapse. *J Neurosci* 1997; 17(16):6256–63.

Joset A, Dodd DA, Halegoua S, Schwab ME. Pincher-generated Nogo-A endosomes mediate growth cone collapse and retrograde signaling. *J Cell Biol* 2010;188(2):271–85.

Jourd'heuil D, Hallén K, Feelisch M, Grisham MB. Dynamic state of S-nitrosothiols in human plasma and whole blood. *Free Radic Biol Med* 2000;28(3):409–417.

Jung H, O'Hare CM, Holt CE. Translational regulation in growth cones. *Current opinion in genetics & development* 2011;21(4):458–64.

Kalcheim C, Teillet MA. Consequences of somite manipulation on the pattern of dorsal root ganglion development. *Development* 1989;106(1):85–93.

Kaneko S, Iwanami A, Nakamura M, Kishino A, Kikuchi K, Shibata S, Okano HJ, Ikegami T, Moriya A, Konishi O, Nakayama C, Kumagai K, Kimura T, Sato Y, Goshima Y, Taniguchi M, Ito M, He Z, Toyama Y, Okano H. A selective Sema3A inhibitor enhances regenerative responses and functional recovery of the injured spinal cord. *Nat Med* 2006;12(12):1380–9.

Kantor DB, Chivatakarn O, Peer KL, Oster SF, Inatani M, Hansen MJ, Flanagan JG, Yamaguchi Y, Sretavan DW, Giger RJ, Kolodkin AL. Semaphorin 5A is a bifunctional axon guidance cue regulated by heparan and chondroitin sulfate proteoglycans. *Neuron* 2004;44(6):961–75.

Kapfhammer JP, Raper JA. Collapse of growth cone structure on contact with specific neurites in culture. *J Neurosci* 1987;7(1):201–12.

Kaplan BB, Gioio AE, Capano CP, Crispino M, Giuditta A. beta-Actin and beta-Tubulin are components of a heterogeneous mRNA population present in the squid giant axon. *Mol Cell Neurosci* 1992; 3(2):133–44.

Katayama M, Kawata M, Yoshida Y, Horiuchi H, Yamamoto T, Matsuura Y, Takai Y. The posttranslationally modified C-terminal structure of bovine aortic smooth muscle rhoA p21. *J Biol Chem* 1991; 266(19):12639–45.

Katoh-Semba R, Matsuda M, Kato K, Oohira A. Chondroitin sulphate proteoglycans in the rat brain: candidates for axon barriers of sensory neurons and the possible modification by laminin of their actions. *Eur J Neurosci* 1995;7(4):613–21.

Keleman K, Rajagopalan S, Cleppien D, Teis D, Paiha K, Huber LA, Technau GM, Dickson BJ. Comm sorts robo to control axon guidance at the Drosophila midline. *Cell* 2002;110(4):415–27.

Kennedy TE, Wang H, Marshall W, Tessier-Lavigne M. Axon guidance by diffusible chemoattractants: a gradient of netrin protein in the developing spinal cord. *J Neurosci* 2006;26(34):8866–74.

Kerschensteiner M, Schwab ME, Lichtman JW, Misgeld T. In vivo imaging of axonal degeneration and regeneration in the injured spinal cord. *Nat Med* 2005;11(5):572–7.

Kessler DS, Melton DA. Vertebrate embryonic induction: mesodermal and neural patterning. *Science* 1994;266(5185):596–604.

van Kesteren RE, Carter C, Dissel HMG, van Minnen J, Gouwenberg Y, Syed NI, Spencer GE, Smit AB. Local synthesis of actin-binding protein beta-thymosin regulates neurite outgrowth. *J Neurosci* 2006; 26(1):152–7.

Ketschek A, Gallo G. Nerve growth factor induces axonal filopodia through localized microdomains of phosphoinositide 3-kinase activity that drive the formation of cytoskeletal precursors to filopodia. *J Neurosci* 2010;30(36):12185–97.

Keynes R, Tannahill D, Morgenstern DA, Johnson AR, Cook GM, Pini A. Surround repulsion of spinal sensory axons in higher vertebrate embryos. *Neuron* 1997;18(6):889–97.

Keynes RJ, Johnson AR, Picart CJ, Dunin-Borkowski OM, Cook GM. A growth cone collapsing activity in chicken gray matter. *Ann N Y Acad Sci* 1991;633:562.

Keynes RJ, Stern CD. Segmentation in the vertebrate nervous system. *Nature* 1984;310(5980):786–9.

Keynes RJ, Stern CD. Mechanisms of vertebrate segmentation. *Development* 1988;103(3):413–29.

Kickhoefer VA, Stephen AG, Harrington L, Robinson MO, Rome LH. Vaults and telomerase share a common subunit, TEP1. *J Biol Chem* 1999;274(46):32712–7.

Kidd T, Brose K, Mitchell KJ, Fetter RD, Tessier-Lavigne M, Goodman CS, Tear G. Roundabout controls axon crossing of the CNS midline and defines a novel subfamily of evolutionarily conserved guidance receptors. *Cell* 1998;92(2):205–15.

Kim GH, Park E, Kong YY, Han JK. Novel function of POSH, a JNK scaffold, as an E3 ubiquitin ligase for the Hrs stability on early endosomes. *Cell Signal* 2006;18(4):553–63.

Kim JE, Bonilla IE, Qiu D, Strittmatter SM. Nogo-C is sufficient to delay nerve regeneration. *Mol Cell Neurosci* 2003;23(3):451–9.

Kimura K, Ito M, Amano M, Chihara K, Fukata Y, Nakafuku M, Yamamori B, Feng J, Nakano T, Okawa K, Iwamatsu A, Kaibuchi K. Regulation of myosin phosphatase by Rho and Rho-associated kinase (Rho-kinase). *Science* 1996;273(5272):245–8.

Kimura-Kuroda J, Teng X, Komuta Y, Yoshioka N, Sango K, Kawamura K, Raisman G, Kawano H. An in vitro model of the inhibition of axon growth in the lesion scar formed after central nervous system injury. *Mol Cell Neurosci* 2010;43(2):177–87.

Kiseleva E, Morozova KN, Voeltz GK, Allen TD, Goldberg MW. Reticulon 4a/NogoA locates to regions of high membrane curvature and may have a role in nuclear envelope growth. *J Struct Biol* 2007; 160(2):224–35.

Klostermann A, Lohrum M, Adams RH, Püschel AW. The chemorepulsive activity of the axonal guidance signal semaphorin D requires dimerization. *J Biol Chem* 1998;273(13):7326–31.

Koestler SA, Rottner K, Lai F, Block J, Vinzenz M, Small JV. F- and G-actin concentrations in lamellipodia of moving cells. *PLoS ONE* 2009;4(3):e4810.

Kolodkin AL, Levengood DV, Rowe EG, Tai YT, Giger RJ, Ginty DD. Neuropilin is a semaphorin III receptor. *Cell* 1997;90(4):753–62.

Kolodkin AL, Matthes DJ, Goodman CS. The semaphorin genes encode a family of transmembrane and secreted growth cone guidance molecules. *Cell* 1993;75(7):1389–99.

Kolodkin AL, Matthes DJ, O'Connor TP, Patel NH, Admon A, Bentley D, Goodman CS. Fasciclin IV: sequence, expression, and function during growth cone guidance in the grasshopper embryo. *Neuron* 1992;9(5):831–45.

Kondoh K, Sano A, Kakimoto Y, Matsuda S, Sakanaka M. Distribution of prosaposin-like immunoreactivity in rat brain. *J Comp Neurol* 1993;334(4):590–602.

Koppel AM, Raper JA. Collapsin-1 covalently dimerizes, and dimerization is necessary for collapsing activity. *J Biol Chem* 1998;273(25):15708–13.

Kotani Y, Matsuda S, Sakanaka M, Kondoh K, Ueno S, Sano A. Prosaposin facilitates sciatic nerve regeneration in vivo. *J Neurochem* 1996;66(5):2019–25.

Kranenburg O, Poland M, Gebbink M, Oomen L, Moolenaar WH. Dissociation of LPA-induced cytoskeletal contraction from stress fiber formation by differential localization of RhoA. *J Cell Sci* 1997; 110 (Pt 1:2417–27.

Kruger RP, Aurandt J, Guan KL. Semaphorins command cells to move. *Nat Rev Mol Cell Biol* 2005; 6(10):789–800.

Krull CE, Collazo A, Fraser SE, Bronner-Fraser M. Segmental migration of trunk neural crest: time-lapse analysis reveals a role for PNA-binding molecules. *Development* 1995;121(11):3733–43.

Kuhn TB, Brown MD, Bamburg JR. Rac1-dependent actin filament organization in growth cones is necessary for beta1-integrin-mediated advance but not for growth on poly-D-lysine. *J Neurobiol* 1998; 37(4):524–40.

Kuhn TB, Brown MD, Wilcox CL, Raper Ja, Bamburg JR. Myelin and collapsin-1 induce motor neuron growth cone collapse through different pathways: inhibition of collapse by opposing mutants of rac1. *J Neurosci* 1999;19(6):1965–75.

Kunda P, Paglini G, Quiroga S, Kosik K, Caceres A. Evidence for the involvement of Tiam1 in axon formation. *J Neurosci* 2001;21(7):2361–72.

Kuwako KI, Kakumoto K, Imai T, Igarashi M, Hamakubo T, Sakakibara SI, Tessier-Lavigne M, Okano HJ, Okano H. Neural RNA-Binding Protein Musashi1 Controls Midline Crossing of Precerebellar Neurons through Posttranscriptional Regulation of Robo3/Rig-1 Expression. *Neuron* 2010;67(3):407–421.

Laforest S, Milanini J, Parat F, Thimonier J, Lehmann M. Evidences that beta1 integrin and Rac1 are involved in the overriding effect of laminin on myelin-associated glycoprotein inhibitory activity on neuronal cells. *Mol Cell Neurosci* 2005;30(3):418–28.

Latov N, Nilaver G, Zimmerman EA, Johnson WG, Silverman AJ, Defendini R, Cote L. Fibrillary astrocytes proliferate in response to brain injury: a study combining immunoperoxidase technique for glial fibrillary acidic protein and radioautography of tritiated thymidine. *Dev Biol* 1979;72(2):381–4.

le Gros Clark WE. The problem of neuronal regeneration in the central nervous system: II. The insertion of peripheral nerve stumps into the brain. *J Anat* 1943;77(Pt 3):251–9.

Lebrand C, Dent EW, Strasser GA, Lanier LM, Krause M, Svitkina TM, Borisy GG, Gertler FB. Critical role of Ena/VASP proteins for filopodia formation in neurons and in function downstream of netrin-1. *Neuron* 2004;42(1):37–49.

Lee JK, Chan AF, Luu SM, Zhu Y, Ho C, Tessier-Lavigne M, Zheng B. Reassessment of corticospinal tract regeneration in Nogo-deficient mice. *J Neurosci* 2009;29(27):8649–54.

Lee JK, Geoffroy CG, Chan AF, Tolentino KE, Crawford MJ, Leal MA, Kang B, Zheng B. Assessing spinal axon regeneration and sprouting in Nogo-, MAG-, and OMgp-deficient mice. *Neuron* 2010;66(5):663–70.

Leeuwen FN, Kain HE, Kammen RA, Michiels F, Kranenburg OW, Collard JG. The guanine nucleotide exchange factor Tiam1 affects neuronal morphology; opposing roles for the small GTPases Rac and Rho. *J Cell Biol* 1997;139(3):797–807.

Letourneau PC, Shattuck TA, Ressler AH. "Pull" and "push" in neurite elongation: observations on the effects of different concentrations of cytochalasin B and taxol. *Cell Motil Cytoskeleton* 1987;8(3):193–209.

Leung KM, van Horck FPG, Lin AC, Allison R, Standart N, Holt CE. Asymmetrical beta-actin mRNA translation in growth cones mediates attractive turning to netrin-1. *Nat Neurosci* 2006;9(10):1247–56.

Leung T, Ng Y, Cheong A, Ng CH, Tan I, Hall C, Lim L. p80 ROKalpha binding protein is a novel splice variant of CRMP-1 which associates with CRMP-2 and modulates RhoA-induced neuronal morphology. *FEBS Lett* 2002;532(3):445–9.

Lewis H, Gray WH. *Gray's Anatomy of the Human Body (20th Edition)* (Lea & Febiger, 1918).

Li C, Bassell GJ, Sasaki Y. Fragile X Mental Retardation Protein is Involved in Protein Synthesis-Dependent Collapse of Growth Cones Induced by Semaphorin-3A. *Front Neural Circuits* 2009;3:11.

Li C, Sasaki Y, Takei K, Yamamoto H, Shouji M, Sugiyama Y, Kawakami T, Nakamura F, Yagi T, Ohshima T, Goshima Y. Correlation between semaphorin3A-induced facilitation of axonal transport and local activation of a translation initiation factor eukaryotic translation initiation factor 4E. *J Neurosci* 2004; 24(27):6161–70.

Li F, Higgs HN. The mouse Formin mDia1 is a potent actin nucleation factor regulated by autoinhibition. *Curr Biol* 2003;13(15):1335–40.

Li L, Lundkvist A, Andersson D, Wilhelmsson U, Nagai N, Pardo AC, Nodin C, Stå hlberg A, Aprico K, Larsson K, Yabe T, Moons L, Fotheringham A, Davies I, Carmeliet P, Schwartz JP, Pekna M, Kubista M, Blomstrand F, Maragakis N, Nilsson M, Pekny M. Protective role of reactive astrocytes in brain ischemia. *J Cereb Blood Flow Metab* 2008;28(3):468–81.

Lin AC, Holt CE. Local translation and directional steering in axons. *EMBO J* 2007;26(16):3729–36.

Liu BP, Fournier A, GrandPré T, Strittmatter SM. Myelin-associated glycoprotein as a functional ligand for the Nogo-66 receptor. *Science* 2002*a*;297(5584):1190–3.

Liu H, Ng CEL, Tang BL. Nogo-A expression in mouse central nervous system neurons. *Neurosci Lett* 2002*b*;328(3):257–60.

Liu K, Lu Y, Lee JK, Samara R, Willenberg R, Sears-Kraxberger I, Tedeschi A, Park KK, Jin D, Cai B, Xu B, Connolly L, Steward O, Zheng B, He Z. PTEN deletion enhances the regenerative ability of adult corticospinal neurons. *Nat Neurosci* 2010;13(9):1075–81.

Liu M, Ma Y. Expression of soluble Nogo-66 receptor and brain-derived neurotrophic factor in transduced rat bone marrow stromal cells. *Journal of Clinical Neuroscience* 2010;17(6):762–5.

Liu Y, Wang X, Lu CC, Kerman R, Steward O, Xu XM, Zou Y. Repulsive Wnt signaling inhibits axon regeneration after CNS injury. *J Neurosci* 2008;28(33):8376–82.

Llorens F, Gil V, Del Río JA. Emerging functions of myelin-associated proteins during development, neuronal plasticity, and neurodegeneration. *FASEB J* 2010;.

Lu C, Shervington A. Chemoresistance in gliomas. *Mol Cell Biochem* 2008;312(1-2):71–80.

Lu M, Witke W, Kwiatkowski DJ, Kosik KS. Delayed retraction of filopodia in gelsolin null mice. *J Cell Biol* 1997;138(6):1279–87.

Lu YB, Iandiev I, Hollborn M, Körber N, Ulbricht E, Hirrlinger PG, Pannicke T, Wei EQ, Bringmann A, Wolburg H, Wilhelmsson U, Pekny M, Wiedemann P, Reichenbach A, Käs JA. Reactive glial cells: increased stiffness correlates with increased intermediate filament expression. *FASEB J* 2011;25(2):624–31.

Luo Y, Raible D, Raper JA. Collapsin: a protein in brain that induces the collapse and paralysis of neuronal growth cones. *Cell* 1993;75(2):217–27.

Luo Y, Wu X, Liu S, Li K. Reactivation of visual cortical plasticity by NEP1-40 from early monocular deprivation in adult rats. *Neurosci Lett* 2011;494(3):196–201.

Ma D, Jan LY. ER transport signals and trafficking of potassium channels and receptors. *Curr Opin Neurobiol* 2002;12(3):287–92.

Maekawa M, Ishizaki T, Boku S, Watanabe N, Fujita A, Iwamatsu A, Obinata T, Ohashi K, Mizuno K, Narumiya S. Signaling from Rho to the actin cytoskeleton through protein kinases ROCK and LIM-kinase. *Science* 1999;285(5429):895–8.

Mallavarapu A, Mitchison T. Regulated actin cytoskeleton assembly at filopodium tips controls their extension and retraction. *J Cell Biol* 1999;146(5):1097–106.

Mandel R, Ryser HJ, Ghani F, Wu M, Peak D. Inhibition of a reductive function of the plasma membrane by bacitracin and antibodies against protein disulfide-isomerase. *Proc Natl Acad Sci U S A* 1993; 90(9):4112–6.

Margeta-Mitrovic M, Jan YN, Jan LY. A trafficking checkpoint controls GABA(B) receptor heterodimerization. *Neuron* 2000;27(1):97–106.

Marsh L, Letourneau PC. Growth of neurites without filopodial or lamellipodial activity in the presence of cytochalasin B. *J Cell Biol* 1984;99(6):2041–7.

Martin KC, Zukin RS. RNA trafficking and local protein synthesis in dendrites: an overview. *J Neurosci* 2006;26(27):7131–4.

Massey JM, Hubscher CH, Wagoner MR, Decker Ja, Amps J, Silver J, Onifer SM. Chondroitinase ABC digestion of the perineuronal net promotes functional collateral sprouting in the cuneate nucleus after cervical spinal cord injury. *J Neurosci* 2006;26(16):4406–14.

Matsuoka RL, Nguyen-Ba-Charvet KT, Parray A, Badea TC, Chédotal A, Kolodkin AL. Transmembrane semaphorin signalling controls laminar stratification in the mammalian retina. *Nature* 2011; 470(7333):259–63.

McGee AW, Yang Y, Fischer QS, Daw NW, Strittmatter SM. Experience-driven plasticity of visual cortex limited by myelin and Nogo receptor. *Science* 2005;309(5744):2222–6.

McMahon JA, Takada S, Zimmerman LB, Fan CM, Harland RM, McMahon AP. Noggin-mediated antagonism of BMP signaling is required for growth and patterning of the neural tube and somite. *Genes Dev* 1998;12(10):1438–52.

Mehlen P, Delloye-Bourgeois C, Chédotal A. Novel roles for Slits and netrins: axon guidance cues as anticancer targets? *Nature reviews. Cancer* 2011;11(3):188–97.

Mi S, Lee X, Shao Z, Thill G, Ji B, Relton J, Levesque M, Allaire N, Perrin S, Sands B, Crowell T, Cate RL, McCoy JM, Pepinsky RB. LINGO-1 is a component of the Nogo-66 receptor/p75 signaling complex. *Nat Neurosci* 2004;7(3):221–8.

Milzani A, DalleDonne I, Colombo R. Prolonged oxidative stress on actin. *Arch Biochem Biophys* 1997; 339(2):267–74.

Ming Gl, Wong ST, Henley J, Yuan Xb, Song Hj, Spitzer NC, Poo Mm. Adaptation in the chemotactic guidance of nerve growth cones. *Nature* 2002;417(6887):411–8.

Minturn JE, Fryer HJ, Geschwind DH, Hockfield S. TOAD-64, a gene expressed early in neuronal differentiation in the rat, is related to unc-33, a C. elegans gene involved in axon outgrowth. *J Neurosci* 1995;15(10):6757–66.

Misgeld T, Nikic I, Kerschensteiner M. In vivo imaging of single axons in the mouse spinal cord. *Nat Protoc* 2007;2(2):263–8.

Mitsui N, Inatome R, Takahashi S, Goshima Y, Yamamura H, Yanagi S. Involvement of Fes/Fps tyrosine kinase in semaphorin3A signaling. *EMBO J* 2002;21(13):3274–85.

Moldovan L, Irani K, Moldovan NI, Finkel T, Goldschmidt-Clermont PJ. The actin cytoskeleton reorganization induced by Rac1 requires the production of superoxide. *Antioxid Redox Signal* 1999; 1(1):29–43.

Moncada S, Higgs A. The L-arginine-nitric oxide pathway. *The New England journal of medicine* 1993; 329(27):2002–12.

Moon LD, Brecknell JE, Franklin RJ, Dunnett SB, Fawcett JW. Robust regeneration of CNS axons through a track depleted of CNS glia. *Exp Neurol* 2000;161(1):49–66.

Mothe A, Tator C. Proliferation, migration, and differentiation of endogenous ependymal region stem/progenitor cells following minimal spinal cord injury in the adult rat. *Neuroscience* 2005;131:177–187.

Muir EM, Fyfe I, Gardiner S, Li L, Warren P, Fawcett JW, Keynes RJ, Rogers JH. Modification of N-glycosylation sites allows secretion of bacterial chondroitinase ABC from mammalian cells. *J Biotechnol* 2010;145(2):103–10.

Müller CM, Best J. Ocular dominance plasticity in adult cat visual cortex after transplantation of cultured astrocytes. *Nature* 1989;342(6248):427–30.

Munnamalai V, Suter DM. Reactive oxygen species regulate F-actin dynamics in neuronal growth cones and neurite outgrowth. *J Neurochem* 2009;108(3):644–61.

Myer DJ, Gurkoff GG, Lee SM, Hovda DA, Sofroniew MV. Essential protective roles of reactive astrocytes in traumatic brain injury. *Brain* 2006;129(Pt 10):2761–72.

Nadella M, Bianchet MA, Gabelli SB, Barrila J, Amzel LM. Structure and activity of the axon guidance protein MICAL. *Proc Natl Acad Sci U S A* 2005;102(46):16830–5.

Nakamae T, Tanaka N, Nakanishi K, Kamei N, Sasaki H, Hamasaki T, Yamada K, Yamamoto R, Izumi B, Ochi M. The effects of combining chondroitinase ABC and NEP1-40 on the corticospinal axon growth in organotypic co-cultures. *Neurosci Lett* 2010;476(1):14–7.

Nakamura F, Kalb RG, Strittmatter SM. Molecular basis of semaphorin-mediated axon guidance. *J Neurobiol* 2000;44(2):219–29.

Nakamura Y, Fujita Y, Ueno M, Takai T, Yamashita T. Paired immunoglobulin-like receptor B knockout does not enhance axonal regeneration or locomotor recovery after spinal cord injury. *J Biol Chem* 2011; 286(3):1876–83.

Nangle MR, Keast JR. Semaphorin 3A inhibits growth of adult sympathetic and parasympathetic neurones via distinct cyclic nucleotide signalling pathways. *Br J Pharmacol* 2010;162(5):1083–95.

Narayanan U, Nalavadi V, Nakamoto M, Pallas DC, Ceman S, Bassell GJ, Warren ST. FMRP phosphorylation reveals an immediate-early signaling pathway triggered by group I mGluR and mediated by PP2A. *J Neurosci* 2007;27(52):14349–57.

Narayanan U, Nalavadi V, Nakamoto M, Thomas G, Ceman S, Bassell GJ, Warren ST. S6K1 phosphorylates and regulates fragile X mental retardation protein (FMRP) with the neuronal protein synthesis-dependent mammalian target of rapamycin (mTOR) signaling cascade. *J Biol Chem* 2008; 283(27):18478–82.

Nédelec S, Peljto M, Shi P, Amoroso MW, Kam LC, Wichterle H. Concentration-dependent requirement for local protein synthesis in motor neuron subtype-specific response to axon guidance cues. *J Neurosci* 2012;32(4):1496–506.

Negishi M, Oinuma I, Katoh H. R-Ras As a Key Player for Signaling Pathway of Plexins. *Mol Neurobiol* 2005;32(3):217–222.

Niederöst B, Oertle T, Fritsche J, McKinney RA, Bandtlow CE. Nogo-A and myelin-associated glycoprotein mediate neurite growth inhibition by antagonistic regulation of RhoA and Rac1. *J Neurosci* 2002; 22(23):10368–76.

Niederöst BP, Zimmermann DR, Schwab ME, Bandtlow CE. Bovine CNS myelin contains neurite growth-inhibitory activity associated with chondroitin sulfate proteoglycans. *J Neurosci* 1999; 19(20):8979–89.

Nikolic M, Chou MM, Lu W, Mayer BJ, Tsai LH. The p35/Cdk5 kinase is a neuron-specific Rac effector that inhibits Pak1 activity. *Nature* 1998;395(6698):194–8.

Nishimura T, Takeichi M. Shroom3-mediated recruitment of Rho kinases to the apical cell junctions regulates epithelial and neuroepithelial planar remodeling. *Development* 2008;135(8):1493–502.

Nobes CD, Hall A. Rho, rac, and cdc42 GTPases regulate the assembly of multimolecular focal complexes associated with actin stress fibers, lamellipodia, and filopodia. *Cell* 1995;81(1):53–62.

Nusser N, Gosmanova E, Zheng Y, Tigyi G. Nerve growth factor signals through TrkA, phosphatidylinositol 3-kinase, and Rac1 to inactivate RhoA during the initiation of neuronal differentiation of PC12 cells. *J Biol Chem* 2002;277(39):35840–6.

O'Brien JS, Carson GS, Seo HC, Hiraiwa M, Kishimoto Y. Identification of prosaposin as a neurotrophic factor. *Proc Natl Acad Sci U S A* 1994;91(20):9593–6.

O'Connor TP, Duerr JS, Bentley D. Pioneer growth cone steering decisions mediated by single filopodial contacts in situ. *J Neurosci* 1990;10(12):3935–46.

Oertle T, van der Haar ME, Bandtlow CE, Robeva A, Burfeind P, Buss A, Huber AB, Simonen M, Schnell L, Brösamle C, Kaupmann K, Vallon R, Schwab ME. Nogo-A inhibits neurite outgrowth and cell spreading with three discrete regions. *J Neurosci* 2003*a*;23(13):5393–406.

Oertle T, Klinger M, Stuermer CAO, Schwab ME. A reticular rhapsody: phylogenic evolution and nomenclature of the RTN/Nogo gene family. *FASEB J* 2003*b*;17(10):1238–47.

Ohata S, Aoki R, Kinoshita S, Yamaguchi M, Tsuruoka-Kinoshita S, Tanaka H, Wada H, Watabe S, Tsuboi T, Masai I, Okamoto H. Dual Roles of Notch in Regulation of Apically Restricted Mitosis and Apicobasal Polarity of Neuroepithelial Cells. *Neuron* 2011;69(2):215–230.

Ohta K, Tannahill D, Yoshida K, Johnson AR, Cook GM, Keynes RJ. Embryonic lens repels retinal ganglion cell axons. *Dev Biol* 1999;211(1):124–32.

Oinuma I, Katoh H, Negishi M. Molecular dissection of the semaphorin 4D receptor plexin-B1-stimulated R-Ras GTPase-activating protein activity and neurite remodeling in hippocampal neurons. *J Neurosci* 2004;24(50):11473–80.

Okada S, Nakamura M, Katoh H, Miyao T, Shimazaki T, Ishii K, Yamane J, Yoshimura A, Iwamoto Y, Toyama Y, Okano H. Conditional ablation of Stat3 or Socs3 discloses a dual role for reactive astrocytes after spinal cord injury. *Nat Med* 2006;12(7):829–34.

Pak CW, Flynn KC, Bamburg JR. Actin-binding proteins take the reins in growth cones. *Nature reviews. Neuroscience* 2008;9(2):136–47.

Park JB, Yiu G, Kaneko S, Wang J, Chang J, He XL, Garcia KC, He Z. A TNF receptor family member, TROY, is a coreceptor with Nogo receptor in mediating the inhibitory activity of myelin inhibitors. *Neuron* 2005;45(3):345–51.

Park KK, Liu K, Hu Y, Smith PD, Wang C, Cai B, Xu B, Connolly L, Kramvis I, Sahin M, He Z. Promoting axon regeneration in the adult CNS by modulation of the PTEN/mTOR pathway. *Science* 2008; 322(5903):963–6.

Paspalas CD, Perley CC, Venkitaramani DV, Goebel-Goody SM, Zhang Y, Kurup P, Mattis JH, Lombroso PJ. Major vault protein is expressed along the nucleus-neurite axis and associates with mRNAs in cortical neurons. *Cereb Cortex* 2009;19(7):1666–77.

Pasterkamp RJ, Anderson PN, Verhaagen J. Peripheral nerve injury fails to induce growth of lesioned ascending dorsal column axons into spinal cord scar tissue expressing the axon repellent Semaphorin3A. *J Neurosci* 2001;13(3):457–71.

Pasterkamp RJ, Dai Hn, Terman JR, Wahlin KJ, Kim B, Bregman BS, Popovich PG, Kolodkin AL. MICAL flavoprotein monooxygenases: expression during neural development and following spinal cord injuries in the rat. *Mol Cell Neurosci* 2006;31(1):52–69.

Pasterkamp RJ, Giger RJ, Ruitenberg MJ, Holtmaat AJ, De Wit J, De Winter F, Verhaagen J. Expression of the gene encoding the chemorepellent semaphorin III is induced in the fibroblast component of neural scar tissue formed following injuries of adult but not neonatal CNS. *Mol Cell Neurosci* 1999; 13(2):143–66.

Pasterkamp RJ, Kolodkin AL. Semaphorin junction: making tracks toward neural connectivity. *Curr Opin Neurobiol* 2003;13(1):79–89.

Perdigoto AL, Chaudhry N, Barnes GN, Filbin MT, Carter BD. A novel role for PTEN in the inhibition of neurite outgrowth by myelin-associated glycoprotein in cortical neurons. *Mol Cell Neurosci* 2011; 46(1):235–44.

Pereira S, Zhang H, Takai T, Lowell CA. The inhibitory receptor PIR-B negatively regulates neutrophil and macrophage integrin signaling. *J Immunol* 2004;173(9):5757–65.

Perron JC, Dodd J. Inductive specification and axonal orientation of spinal neurons mediated by divergent bone morphogenetic protein signaling pathways. *Nat Dev* 2011;6:36.

Piper M, Anderson R, Dwivedy A, Weinl C, van Horck F, Leung KM, Cogill E, Holt C. Signaling mechanisms underlying Slit2-induced collapse of Xenopus retinal growth cones. *Neuron* 2006;49(2):215–28.

Piper M, Holt C. RNA translation in axons. *Annu Rev Cell Dev Biol* 2004;20:505–523.

Piper M, Salih S, Weinl C, Holt CE, Harris WA. Endocytosis-dependent desensitization and protein synthesis-dependent resensitization in retinal growth cone adaptation. *Nat Neurosci* 2005;8(2):179–86.

Pizzorusso T, Medini P, Berardi N, Chierzi S, Fawcett JW, Maffei L. Reactivation of ocular dominance plasticity in the adult visual cortex. *Science* 2002;298(5596):1248–51.

Plantman S, Patarroyo M, Fried K, Domogatskaya A, Tryggvason K, Hammarberg H, Cullheim S. Integrin-laminin interactions controlling neurite outgrowth from adult DRG neurons in vitro. *Mol Cell Neurosci* 2008;39(1):50–62.

Polleux F, Giger RJ, Ginty DD, Kolodkin AL, Ghosh A. Patterning of cortical efferent projections by semaphorin-neuropilin interactions. *Science* 1998;282(5395):1904–6.

Polleux F, Morrow T, Ghosh A. Semaphorin 3A is a chemoattractant for cortical apical dendrites. *Nature* 2000;404(6778):567–73.

Pot C, Simonen M, Weinmann O, Schnell L, Christ F, Stoeckle S, Berger P, Rülicke T, Suter U, Schwab ME. Nogo-A expressed in Schwann cells impairs axonal regeneration after peripheral nerve injury. *J Cell Biol* 2002;159(1):29–35.

Pourquié O. The chick embryo: a leading model in somitogenesis studies. *Mech Dev* 2004;121(9):1069–79.

Pruyne D, Evangelista M, Yang C, Bi E, Zigmond S, Bretscher A, Boone C. Role of formins in actin assembly: nucleation and barbed-end association. *Science* 2002;297(5581):612–5.

Ramachandran N, Root P, Jiang XM, Hogg PJ, Mutus B. Mechanism of transfer of NO from extracellular S-nitrosothiols into the cytosol by cell-surface protein disulfide isomerase. *Proc Natl Acad Sci U S A* 2001;98(17):9539–44.

Ramón-Cueto A, Plant GW, Avila J, Bunge MB. Long-distance axonal regeneration in the transected adult rat spinal cord is promoted by olfactory ensheathing glia transplants. *J Neurosci* 1998;18(10):3803–15.

Ramón y Cajal S. *Textura del Sistema Nervioso del Hombre y de los Vertebrados* (Moya, Madrid, 1899).

Ramón y Cajal S. *Degeneration and Regeneration of the Nervous System* (Hafner, New York, 1928).

Reier PJ. Penetration of grafted astrocytic scars by regenerating optic nerve axons in Xenopus tadpoles. *Brain Res* 1979;164:61–8.

Reiner O, Sapir T. Polarity regulation in migrating neurons in the cortex. *Mol Neurobiol* 2009;40(1):1–14.

Rentería RC, Constantine-Paton M. Exogenous nitric oxide causes collapse of retinal ganglion cell axonal growth cones in vitro. *J Neurobiol* 1996;29(4):415–28.

Rhodes KE, Raivich G, Fawcett JW. The injury response of oligodendrocyte precursor cells is induced by platelets, macrophages and inflammation-associated cytokines. *Neuroscience* 2006;140(1):87–100.

Ridet JL, Malhotra SK, Privat a, Gage FH. Reactive astrocytes: cellular and molecular cues to biological function. *Trends Neurosci* 1997;20(12):570–7.

Ridley AJ. Rho GTPases and actin dynamics in membrane protrusions and vesicle trafficking. *Trends Cell Biol* 2006;16(10):522–9.

Ridley AJ, Hall A. Distinct patterns of actin organization regulated by the small GTP-binding proteins Rac and Rho. *Cold Spring Harb Symp Quant Biol* 1992;57:661–71.

Riento K, Guasch RM, Garg R, Jin B, Ridley AJ. RhoE binds to ROCK I and inhibits downstream signaling. *Mol Cell Biol* 2003;23(12):4219–29.

Robles E, Gomez TM. Focal adhesion kinase signaling at sites of integrin-mediated adhesion controls axon pathfinding. *Nat Neurosci* 2006;9(10):1274–83.

Robles E, Huttenlocher A, Gomez TM. Filopodial calcium transients regulate growth cone motility and guidance through local activation of calpain. *Neuron* 2003;38(4):597–609.

Roche FK, Marsick BM, Letourneau PC. Protein synthesis in distal axons is not required for growth cone responses to guidance cues. *J Neurosci* 2009;29(3):638–52.

Root P, Sliskovic I, Mutus B. Platelet cell-surface protein disulphide-isomerase mediated S-nitrosoglutathione consumption. *Biochem J* 2004;382(Pt 2):575–80.

Ross AF, Oleynikov Y, Kislauskis EH, Taneja KL, Singer RH. Characterization of a beta-actin mRNA zipcode-binding protein. *Mol Cell Biol* 1997;17(4):2158–65.

Sabatier C, Plump AS, Le Ma, Brose K, Tamada A, Murakami F, Lee EYHP, Tessier-Lavigne M. The divergent Robo family protein rig-1/Robo3 is a negative regulator of slit responsiveness required for midline crossing by commissural axons. *Cell* 2004;117(2):157–69.

Sandvig A. *Investigation of Axon Regeneration in the Higher Vertebrate Nervous System*. Ph.D. thesis, Department of Anatomy, University of Cambridge, 1999.

Sandvig A, Berry M, Barrett LB, Butt A, Logan A. Myelin-, reactive glia-, and scar-derived CNS axon growth inhibitors: expression, receptor signaling, and correlation with axon regeneration. *Glia* 2004; 46(3):225–51.

Sanes DH, Reh TA, Harris WA. *Development of the Nervous System* (Elsevier Inc., 2006), 2nd ed.

Sarmiere PD, Bamburg JR. Regulation of the neuronal actin cytoskeleton by ADF/cofilin. *J Neurobiol* 2004;58(1):103–17.

Sarner S, Kozma R, Ahmed S, Lim L. Phosphatidylinositol 3-kinase, Cdc42, and Rac1 act downstream of Ras in integrin-dependent neurite outgrowth in N1E-115 neuroblastoma cells. *Mol Cell Biol* 2000; 20(1):158–72.

Sasaki M, Black JA, Lankford KL, Tokuno HA, Waxman SG, Kocsis JD. Molecular reconstruction of nodes of Ranvier after remyelination by transplanted olfactory ensheathing cells in the demyelinated spinal cord. *J Neurosci* 2006;26(6):1803–12.

Sasaki Y, Cheng C, Uchida Y, Nakajima O, Ohshima T, Yagi T, Taniguchi M, Nakayama T, Kishida R, Kudo Y, Ohno S, Nakamura F, Goshima Y. Fyn and Cdk5 mediate semaphorin-3A signaling, which is involved in regulation of dendrite orientation in cerebral cortex. *Neuron* 2002;35(5):907–20.

Sasaki Y, Welshhans K, Wen Z, Yao J, Xu M, Goshima Y, Zheng JQ, Bassell GJ. Phosphorylation of Zipcode Binding Protein 1 Is Required for Brain-Derived Neurotrophic Factor Signaling of Local {beta}-Actin Synthesis and Growth Cone Turning. *J Neurosci* 2010;30(28):9349–58.

Schaefer AW, Schoonderwoert VTG, Ji L, Mederios N, Danuser G, Forscher P. Coordination of actin filament and microtubule dynamics during neurite outgrowth. *Dev Cell* 2008;15(1):146–62.

Scheffer GL, Wijngaard PL, Flens MJ, Izquierdo MA, Slovak ML, Pinedo HM, Meijer CJ, Clevers HC, Scheper RJ. The drug resistance-related protein LRP is the human major vault protein. *Nat Med* 1995; 1(6):578–82.

Schnell L, Schwab ME. Axonal regeneration in the rat spinal cord produced by an antibody against myelin-associated neurite growth inhibitors. *Nature* 1990;343(6255):269–72.

Schuman EM, Dynes JL, Steward O. Synaptic regulation of translation of dendritic mRNAs. *J Neurosci* 2006;26(27):7143–6.

Schwab ME. Myelin-associated inhibitors of neurite growth. *Exp Neurol* 1990;109(1):2–5.

Schwab ME, Caroni P. Oligodendrocytes and CNS myelin are nonpermissive substrates for neurite growth and fibroblast spreading in vitro. *J Neurosci* 1988;8(7):2381–93.

Schweigreiter R. The natural history of the myelin-derived nerve growth inhibitor Nogo-A. *Neuron glia biology* 2008;4(2):83–9.

Sebök A, Nusser N, Debreceni B, Guo Z, Santos MF, Szeberenyi J, Tigyi G. Different roles for RhoA during neurite initiation, elongation, and regeneration in PC12 cells. *J Neurochem* 1999;73(3):949–60.

Shah CM, Bell SE, Locke IC, Chowdrey HS, Gordge MP. Interactions between cell surface protein disulphide isomerase and S-nitrosoglutathione during nitric oxide delivery. *Nitric Oxide* 2007;16(1):135–42.

Shao Y, Akmentin W, Toledo-Aral JJ, Rosenbaum J, Valdez G, Cabot JB, Hilbush BS, Halegoua S. Pincher, a pinocytic chaperone for nerve growth factor/TrkA signaling endosomes. *J Cell Biol* 2002;157(4):679–91.

Shao Z, Browning JL, Lee X, Scott ML, Shulga-Morskaya S, Allaire N, Thill G, Levesque M, Sah D, McCoy JM, Murray B, Jung V, Pepinsky RB, Mi S. TAJ/TROY, an orphan TNF receptor family member, binds Nogo-66 receptor 1 and regulates axonal regeneration. *Neuron* 2005;45(3):353–9.

Shelly M, Cancedda L, Lim BK, Popescu AT, Cheng Pl, Gao H, Poo Mm. Semaphorin3A regulates neuronal polarization by suppressing axon formation and promoting dendrite growth. *Neuron* 2011; 71(3):433–46.

Shi SH, Jan LY, Jan YN. Hippocampal neuronal polarity specified by spatially localized mPar3/mPar6 and PI 3-kinase activity. *Cell* 2003;112(1):63–75.

Shibata Y, Voss C, Rist JM, Hu J, Rapoport TA, Prinz WA, Voeltz GK. The reticulon and DP1/Yop1p proteins form immobile oligomers in the tubular endoplasmic reticulum. *J Biol Chem* 2008; 283(27):18892–904.

Shirao S, Kashiwagi S, Sato M, Miwa S, Nakao F, Kurokawa T, Todoroki-Ikeda N, Mogami K, Mizukami Y, Kuriyama S, Haze K, Suzuki M, Kobayashi S. Sphingosylphosphorylcholine is a novel messenger for Rho-kinase-mediated Ca2+ sensitization in the bovine cerebral artery: unimportant role for protein kinase C. *Circ Res* 2002;91(2):112–9.

Shirasaki R, Mirzayan C, Tessier-Lavigne M, Murakami F. Guidance of circumferentially growing axons by netrin-dependent and -independent floor plate chemotropism in the vertebrate brain. *Neuron* 1996; 17(6):1079–88.

Shypitsyna A, Málaga-Trillo E, Reuter A, Stuermer CAO. Origin of nogo-a by domain shuffling in an early jawed vertebrate. *Mol Biol Evol* 2011;28(4):1363–70.

Siebold C, Berrow N, Walter TS, Harlos K, Owens RJ, Stuart DI, Terman JR, Kolodkin AL, Pasterkamp RJ, Jones EY. High-resolution structure of the catalytic region of MICAL (molecule interacting with CasL), a multidomain flavoenzyme-signaling molecule. *Proc Natl Acad Sci U S A* 2005;102(46):16836–41.

da Silva JS, Dotti CG. Breaking the neuronal sphere: regulation of the actin cytoskeleton in neuritogenesis. *Nature reviews. Neuroscience* 2002;3(9):694–704.

Sofroniew MV. Molecular dissection of reactive astrogliosis and glial scar formation. *Trends Neurosci* 2009;32(12):638–47.

Soker S, Takashima S, Miao HQ, Neufeld G, Klagsbrun M. Neuropilin-1 is expressed by endothelial and tumor cells as an isoform-specific receptor for vascular endothelial growth factor. *Cell* 1998;92(6):735–45.

Sørensen A, Alekseeva T, Katechia K, Robertson M, Riehle MO, Barnett SC. Long-term neurite orientation on astrocyte monolayers aligned by microtopography. *Biomaterials* 2007;28(36):5498–508.

Spassky N, de Castro F, Le Bras B, Heydon K, Quéraud-LeSaux F, Bloch-Gallego E, Chédotal A, Zalc B, Thomas JL. Directional guidance of oligodendroglial migration by class 3 semaphorins and netrin-1. *J Neurosci* 2002;22(14):5992–6004.

Speidel CC. Adjustments of Nerve Endings: Harvey Lecture, January 16, 1941. *Bull N Y Acad Med* 1942; 18(10):625–53.

Spillane M, Ketschek A, Jones SL, Korobova F, Marsick B, Lanier L, Svitkina T, Gallo G. The actin nucleating Arp2/3 complex contributes to the formation of axonal filopodia and branches through the regulation of actin patch precursors to filopodia. *Dev Neurobiol* 2011;n/a–n/a.

Stephens GJ, Cholewinski AJ, Wilkin GP, Djamgoz MB. Essential protective roles of reactive astrocytes in traumatic brain injury. *Glia* 1993;9:269–79.

Stern CD, Sisodiya SM, Keynes RJ. Interactions between neurites and somite cells: inhibition and stimulation of nerve growth in the chick embryo. *J Embryol Exp Morphol* 1986;91:209–26.

Steward O, Schuman EM. Compartmentalized synthesis and degradation of proteins in neurons. *Neuron* 2003;40(2):347–59.

Stiess M, Maghelli N, Kapitein LC, Gomis-Rüth S, Wilsch-Bräuninger M, Hoogenraad CC, Tolić-Nø rrelykke IM, Bradke F. Axon extension occurs independently of centrosomal microtubule nucleation. *Science* 2010;327(5966):704–7.

Strochlic L, Dwivedy A, van Horck FPG, Falk J, Holt CE. A role for S1P signalling in axon guidance in the Xenopus visual system. *Development* 2008;135(2):333–42.

Sun F, Park KK, Belin S, Wang D, Lu T, Chen G, Zhang K, Yeung C, Feng G, Yankner BA, He Z. Sustained axon regeneration induced by co-deletion of PTEN and SOCS3. *Nature* 2011;480(7377):372–5.

Suzuki T, Nakamoto T, Ogawa S, Seo S, Matsumura T, Tachibana K, Morimoto C, Hirai H. MICAL, a novel CasL interacting molecule, associates with vimentin. *J Biol Chem* 2002;277(17):14933–41.

Swaney KF, Huang CH, Devreotes PN. Eukaryotic chemotaxis: a network of signaling pathways controls motility, directional sensing, and polarity. *Annu Rev Biophys* 2010;39:265–89.

Syken J, Grandpre T, Kanold PO, Shatz CJ. PirB restricts ocular-dominance plasticity in visual cortex. *Science* 2006;313(5794):1795–800.

Takahashi T, Fournier A, Nakamura F, Wang LH, Murakami Y, Kalb RG, Fujisawa H, Strittmatter SM. Plexin-neuropilin-1 complexes form functional semaphorin-3A receptors. *Cell* 1999;99(1):59–69.

Takahashi T, Strittmatter SM. Plexina1 autoinhibition by the plexin sema domain. *Neuron* 2001; 29(2):429–39.

Tanaka M, Ohashi R, Nakamura R, Shinmura K, Kamo T, Sakai R, Sugimura H. Tiam1 mediates neurite outgrowth induced by ephrin-B1 and EphA2. *EMBO J* 2004;23(5):1075–88.

Taylor AM, Berchtold NC, Perreau VM, Tu CH, Li Jeon N, Cotman CW. Axonal mRNA in uninjured and regenerating cortical mammalian axons. *J Neurosci* 2009;29(15):4697–707.

Taylor J, Chung KH, Figueroa C, Zurawski J, Dickson HM, Brace EJ, Avery AW, Turner DL, Vojtek AB. The scaffold protein POSH regulates axon outgrowth. *Mol Biol Cell* 2008;19(12):5181–92.

Terman JR, Mao T, Pasterkamp RJ, Yu HH, Kolodkin AL. MICALs, a family of conserved flavoprotein oxidoreductases, function in plexin-mediated axonal repulsion. *Cell* 2002;109(7):887–900.

Tessier-Lavigne M. NEUROBIOLOGY:Regeneration in the Nogo Zone. *Science* 2000;287(5454):813–814.

Tester NJ, Howland DR. Chondroitinase ABC improves basic and skilled locomotion in spinal cord injured cats. *Exp Neurol* 2008;209(2):483–96.

The PubChem Database. Oxophenylarsine. 2012.

Thermo-Scientific/Pierce. GST-tagged Proteins. 2012.

Tilney LG, Hatano S, Ishikawa H, Mooseker MS. The polymerization of actin: its role in the generation of the acrosomal process of certain echinoderm sperm. *J Cell Biol* 1973;59(1):109–26.

Tilney LG, Portnoy DA. Actin filaments and the growth, movement, and spread of the intracellular bacterial parasite, Listeria monocytogenes. *J Cell Biol* 1989;109(4 Pt 1):1597–608.

Togashi K, von Schimmelmann MJ, Nishiyama M, Lim CS, Yoshida N, Yun B, Molday RS, Goshima Y, Hong K. Cyclic GMP-gated CNG channels function in Sema3A-induced growth cone repulsion. *Neuron* 2008;58(5):694–707.

Toh BH, Lolait SJ, Mathy JP, Baum R. Association of mitochondria with intermediate filaments and of polyribosomes with cytoplasmic actin. *Cell Tissue Res* 1980;211(1):163–9.

Tojima T, Hines JH, Henley JR, Kamiguchi H. Second messengers and membrane trafficking direct and organize growth cone steering. *Nature reviews. Neuroscience* 2011;12(4):1–13.

Tojima T, Itofusa R, Kamiguchi H. The nitric oxide-cGMP pathway controls the directional polarity of growth cone guidance via modulating cytosolic Ca2+ signals. *J Neurosci* 2009;29(24):7886–97.

Tojima T, Itofusa R, Kamiguchi H. Asymmetric clathrin-mediated endocytosis drives repulsive growth cone guidance. *Neuron* 2010;66(3):370–7.

Tom VJ, Steinmetz MP, Miller JH, Doller CM, Silver J. Studies on the development and behavior of the dystrophic growth cone, the hallmark of regeneration failure, in an in vitro model of the glial scar and after spinal cord injury. *J Neurosci* 2004;24(29):6531–9.

Toyofuku T, Yoshida J, Sugimoto T, Zhang H, Kumanogoh A, Hori M, Kikutani H. FARP2 triggers signals for Sema3A-mediated axonal repulsion. *Nat Neurosci* 2005;8(12):1712–9.

Tsai SY, Papadopoulos CM, Schwab ME, Kartje GL. Delayed anti-nogo-a therapy improves function after chronic stroke in adult rats. *Stroke; a journal of cerebral circulation* 2011;42(1):186–90.

Turney SG, Bridgman PC. Laminin stimulates and guides axonal outgrowth via growth cone myosin II activity. *Nat Neurosci* 2005;8(6):717–9.

Uehara T, Bléry M, Kang DW, Chen CC, Ho LH, Gartland GL, Liu FT, Vivier E, Cooper MD, Kubagawa H. Inhibition of IgE-mediated mast cell activation by the paired Ig-like receptor PIR-B. *J Clin Invest* 2001;108(7):1041–50.

Valdez G, Akmentin W, Philippidou P, Kuruvilla R, Ginty DD, Halegoua S. Pincher-mediated macroendocytosis underlies retrograde signaling by neurotrophin receptors. *J Neurosci* 2005;25(21):5236–47.

Varga ZM, Bandtlow CE, Erulkar SD, Schwab ME, Nicholls JG. The critical period for repair of CNS of neonatal opossum (Monodelphis domestica) in culture: correlation with development of glial cells, myelin and growth-inhibitory molecules. *Eur J Neurosci* 1995*a*;7(10):2119–29.

Varga ZM, Schwab ME, Nicholls JG. Myelin-associated neurite growth-inhibitory proteins and suppression of regeneration of immature mammalian spinal cord in culture. *Proc Natl Acad Sci U S A* 1995*b*; 92(24):10959–63.

van de Velde HJ, Roebroek AJ, Senden NH, Ramaekers FC, Van de Ven WJ. NSP-encoded reticulons, neuroendocrine proteins of a novel gene family associated with membranes of the endoplasmic reticulum. *J Cell Sci* 1994;107 (Pt 9:2403–16.

Venance L, Stella N, Glowinski J, Giaume C. Mechanism involved in initiation and propagation of receptor-induced intercellular calcium signaling in cultured rat astrocytes. *J Neurosci* 1997;17(6):1981–92.

Verdú E, García-Alías G, Forés J, López-Vales R, Navarro X. Olfactory ensheathing cells transplanted in lesioned spinal cord prevent loss of spinal cord parenchyma and promote functional recovery. *Glia* 2003;42(3):275–86.

Vermeren MM, Cook GM, Johnson aR, Keynes RJ, Tannahill D. Spinal nerve segmentation in the chick embryo: analysis of distinct axon-repulsive systems. *Dev Biol* 2000;225(1):241–52.

Voeltz GK, Prinz WA, Shibata Y, Rist JM, Rapoport TA. A class of membrane proteins shaping the tubular endoplasmic reticulum. *Cell* 2006;124(3):573–86.

Voiculescu O. Co-operation between ingressing cells concentrates gastrulation at the primitive streak. *Unpublished work* 2011;.

Walter J, Henke-Fahle S, Bonhoeffer F. Avoidance of posterior tectal membranes by temporal retinal axons. *Development* 1987;101(4):909–13.

Walzer T, Galibert L, Comeau MR, De Smedt T. Plexin C1 engagement on mouse dendritic cells by viral semaphorin A39R induces actin cytoskeleton rearrangement and inhibits integrin-mediated adhesion and chemokine-induced migration. *J Immunol* 2005;174(1):51–9.

Wang KC, Kim JA, Sivasankaran R, Segal R, He Z. P75 interacts with the Nogo receptor as a co-receptor for Nogo, MAG and OMgp. *Nature* 2002*a*;420(6911):74–8.

Wang KC, Koprivica V, Kim JA, Sivasankaran R, Guo Y, Neve RL, He Z. Oligodendrocyte-myelin glycoprotein is a Nogo receptor ligand that inhibits neurite outgrowth. *Nature* 2002*b*;417(6892):941–4.

Wang T, Wang J, Yin C, Liu R, Zhang JH, Qin X. Down-regulation of Nogo receptor promotes functional recovery by enhancing axonal connectivity after experimental stroke in rats. *Brain Res* 2010;.

Ward Y, Yap SF, Ravichandran V, Matsumura F, Ito M, Spinelli B, Kelly K. The GTP binding proteins Gem and Rad are negative regulators of the Rho-Rho kinase pathway. *J Cell Biol* 2002;157(2):291–302.

Welshhans K, Bassell GJ. Netrin-1-Induced Local {beta}-Actin Synthesis and Growth Cone Guidance Requires Zipcode Binding Protein 1. *J Neurosci* 2011;31(27):9800–13.

Wenzel J, Lammert G, Meyer U, Krug M. The influence of long-term potentiation on the spatial relationship between astrocyte processes and potentiated synapses in the dentate gyrus neuropil of rat brain. *Brain Res* 1991;560(1-2):122–31.

Westmark CJ, Westmark PR, O'Riordan KJ, Ray BC, Hervey CM, Salamat MS, Abozeid SH, Stein KM, Stodola LA, Tranfaglia M, Burger C, Berry-Kravis EM, Malter JS. Reversal of Fragile X Phenotypes by Manipulation of AβPP/Aβ Levels in Fmr1KO Mice. *PLoS ONE* 2011;6(10):e26549.

Whitford KL, Dijkhuizen P, Polleux F, Ghosh A. Molecular control of cortical dendrite development. *Annu Rev Neurosci* 2002;25:127–49.

Wiesel TN, Hubel DH. Single-cell responses in striate cortex of kittens deprived of vision in one eye. *J Neurophysiol* 1963;26:1003–17.

Winberg ML, Tamagnone L, Bai J, Comoglio PM, Montell D, Goodman CS. The transmembrane protein Off-track associates with Plexins and functions downstream of Semaphorin signaling during axon guidance. *Neuron* 2001;32(1):53–62.

Winter JN, Jefferson LS, Kimball SR. ERK and Akt signaling pathways function through parallel mechanisms to promote mTORC1 signaling. *American journal of physiology. Cell physiology* 2011; 300(5):C1172–80.

Winzeler AM, Mandemakers WJ, Sun MZ, Stafford M, Phillips CT, Barres BA. The Lipid Sulfatide Is a Novel Myelin-Associated Inhibitor of CNS Axon Outgrowth. *J Neurosci* 2011;31(17):6481–6492.

Wright JH, Drueckes P, Bartoe J, Zhao Z, Shen SH, Krebs EG. A role for the SHP-2 tyrosine phosphatase in nerve growth-induced PC12 cell differentiation. *Mol Biol Cell* 1997;8(8):1575–85.

Wu KY, Hengst U, Cox LJ, Macosko EZ, Jeromin A, Urquhart ER, Jaffrey SR. Local translation of RhoA regulates growth cone collapse. *Nature* 2005;436(7053):1020–4.

Xia H, Hornby ZD, Malenka RC. An ER retention signal explains differences in surface expression of NMDA and AMPA receptor subunits. *Neuropharmacology* 2001;41(6):714–23.

Xiao F, Gordge MP. Cell surface thiol isomerases may explain the platelet-selective action of S-nitrosoglutathione. *Nitric Oxide* 2011;25(3):303–8.

Yamaguchi Y, Katoh H, Yasui H, Mori K, Negishi M. RhoA inhibits the nerve growth factor-induced Rac1 activation through Rho-associated kinase-dependent pathway. *J Biol Chem* 2001;276(22):18977–83.

Yamashita T, Tohyama M. The p75 receptor acts as a displacement factor that releases Rho from Rho-GDI. *Nat Neurosci* 2003;6(5):461–7.

Yang B, Chang Y, Weyers AM, Sterner E, Linhardt RJ. Disaccharide analysis of glycosaminoglycan mixtures by ultra-high-performance liquid chromatography-mass spectrometry. *J Chromatogr A* 2012; 1225:91–8.

Yang L, Garbe DS, Bashaw GJ. A frazzled/DCC-dependent transcriptional switch regulates midline axon guidance. *Science* 2009;324(5929):944–7.

Yang N, Higuchi O, Ohashi K, Nagata K, Wada A, Kangawa K, Nishida E, Mizuno K. Cofilin phosphorylation by LIM-kinase 1 and its role in Rac-mediated actin reorganization. *Nature* 1998;393(6687):809–12.

Yang YS, Strittmatter SM. The reticulons: a family of proteins with diverse functions. *Genome Biol* 2007; 8(12):234.

Yao J, Sasaki Y, Wen Z, Bassell GJ, Zheng JQ. An essential role for beta-actin mRNA localization and translation in Ca2+-dependent growth cone guidance. *Nat Neurosci* 2006;9(10):1265–73.

Yazdani U, Terman JR. The semaphorins. *Genome Biol* 2006;7(3):211.

Yeh TH, Lee DY, Gianino SM, Gutmann DH. Microarray analyses reveal regional astrocyte heterogeneity with implications for neurofibromatosis type 1 (NF1)-regulated glial proliferation. *Glia* 2009; 57(11):1239–49.

York RD, Molliver DC, Grewal SS, Stenberg PE, McCleskey EW, Stork PJ. Role of phosphoinositide 3-kinase and endocytosis in nerve growth factor-induced extracellular signal-regulated kinase activation via Ras and Rap1. *Mol Cell Biol* 2000;20(21):8069–83.

Yuan Q, Scott DE, So KF, Wu W. A subpopulation of reactive astrocytes at affected neuronal perikarya after hypophysectomy in adult rats. *Brain Res* 2007;1159:18–27.

Yuan Xb, Jin M, Xu X, Song Yq, Wu Cp, Poo Mm, Duan S. Signalling and crosstalk of Rho GTPases in mediating axon guidance. *Nat Cell Biol* 2003;5(1):38–45.

Zai A, Rudd MA, Scribner AW, Loscalzo J. Cell-surface protein disulfide isomerase catalyzes transnitrosation and regulates intracellular transfer of nitric oxide. *J Clin Invest* 1999;103(3):393–9.

Zanata SM, Hovatta I, Rohm B, Püschel AW. Antagonistic effects of Rnd1 and RhoD GTPases regulate receptor activity in Semaphorin 3A-induced cytoskeletal collapse. *J Neurosci* 2002;22(2):471–7.

Zander H, Hettich E, Greiff K, Chatwell L, Skerra A. Biochemical characterization of the recombinant human Nogo-A ectodomain. *The FEBS journal* 2007;274(10):2603–13.

Zhao G, London E. An amino acid "transmembrane tendency" scale that approaches the theoretical limit to accuracy for prediction of transmembrane helices: relationship to biological hydrophobicity. *Protein Sci* 2006;15(8):1987–2001.

Zhao J, Lurie DI. Loss of SHP-1 phosphatase alters cytokine expression in the mouse hindbrain following cochlear ablation. *Cytokine* 2004;28(1):1–9.

Zhao X, Wu J, Kuang F, Wang J, Ju G. Silencing of Nogo-A in rat oligodendrocyte cultures enhances process branching. *Neurosci Lett* 2011;499(1):32–6.

Zheng B, Atwal J, Ho C, Case L, He Xl, Garcia KC, Steward O, Tessier-Lavigne M. Genetic deletion of the Nogo receptor does not reduce neurite inhibition in vitro or promote corticospinal tract regeneration in vivo. *Proc Natl Acad Sci U S A* 2005;102(4):1205–10.

Zhou X, Lin DS, Zheng F, Sutton MA, Wang H. Intracellular calcium and calmodulin link brain-derived neurotrophic factor to p70S6 kinase phosphorylation and dendritic protein synthesis. *J Neurosci Res* 2010;88(7):1420–32.

Zivraj KH, Tung YCL, Piper M, Gumy L, Fawcett JW, Yeo GSH, Holt CE. Subcellular Profiling Reveals Distinct and Developmentally Regulated Repertoire of Growth Cone mRNAs. *J Neurosci* 2010; 30(46):15464–15478.

Zörner B, Schwab ME. Anti-Nogo on the go: from animal models to a clinical trial. *Ann N Y Acad Sci* 2010;1198:E22–E34.

Zuo J, Neubauer D, Dyess K, Ferguson TA, Muir D. Degradation of chondroitin sulfate proteoglycan enhances the neurite-promoting potential of spinal cord tissue. *Exp Neurol* 1998;154(2):654–62.

Appendix A

Additional Results

A.1 Effects of Growth Media and Assay Time-Course Upon PS Dependence of Sema3A Growth Cone Collapse

Neither time-course or differences in growth medium affect the synthesis dependence of Sema3A-induced growth cone collapse (figure A.1).

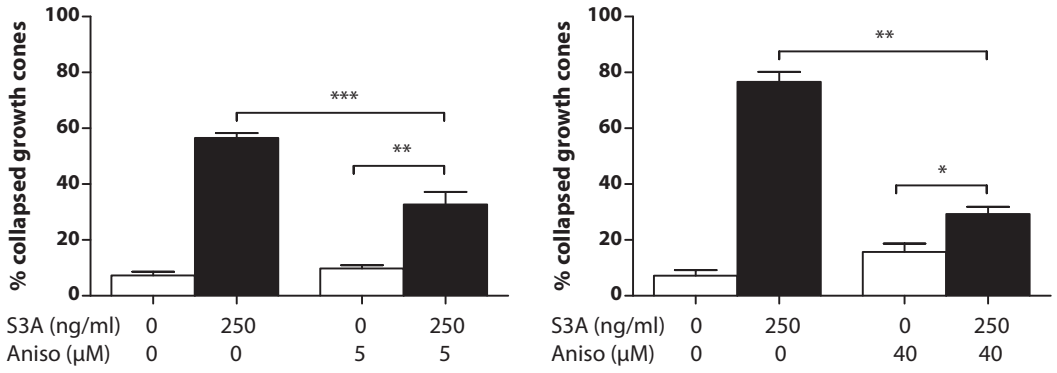

(a) Sema3A and F-12+B-27 Medium

(b) Pre-Incubation with 40 μM Anisomycin

Figure A.1: The Effects of Differing Media and Anisomycin Incubation on Collapse
(a) Using the same medium as Roche et al. (2009), protein synthesis inhibition with anisomycin inhibited the majority of Sema3A-induced collapse, but not all. (b) Pre-incubation with 20 μM anisomycin for 15 minutes prior to the application of Sema3A similarly did not change the effects of anisomycin on Sema3A-induced collapse.

A.2 The Time-Course of Anisomycin-Induced Growth Cone Collapse

As 30 minutes' exposure to cycloheximide or anisomycin consistently induces small but significant levels of collapse (Figure A.2), whereas 45 minutes' exposure used by Roche et al. (2009) found no significant effect of anisomycin on Sema3A-induced collapse.

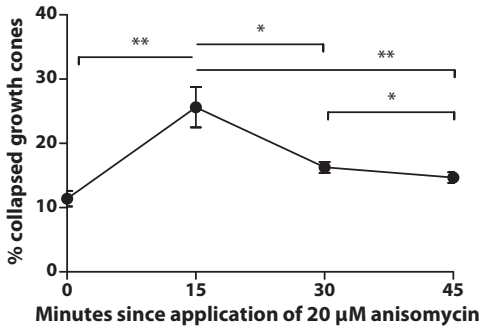

Figure A.2: Reversible Collapse Induced by Anisomycin
20 µM anisomycin induces significant collapse within 15 minutes, which falls after 30 minutes, and further at the 45-minute point.

A.3 Direct Confirmation of Inhibition of Growth Cone Protein Synthesis

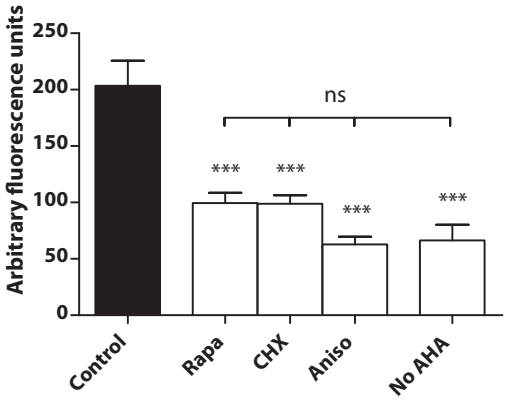

Figure A.3: Protein Synthesis in Growth Cones Labelled By AHA-TAMRA Click Reaction
Growth cones growth in 80 ng/ml NGF and methionine-free L-15 medium were exposed to AHA for 30 minutes, then washed and fixed. Newly synthesised proteins incorporating AHA in place of methionine were labelled with TAMRA and fluorescence measured, in the presence of 100 nM rapamycin (Rapa), 25 μM cycloheximide (CHX) and 20 μM anisomycin (Aniso), and in the absence of AHA (No AHA) as a negative control. All three inhibitors and the absence of AHA reduce levels of fluorescence relative to control, and the inhibitors reduce fluorescence to levels that do not differ significantly from the absence of AHA. Labelling performed by Roger Keynes, image analysis by Richard Manns.

A.4 280 nm Absorptions of Antibody Fractions

During purification of the 3004.2KLH antibody, the concentration of protein in the eluted fractions was measured by absorbance at 280 nm.

Elution Fraction	#1	#2	#3	#4	#5
Optical Density @ 280 nm	3.000+	3.000+	0.347	0.184	0.179

Table A.1: 280 nm Absorbance of Antibody Elution Fractions

Fractions #1 and #2 were pooled for dialysis against PBS; the remaining fractions were discarded.

A.5 Protein Purification

The 3004.2KLH-binding protein bears *O*-glycans (Keynes and Cook, *unpublished data*), whereas MVP does not, from published data (Herrmann et al., 1997) and apparent molcular weight (Figure 5.5(d)). Biochemical methods were therefore employed to differentiate the two molecules.

A.5.1 Protein Purification *via* Lectin Binding

Jacalin (a jackfruit-derived lectin) has a specificity for *O*-glycosylated glycoproteins, and reduces the growth cone collapse activity of extracts of CRL 1718 cells. The protein sample was incubated in the presence of jacalin-coated beads, to be eluted later, free of MVP. Although the beads reduced the amount of the 3004.2KLH-binding protein in the supernatant (Figure A.4(a)). Incubation of Fraction II proteins with jacalin-coated beads reduced the amount of the 3004.2KLH-binding protein, confirming that the 3004.2KLH-binding protein bound to the jacalin-coated beads. Immobilised jacalin has also been shown to remove growth cone collapsing activity from extracts of CRL 1718 cells (Cook, *personal communication*). However, application of various lectin-specific sugars, SDS or urea/thiourea (see *Methods: Purification with Lectins*) failed to recover detectable quantities of intact the 3004.2KLH-binding protein.

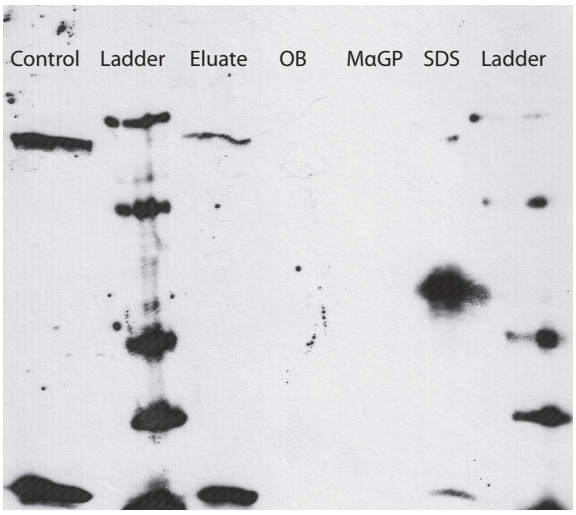

(a) Elution Using Elution Buffer OB, Methyl-α-GP and SDS

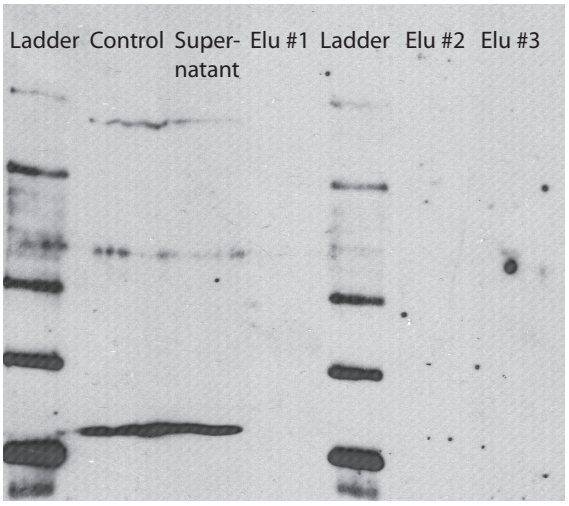

(b) Elution Using Methyl-α-GP, Urea and Thiourea

Figure A.4: Elution of the 3004.2KLH-binding protein from Jacalin Beads

(a) The the 3004.2KLH-binding protein band in the 'Eluate' lane, the supernatant after incubation with jacalin-coated beads, is reduced compared to 'Control'. Sequential use of neither the supplied protein elution buffer (OB), nor 0.5 M methyl-α-*D*-galactopyranoside (MαGP) or 1% w/v sodium dodecyl sulphate (SDS) released a detectable band of undegraded the 3004.2KLH-binding protein. There is a diffuse 70 kDa signal in the SDS lane and a sharper band at the base of the gel. These may be degradation products of the 3004.2KLH-binding protein. The previous two lanes do not reveal immunoreactive bands. (b) Attempted elution of the 3004.2KLH-binding protein using Elution Buffers 1–3 (Elu #1–3), combinations of urea, thio-urea and methyl-α-*D*-galactopyranoside. None eluted significant bands.

A.5.2 Protein Purification *via* Deglycosylation

Previous data suggest that deglycosylation of the 3004.2KLH-binding protein causes a shift in apparent molecular weight (Keynes and Cook, *unpublished data*). Combining this with SDS-PAGE to separate proteins by apparent molecular weight before and after deglycosylation would isolate the 3004.2KLH-binding protein with a 'double sieve' effect: proteins that shared its initial apparent molecular weight prior to SDS-PAGE are unlikely to share it after deglycosylation.

Non-enzymatic β-elimination released glycans from fetuin while the protein was not extensively degraded (Figure A.5). However, application of this protocol to CRL 1718 protein samples containing the 3004.2KLH-binding protein rapidly degraded the 3004.2KLH-binding protein (Figure 5.8) despite protocol modification (see *Methods: Non-Enzymatic Deglycosylation*).

A.5.3 Isolation of the 3004.2KLH-binding protein *via* Enzymatic Deglycosylation and Serial SDS-PAGE Electrophoresis

the 3004.2KLH-binding protein was also deglycosylated with sialidase and *O*-glycosidase (see *Methods: Enzymatic Deglycosylation*). The method employed the SDS-PAGE gel twice, with an intervening deglycosylation step. After separation by apparent molecular weight with each SDS-PAGE gel, the appropriate band was excised.

Repeated trial deglycosylations (*not shown*) demonstrated that the process resulted in a shift from 115 kDa to approximately 50 kDa, irrespective of the incubation length (Figure A.6(a)). This differed from the 80–90 kDa band observed in previous experiments (Keynes and Cook, *unpublished observations*). During the two-step sieve, it appeared after deglycosylation despite only the 115-kDa band being selected for incubation (Figures A.6(b) and A.6(c), respectively). It was concluded that this new band must be a fragment of the 3004.2KLH-binding protein, and was thus sent for MALDI-TOF analysis. The result revealed that the signal from contamination with bovine serum albumin (BSA) prevented identification of other proteins; the 3004.2KLH-binding protein remains unidentified. BSA was included during the deglycosylation step to prevent adsorption of the enzymes to the nitrocellulose strip, onto which the the 3004.2KLH-

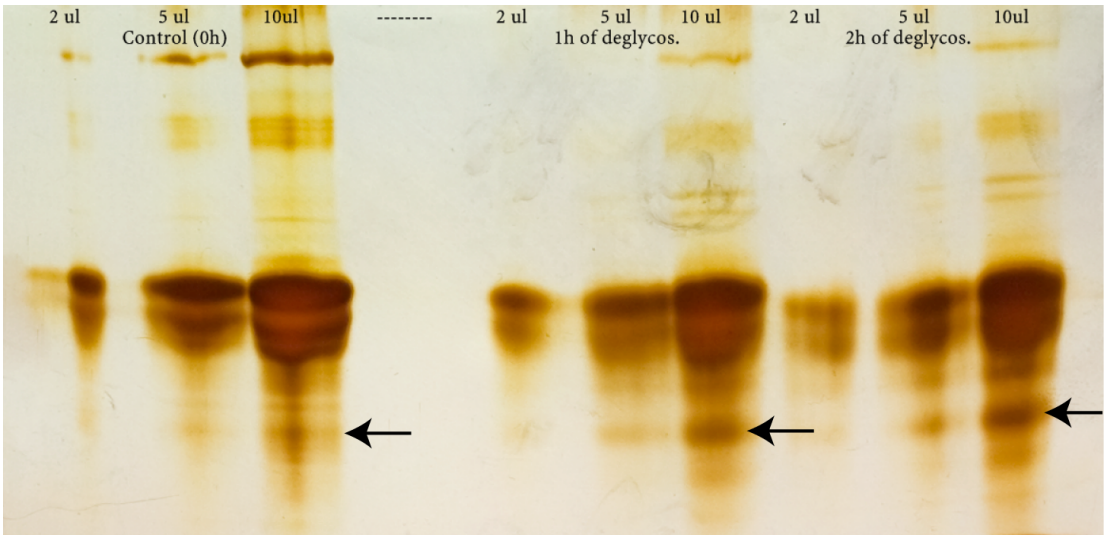

(a) Fetuin Protein Moiety Stability

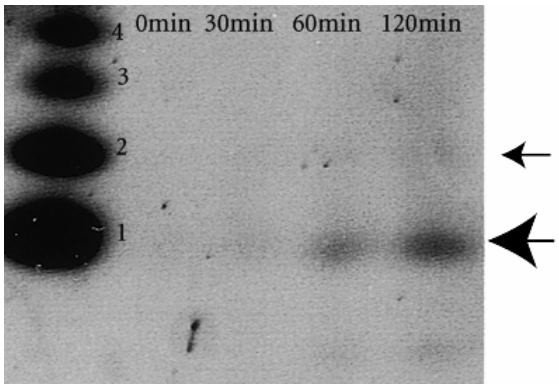

(b) Glycan Release over Time

Figure A.5: Time-Course of β-Elimination of Glycans from Fetuin

Fetuin proteins are stable (a) during the modified β-elimination process over 1–2 hours at a range of protein concentrations (2–10 µl of 1 mg/ml fetuin per reaction) as assessed by silver stain reaction. A secondary band of lower apparent molecular weight increases in intensity over time (arrowed). During this time, glycans (b) are released progressively, equivalent in apparent molecular weight to a mono- or disaccharide (large and small arrow, respectively). The molecular weight markers (labelled 1–4) consist of oligosaccharides derived from starch of varying numbers of component glucose moieties.

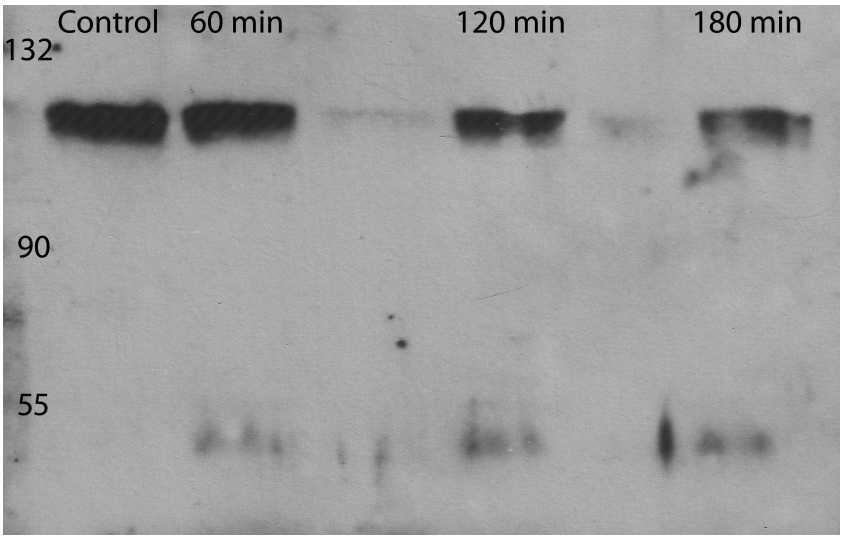

(a) Deglycosylation Time Course

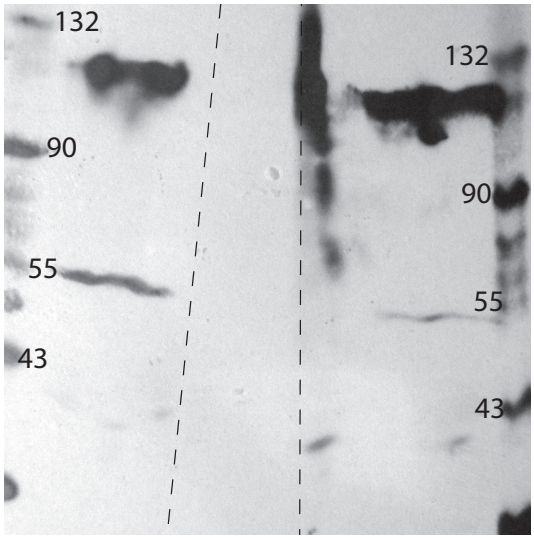

(b) 1st Stage of 2-Step Purification

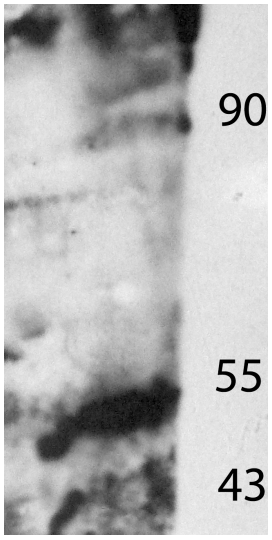

(c) 2nd Stage of 2-Step Purification

Figure A.6: Enzymatic Deglycosylation of the 3004.2KLH-binding protein

(a) A Western blot of the effect of enzymatic deglycosylation upon the 3004.2KLH-binding protein over time. A 50 kDa band develops over time, as the intensity of the 115 kDa band fades inversely. (b) Western blot of the side strips of the first SDS-PAGE gel. Reference lanes either side of the excised central lane show the 115 kDa band as a guide for mass-guided excision of the central the 3004.2KLH-binding protein-rich band. The dashed lines indicate the side of the two developed strips. The large signal on the right-hand side is part of the central band, indicating the abundance of the 3004.2KLH-binding protein. (c) Western blot of the SDS-PAGE gel after deglycosylation. The reporter lane shows a strong 50-kDa band . This position was correlated with the band on the silver-stained section of the gel, and the band excised for MALDI-TOF sequencing.

binding protein band had been transferred (See *Methods: Enzymatic Deglycosylation*)

A.6 cDNA Amplification and Prosaposin

A.6.1 DNA Concentrations after PCR and Midi-Prep Plasmid Synthesis

After selection and amplification of strong bands, I measured the concentration of cDNA *via* nano-drop spectrometry:

I and IV were selected for transformation into the pGEM-T-Easy plasmid with axolotl (*Ambystoma mexicanum*) *Sox8* as a control.

After sequencing, plasmid 'I2', *Homo sapiens prosaposin* was selected for *in situ* hybridisation, and axolotl *Sox8*, 'C2' was used as a control.

A.7 Primary Sequence of *Homo sapiens* Prosaposin

A.7.1 Confirmation of the Integrity of the cDNA Sample

Integrity of cDNA was confirmed by amplifying the cDNA sequence for *SEMA3A* (Figure A.7). The KOD Hot-Start Polymerase protocol and programme (see *Methods*) was used with 2% CRL 1718 cDNA solution and 20 μM of *SEMA3A* forward and reverse primers (see Table A.2). Gel electrophoresis of the products of the polymerase chain reaction (PCR) (Figure A.7) revealed one band per lane of ~2 400 bp, similar to the predicted length of 2 316 bp. No signs of smaple deterioriation such as loss of the ~2 400 bp band, of the appearance of shorted fragments of *SEMA3A* cDNA, was observed.

cDNA Template	Forward/Reverse	Sequence (5′ → 3′)	T_m	CG %
Sfi 5′	Forward	GAGTGGCCATTACGGCCGGG	74.5	70
Sfi 3′	Reverse	GGCCGAGGCGGCCGACATGT	79.4	75
Sema3A	Forward	AGCGTGTGCTGAGTGTTGCCTCG	69.7	60.9
Sema3A	Reverse	CCTTTCTTATTTTCTTGTAAGTG	51.0	30.4
AP 1	Forward	GAATGGACAGTTAGGCTAATT	50	38.1
AP 2	Forward	CTGGAGGACTTCAAACTC	49.7	50
AP 3	Forward	CTTGATCTAGACTACTAT	40.9	33.3
AP –1	Reverse	AATTAGCCTAACTGTCCATTC	50	38.1
AP –2	Reverse	GAGTTTGAAGTCCTCCAG	49.7	50
AP –3	Reverse	ATAGTAGTCTAGATCAAG	40.9	33.3

Table A.2: Sequences of Primers Used in PCR

The SfaI (Sfi) sequences were used to allow amplification in either direction knowing only one other sequence. The Sema3A sequences encoded the start of the exon, allowing the entire sequence to be amplified. Three peptide sequences from the 3004.2KLH-binding protein were used to generate the AP primers. Each primer was synthesised in both forward (x) and reverse (-x) directions to allow amplification of binding cDNA in both directions from a single bound primer.

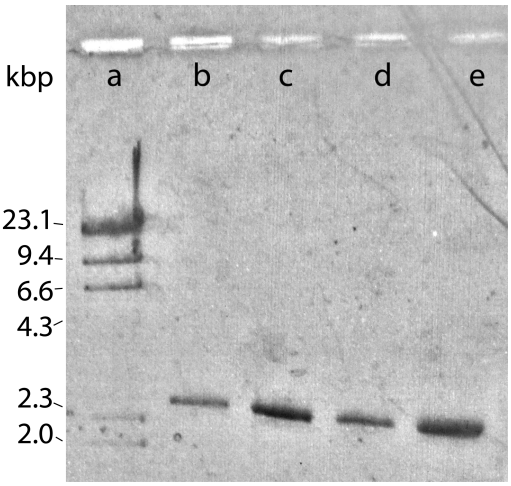

Figure A.7: The cDNA Sample Contains Full-Length *SEMA3A* cDNA

Gel electrophoresis of the products of PCR with *SEMA3A* primers and the astrocyte cDNA sample. Left to right, the lanes are a) HindIII as a molecular weight standard, b) PCR using 0.1× concentrate of cDNA template, (c) as previous, but twice the amount of sample, (d) using undiluted cDNA template, and (e) as previous, but twice the amount of sample.

Band	Absorption	260/280 nm Ratio	260/230 nm Ratio	Concentration (ng/µl)
I	1.999	1.97	2.22	16.6
II	2.833	1.89	2.14	13.3
III	2.776	1.87	2.49	9.1
IV	2.910	1.88	2.51	11.8
V	5.399	1.85	2.22	13.9
VI	4.030	1.86	1.40	16.7

Table A.3: cDNA Concentration prior to Sequencing

Sample	Absorption	260/280 nm Ratio	260/230 nm Ratio	Concentration (ng/µl)
C1	4.731	1.82	2.21	523.7
I2	2.937	1.85	2.28	335.5

Table A.4: cDNA Concentration prior to RNA Probe Synthesis

1	myalfllasl	lgaalagpvl	glkectrgsa	vwcqnvktas	dcgavkhclq	tvwnkptvks
61	lpcdickdvv	taagdmlkdn	ateeeilvyl	ektcdwlpkp	nmsasckeiv	dsylpvildi
121	ikgemsrpge	vcsalnlces	lqkhlaelnh	qkqlesnkip	eldmtevvap	fmanipllly
181	pqdgprskpq	pkdngdvcqd	ciqmvtdiqt	avrtnstfvq	alvehvkeec	drlgpgmadi
241	cknyisqyse	iaiqmmmhmq	pkeicalvgf	cdevkempmq	tlvpakvask	nvipalelve
301	pikkhevpak	sdvycevcef	lvkevtklid	nnktekeild	afdkmcsklp	kslseecqev
361	vdtygssils	illeevspel	vcsmlhlcsg	trlpaltvhv	tqpkdggfce	vckklvgyld
421	rnleknstkq	eilaalekgc	sflpdpyqkq	cdqfvaeyep	vlieilvevm	dpsfvclkig
481	acpsahkpll	gtekciwgps	ywcqntetaa	qcnavehckr	hvwn	

Table A.5: Amino Acid Sequence of Prosaposin

Appendix B

Published Work